ISTANBUL TECHNICAL UNIVERSITY ★ GRADUATE SCHOOL

AIR-SEA INTERACTIONS IN THE FORMATION OF THUNDERSTORMS OVER MARMARA REGION: PHYSICAL PROCESSES AND MODELLING

Ph.D. THESIS

Veli YAVUZ

Department of Meteorological Engineering

Atmospheric Sciences Programme

OCTOBER 2022

ISTANBUL TECHNICAL UNIVERSITY ★ GRADUATE SCHOOL

AIR-SEA INTERACTIONS IN THE FORMATION OF THUNDERSTORMS OVER MARMARA REGION: PHYSICAL PROCESSES AND MODELLING

Ph.D. THESIS

Veli YAVUZ
(511162006)

Department of Meteorological Engineering

Atmospheric Sciences Programme

Thesis Advisor: Prof. Dr. Ali DENİZ

OCTOBER 2022

ISTANBUL TEKNİK ÜNİVERSİTESİ ★ LİSANSÜSTÜ EĞİTİM ENSTİTÜSÜ

MARMARA BÖLGESİ'NDE ORAJLARIN OLUŞUMUNDA HAVA-DENİZ ETKİLEŞİMLERİNİN ETKİSİ: FİZİKSEL SÜREÇLER VE MODELLEME

DOKTORA TEZİ

Veli YAVUZ
(511162006)

Meteoroloji Mühendisliği Anabilim Dalı

Atmosfer Bilimleri Programı

Tez Danışmanı: Prof. Dr. Ali DENİZ

EKİM 2022

Veli YAVUZ, a Ph.D. student of ITU Graduate School student ID 511162006, successfully defended the thesis/dissertation entitled "AIR-SEA INTERACTIONS IN THE FORMATION OF THUNDERSTORMS OVER MARMARA REGION: PHYSICAL PROCESSES AND MODELLING", which he prepared after fulfilling the requirements specified in the associated legislations, before the jury whose signatures are below.

Thesis Advisor : **Prof. Dr. Ali DENİZ** ....
İstanbul Technical University

Jury Members : **Prof. Dr. Ahmet Duran ŞAHİN** ....
Istanbul Technical University

Assoc. Prof. Dr. Ahmet ÖZTOPAL ....
Istanbul Technical University

Assoc. Prof. Dr. Haldun KARAN ....
TÜBİTAK

Assoc. Prof. Dr. Hakkı BALTACI ....
Gebze Technical University

Date of Submission : 27 September 2022
Date of Defense : 28 October 2022

To my family,

FOREWORD

Thunderstorms and sea-effect snowfalls are two of the most important atmospheric phenomena in our country and in the world, especially since the 21st century, depending on global climate change. In the Marmara Region, which is the most developed region of Turkey in terms of industry and economy, thunderstorms and heavy snowfalls as a result of air-sea interactions cause negativities both in all types of transportation and in daily life. This thesis study examines the air-sea interactions in a cause-effect relationship, and discusses two important meteorological phenomena for the Marmara Region in terms of both their impact on daily life and the aviation sector. It is expected that the thesis study outputs will contribute to decision makers in both operational aviation activities and meteorology.

First of all, I would like to thank my supervisors Prof. Dr. Ali DENİZ, Prof. Dr. Anthony R. Lupo, and Prof. Dr. Neil I. Fox for their guidance and support. I also would like to thank my committee members Prof. Dr. Ahmet Duran ŞAHİN, Assoc. Prof. Dr. Ahmet ÖZTOPAL, and Assoc. Prof. Dr. Haldun KARAN for their contributions to my thesis.

Secondly, I dedicate the most special and precious thanks to my dear family. I am grateful to them for always being there for me and supporting me in all circumstances.

Thirdly, I would like to thank my dear friends Caner TEMİZ, Cem ÖZEN, Emrah UZUN, Gürkan ERGİN, İbrahim AKBAYIR, Mesut ONAY, Muharrem ZORBA, and Samet YÜKSEL for their support in alphabetical order.

Finally, I would like to thank my country, Istanbul Technical University, TUBITAK, University of Missouri, and Turkish State Meteorological Service for their support.

This thesis has been supported by TUBITAK 2214-A program with grant number 1059B142000051.

October 2022 Veli YAVUZ
(Meteorological Engineer)

TABLE OF CONTENTS

Page

ABBREVIATIONS

AD : Anno Domini
AMD : Amended
AMSL : Above Mean Sea Level
APDRC : Asia Pacific Data Research Centre
ATDnet : Arrival Time Differencing Network
B : Backing
BKN : Broken
BRN : Bulk Richardson Number
BS : Black Sea
CAPE : Convective Available Potential Energy
CB : Cumulonimbus
CIN : Convective Inhibition
CML : Convective Mixing Layer
COL : Cut-Off-Low
CT : Cross Total
ESWD : European Severe Weather Database
FEW : Few
G : Gust
GOES : Geostationary Operational Environmental Satellite
HZ : Haze
ICAO : International Civil Aviation Organisation
IR : Infrared
KI : K Index
LCL : Lifted Condensation Level
LCLP : Pressure Of Lifted Condensation Level
LES : Lake-Effect Snow
LHF : Latent Heat Flux
LI : Lifted Index
LS : Lake Surface
LT : Local Time
LW : Long Wave
LWT : Long Wave Trough
MAPLE : McGill Algorithm for Precipitation Nowcasting by Lagrangian Extrapolation
MAX : Max Display
METAR : Meteorological Aerodrome Report
MODIS : Moderate Resolution Imaging Spectroradiometer
MSG : Meteosat Second Generation
MSL : Mean Sea Level
NASA : National Aeronautics and Space Administration
NAO : North Atlantic Oscillation
NCEP : National Centres for Environmental Prediction
NIR : Near Infrared
NOAA : National Oceanic and Atmospheric Administration

NTT : Negative Tilted Trough
OAFLUX : Objectively Analysed Air-Sea Flux
OLC : Over Lake Convergence
OSC : Over Sea Convergence
P : Pressure
PPI : Plan Position Indicator
PROB : Probability
PTT : Positive Tilted Trough
PSWC : Plymouth State Weather Centre
PWAT : Precipitable Water
RA : Rain
RGB : Red-Green-Blue
RH : Relative Humidity
SCT : Scattered
SES : Sea-Effect Snow
SEVIRI : Spinning-Enhanced Visible and Infrared Imager
SH : Specific Humidity / Shower
SHF : Sensible Heat Flux
SI : Showalter Index
SN : Snow
SPECI : Special Aerodrome Report
SS : Sea Surface
SST : Sea Surface Temperature
STEPS : Short-Term Ensemble Prediction System
SW : Short Wave
SWEAT : Severe Weather Index
SWIRLS : Short-range Warnings of Intense Rainstorm in Localized
SWT : Short Wave Trough
SYNOP : Surface Synoptic Observations
T : Actual Temperature
TAF : Terminal Aerodrome Forecast
Td : Dew Point Temperature
TEMPO : Temporary
TITAN : Thunderstorm Identification Tracking Analysis and Nowcasting Systems
TKE : Turbulence Kinetic Energy
TQI : TQ Index
TRANS : Transition
TS : Thunderstorm
TSMS : Turkish State Meteorological Service
TTI : Total Total Index
USA : United States of America
UTC : Universal Time Coordinated
V : Veering
VC : Vicinity
VIS : Visible
VRB : Variable
VT : Vertical Total
WD : Wind Direction
WHOI : Woods Hole Oceanographic Centre

WMO **:** World Meteorological Organisation
WS **:** Wind Speed
WV **:** Water Vapor

SYMBOLS

°C	: Celcius Degrees
cm	: Centimeter
hPa	: Hecto Pascal
hr	: Hour
J	: Joule
kg	: Kilogram
km	: Kilometer
kn	: Knot
m	: Meter
min	: Minute
s	: Second
W	: Watt
µm	: Mikrometer
Ω	: Omega
µ	: Average Duration
Δ	: Difference

LIST OF TABLES

Page

LIST OF FIGURES

Page

AIR-SEA INTERACTIONS IN THE FORMATION OF THUNDERSTORMS OVER MARMARA REGION: PHYSICAL PROCESSES AND MODELLING

SUMMARY

Thunderstorm and sea-effect snow (SES) are meteorological events that adversely affect both daily life and the transportation sector, and occur as a result of air-sea interaction. Thunderstorm, is a meteorological phenomenon that usually contains strong winds and causes strong precipitation (e.g., rain, hail) accompanied by lightning. Intense atmospheric instability, high humidity, vertical triggering mechanisms, and wind shears are essential components for thunderstorm formation. Thunderstorms caused by cumulonimbus clouds occur both with precipitation and without precipitation. On the other hand, they occur not only with rain, but also with snow and hail. This phenomenon, known as a severe weather event, occurs as a result of convectional movements. For this reason, the increasing differences between the upper atmospheric level air parcel temperature and the sea or lake surface temperatures play an intensifying role in thunderstorm activities.

SES occurs as a result of atmospheric instability, which occurs as a result of dry and cold air masses gaining heat and moisture fluxes as they pass over warmer water bodies. As a result of the instability of very cold and dry air parcels of arctic or polar origin during their passage over the Black Sea located in the north of our country, the Marmara Region and the Black Sea Region are exposed to SES in the winter months. Although SES cause heavy snowfalls in regions where they are effective as severe weather events, they do not need synoptic-scale systems to occur. SES that occur in a region where synoptic-scale systems are currently dominant are called as snowfall with increased sea effect. This type of snowfall causes more intense snow on the regions where the SES bands pass.

In our country, there are studies on both severe weather events mentioned above. There are both case studies and climatological analyses in the literature regarding the thunderstorm event. However, climatological analyses and short-term forecast models are limited in terms of their effects on the Marmara Region and especially on the aviation sector. On the other hand, there are a very limited number of studies in the literature regarding the SES events for our country. There is no climatological comprehensive analysis or a prediction mechanism established for certain sectors for this event, where only a few assessments and case studies are included in the international literature. Both a knowledge and a scientific base are needed for this severe weather event, which is very effective in the northern parts of our country during the winter months and directly affects both daily life and transportation activities. In this context, in this thesis, a total of nine articles, two on thunderstorm events and seven articles on SES, were published in six different internationally refereed journals.

In the first article, a short-term forecast of the thunderstorm that occurred at Istanbul Atatürk International Airport on February 2, 2015 was made. It has been determined that the thunderstorm and its severity can be predicted in the range of 42-57 minutes

in advance by analysing radar images, Lightning Detection Tracking System (LDTS), sea surface temperature information, and surface/upper level atmospheric information. It has been revealed that this result is important for the decision makers working in the meteorology office.

In the second article, various 15-year long-term statistics of thunderstorm events were investigated at 11 airports in the Marmara Region. Atmospheric conditions in which thunderstorm events occur and the effects of air-sea interaction were examined. Intraday, monthly, and annual distributions were analszed. No trend was determined on an annual basis, and the most observations were made in September on a monthly basis. In the daytime thunderstorm distribution, the most observations occurred between 1100-1900 hours. 72% of thunderstorms occurred with rain and 22% without any precipitation. One of the most important results of the study is that the Convective Available Potential Energy (CAPE) is zero in approximately 50% of the events.

In the third article, the morphological classification of SES bands was made for the Danube Sea Area (western Black Sea) in the Black Sea. Between 2009 and 2018, SES bands were observed over the region in a total of 83 days, and these bands caused snowfall within the borders of the Marmara Region in 75 days. Various satellite and radar images obtained from the Turkish State Meteorological Service (TSMS) were used for the detection of SES bands. In total, five different types of SES bands have been defined for the region. The most common type of band among all events was Type-2 SES band with 85%. The most important reason for this is that this band type consists of parallel bands in the longitudinal direction. The north-south movements of polar and arctic air masses along the long fetch distance of the western Black Sea have created suitable atmospheric conditions for the Type-2 band. On average, the lowest sea surface temperatures (SESs) occurred in the northernmost part of the Danube Sea Area. This region is the region where SES bands mostly begin to form and are of weak intensity. The intensity of the bands increased due to the increasing SST towards the south.

In the fourth article, the analysis of vortex (Type-5) SES bands that occurred in the western Black Sea on January 30-31, 2012 was carried out. The vortex band, which was detected with various images of two different satellites (Terra and MSG satellites), continued its effect on the region for approximately 24 hours. The structure of the vortex was analysed by analysing the surface level meteorological data obtained from 12 airports, 16 meteorological stations, and 5 radiosonde stations belonging to the countries surrounding the western Black Sea and various charts of the upper atmospheric levels. The 24 cm of snow depth was measured at the İnebolu meteorology station, where the SES bands connected to the vortex were effective, and a total of 102 flights were canceled across the countries surrounding the western Black Sea. In addition to these, many traffic accidents have also occurred due to heavy and sudden snowfalls. The surface and upper level atmospheric conditions that create the vortex were found as follows: presence of a strong/deep inversion layer between the surface and 700 hPa, the wind direction change being limited to a maximum of 50° in the same vertical range, the temperature difference reaches 25.8 °C in between the sea surface and 850 hPa at the point where the vortex core is located. In addition, in the analyses made with the synoptic charts, it was determined that the vortex was formed during the two-day period and there was a low pressure centre in the region where the core is located.

In the fifth article, the statistical characteristics of SES events for the western Black Sea were analysed for the years 2009-2018. The main purpose of the study is to determine the meso- and synoptic-scale structures of SES events for the region in general and to create knowledge for nowcasting and forecasting applications to be made later. A total of 95 events were detected using satellite and radar images. These events were determined according to four different scale categories. As a result, 36 events (38%) are determined as Black Sea (BS) Events, 24 (25%) as Synoptic-scale (SYNOP) Events, 23 (24%) as Over Sea Convergence (OSC) Events, and 12 (13%) as Transition (TRANS) Events. While the average duration of SES events in four different categories was 15.9 hours, the longest time was 59 hours in the SYNOP Events. Except for the OSC Events, the prevailing wind direction under the inversion layer was northerly in all three categories. Inversion layer was detected in most of the BS Events and SYNOP Events, and the sea surface and upper level temperature difference was 4 °C to 6 °C higher on average compared to the other two categories. The highest number of events occurred in January with 51, and the lowest in March with 2.

In the sixth article, the effect of short-wave troughs on the formation and development of SES bands in the western Black Sea was investigated. Between 2010 and 2018, a total of 48 short-wave troughs and long waves were detected in the presence of SES bands throughout the region. The most important role of long waves has been realized as a result of determining the direction of short-wave troughs. Afterwards, short-wave troughs and long waves were classified based on their direction of motion. Five different types of short-wave troughs and five different types of long waves were determined, and their monthly and annual statistics, and their durations were revealed. In addition, the temperature differences between sea surface and upper atmospheric levels were analysed for each type, and inversion conditions were examined. The average duration of short-wave troughs was found to be 27.8 hours, and the longest time was observed in LWT type with 60 hours. In 77% and 79% of all events, respectively, short-wave troughs and long waves were found to have the same direction of motion as the current SES bands.

In the seventh article, thundersnows occurring in the Marmara Region within a 22-year period were investigated. For these events, the formation mechanisms, suitable surface, sea, and upper level atmospheric conditions were investigated. Based on the reports of 11 airports in the region, a total of 19 incidents were identified. In 17 of these events, the SES mechanism was found to be effective. After statistical temporal analysis, the predictability of these events was investigated with atmospheric stability indices. Accordingly, the most successful stability indices were Total Total Index and TQ Index.

In the eighth article, a comparison of SES and non-SES for two international airports in Istanbul is made. A SES event prediction algorithm was developed for both airports using 10 years of atmospheric data. At the same time, suitable atmospheric conditions were determined according to the snow depths.

Finally, in the ninth article, historical extreme winters in Istanbul were investigated. The events that took place within the scope of the 17-century period are shown, and based on the events that took place in the last few centuries, heavy snowfall and harsh winter forecasts are made for the period up to 2050 and 2100.

MARMARA BÖLGESİ'NDE ORAJLARIN OLUŞUMUNDA HAVA-DENİZ ETKİLEŞİMLERİNİN ETKİSİ: FİZİKSEL SÜREÇLER VE MODELLEME

ÖZET

Oraj ve deniz etkili kar (DEK) yağışı, hem günlük yaşamı hem de ulaşım sektörünü olumsuz etkileyen ve hava-deniz etkileşiminin bir sonucu olarak meydana gelen meteorolojik olaylardır. Oraj ya da diğer bilinen ismiyle gök gürültülü fırtına, bünyesinde genellikle güçlü rüzgarları ihtiva eden, yıldırım ve şimşek eşliğinde güçlü yağışlara (örneğin; yağmur ve dolu) sebebiyet veren bir meteorolojik fenomendir. Yoğun atmosferik kararsızlık, yüksek nem oranı, düşey tetikleyici mekanizmalar, ve rüzgar kaymaları oraj oluşumunda gerekli olan temel bileşenleri oluşturmaktadır. Kümülonimbüs bulutlarının neden olduğu orajlar, yağışlı meydana geldiği gibi yağışsız olarak da meydana gelmektedir. Diğer yandan yalnızca yağmur eşliğinde değil, kar ve dolu ile birlikte de meydana gelmektedirler. Şiddetli hava olayı olarak bilinen bu fenomen, konveksiyonel hareketlerin bir sonucu olarak oluşmaktadır. Bu sebeple yukarı atmosferik seviye hava parsel sıcaklığı ile deniz ya da göl yüzey sıcaklıkları arasındaki artan farklar oraj aktivitelerini şiddetlendirici rol oynamaktadır.

DEK ya da deniz etkisinde meydana gelen yağışlar, kuru ve soğuk hava kütlelerinin kendine göre daha sıcak su kütleleri üzerinden geçerken ısı ve nem akılarını kazanması sonucunda ortaya çıkan atmosferik kararsızlığın bir sonucu olarak meydana gelmektedir. Arktik ya da polar kökenli çok soğuk ve kuru hava parsellerinin ülkemizin kuzeyinde yer alan Karadeniz üzerinden geçişi esnasında kararsızlaşması sonucunda Marmara Bölgesi ve Karadeniz Bölgesi kış aylarında DEK yağışlarına maruz kalmaktadır. DEK yağışları şiddetli hava olayı olarak etkili olduğu bölgelerde yoğun kar yağışlarına sebep olsa da, meydana gelmek için sinoptik-ölçek sistemlere ihtiyaç duymamaktadır. Hali hazırda sinoptik-ölçek sistemlerin hakim olduğu bir bölgede meydana gelen DEK yağışları ise deniz etkisi arttırılmış kar yağışı olarak tabir edilmektedir. Bu tür yağışlar nispeten DEK bantlarının geçtiği bölgeler üzerinde daha yoğun yağışa sebep olmaktadır.

Ülkemizde, yukarıda bahsi geçen her iki şiddetli hava olayı ile ilgili olarak yapılan çalışmalar yer almaktadır. Oraj hadisesi ile ilgili olarak hem durum analizleri hem de klimatolojik analizler literatürde bulunmaktadır. Fakat Marmara Bölgesi genelinde ve özellikle havacılık sektörüne etkileri açısından yapılan klimatolojik analizler ve kısa süreli tahmin modelleri kısıtlı sayıdadır. Diğer yandan ülkemiz için DEK hadisesi ile ilgili olarak oldukça kısıtlı sayıda çalışma literatürde yer almaktadır. Yalnızca birkaç çeşitli değerlendirme ve durum analizinin uluslararası literatürde yer aldığı bu olay için klimatolojik kapsamlı bir analiz ya da belirli sektörler için oluşturulmuş bir tahmin mekanizması bulunmamaktadır. Ülkemizin kuzey kesimlerinde kış aylarında oldukça etkili olan ve hem günlük yaşamı hem de ulaşım faaliyetlerini doğrudan etkileyen bu şiddetli hava olayı için hem bir bilgi birikimine hem de bilimsel bir altlığa ihtiyaç duyulmaktadır. Bu bağlamda, bu doktora tez çalışmasında, hava-deniz etkileşiminin bir sonucu olarak meydana gelen oraj hadiseleri ile ilgili iki adet, DEK hadisesi ile

ilgili yedi adet olmak üzere toplamda dokuz adet makale uluslararası hakemli altı farklı dergide yayımlanmıştır.

İlk makalede, 2 Şubat 2015 tarihinde İstanbul Atatürk Uluslararası Havalimanı'nda meydana gelen oraj hadisesinin kısa süreli tahmini gerçekleştirilmiştir. Radar görüntüleri, Yıldırım Tespit Takip Sistemi (YTTS), deniz suyu sıcaklık bilgileri ve yer/yukarı seviye atmosferik bilgiler analiz edilerek, orajın ve şiddetinin 42-57 dakika aralığında önceden tahmin edilebileceği tespit edilmiştir. Bu sonucun meteoroloji ofisinde çalışan karar verici merciiler için önemli olduğu ortaya konulmuştur.

İkinci makalede, Marmara Bölgesi'nde yer alan 11 havalimanı için oraj olaylarının 15 yıllık uzun dönem çeşitli istatistikleri çıkartılmıştır. Oraj olaylarının meydana geldiği atmosferik koşullar ve hava-deniz etkileşiminin etkileri araştırılmıştır. Gün içi, aylık, ve yıllık dağılımları analiz edilmiştir. Yıllık bazda herhangi bir trend belirlenmemiş, aylık bazda ise en çok gözlem Eylül ayında yapılmıştır. Gün içi oraj dağılımlarında ise en çok gözlem 1100-1900 saatleri arasında meydana gelmiştir. Orajların %72'si yağmurla birlikte, %22'si ise yağışsız olarak meydana gelmiştir. Çalışmanın en önemli sonuçlarından birisi ise konvektif hazır potansiyel enerji (CAPE) olayların yaklaşık %50'sinde sıfır değerini almıştır.

Üçüncü makalede, Karadeniz'de yer alan Danube Deniz Sahası (batı Karadeniz) için DEK bantlarının morfolojik sınıflandırması yapılmıştır. 2009-2018 yılları arasında toplamda 83 günde bölge üzerinde DEK bantları gözlenmiş, 75 günde ise bu bantlar Marmara Bölgesi sınırları içerisinde kar yağışına sebep olmuştur. DEK bantlarının tespiti için Meteoroloji Genel Müdürlüğü'nden temin edilen çeşitli uydu ve radar görüntüleri kullanılmıştır. Toplamda beş farklı tipte DEK bantı bölge için tanımlanmıştır. Tüm olaylar içerisinde en çok meydana gelen bant tipi ise %85 oranla Tip-2 DEK bantı olmuştur. Bunun en önemli sebebi ise bu bant tipinin boylamsal doğrultuda birbirine paralel bantlardan meydana gelmesidir. Batı Karadeniz'in uzun feç mesafesi boyunca polar ve arktik hava kütlelerinin kuzeyden güneye doğru hareketleri Tip-2 bant için uygun atmosferik koşulları meydana getirmiştir. Ortalama olarak en düşük deniz suyu sıcaklıkları Danube Deniz Sahası'nın en kuzeyinde meydana gelmiştir. Bu bölge çoğunlukla DEK bantlarının oluşmaya başladığı ve zayıf şiddette olduğu bölgedir. Güneye doğru inildikçe artan deniz suyu sıcaklığına bağlı olarak bantların şiddeti de artmıştır.

Dördüncü makalede, 30-31 Ocak 2012 tarihinde batı Karadeniz'de meydana gelen vorteks (Tip-5) şeklindeki DEK bantlarının analizi gerçekleştirilmiştir. İki farklı uyduya (Terra ve MSG uyduları) ait çeşitli görüntülerle tespit edilen vorteks bant, bölge üzerinde etkisini yaklaşık 24 saat sürdürmüştür. Batı Karadeniz'i çevreleyen ülkelere ait 12 havalimanı, 16 meteoroloji istasyonu ve 5 radyozonde istasyonundan temin edilen yer seviyesi meteorolojik veriler ve yukarı atmosferik seviyelere ait çeşitli kartlar analiz edilerek vorteksin yapısı incelenmiştir. Vortekse bağlı DEK bantlarının etkili olduğu İnebolu meteoroloji istasyonunda 24 cm kar yüksekliği ölçülmüş, ayrıca batı Karadeniz'i çevreleyen ülkeler genelinde toplamda 102 uçuş iptal edilmiştir. Bunların yanı sıra çeşitli trafik kazaları da yoğun ve ani kar yağışlarına bağlı olarak meydana gelmiştir. Vorteksi meydana getiren yer ve yukarı seviye atmosferik koşullar şu şekilde bulunmuştur: yer yüzeyi ve 700 hPa arasında kuvvetli/derin enverziyon tabakasının mevcudiyeti, aynı düşey aralıkta rüzgar yön değişiminin maksimum 50° ile kısıtlı olması, vorteks çekirdeğinin bulunduğu noktada deniz yüzeyi ve 850 hPa seviyesi arasında sıcaklık farkının 25.8 °C'ye ulaşmasıdır. Ayrıca sinoptik kartlarla yapılan analizlerde iki günlük periyot boyunca vorteksin oluştuğu ve çekirdeğinin yer aldığı bölgede alçak basınç merkezinin bulunduğu tespit edilmiştir.

Beşinci makalede, batı Karadeniz için DEK olaylarının istatistiksel karakteristikleri 2009-2018 yılları arası için analiz edilmiştir. Çalışmanın temel amacı SES olaylarının bölge geneli için mezo- ve sinoptik-ölçek yapılarının belirlenerek daha sonra yapılacak kısa ve uzun süreli tahminler için bilgi birikimi oluşturulmasıdır. Uydu ve radar görüntüleri kullanılarak toplamda 95 olay tespit edilmiştir. Bu olaylar dört farklı ölçek kategorisine göre belirlenmiştir. Sonuç olarak, 36 olay (%38) Black Sea (BS) Event, 24 (%25) olay Synoptic-scale (SYNOP) Event, 23 olay (%24) Over Sea Convergence (OSC) Event, ve 12 olay (%13) Transition (TRANS) Event olarak tespit edilmiştir. Dört farklı kategoride DEK olaylarının ortalama yaşam süresi 15.9 saat olurken, en uzun süre 59 saat ile SYNOP Event kategorisinde gerçekleşmiştir. OSC Event kategorisi hariç diğer üç kategoride de enverziyon tabakası altı hakim rüzgar yönü kuzeyli olmuştur. BS Event ve SYNOP Event kategorilerinin çoğunda enverziyon tabakası tespit edilmiş, deniz yüzeyi ve yukarı seviye sıcaklık farkı ise diğer iki kategoriye göre ortalamada 4 °C to 6 °C yüksek meydana gelmiştir. En yüksek sayıda olay 51 ile Ocak ayında, en düşük ise 2 ile Mart ayında meydana gelmiştir.

Altıncı makalede, batı Karadeniz'de meydana gelen DEK bantlarının formasyonunda ve gelişiminde kısa dalga troflarının etkisi araştırılmıştır. 2010-2018 yılları araında bölge genelinde SES bantlarının mevcudiyetinde toplamda 48 adet kısa dalga trofu ve uzun dalga tespit edilmiştir. Uzun dalgaların en önemli rolü kısa dalga troflarının yönünü tayin etmesi neticesinde gerçekleşmiştir. Sonrasında kısa dalga trofları ve uzun dalgalar hareket yönleri baz alınarak sınıflandırmaya tabii tutulmuştur. Beş farklı tip kısa dalga trofu ve beş farklı tip uzun dalga tespit edilerek, bunların aylık ve yıllık bazda istatistikleri ile devam süreleri ortaya konulmuştur. Ayrıca her bir tip için deniz yüzey sıcaklığı ve yukarı atmosferik seviyeler arasındaki sıcaklık farkları analiz edilmiş, ve enverziyon durumları incelenmiştir. Kısa dalga troflarının ortalama yaşam süresi 27.8 saat olarak bulunmuş, en uzun süre ise 60 saat ile LWT tipinde gözlenmiştir. Tüm olayların %77 ve %79'unda sırasıyla kısa dalga troflarının ve uzun dalgaların mevcut DEK bantları ile aynı hareket doğrultusuna sahip olduğu tespit edilmiştir.

Yedinci makalede, 22 yıllık periyot kapsamında Marmara Bölgesi'nde meydana gelen orajlı kar yağışları araştırılmıştır. Bu olaylar için oluşum mekanizmaları, uygun yer, deniz ve yukarı seviye atmosferik koşullar incelenmiştir. Bölgede yer alan 11 havalimanı raporlarından hareketle toplamda 19 olay tespit edilmiştir. Bu olayların 17'sinde DEK mekanizmasının etkili olduğu belirlenmiştir. İstatistiki olarak yapılan zamansal analizlerin ardından, atmosferik kararlılık indeksleri ile bu olayların tahmin edilebilirliği araştırılmıştır. Buna göre en başarılı kararlılık indeksleri Total Total İndeks ve TQ İndeks olmuştur.

Sekizinci makalede, İstanbul'da yer alan iki uluslararası havalimanı için DEK ve DEK olmayan kar yağışlarının karşılaştırılması yapılmıştır. 10 yıllık birçok atmosferik veri kullanılarak her iki havalimanı için DEK olayı tahmin algoritması geliştirilmiştir. Aynı zamanda kar derinlikleri baz alınarak uygun atmosferik koşullar belirlenmiştir.

Son olarak dokuzuncu makalede, İstanbul'da meydana gelen tarihi ekstrem kışlar araştırılmıştır. 17 yüzyıllık periyot kapsamında meydana gelen olaylar gösterilmiş, son birkaç yüzyılda meydana gelen olaylar baz alınarak 2050 ve 2100 yıllarına kadar olan süreçte yoğun kar yağışı ve sert kış tahminlerinde bulunulmuştur.

1. INTRODUCTION

Air-sea interaction, briefly, is the whole of dynamic and thermodynamic processes that occur between the atmosphere and various water bodies (e.g., lake, sea, ocean). This interaction plays an important role in most of the meteorological disasters that constitute a large part of natural disasters. Turkey has a geographical location surrounded by seas and mountains on three sides. The mountains in the Black Sea Region lie parallel to the sea, and the mountains in the Aegean Region lie perpendicular to the sea. Therefore, meteorological events due to air-sea interactions occur in every geographical region of the country, less frequently in the eastern and inner parts. Turkey is exposed to the transitions of tropical air masses in warm months and polar air masses in cold months. Thunderstorms that occur in the spring and summer seasons begin to develop a few hours after sunrise after the atmospheric boundary layer (ABL) modulates with vertical heat, moisture and momentum fluxes. Flux transfers activated due to solar radiation continue until a few hours after sunset. Convective clouds (e.g., cumulonimbus, cumulus) that occur due to the development of the convective boundary layer (CBL) can cause heavy precipitation, hail and lightning. The development of the convective layer and the intensity of the convective clouds formed due to it are parallel to the temperature difference of the air parcel and the water mass over which it passes. Therefore, the fact that sea surface temperature (SST) anomalies are above normal in spring and summer affects the frequency and severity of thunderstorms. Turkey is frequently exposed to the effects of Siberian Thermal High Pressure (Siberian Anticyclone) and Icelandic Dynamic Low Pressure (Icelandic Cyclone) during the winter months. As a result of the passage of cold air masses over the Black Sea, located in the north of the country, systems occur depending on air-sea interactions. The meteorological phenomenon, which is mostly called lake effect snow (LES) in the literature and known as sea effect snow (SES) because it occurs under the effect of the Black Sea in our country, affects the Marmara Region and the northern parts of the Black Sea Region every year. The SES event is the result of cold air masses transferring heat and moisture fluxes to their bodies as they pass over relatively warmer water bodies, intensifying and leaving heavy snowfall to the places on their trajectories.

Case studies and climatological analyses related to thunderstorms were carried out for Turkey. However, the number of studies that take into account aviation activities in the Marmara Region is very limited. Similarly, there are only a few case studies for Turkey in the literature on SESs. It is an important need to carry out the climatological analysis of this event, which plays an important role in the snowfalls that occur especially in the Marmara Region and the northern parts of the Black Sea Region of Turkey, to reveal the atmospheric conditions in which it occurred, and to develop a forecasting system for the directly affected sectors. Many articles and projects have been carried out on LES bands and the snowfalls they cause in many countries around the world, especially in the United States and Canada. In addition, there are various studies in the literature examining the snow bands that occur in many sea effects such as the Japan Sea, the Adriatic Sea, and the Baltic Sea. As a result, thanks to the knowledge and scientific base that will be prepared for this meteorological phenomenon for our country, it will be beneficial for many decision-makers in the future.

In this thesis, studies were carried out for the short-term prediction of the thunderstorm event for an airport in the Marmara Region, and the atmospheric conditions that caused these events were investigated by performing climatological analysis on the basis of airports in the region for many years. In addition, various statistics of thunderstorm events were investigated, and their differences and similarities were examined around the world. Regarding the SESs, the morphological structures of the SES bands that cause these snowfalls were analysed, the atmospheric conditions that created them were analysed in depth, the effects they created throughout the Marmara Region were evaluated, and important findings were obtained especially for the aviation sector.

2. NOWCASTING OF A THUNDERSTORM: THE CASE STUDY OF 2 FEBRUARY, 2015 AT ISTANBUL ATATURK INTERNATIONAL AIRPORT [1]

2.1 Introduction

Nowcasting is performed in order to estimate the short-term future changes that may occur in the atmosphere for several hours (Mass and Mass, 2011). Such estimates are particularly important for commercial and general aviation, outdoor sport activities, construction, power plants, and ground transportation (Wilson et al., 1998). In particular, weather forecasting requires a lot of decision-making (Stuart et al., 2007). Together with advances in technology, it is desirable that the forecasters be trained in the most current techniques of nowcasting (Stuart et al., 2006). Convective nowcasting requires spatially (e.g. 1 km) and temporally (e.g. 10 min.) high-resolution prediction products. Forecasters now have the use satellite and radar images, lightning observations, and ground observations at their disposal. There is also a need for high-resolution model outputs and artificial intelligence products that can quickly auto-update, and, for example, show the direction and intensity of the storm or cell that will be emerging (Sills, 2009). Wilson et al. (1998) have discussed thunderstorm nowcasting techniques as classified into three categories; extrapolation, convection initiation/dissipation, and numerical prediction.

When an air mass passes over a warmer surface, the lower layer of the air mass (Meteorology, 2005; Türkeş, 2010; Ackerman and Knox, 2013) does the following; a) becomes warmer, b) more unstable, and c) the relative humidity decreases. For the opposite conditions, an air mass passing over a cold surface, it a) becomes cooler, b) more stable, and c) more humid.

An examination of the relationship between sea surface temperatures (SSTs) and thunderstorm occurrence demonstrates that positive temperature anomalies leads to

---

[1] This chapter is based on the research paper: Yavuz, V., Özdemir, E.T. and Deniz, A. (2020). Nowcasting of a thunderstorm: the case study of 2 February, 2015 at Istanbul Ataturk International Airport. *Mausam*, 71(1), 21-32, doi: https://doi.org/10.54302/mausam.v71i1.3

cloud formation because they contain a sufficient amount of latent heat. Studies have demonstrated that convective clouds (such as; cumulonimbus, cumulus) generally form or are enhanced. Ismail and Siadari (2015) have analysed the relationship between daily SST by using model output for their case study about a thunderstorm. They found that increasing temperatures over the sea surface cause instability, formation of convective clouds, and thunderstorms. SSTs also play an important role on the intensity of thunderstorm. Many computer-based model studies have indicated that small-scale changes in temperature also affected the wind patterns. It can lead to formation of the convective clouds by causing surface wind convergence (Hoyle, 2008). Das et al., (2014) tried to reveal the characteristics of a thunderstorm case study that was examined at the Guwahati Airport. The results show that warm and moist advection had progressed at low levels over the region and this generally happens in the pre-monsoon season. Additionally, there are many studies about thunderstorms in the scientific literature that examined the formation mechanisms and its effects on nearby airports (Young, 2007; Jebson, 2011; Pradhan et al., 2012; Sibley, 2012; Singh, et al., 2014; Özdemir and Deniz, 2016).

Thunderstorms at airports have caused flights to be cancelled or to be diverted because of turbulence, low visibility, heavy rain, etc. Although the consistency of meteorological forecasts is increasing today, there are still difficulties associated with the formation of convective systems. The use of radar products and lightning observations for nowcasting applications are increasingly important as well as the evaluation of model outputs.

The most common season for thunderstorms at Istanbul Ataturk International Airport is the boreal autumn for the period between 2008 and 2012. September and June are the months thunderstorms most frequently occur in general, while February and January are the months when the thunderstorms have occurred least. Regarding most frequent occurrence by time of day 42.16% of thunderstorms occurred between 1700 UTC (Universal Coordinated Time) and 2400 UTC; with 17.48% of storms occurring between 0900 UTC and 1300 UTC (Yazmuhammedov et al., 2014; Özdemir et al., 2017).

According to Terminal Aerodrome Forecast (TAF) reports prepared on 2 February 2015, at 1040 UTC and 1640 UTC at LTBA, a thunderstorm with light rain (-TSRA) was expected between 2 February 2015, at 2200 UTC and 3 February 2015, at 0200 UTC (Table 2.1).

Table 2.1 : TAFs that LTBA prepared on 2 February 2015, at 1040 UTC and 1640 UTC.

TAF LTBA 021040Z 0212/0318 20015KT 9999 SCT035 BKN100
TEMPO 0212/0216 –SHRA BKN030 BKN080
TEMPO 0222/0302 21015G25KT 4000 –TSRA FEW020CB BKN025
TEMPO 0303/0307 21017G27KT=
TAF LTBA 021640Z 0218/0324 22015KT 9999 SCT035 BKN100
BECMG 0218/0221 –SHRA BKN030 BKN080
TEMPO 0222/0302 23015G25KT 4000 –TSRA FEW020CB BKN025
TEMPO 0303/0307 21017G27KT
PROB30 TEMPO 0307/0310 4000 –TSRA FEW020CB BKN030=

Note: TAF: terminal aerodrome forecast; Z: Coordinated Universal Time; KT: knots; SCT: scattered; BKN: broken; TEMPO: temporary; (-): light; SHRA: showers with rain; G: gust; TSRA: thunderstorm with rain; CB: cumulonimbus; FEW: few; PROB: probability.

At LTBA, a thunderstorm with light rain began at 1757 UTC and ended at 1920 UTC (duration: 1 h 23 min). The TAF previously prepared at 1640 UTC was republished as TAF AMD (Amended) (Table 2.2). The LTBA Meteorological Office changed the forecast at 1753 UTC. It was then expected that a thunderstorm with light rain showers would occur between 1800 UTC and 2200 UTC. In this study, the thunderstorm that took place on 2 February 2015, at Istanbul Ataturk International Airport (LTBA) was examined, and the importance of "nowcasting" was emphasized. The purpose of this study is to carry out a search for predictability (nowcasting) of thunderstorm beforehand from the expected time by using radar and lightning images from nowcasting applications.

Table 2.2 : Amortized TAF (AMD-amended) that LTBA has issued on 2 February 2015, at 1753 UTC.

TAF AMD LTBA 021753Z 0218/0324 22015KT 9999 –SHRA SCT030 BKN080
TEMPO 0218/0222 4000 –TSRA FEW020CB BKN025
PROB30 TEMPO 0222/0301 23015G25KT –TSRA FEW020CB BKN030
TEMPO 0303/0307 21017G27KT
PROB40 TEMPO 0307/0310 4000 –TSRA FEW020CB BKN030=

Note: TAF: terminal aerodrome forecast; Z: Coordinated Universal Time; KT: knots; SCT: scattered; BKN: broken; TEMPO: temporary; (-): light; SHRA: showers with rain; G: gust; TSRA: thunderstorm with rain; CB: cumulonimbus; FEW: few; PROB: probability.

2.2 Data and Methodology

LTBA is located southwest of Istanbul and north of the Marmara Sea (Figure 2.1). According to the 2014 annual flight statistics, LTBA is ranked 13th in the world for the number of air traffic operations (ACI, 2015). According to the statistics conducted for Turkey, LTBA ranks first in terms of total number of passengers (GDSAA, 2015).

The products used in this study to obtain data were the Aerodrome Routine Weather Reports (METAR) and Aerodrome Special Weather Reports (SPECI) prepared by Ataturk International Airport Meteorology Office, TAF reports, routine synoptic maps, Skew-T Log-P diagrams, radar images, lightning observations, and SSTs (it measured by the Turkish State Meteorology Service at the stations on the Marmara Sea). SSTs are temperatures measured by TSMS and obtained from breakwaters and sea buoys located at points indicated on Figure 2.1 and these were measured every minute. However, hourly mean values were used in this study.

The Max radar products (41°20’28” N - 28°21’24” E; altitude: 378 m; tower: 41 m; distance to LTBA: ~56 km; C-band Doppler radar) were obtained from TSMS and also used for nowcasting. The Max product shows the maximum values measured by the radar between two defined horizontal levels using volumetric scanning data. It provides information about levels in which the events are more active and the condensation nuclei of air masses. Max radar images are products that are capable of displaying echo height and intensity on a single image and is used when weather conditions are severe. The lightning observations were evaluated also and these were obtained from the TSMS. Figure 1 shows the locations of LTBA, Kartal (Istanbul Rawinsonde Station) and sea water measuring stations.

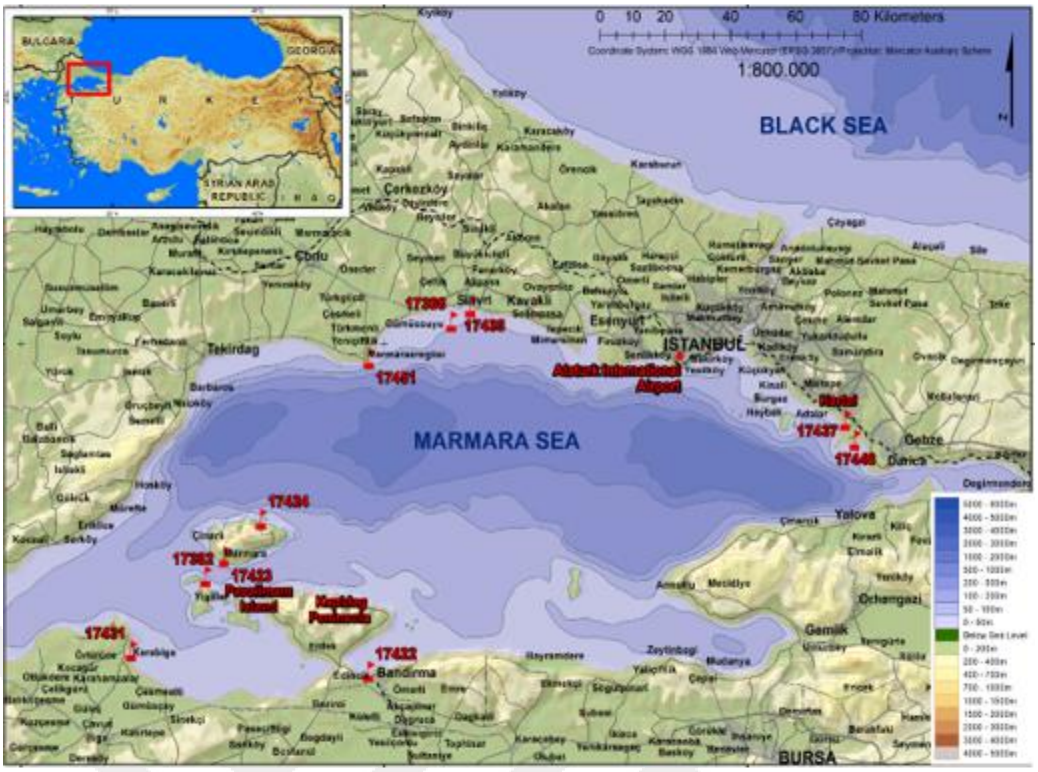

Figure 2.1 : Locations of LTBA, Kartal (Istanbul Rawinsonde Station) and sea water measuring stations.

2.3 Analysis and Nowcasting

2.3.1 Synoptic condition

On 2 February 2015, at 1200 UTC, according to the Met Office synoptic charts, a cold front and low pressure with a minimum value of 996 hPa near the Romanian Black Sea coast, stretching east of Istanbul and Marmara Sea and reaching to Crete Island. At 1800 UTC, this cold front continued moving the northeast by passing through Istanbul and reached the eastern parts of Turkey's western regions. At 1800 UTC, there was a trough from Bulgaria through Greece to the North Aegean (Figure 2.2). At 1200 UTC and 1800 UTC, 90% relative humidity was observed at 700 hPa over the western and southwestern regions. At the 500 hPa level at 1200 UTC, a splayed trough entered into Turkey’s western region. In particular, Istanbul is located at the left front side of the trough where positive vorticity values are high. Positive high vorticity values generally contributes to the lifting mechanism.

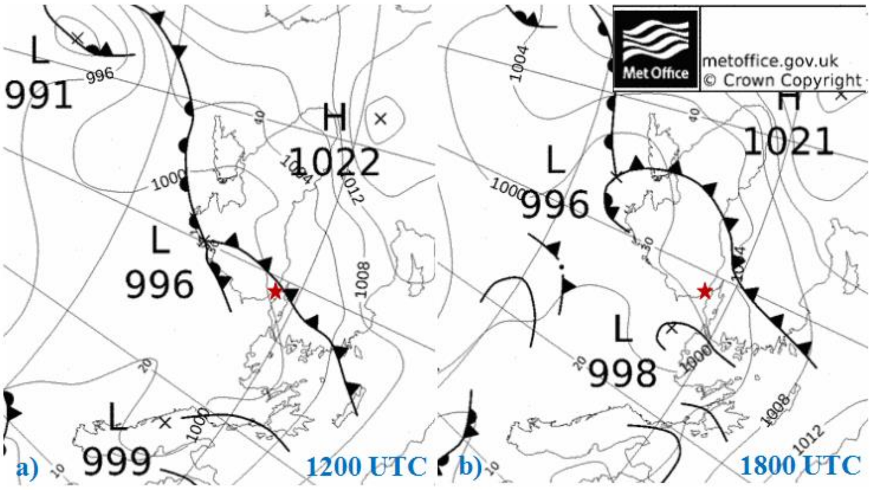

Figure 2.2 : Surface chart (lines, units in hPa) on 2 February 2015, at 1200 UTC. A red star shows the location of Istanbul.

2.3.2 Skew-T Log-P Diagram of Kartal (Istanbul Rawinsonde Station)

The distance between LTBA and Kartal (Istanbul) Rawinsonde Station is about 30 km. According to the 1200 UTC skew-T Log-P diagram (Figure 2.3), K Index and Totals Totals Index values indicate that it may be a moderate thunderstorm (Table 2.3) (NOAA, 2015). The relative humidity in the layer between 825 hPa (1585 m) and 415 hPa (6769 m) is over 81%.

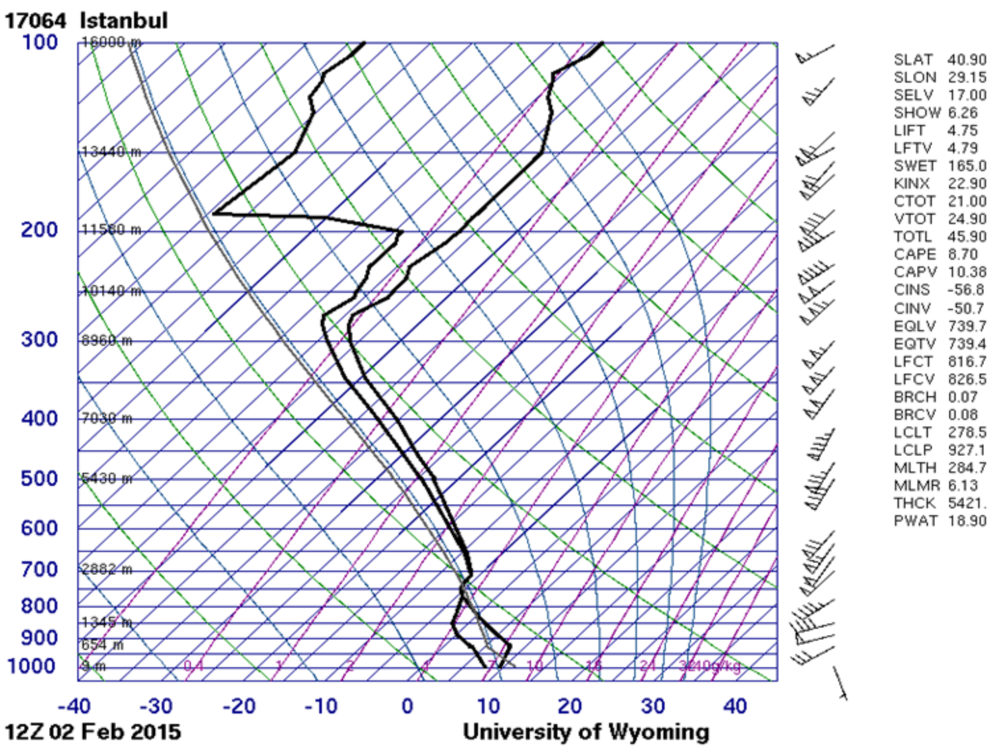

Figure 2.3 : Skew-T Log-P Diagram on 2 February 2015, at 1200 UTC in Kartal (Istanbul).

Table 2.3 : Various instability values at 1200 UTC on 2 February 2015.

Index	Value	Interpretation
Showalter Stability Index (SSI)	6.26	SI ≥ 3, no significant activity expected
Lifted Index (LI)	4.75	LI ≥ 3, no significant activity expected
K Index (KI)	22.90	21 ≤ KI ≤ 25, 20%-40% probability of thunderstorm occurrence
Totals Totals Index (TTI)	45.90	45 ≤ TTI ≤ 47, partial/moderate thunderstorm
Convective Available Potential Energy (CAPE)	8.70	CAPE < 1000, poor instability

2.3.3 METAR and SPECI reports

METAR and SPECI reports obtained from TSMS were examined. On 2 February 2015, at LTBA, a shower with rain started at 0420 UTC occasionally becoming of moderate intensity and continuing intermittently throughout the day. The thunderstorm with rain showers started at 1757 UTC and ended at 1920 UTC, continuing for 1 h and 23 min (Table 2.4).

Table 2.4 : METAR and SPECI reports at LTBA on 2 February, 2015.

Time (UTC)	Wind Dir. (º)	Wind Sp.	Phenome na	Prevailing Vis. (m)	Cloudiness	T & Td (ºC)	P (hPa)
14:50	180	8	(-) SHRA	10,000	SCT030 BKN080	11-08	1000
15:20	190	10	(-) SHRA	10,000	SCT030 BKN080	11-08	1000
15:50	180	11	-	10,000	SCT030 BKN080	11-08	1000
16:20	190	10	-	10,000	SCT030 BKN080	11-07	1001
16:50	180	10	-	10,000	SCT030 BKN080	11-08	1001
17:15	170	12	(-) SHRA	10,000	SCT030 BKN080	11-08	1000
17:20	170	14	(-) SHRA	10,000	SCT030 BKN080	10-08	1001
17:50	190	10	(-) SHRA	10,000	FEW020CB BKN030	11-07	1001
17:57	200	8	(-) TSRA	8,000	FEW020CB BKN025	11-07	1001
18:20	200 / 180V240	11	(-) TSRA	8,000	FEW020CB BKN025	10-07	1001
18:50	220 / 190V270	10	(-) TSRA	4,000	FEW020CB BKN030	10-07	1002
19:20	280 / 220V340	4	(-) SHRA	8,000	FEW020CB BKN030	09-07	1002
19:50	150 / 100V200	3	(-) SHRA	8,000	FEW020CB BKN030	09-07	1002
20:20	140 / 030V180	3	(-) SHRA	8,000	FEW020CB BKN035	09-07	1002
20:50	150 / 100V180	6	(-) SHRA	7,000	FEW017CB BKN030	09-07	1002

Note: T: temperature; Td: dew point temperature; (-): light; SCT: scattered; BKN: broken; CB: cumulonimbus; TSRA: thunderstorm with rain; FEW: few; SHRA: heavy rain showers

2.3.4 Marmara Sea surface temperatures

The hourly averaged SSTs obtained from measuring stations in the Marmara Sea and available through TSMS are shown in Table 2.5. Between 1000 UTC and 1500 UTC, the increase in sea surface temperature is 0.30 °C at station 17424 (daytime maximum value is 10.63 °C at 1400 UTC) and 0.24 °C at station 17423 (daytime maximum value is 10.05 °C at 1400 UTC).

Table 2.5 : Sea surfacetemperatures of the Marmara Sea on 2 February, 2015.

Station No & Time (UTC)	17382	17388	17422	17423	17424	17431	17437	17438	17448	17451
0100	9.99	9.54	10.58	9.64	9.53	11.20	9.28	8.14	9.72	8.38
0200	9.90	9.60	10.59	9.73	9.45	11.19	9.30	8.10	9.70	8.37
0300	9.83	9.60	10.43	9.74	9.40	11.11	9.31	8.10	9.70	8.38
0400	9.90	9.60	9.85	9.81	9.73	11.07	9.30	8.09	9.77	8.36
0500	9.85	9.60	9.80	9.85	10.24	11.09	9.30	8.08	9.79	8.33
0600	9.50	9.60	9.82	9.90	10.40	10.92	9.30	8.06	9.80	8.31
0700	9.50	9.60	9.78	9.90	10.52	10.53	9.30	8.01	9.78	8.29
0800	9.47	9.60	9.41	9.90	10.61	10.34	9.30	8.00	9.78	8.29
0900	9.57	9.60	9.20	9.82	10.53	10.47	9.25	8.07	9.80	8.29
1000	9.60	9.68	9.12	9.79	10.21	10.55	9.25	8.03	9.79	8.28
1100	9.62	9.70	8.96	9.81	10.39	10.59	9.29	7.96	9.79	8.37
1200	9.68	9.71	8.94	9.93	10.40	10.66	9.28	7.99	9.80	8.37
1300	9.81	9.77	9.02	10.03	10.60	10.69	9.30	7.99	9.80	8.32
1400	9.94	9.79	8.96	10.05	10.63	10.70	9.30	8.00	9.79	8.35
1500	9.98	9.79	8.90	9.93	10.60	10.58	9.31	7.95	9.77	8.22
1600	9.88	9.71	8.90	9.92	10.40	10.49	9.29	7.90	9.79	8.09
1700	9.90	9.70	8.90	9.86	10.31	10.57	9.31	7.90	9.80	8.06
1800	9.99	9.70	8.90	9.84	10.39	10.65	9.30	7.90	9.74	8.08
1900	9.98	9.70	8.83	9.81	10.45	10.73	9.30	7.90	9.76	8.05
2000	9.86	9.70	8.82	9.80	10.50	10.69	9.31	7.98	9.70	8.11
2100	9.83	9.70	8.82	9.79	10.52	10.72	9.30	7.94	9.70	8.19
2200	9.80	9.68	8.91	9.80	10.49	10.71	9.28	7.96	9.70	8.22
2300	9.67	9.60	8.90	9.80	10.45	10.56	9.29	7.90	9.71	8.28
0000	9.53	9.60	8.90	9.78	10.39	10.27	9.30	7.90	9.70	8.19

2.3.5 Nowcasting

2.3.5.1 Radar images

Max display images of Istanbul Radar for the period 1608 UTC to 1815 UTC on 2 February 2015 obtained from TSMS are shown in Figure 2.4. At 1608 UTC, a thunderstorm cell was seen in the southwest part of Istanbul's Anatolian side (Figure 2.4a). There was no convective activity over the Marmara Sea and at LTBA. At 1615 UTC, cloudiness (Figure 2.4b) on Pasalimani Island moved northeast and convectively developed, reaching a vertical height of approximately 10 km (Figure 2.4c). At 1638 UTC, two more thunderstorm cells appeared on the Marmara Sea over the northeast part of the Kapidag Peninsula (Figure 2.4e). At 1708 UTC, large thunderstorm cells were observed over the middle and southwest parts of the Marmara Sea (Figure 2.4i).

At 1738 UTC, the thunderstorm cell, which was spread over a large portion of the middle Marmara Sea region, moved a northeast direction parallel to the movement of the cold front (Figure 2.4m). At 1808 UTC, the thunderstorm cell was close to LTBA (Figure 2.4q). By 1816 UTC, the northern parts of the thunderstorm cell was on the LTBA (Figure 2.4r).

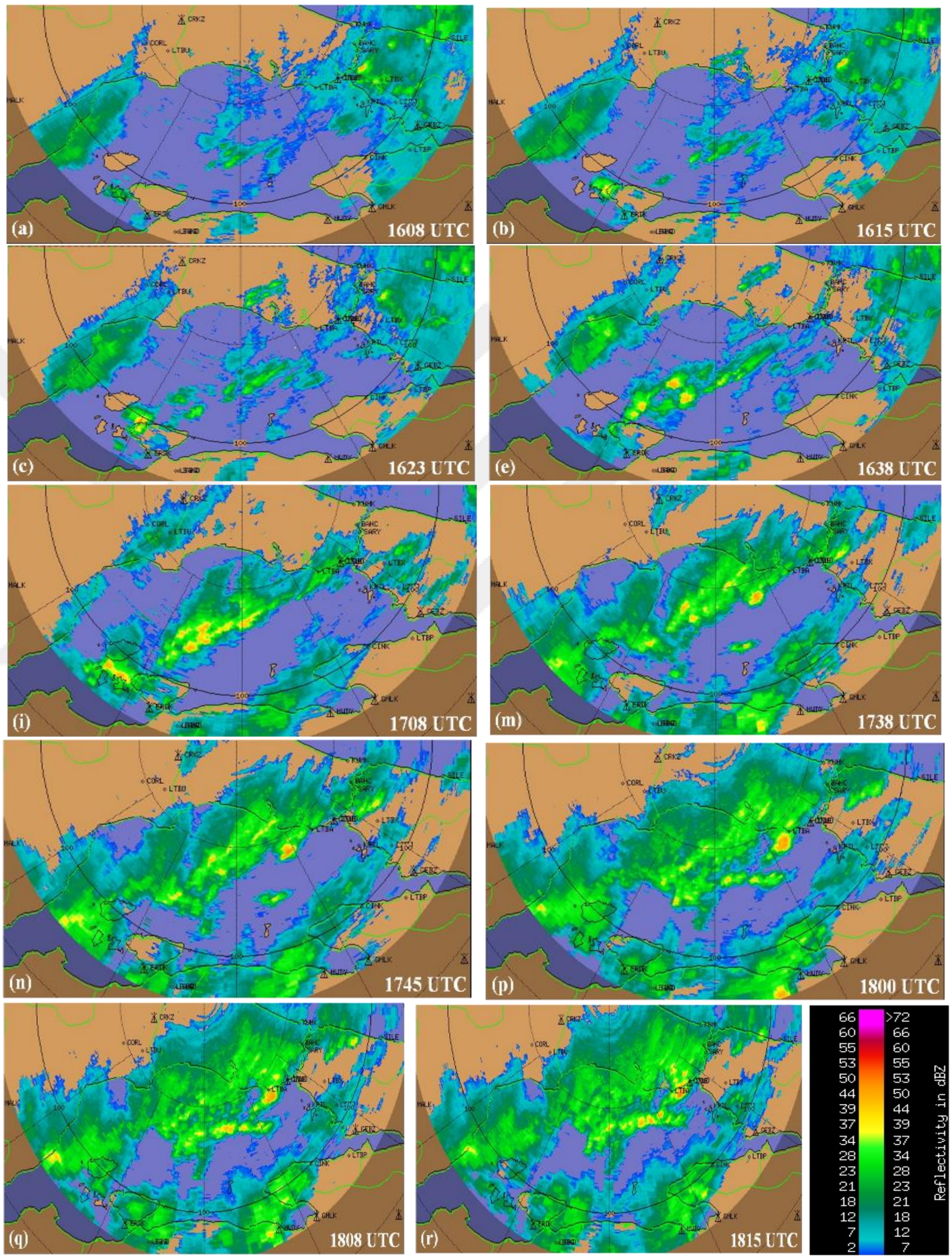

Figure 2.4 : (a-r) Max display images of Istanbul Radar.

Figure 2.5(a-c) shows vertical sections of Max display radar products for the time period between 1753 UTC and 1808 UTC. Examining the vertical cross-section of the

Max radar product at 1800 UTC, it is demonstrated that the thunderstorm cell reached a maximum reflectivity value of 53.5 dBZ (Figure 2.5b).

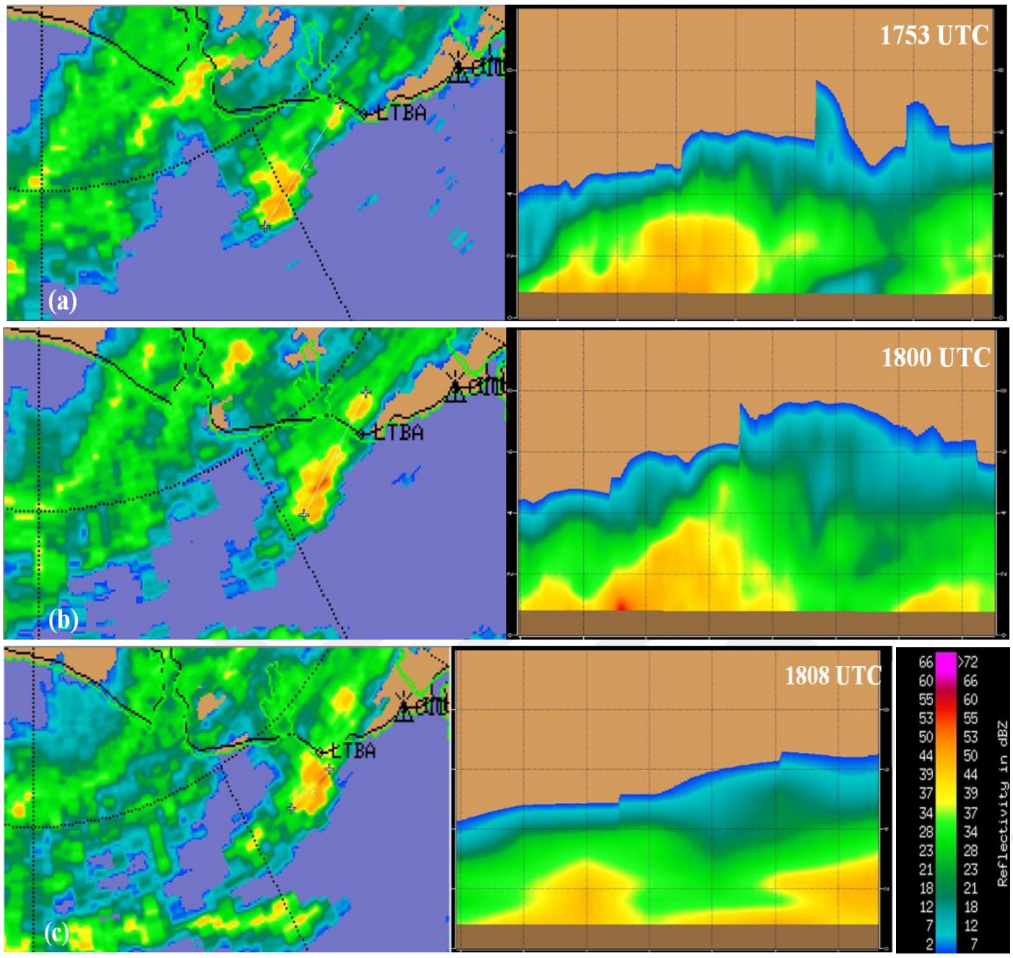

Figure 2.5 : Max display images from Istanbul Radar, the vertical sections of the Max radar images for a) at 1753 UTC, b) 1800 UTC, c) 1808 UTC.

2.3.5.2 Lightning observations

The lightning observations in the Marmara Sea between 1600 UTC and 1800 UTC are shown in Figure 2.6 (the position of LTBA is shown using the red circle). Between 1600 UTC and 1630 UTC, lightning was observed over and around Kapidag Peninsula (Figure 2.6a). It is seen that the lightning observations spread along the northeast-southwest direction in the middle of Marmara Sea between 1700 UTC and 1730 UTC (Figure 2.6c). In Figure 2.6d, increased lightning activity is approaching LTBA from the southwest between 1730 UTC and 1800 UTC.

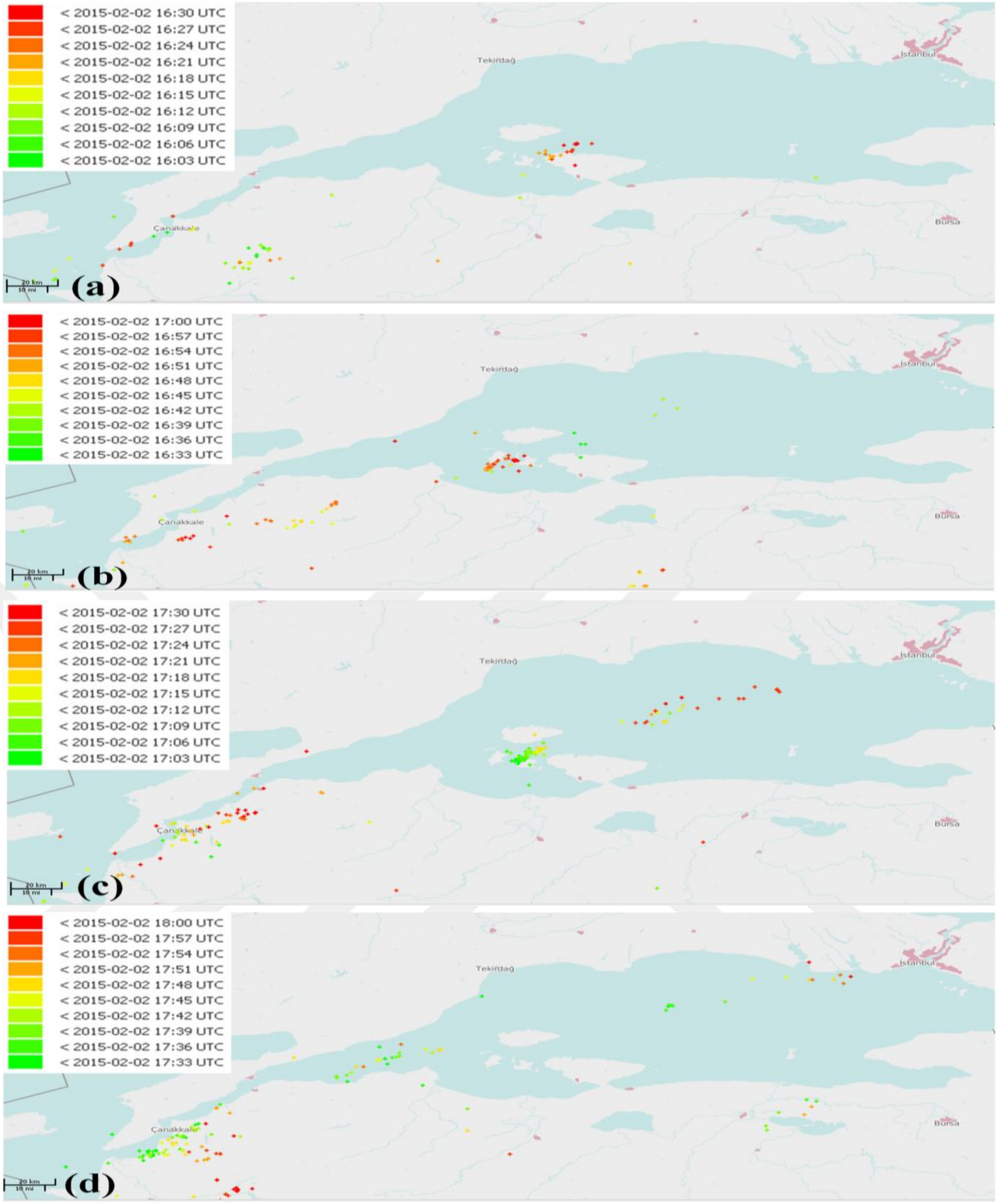

Figure 2.6 : Lightning observations in the Marmara Sea region for a) 1600 UTC-1630 UTC, b) 1630 UTC-1700 UTC, c) 1700 UTC-1730 UTC, d) 1730 UTC-1800 UTC.

2.4 Discussion

Öztopal (2017) has examined the temporal and spatial distribution of thunder and lightning events for the period 2010-2014 within Turkey, using the Arrival Time Differencing Network (Atdnet) observation data operated by the UK Meteorological Office (Figure 2.7). The highest value shown for lightning activity in Turkey is about 7.1 strokes $km^{-2}.year^{-1}$. The shores of the Hatay province, Gulf of Iskenderun, many districts of Antalya and Muğla provinces (Belek, Side, Alanya, Dalaman, Fethiye and

Marmaris) and coastlines of Marmaris especially observed the highest density of lightning activity 5.0 - 7.1 strokes $km^{-2}.year^{-1}$. When we look at the frequency of lightning activity in the LTBA region, it was not observed to be as intense as the regions mentioned above. The value is approximately between 2.5 and 3.5 strokes $km^{-2}.year^{-1}$. These results show that the LTBA and its surroundings were not the place where the convection was initiated and intensifying, but that the thunderstorm was entering the mature stage and then the disintegration phase.

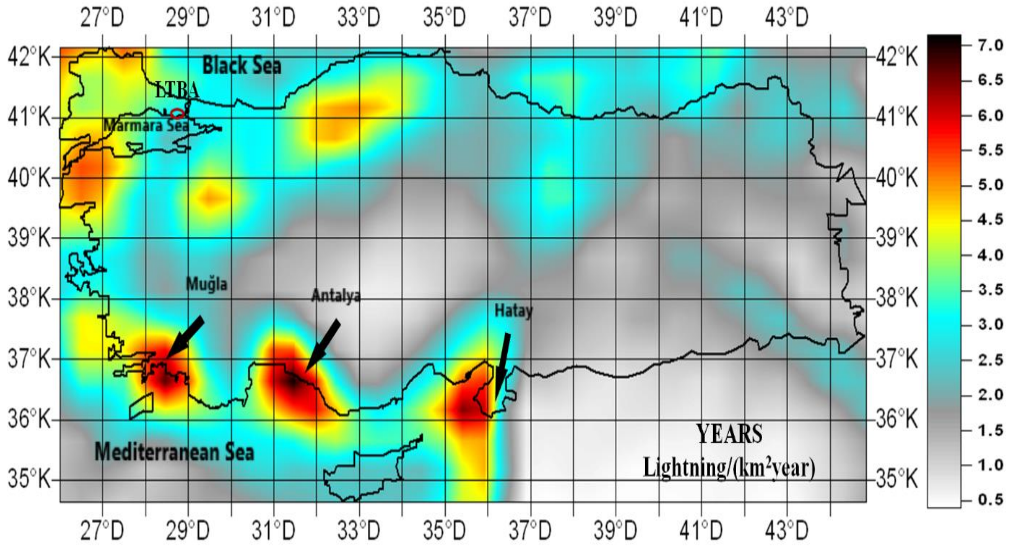

Figure 2.7 : Temporal and spatial distribution of lightning events in Turkey, 2010-2014 (Öztopal, 2017).

Yavuz (2016) reviewed the METAR and SPECI reports that were prepared by LTBA over a period of 15 years from 2001 and 2015 inclusive. Lightning events were observed mainly between 1700 UTC and 2200 UTC (Figure 2.8). Over that period, there was an increasing trend towards 1700 UTC to 2200 UTC occurrences. Also in the same study, the author examined ATDnet lightning strike data for the seven year period covering 2008 and 2014 (Figure 2.9). A total of 623 lightning events per hour were detected within a 25 km radius for the selected period in LTBA. Also, in this region, the maximum number of lightning events for one particular hour was 44 (7% - 1000 UTC and 1100 UTC); and then 38 (6% - between 1700 UTC and 1800 UTC).

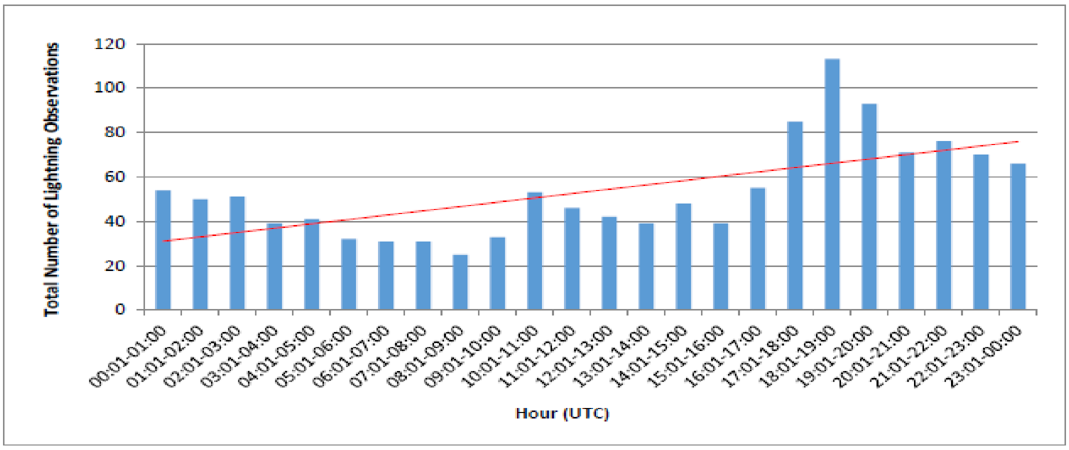

Figure 2.8 : Hourly lightning observations at LTBA, 2001-2015 (Yavuz, 2016).

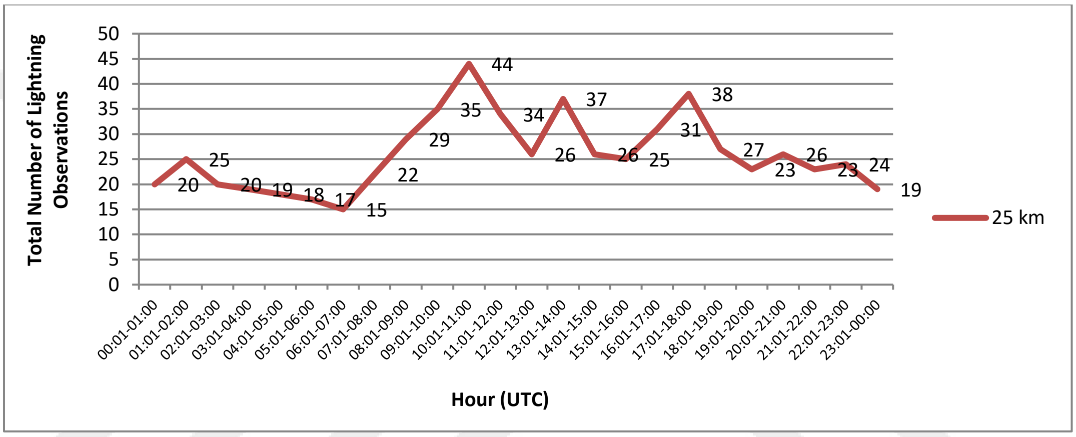

Figure 2.9 : Total number of hourly lightning observations at LTBA within the 25 km radius, 2008-2014 (Yavuz, 2016).

High SST values are directly related to water vapor in the lower atmosphere (lower troposphere). Similarly, changes and trends in water vapor have a direct correlation with SST anomalies. Theoretically and observed in the model studies, the observed increase in SST and associated with water vapor in the case of constant relative humidity conditions has a positive effect on atmospheric convection (such as the development of thunderstorms and tropical cyclones, see Trenberth, 2005). The increase in the insolation that occurs on a daily basis causes SST values to increase. Therefore, changes in surface fluxes are observed in association with shortwave length radiation. Even increases on the order of a few degrees Centigrade can lead to high variations in the net surface flux. This can lead to an instability effect in the lower atmosphere (Kawai and Wada, 2007).

Due to the location of LTBA (the Black Sea to the north, the Marmara Sea to the south and the Bosphorus to the north-east), it constitutes a transit zone for thunderstorm and lightning activities because there are large water sources around it (three sides) to provide the moisture required for convective movements. The surface circulation of the Marmara Sea, which was constructed and synthesized here using data from March 1992 to October 1999 is shown in Fig. 10. The circulation of the Marmara Sea surface waters (Figure 2.10) can be described as a current circulating from the Black Seas through the Bosphorus and into the Mediterranean establishing a clockwise gyre within a large portion of the basin. This general structure may vary due to the wind and/or the amount of water coming from the Black Sea (Beşiktepe et al. 2000). In the southern part of the Marmara Sea, the relatively warm sea surface currents move to the north part of the Marmara Sea, and it causes increasing instability in the atmosphere to the north of the Marmara Sea. Conversely, these same surface currents increases the stability of the atmosphere to the south by causing the surface temperature to decrease in the Marmara Sea (which is located just south of LTBA). The authors note that most thunderstorms that took place at LTBA have occured between 1700 UTC and 2200 UTC (Yavuz, 2016), and between 1700 UTC and 2400 UTC (Özdemir et al., 2015). Moreover, it is postulated that there was a contribution by the sea surface currents and the location and timing of thunderstorms. These issues have been raised in this study by the authors for the first time in Turkey. Future work should be done investigating this topic as it would influence nowcasting for these regions.

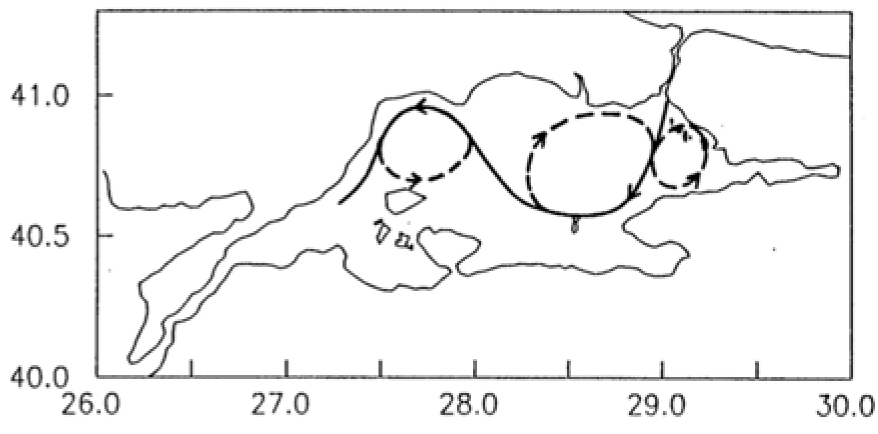

Figure 2.10 : Sea surface circulation of the Marmara Sea (Beşiktepe et. al., 2000).

There are many different nowcasting systems that are in use today. Some of the most commonly used are; Thunderstorm Identification Tracking Analysis and Nowcasting (TITAN) (Dixon and Wiener, 1993), McGill Algorithm for Precipitation Nowcasting by Lagrangian Extrapolation (MAPLE) (Germann and Zawadzki, 2002), Short-Term Ensemble Prediction System (STEPS) (Bowler et al., 2006) and the Short-range

Warnings of Intense Rainstorm in Localized Systems (SWIRLS) (Li and Lai, 2004). In Turkey, TSMS operates the meteorological radars of which there are a total of 18 of them including 17 C-band and 1 X-band in Turkey. The C-band radars are mountain radars (These radars are located on the high hills, not on the airport plain). Including LTBA, the nowcasting systems mentioned above are not used in Turkey. As with many countries using radar, Turkey has also performed nowcasting based on human prediction.

The modification of a predictive TAF report that thunderstorm cells observed over the Marmara Sea are being monitored by radar products should not mean that definitely there will be a thunderstorm at LTBA. On 23 September 2015, LTBA Meteorological Office surveyed convective activity over the Marmara Sea by evaluating radar products. The TAF published at 1640 UTC was corrected at 1957 UTC and a thunderstorm was expected between 2000 UTC and 2200 UTC. However, the thunderstorm cell collapsed and only a shower with rain occurred at LTBA. The authors believe that local SST anomalies (10-20 km) in the proximity of LTBA over the Marmara Sea contribute to sea surface water flow, which will either increase or decrease the effect of warm water or relatively cold water from runoff due to thunderstorms. Air masses undergo thermodynamic changes as they pass through relatively warm or cold surfaces. As a result, the stability of the lower layer of air mass is changing (Meteorology, 2005; Türkeş, 2010; Ackerman and Knox, 2013).

2.5 Conclusion

In this study, a thunderstorm accompanied by rain showers at LTBA on 2 February 2015 was investigated for its predictability by using radar and lightning images (nowcasting) before it occurred.

On 2 February 2015, at 1200 UTC, a cold front passed over LTBA and the airport was behind the cold front by the afternoon and evening. After evaluation of meteorological model outputs and actual maps, the thunderstorm incident is expected due to the passage of the trough behind the cold front between 2200 UTC and 0200 UTC (February 2 to 3, 2015). According to the 1200 UTC sounding data, important activity was not expected or the probability of precipitation associated with the trough was expected to be very low due to solar heating. According to the sea surface temperature data obtained from Marmara Sea water measuring stations, there was an increase in the temperature anomaly to a maximum value of +0.30 °C between 0900 UTC and 1500 UTC. The increase in sea surface temperature caused the increase in the instability on the Marmara Sea. Depending on this instability, thunderstorm cells formed in different parts of the Marmara Sea. Between 1615 UTC and 1630 UTC, the thunderstorm cells began to form over the southwestern part of the Marmara Sea, particularly; Marmara Island, Avsa Island and the Kapidag Peninsula. These thunderstorm cells formed and then moved parallel to the movement of the cold front to the northeast of Istanbul, and the system continued to move towards the northeast. At 1700 UTC, there was a wide range of thunderstorm cells over the Marmara Sea. Small increases in Marmara Sea SSTs between 1700 UTC and 2100 UTC, have increased the activity of the thunderstorm cells. These small increases in SSTs (maximum of +0.16 °C) are due to the changes in the flow of sea surface waters. At 1723 UTC, the thunderstorm cell that would affect LTBA continued to evolve by ingesting enough humidity from the sea. At 1808 UTC, the northern parts of these cells were located at LTBA. The thunderstorm with shower activity was reported commencing at 1757 UTC by LTBA and ended at 1920 UTC. Thus, the thunderstorm continued at the airport for 1 hour and 23 minutes.

This thunderstorm activity, which was expected by the LTBA Meteorology Office at 1753 UTC, could have been estimated sooner by using Max radar images and lightning observations. If the thunderstorm cell observed on Pasalimanı Island and Kapidag Peninsula at 1615 UTC was tracked, and then later the distribution and direction of movement of this cell over the Marmara Sea were also monitored, the TAF estimate could have been corrected by LTBA Meteorological Office between 1700 UTC and 1715 UTC. Revising the TAF forecasts by monitoring thunderstorm cells from the Marmara Sea using radar products and lightning observations, should not mean that will be automatically a thunderstorm observed at LTBA. On 23 September 2015, the LTBA Meteorological Office assessed the radar products to track convective activity over the Marmara Sea. The TAF published at 1640 UTC was revised at 1957 UTC and a thunderstorm was expected to occur between 2000 UTC and 2000 UTC. However, the thunderstorm cell decayed and it only caused shower with rain at LTBA.

The work done by Özdemir et al. (2017) for the period 2008-2012 included the fact that 42.2% of the thunderstorms that took place at LTBA occurred between 1700 UTC and 2400 UTC. On 2 February 2015, the timing of the thunderstorm activity at LTBA and the Özdemir’s results are consistent with each other. The occurrence of the thunderstorm activities should be observed normally at about noon when convective activity is greatest. However, these activities occurred between 1700 UTC and 2400 UTC at LTBA.

3. LONG-TERM THUNDERSTORM ANALYSIS AT AIRPORTS IN THE MARMARA REGION: TYPES AND FAVOURABLE ATMOSPHERIC CONDITIONS [2]

3.1 Introduction

Thunderstorm and lightning are the most important meteorological phenomena affecting the aviation sector. Regarding these phenomena around the world, case studies and climatological analyses have been carried out for many airports and their surroundings (Kohn et al., 2011; Drozdov et al., 2013; Özdemir et al., 2017; Chen and Wang, 2019; Ryley et al., 2020; Taszarek et al., 2020; Yavuz et al., 2020). In the studies conducted within the Mediterranean Region, a linear relationship between the intensity of thunderstorm and precipitation was determined, and the importance of local topography in daily changes were revealed (Piper and Kunz, 2017). In the studies carried out for the northern regions of China, the conditions of occurrence of short-duration excessive rainfall, strong winds and hail events caused by severe thunderstorms were examined (Yang et al., 2017; Ma et al., 2021). In the studies conducted for the European Region, the effects of thunderstorm in terms of aviation were investigated. In accidents caused by thunderstorm, it was determined that sudden changes in wind speed (gust) and direction were the most important factors in losing control for pilots (Proseus, 2000, Tafferner et al., 2010). In addition, it was determined in many studies that gust of 80 kt and above often occurs in the thunderstorm climatology analysis conducted for the European Region (Punkka et al., 2006; Taszarek et al., 2019). Weather conditions are one of the most critical parameters in the occurrence of delays as well as accidents in aviation operations. It was stated that the most important factor in the delays was the weather conditions and its rate in all meteorological events was 87% in the investigations made for the United States. Among the weather events, thunderstorm ranked 3rd with 16% (Wang and Kulkarni,

---

[2] This chapter is based on the research paper: Yavuz, V., Deniz, A., Özdemir, E.T., Karan, H. and Temiz, C. (2022). Long-term thunderstorm analysis at airports in the Marmara Region: types and favourable atmospheric conditions. *International Journal of Global Warming*, 28(1), 81-95, doi: https://doi.org/10.1504/IJGW.2022.125083

2011). This phenomenon had the greatest impact rate from May, when the air traffic was at its peak, to the end of September because the thunderstorm activities reach their highest numbers especially in the spring start and end times (Taszarek et al., 2019).

Manzato (2007) examined the climatology of thunderstorm and precipitation over a 10-year period in his study for the Friuli Venezia Giulia Region. In the daily investigations, the highest number of observations occurred between 1100 UTC and 1700 UTC, and the least observation occurred between 0500 UTC and 1100 UTC. In monthly analysis, thunderstorm was observed more frequently between May and October, reaching its maximum number especially in June. Raghavendra et al. (2018) analysed the thunderstorms for the Congo Basin over a 35-year period. While there was an increasing trend in thunderstorm activities during the period, on the other hand, there was a decrease in the precipitation trend. Enno et al. (2020) found that the highest number of lightning strikes was in July, and the least number was in February, in their study within a 10-year period for the European Region in general. These months were followed by June, August, May and September, respectively. In addition, in the daily study conducted by the authors, it was determined that the highest number of lightning activities were between 1400 UTC -1600 UTC and the lowest number of activities was between 0000 UTC and 0300 UTC. Agnihotri et al. (2013), in their study of the climatological analysis of thunderstorm events for Bangalore, made statistical analyses based on annual, monthly and hourly for 1981-2010. The prominent results of the study were that thunderstorms generally occur between 1500 UTC - 0300 UTC. In addition, in the analysis made on the relationship between rainfall and thunderstorm, it was revealed that thunderstorm events caused excessive rainfall. Kaltenböck et al. (2009) analysed a total of 3406 severe weather events using European Severe Weather Database (ESWD) data in their study, taking into account environmental atmospheric conditions over Europe during the warm seasons between 2006-2007. As a result of the analysis, thunderstorm activities were examined in 7 sub-categories, and detailed analyses were made for most of the meteorological parameters that caused them. In general, as a result of the study, it was determined that there was hail between 50% and 90% when lightning was observed. In addition, when lightning was seen, excessive rainfalls, high convective available potential energy (CAPE) values, high humidity levels with low flow, warm season storms, storms in the F2 and F3 categories were observed. Williams and Stanfill (2002) compared the events occurring over the land and sea in their study on the frequency of occurrence of lightning events. According to the analysis results, the lightning events on the land were higher than those in the seas, the main reason for this was that the lands were warmer than the seas. Christian et al. (2003) found that changes in atmospheric temperature gradient had a direct relationship with lightning events. Even a small change in atmospheric temperature locally caused a change on the hydrostatic balance. With the strengthening of buoyancy force, unstable weather conditions occurred and storm clouds formed. The main criteria for the formation of this cloud type were warm air and the amount of humidity at the respective altitude.

In this study, Meteorological Aerodrome Reports (METARs) and Special Meteorological Aerodrome Reports (SPECIs) published by 11 airports in the Marmara Region were analysed for the 2001-2015 period. Analyses were carried out by adapting the reports published every half an hour at international airports and every hour at national airports to an hourly scale. First, the times when thunderstorms occurred were determined at all airports. The thunderstorms were analysed on a daily, monthly, seasonal and annual basis. Second, it was determined whether the thunderstorms were singular or occurred together with any kind of a precipitation. Third, changes in ground level temperature values were investigated in the study of atmospheric conditions in which thunderstorms occurred. Lastly, many stability indices and meteorological parameters analysed. CAPE and CIN values were also analysed throughout the period.

3.2 Data and Methodology

The Marmara Region, which is one of the Turkey's seven geographical regions, contains the most popular provinces (such as Istanbul, Kocaeli, Bursa, Balikesir, etc.) of the country in terms of population, industrialization, economy and tourism. There are 11 airports in the region and three of these airports operate as international, four as national and four as military airports. In this study, long-term analyses, types and atmospheric conditions of thunderstorm occurring at airports were examined by using METAR and SPECI reports published by selected airports.

METAR and SPECI reports were obtained from the Turkish State Meteorological Service (TSMS) for 11 airports in the Marmara Region for the 15-year period between 2001-2015 (TSMS, 2021). All the information about the airports is given in Table 3.1. In addition, the locations of the airports are shown in Figure 3.1. Aviation reports published in half-hour periods at international and in hourly periods at national airports. In this study, the analyses were made by converting the data of all airports to hourly format. In order to obtain information about the vertical structure of the atmosphere and to obtain various stability indices, the sounding data published by Istanbul Kartal Radiosonde Station were used (Source University of Wyoming, 2021).

Table 3.1 : Information about airports within the boundaries of the Marmara Region (FGA, 2021).

City	Airport	Utilization	ICAO Code	Altitude	Distance to Sea
Istanbul	Ataturk	Civilian	LTBA	49 m	1800 m
Istanbul	Sabiha Gokcen	Civilian	LTFJ	95 m	5320 m
Bursa	Yenisehir	Civilian - Military	LTBR	100 m	14000 m
Tekirdag	Corlu	Civilian - Military	LTBU	31 m	14100 m
Yalova	Yalova	Civilian - Military	LTBP	-	12000 m
Istanbul	Samandira	Civilian	LTBX	123 m	11000 m
Balikesir	Bandirma	Civilian - Military	LTBG	52 m	4000 m
Balikesir	Balikesir	Civilian - Military	LTBF	104 m	86000 m
Kocaeli	Cengiz Topel	Civilian - Military	LTBQ	56 m	1400 m
Canakkale	Canakkale	Civilian - Military	LTBH	7 m	2000 m
Balikesir	Kocaseyit	Civilian	LTFD	5 m	5080 m

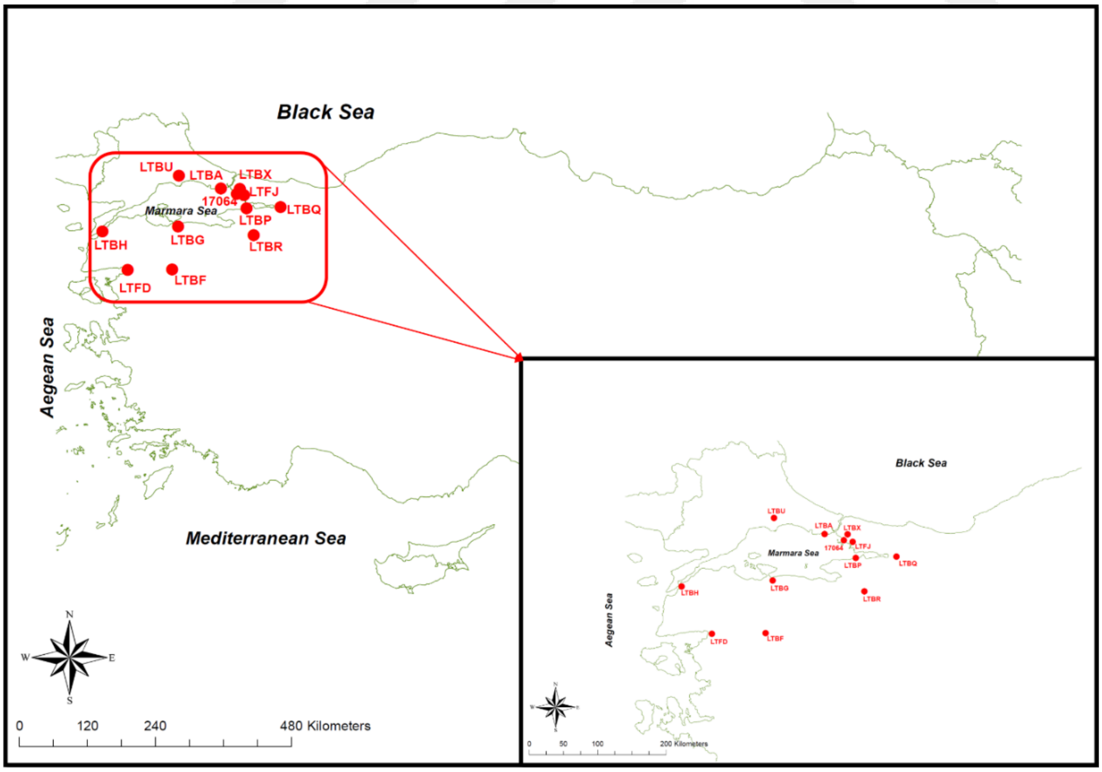

Figure 3.1 : Locations of the airports and Kartal Radiosonde Station.

3.3 Results

In the first stage of the study, METAR and SPECI reports were analysed for 11 airports between the years 2001 and 2015. For each airport, separately, thunderstorm observations were sorted out on a daily-hourly basis. In this direction, hourly statistics were analysed. Later, again for each station, the statistics were evaluated on a monthly and annual total basis. The analysis results are presented individually at LTBA because its operation number was much more than other airport. In the second stage, some threshold values have been determined in the literature regarding temperature information on the ground level, which is one of the most important meteorological parameters that play a role in the thunderstorm formation. In this study, analysis was made on the basis of each airport, and average threshold values were determined. In the third stage of the study, it was analysed whether the thunderstorms accompanied by any dependent meteorological phenomenon (such as rain, snow, snow with rain, haze, fog, etc.) or alone. In the final stage of the study, CAPE and CIN analyses were performed extensively.

METAR and SPECI reports at Istanbul Ataturk International Airport are carried out within half an hour since this airport is an international airport. The analyses based on annual-hourly totals by converting hourly periodicals and then were examined in three different time periods of the day as shown in Figure 3.2, taking into account the widespread and typically known daily variations of the mid-latitude terrestrial Atmospheric Boundary Layer (ABL) (Karan, 2007). In the 1st time period (0300-1100 UTC), both the average and maximum observations showed less lightning than the other time periods. In this time period, turbulent eddies could still be active and remain within the residual layer just above the Convective Mixing Layer (CML) from the previous day. This time period, as mentioned earlier, is also characterized by a shallow, statically stable ABL with weak turbulence. Figure 3.2 shows that there are many lightning strikes observed both at the average and at the maximum values in the 2nd time period which covers the times between sunrise and a few hours in the afternoon. ABL in the 2nd time period can be characterized by buoyancy-influenced Turbulence Kinetic Energy (TKE) generation, vertical wind shear, static stability, turbulent momentum and heat fluxes. The high number of lightning observation can be explained by the atmospheric conditions favorable form storm formation and development. Finally, during sunsets and evening hours represented by the 3rd time period, the average observed lightning becomes the highest when compared with the other two time periods, yet the maximum occurrences still took place in the 2nd time period. Observation of a high number of lightning may be related to the presence of the CML and the other high parameters in the second time period.

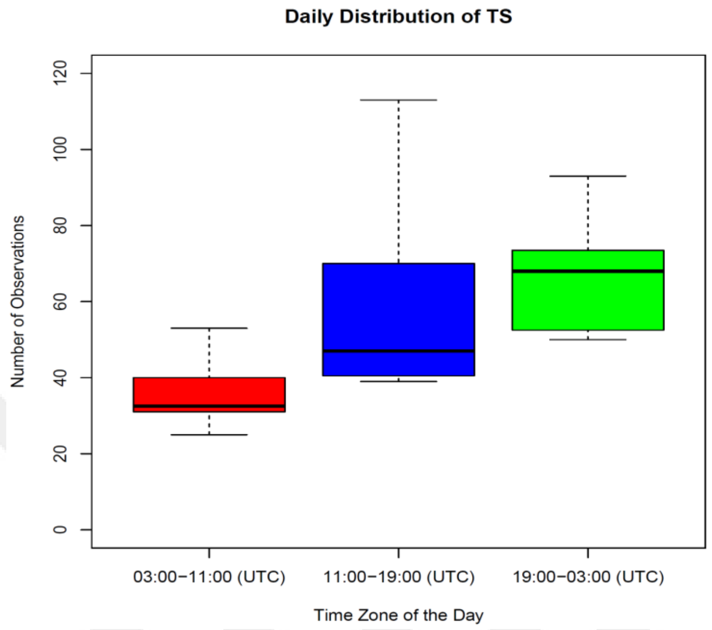

Figure 3.2 : Daily distribution of thunderstorms at LTBA, 2001-2015.

Annual and monthly analyses of the total number of thunderstorm observations per hour within the selected period are given in Figure 3.3. The most thunderstorm observations were made in 2002 and the least thunderstorm took place in 2003 and 2011. When the monthly distributions were examined, it was seen that the most thunderstorm occurs in September, August and June, respectively.

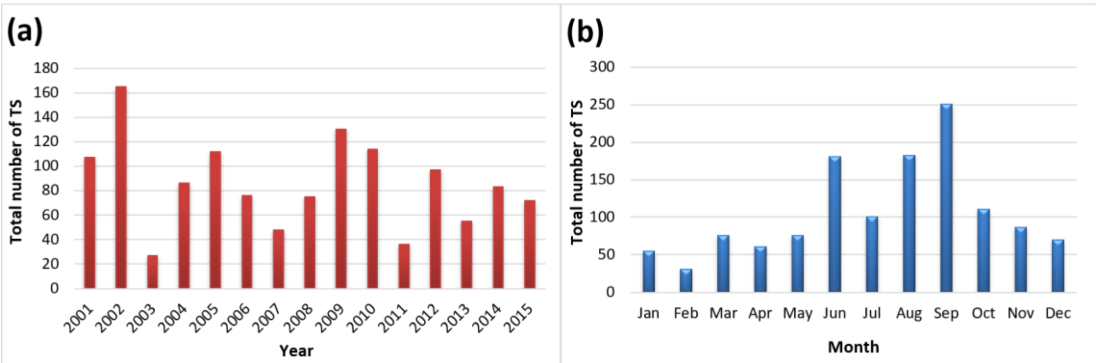

Figure 3.3 : a) Annual total and b) monthly total numbers of thunderstorms at LTBA.

The 15-year average of the thunderstorm observations belonging to 11 airports in the Marmara Region are shown in Figure 3.4. The missing hours for airports without

METAR and SPECI reports were not included in the average. Figure 3.5 is so important for clarifying the situation of lightning for the Marmara Region during the day. As can be seen from this Figure 3.5, the most observed time periods of thunderstorms were the 2nd, belonging to the Marmara Region during the day, which was similar to the Istanbul-LTBA Airport thunderstorm distribution (Figure 3.3). This was due to the convective activities and the thermal instability related to them.

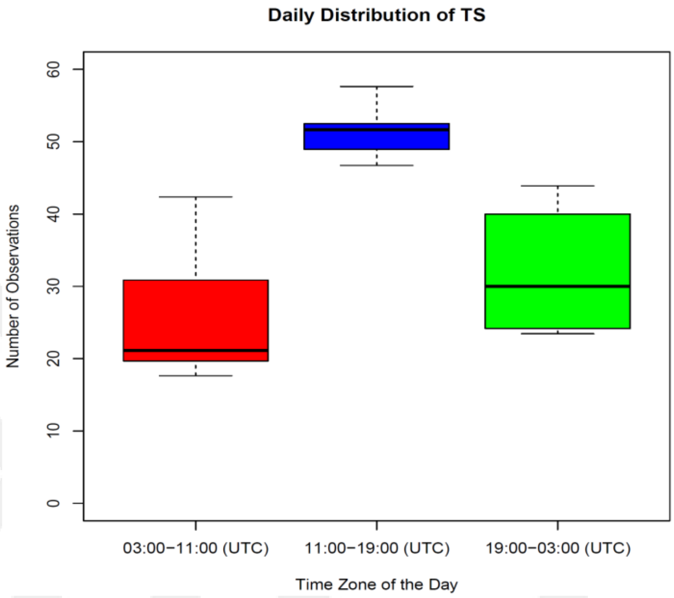

Figure 3.4 : Daily average distribution of thunderstorms in Marmara Region, 2001-2015.

In a further analysis for the 11 airports in the Marmara Region, annual and yearly total analyses were performed for all stations. Looking at annual average analyses, a trend that was increasing day by day in the period was observed. Maximum average thunderstorms in 2012, 2010 and 2009 were noteworthy, especially in 2014. On the other hand, when looking at the total hourly analyses, the thunderstorm observed over 1000 in 2014 was most noticeable. The station where the most thunderstorm occurred was Tekirdag Corlu Airport (LTBU). Following this, the highest number of thunderstorms were seen Istanbul Sabiha Gokcen Airport (LTFJ), Istanbul Ataturk Airport (LTBA) and Kocaeli Cengiz Topel Airport (LTBQ), respectively. Most of the thunderstorms occurred in 2014 and most of these were seen in Istanbul Sabiha Gokcen Airport (LTFJ). Looking at the 15-year data set, airports in the northern Marmara Region generally had more number of thunderstorms.

Monthly average and monthly total analyses were performed similarly after the annual analyses. The monthly average number of thunderstorms in the Marmara Region was the maximum of its values in June with an average observation value of 157 per month and followed by September, May and August, respectively. The maximum value of monthly total number of thunderstorm occurred in June with a total observed value of 1729. The months of the highest number of thunderstorm were seen as September, May and August, respectively. Looking at the monthly totals over a 15-year period, the highest number of thunderstorms was observed in June at LTFJ and LTBU, with a total value of 320. In general, the seasonal surveys showed that the maximum total number of thunderstorms were seen in summer as 3359, in autumn as 2594, in the spring as 1880, and in the winter as 775, respectively.

Figure 3.5a shows which meteorological events took place during the thunderstorm occurrence. According to this Figure, it can be seen that thunderstorms were most likely to occur with rain than they were to occur alone. If we look at the Marmara Region in general (Figure 3.5b), it can be seen that there was a similar distribution. One of the most observed cases was the "VCTS" code, which indicates that the thunderstorm is observed along the whole airport. It is noteworthy that for all airports, the thunderstorm and lightning incidents were occurred mostly in the first place (about 72 %) with rain and in the second place, thunder and lightning without rain.

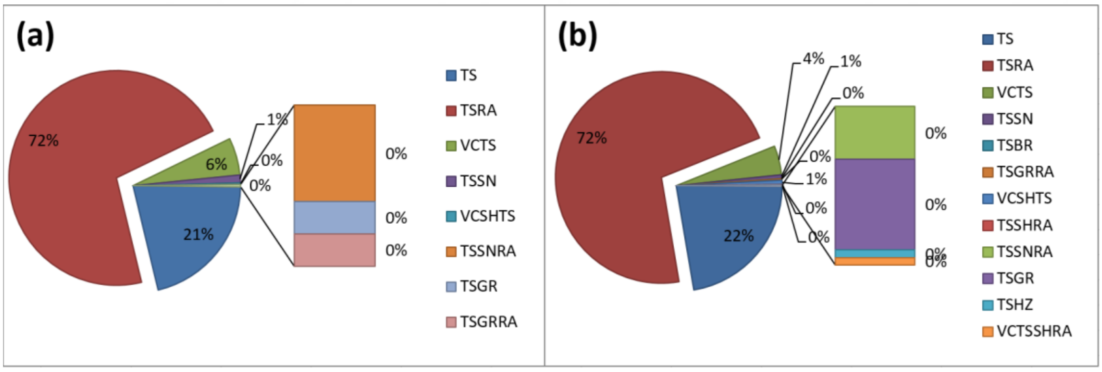

Figure 3.5 : Total number of observations per hour according to types of thunderstorm a) at LTBA, and (b) in Marmara Region. "TS" thunderstorm; "TSRA" thunderstorm with rain; "VCTS" a thunderstorm in the vicinity, "TSSN" thunderstorm with snow; "TSBR" thunderstorm with mist; "TSGRRA" thunderstorm with hail and rain; "TSSHRA" thunderstorm with rain showers; "TSSNRA" thunderstorm with snow showers; "TSGR" thunderstorm with hail; "TSHZ" thunderstorm with haze; "VCTSSHRA" thunderstorm with rain showers in the vicinity.

Figure 3.6 shows the results of the analysis for Istanbul-LTBA, at which temperature thunderstorm and lightning events were observed. In the bimodal distribution histogram, it was seen that most lightning events (corresponding to the May-October period) were found in the first mode at 19-23 °C. In the other maximum observation period (November-April period), temperatures were observed at 10-11 °C range.

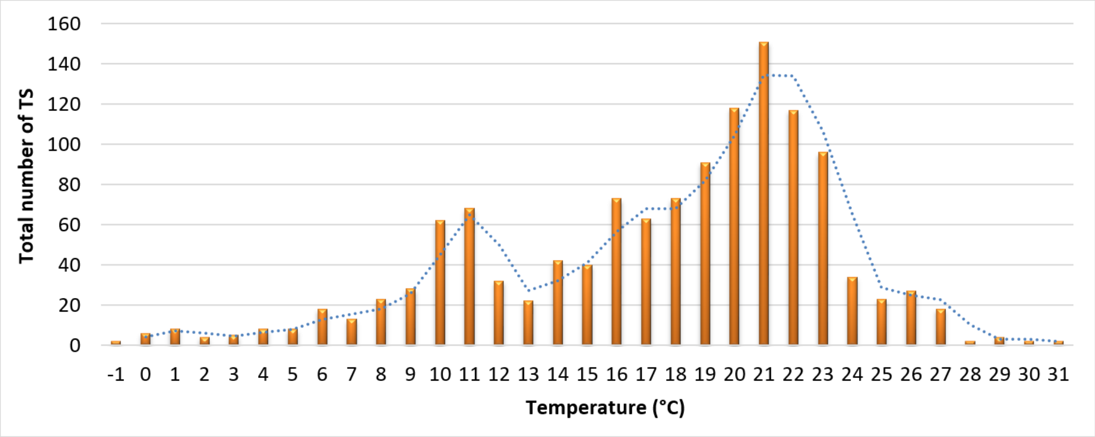

Figure 3.6 : Total number of observations per hour of thunderstorms at LTBA.

A similar analysis was made for all stations. The results show a trend almost similar to the result obtained by examining each station, separately. Although the average of 11 airports was used in the Marmara Region, the temperature-rain histogram distribution approaches a bimodal distribution at LTBA. The temperature range at which most lightning events were observed was found at 17-23 °C. The second mode occurred at a 10-13 °C range. It should also be noted that lightning was observed when the temperature falls below zero (at least -5 °C). Similarly, lightning events were observed at a maximum temperature of 35 °C. Generally, average maximum number of lightning was observed between 15 and 25 °C, which represent the spring months and the beginning and end of summer.

Monthly analysis results of CAPE and CIN are given in Table 3.2. It is seen that the average and maximum CAPE values occurred in the summer season. The highest CAPE value was observed in May with 4941 J/kg. Spring and autumn were the seasons with the highest CAPE values, respectively. On the other hand, minimum CIN values were observed in summer, followed by Spring and Autumn seasons. The CAPE and CIN values in Table 3.2 were calculated by analysing the published observations during the whole period.

Table 3.2 : Analysis of CAPE and CIN values on a monthly basis.

Month	Jan	Feb	Mar	Apr	May	Jun	Jul	Aug	Sep	Oct	Nov	Dec
CAPE	4	6	4	6	59	154	261	325	147	43	8	5
$CAPE_{(max)}$	611	1034	589	564	4941	2085	2841	2864	2831	1348	459	799
CIN	-5	-7	-7	-13	-50	-89	-109	-117	-66	-34	-11	-4
$CIN_{(min)}$	-216	-1598	-218	-685	-1879	-1064	-931	-899	-888	-1109	-628	-247

Wallace and Hobbs (2006) classified the CAPE values to show the degree of instability of the atmosphere. The results obtained according to this classification method are given in Table 3.3. In analyses performed on a monthly basis, it was observed that CAPE values mostly vary in the range of 0-1000 J/kg. In Table 3.3, all observations made twice a day during the period were evaluated.

Table 3.3 : Classification of CAPE values on a monthly basis according to Wallace and Hobbs' classification (2006).

0000 UTC	**Jan**	**Feb**	**Mar**	**Apr**	**May**	**Jun**	**Jul**	**Aug**	**Sep**	**Oct**	**Nov**	**Dec**
CAPE = 0	384	344	379	382	307	220	189	169	219	272	314	395
0 < CAPE ≤ 1000	77	10	75	64	152	217	234	235	219	188	103	67
1000 < CAPE ≤ 2500	0	0	0	0	1	7	27	51	8	2	0	0
2500 < CAPE ≤ 4000	0	0	0	0	1	0	0	1	0	0	0	0
CAPE ≥ 4000	0	0	0	0	0	0	0	0	0	0	0	0
1200 UTC	**Jan**	**Feb**	**Mar**	**Apr**	**May**	**Jun**	**Jul**	**Aug**	**Sep**	**Oct**	**Nov**	**Dec**
CAPE = 0	351	314	353	342	288	173	164	162	184	255	286	349
0 < CAPE ≤ 1000	102	12	102	101	167	252	247	246	211	205	133	108
1000 < CAPE ≤ 2500	0	0	0	0	3	18	37	54	26	1	0	0
2500 < CAPE ≤ 4000	0	0	0	0	1	0	1	2	1	0	0	0
CAPE ≥ 4000	0	0	0	0	1	0	0	0	0	0	0	0
Meaningful data	0.98	0.80	0.98	0.99	0.99	0.99	0.97	0.99	0.96	0.99	0.93	0.99

The analysis results in Table 3.2 and Table 3.3 are the results obtained using all the sounding data obtained during the whole period. In addition to these, a separate analysis was carried out regarding the CAPE and CIN values at the time of thunderstorm at two airports located close to Kartal Radiosonde Station in Istanbul. Based on the METAR reports published by LTBA and LTFJ for a period of 15 years, the analysis was performed by assigning the value corresponding to the closest sounding measurement for each observation where thunderstorm occurred. The analysis results obtained are given in Table 3.4. In analyses performed on a monthly basis, CAPE and CIN values show the average values when thunderstorms occur. On the other hand, CAPE* and CIN* values show the averages of values where CAPE and CIN values were different from zero. In the last column of Table 3.4, the ratio of non-zero CAPE values to all CAPE values at the time of thunderstorm is shown. Although thunderstorms occurred in most months at both airports, it was seen that the CAPE value was approximately 50% zero. In addition, when CAPE* values are considered, the highest average value was found to be 343 J/kg.

Table 3.4 : CAPE and CIN values during thunderstorm at LTBA and LTFJ.

LTBA	CAPE	CIN	CAPE*	CIN*	Ratio of nonzero CAPEs to all CAPEs
Jan	25	-20	116	-90	22%
Feb	199	-58	343	-90	59%
Mar	120	-28	284	-49	42%
Apr	28	-15	89	-49	32%
May	38	-28	143	-93	26%
Jun	59	-31	239	-117	25%
Jul	137	-45	274	-89	50%
Aug	86	-19	384	-85	22%
Sep	88	-31	246	-102	36%
Oct	95	-101	175	-223	54%
Nov	185	-37	374	-74	49%
Dec	94	-74	219	-173	43%
LTFJ	CAPE	CIN	CAPE*	CIN*	Ratio of nonzero CAPEs to all CAPEs
Jan	7	-21	36	-78	20%
Feb	137	-93	190	-119	72%
Mar	102	-66	248	-178	41%
Apr	88	-62	256	-182	34%
May	50	-48	171	-176	29%
Jun	67	-55	202	-155	33%
Jul	125	-80	277	-176	45%
Aug	64	-44	234	-167	27%
Sep	71	-30	214	-133	33%
Oct	67	-105	208	-347	32%
Nov	163	-71	289	-127	56%
Dec	122	-51	317	-126	39%

3.4 Summary and Discussions

According to the results of the analysis made with METAR and SPECI reports, the 2nd time zone (1100-1900 UTC) was the time when the thunderstorm activity was highest. The least observed time was the first time zone (0300-1100 UTC). Physical processes of the atmosphere, especially within the ABL, are closely related to the thunderstorms and lightning incidents. The sensible heat flux originating from the ground surface is activated within a few hours with the sunrise and the ABL development is modulated by vertical heat, humidity and momentum fluxes. The ABL exhibits a statically stable structure, usually a few hours before and after sunrise, reaching a maximum height a few hours after noon (1500-1700 LT – Local Time) as the vertical momentum, heat and moisture transports become active due to solar radiation. This time slot can be characterized by two statically unstable shallow layers: a layer near the earth's surface and a layer just beneath the top of the convective boundary layer (CBL). The mixed layer (Convective Mixing Layer – CML) between these two unstable layers exhibits statically weak-stable characteristics, yet has the potential to become convectively unstable if/when there are strong upward turbulent eddies. During the afternoon hours of the hot summer days, the virtual potential temperature profile within the shallow layer near the surface becomes super-adiabatic while within the CML, if it is well-mixed, the virtual potential temperature profile becomes almost constant with height. The mean Turbulence Kinetic Energy (TKE) increases its intensity during this time as the surface temperature remains much higher than the air temperature. The time of the maximum buoyant TKE coincides with the significant upward turbulent transport, high surface temperature, and the significant temperature difference between the surface and the air above. Once the Sun sets, the turbulence intensity ceases and the height of the ABL gradually decreases. During the time period between sunset and sunrise, there still remains some pockets of turbulent eddies above the ABL as the sensible heat fluxes experience sudden drops and its directional changes cause shallow, statically stable ABL. However, it should also be noted that the ABL structure and its daily change may be of different character depending on geographical location (such as the ABL over the oceans and poles) and large-scale atmospheric movements.

In the analyses conducted to examine the changes on a monthly basis, it was determined that the thunderstorm occurred mostly in June and at least in January during the period. In the seasonal analysis, thunderstorms mostly occurred in the summer season (39%) and then in the autumn (30%), spring (22%) and winter (9%) seasons, respectively. It was observed that thunderstorms mostly occurred with rain (72%) and were less likely to occurred without rain (22%). It was also observed that thunderstorms occurred in the range of 17-23 °C. CAPE values were quite low when thunderstorm occurred. Almost 50% of the times a thunderstorm occurred, the CAPE was set to zero.

A significantly higher amount of thunderstorm has been observed at the airports located in the north of the Marmara Region compared to the airports located in the south. There are several reasons for this. First, the northern airports are exposed to the effect of the Black Sea (land-sea interaction), that is, the cold air systems from the north move through the Black Sea with northern flows, especially in winter, causing an increase in convective activity as a result of their interaction with the relatively warmer water mass. Second, the fact that the Black Sea is at least several times bigger than the Marmara Sea in terms of water body, the sea surface temperatures are relatively lower in spring and summer (the difference between the upper air masses and the temperature difference is higher in these seasons). In addition to these, topographic effects and altitude differences are effective especially in daytime oscillations, monthly and seasonal changes.

4. CLASSIFICATION AND ANALYSIS OF SEA-EFFECT SNOWBANDS FOR DANUBE SEA AREA IN BLACK SEA [3]

4.1 Introduction

Sea effect snow (SES), unlike normal snowfall, is a meteorological phenomenon that is effective in narrower areas with the help of snow bands that the cold air parcel creates by passing over the relatively warm water surface. Snow showers and heavy snowfalls can be seen in areas affected by these snow bands (Cordeira and Laird, 2008).

SES across the globe, occurs in the Great Lakes Region in the United States, in many parts of Ontario-Canada (Laird et al., 2009; Sikora and Halverson, 2002), in the west coasts of northern Japan (Tuskobi et al., 1989; Nakai et al., 2005), in the coastal regions of the Black Sea (Kindap, 2010), in the Kamchatka Peninsula of Russia, and areas near the Caspian Sea (Ghafarian et al., 2008), Baltic Sea (Olsson et al., 2018), Adriatic Sea (Paolo and Silvio, 2017), and Great Salt Lake (Alcott et al., 2012). SES particularly effective in the Marmara and Black Sea Regions in Turkey and can be seen in many cities along the coastline. It can also be seen when appropriate atmospheric conditions occur around Lake Van (Figure 4.1). When looking at the first studies examining the SES and snow bands that cause SES; Wiggin (1950) determined the atmospheric conditions necessary for the formation of SES bands for SESs occurring in the United States. Magono et al. (1996) made some determinations for SESs formed based on the Sea of Japan, taking into account the topography, orography, winter monsoons and many meteorological parameters. In later studies, SES bands in the meso-scale (Peace and Sykes, 1966) and synoptic-scale (Niziol, 1987) structure were examined, many studies were conducted for the prediction system and numerical simulation (Ballentine et al., 1998; Kristovich et al., 2000; Steiger et al., 2003), and threshold ranges for some meteorological parameters for determining the formation criteria of SES have been

[3] This chapter is based on the research paper: Yavuz, V., Deniz, A., Özdemir, E.T., Kolay, O. and Karan, H. (2022). Classification and analysis of sea-effect snowbands for Danube Sea area in Black Sea. *International Journal of Climatology*, 41(5), 3139-3152, doi: https://doi.org/10.1002/joc.7010

revealed (Holroyd, 1971; Niziol, 1987). In the studies ongoing in the 21st century, climatological analysis and many case studies on lakes in the United States have continued in terms of SES (Suriano and Leathers, 2016; Suriano and Leathes, 2017). Regarding SES, in studies conducted across the Black Sea Region, the investigations conducted for Turkey's coastal areas is very limited. Kindap (2010) analysed certain meteorological parameters in the study of SES that occurred in February 2005 for the province of Istanbul, and carried out simulations using the MM5 Model. In another study, Özdemir and Yetemen (2019) analysed the meteorological situation of the enhanced SES that occured on February 15, 2015.

Figure 4.1 : Total number of observations per hour of thunderstorms at LTBA.

When looking at the general findings in the studies conducted to determine the atmospheric conditions at the time of occurrence of SES, it is seen that the following summarized determinations are made:

- Temperature difference between sea surface and 850 hPa level should be a minimum of 13°C (Rothrock, 1969; Niziol et al., 1995, Kunkel et al., 2002, Notaro et al., 2013),
- Wind direction change should be less than 60° between ground level and 700 hPa level (30° and below creates a stronger band structure) (Niziol, 1987),

- There should be an inversion layer(s) between ground level and 700 hPa level (Usually at the level of 1-2 km from the ground, it can be 3 km or more in denser bands) (Niziol, 1987; Özdemir and Yetemen, 2019),
- The cold air transport over the water body should be at least 80 km (Kindap, 2010). Also, he stated in his study on the Black Sea for Istanbul that this distance is around 600 km (Kindap, 2010).

As a result of the first studies in the literature on the classification of SES bands, the bands were divided into four types according to their morphological structures (Braham, 1990). Explanations of the band types are given below:

a) Broad area: Bands or open cells parallel to the wind covering a large area (Kelly, 1982; Braham, 1983),
b) Shoreline band: A convection line parallel to the lee shore and a well-developed land breeze along the coastline (Braham, 1983),
c) Midlake band: Midbands with lower convergence centered on the lake (Passarelli and Braham, 1981),
d) Vortex: Meso-scale vortexes with a well-developed cyclonic flow pattern within the boundary layer (Forbes and Merritt, 1984).

Regarding the classification of SES bands, Niziol et al. (1995) examined five types of SES bands for operational purposes. Based on Geostationary Operational Environmental Satellite (GOES) images, the following results have been obtained for the Great Lakes Region:

- Type-1 (T-1): It is also expressed as a singular band. It occurs parallel to the prevailing wind between sea/lake - inversion layer. Due to its long fetch distance, it causes excessive precipitation in parallel with the occurrence of a strong and organized meso-scale convergence zone on the sea/lake. Bands of 20-50 km width and 50-200 km length are formed (Figure 4.2c).
- Type-2 (T-2): It is also referred to as multiple bands. Bands are formed parallel to the wind direction similar to Type-1, but the fetch distance is shorter. Bands of 5-20 km width and 20-50 km length occur. A strong meso-scale convergence zone is not observed. Multiple bands are observed (Figures 4.2a, b).
- Type-3 (T-3): It is a mixture of Type-1 and Type-2 bands. Also known as hybrid band. The bands parallel to the wind do not develop in the sea/lake just

above it. The system develops from the water source located behind it (Figure 4.2c).

- Type-4 (T-4): This band is also called as parallel to the shore. It is the result of a land breeze generated in a very cold environment with a weak synoptic-scale pressure gradient. It does not leave as much rainfall as in Type-1. Since it usually develops in the presence of high pressure, a strong collapse inversion prevents vertical development (Figures 4.2a, b).
- Type-5 (T-5): It is also expressed as a meso-scale vortex. It usually occurs under very stable atmospheric conditions. It has a formation structure similar to Type-4 bands. It has pronounced spiral band properties with shallow cloud structure and vortex cloud structures. Convergence zone develops depending on the coastal topography (Figure 4.2a).

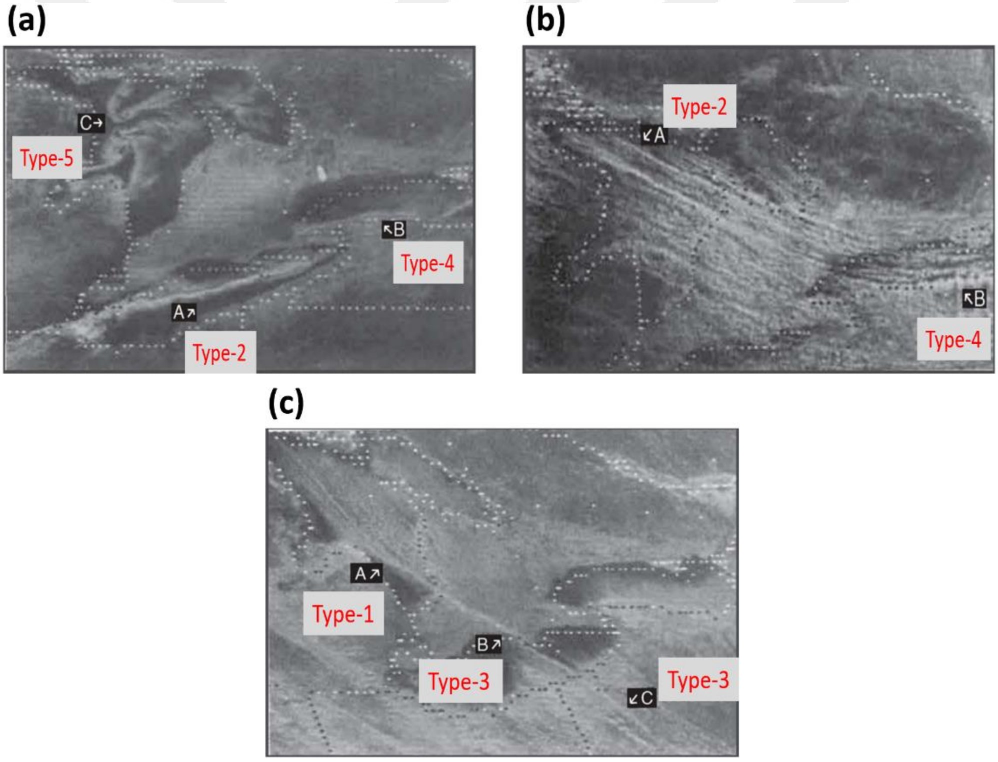

Figure 4.2 : SES band types on GOES satellite images: (a) type 2-4-5, (b) type 2-4, (c) type 1-3 (Sousounis, 2001).

In this study, SES band structures have been examined that cause snowfall in the area up to the coasts and inland parts of the Marmara Region. These bands are formed by polar and arctic air masses that are saturated by meeting the moisture need from the Black Sea, and other air masses following a similar route. SES bands occurring over Danube Region were classified based on five different types of band structures presented by Niziol et al. (1995) within a 10-year period between 2009-2018 (Figure 4.3). Classification of band types occurring on the Black Sea is made for the first time in the Danube Region. The Region is divided into six sub-regions within itself, and the band types and the meteorological conditions that occur in each area are discussed separately. Considering its morphological structure, the Danube Region is divided into six sub-regions in order to best reveal the changes in the SST in the north-south direction. In this context, firstly, SES bands were determined with the help of satellite images, then wind characteristics were determined for upper levels by using upper level synoptic cards, and inversion layers were determined using sounding observations. Finally, the difference between SSTs and upper level temperatures, band types, band formation mechanisms and its orbits have been examined in terms of air-sea interaction.

4.2 Data and Methodology

A period of 10 years (2009-2018) was preferred as the study period. During this period, aviation reports, satellite images, sounding data, upper level atmospheric data and sea surface temperature data were obtained from related sources. There are several reasons for limiting the working period to 10 years. Firstly, considering the many types of data and observations used for such an intensive study, it was not considered possible for a longer study period to occur within the scope of this study. In addition, it has been taken into consideration that the snowy times should have the highest temporal resolution and reflect the region in general. In this context, the opening of Kocaeli Cengiz Topel Airport to civil aviation in 2011, has been an important detail (previously serving as a military airport, aviation reports were rarely prepared when there were flights). In addition, it took a long time to obtain multiple satellite images from Turkish State Meteorological Service at high temporal resolution, and their analysis and interpretation required a great deal of effort. It is planned to carry out a detailed study within different methods for the region in general, to cover a longer study period. Detailed information about the data used in the study is included in the subsections.

4.2.1 Aviation reports

Aviation reports published by the Turkish State Meteorological Service (TSMS) were used in the determination of snowy times that occurred in the borders of the Marmara

Region within a 10-year period between 2009 and 2018. Tekirdag Corlu Airport (ICAO Code: LTBU; 41°8′21″N - 27°55′15″E; altitude: 16 m), Istanbul Ataturk International Airport (ICAO Code: LTBA; 40°58´55"N - 28°49´14"E; altitude: 50 m) Istanbul Sabiha Gokcen International Airport (ICAO Code: LTFJ; 40°53'55"N- 29°18'33"E; altitude: 95 m), and Kocaeli Cengiz Topel Airport (ICAO Code: LTBQ; 40°44´10"N- 30°5´0"E; altitude: 55 m) were selected in this context (Figure 4.3). The Aerodrome Routine Weather Reports (METAR) and the Aerodrome Special Weather Reports (SPECI) have been analysed and the times when the snowfall begins and ends are determined on the basis of selected airports.

4.2.2 Satellite images

Satellite images taken from the Spinning-Enhanced Visible and Infrared Imager (SEVIRI) device on the second generation MSG-2 (Meteosat-9) and MSG-3 (Meteosat-10) satellites were used to distinguish between snowy and sea-effect snowy times. MSG-2 and MSG-3 satellites were launched into space in 2005 and 2012, respectively, and started collecting data (Hall et al., 2019). These second generation satellites are fixed to the earth axis and positioned at an altitude of 36 km. Multispectral images with a frequency of 15-minute are regularly produced on 12 observation channels from visible to infrared (Lazri et al., 2020). For the whole selected period, Infrared (Channel-9; IR), Natural Color RGB, Airmass RGB and Water Vapor (Channel-6, WV) products were used for all analyses.

The Danube Region was chosen for the analysis made with satellite images. This region was divided into six sub-regions and analyses were made separately for each region (Figure 4.3).

4.2.3 Sounding data

In the study, in order to obtain atmospheric information in the vertical and to determine the inversion layers, sounding data belonging to the radiosonde balloon thrown from Istanbul at 0000 UTC and 1200 UTC by Kartal Station was used (Figure 4.3).

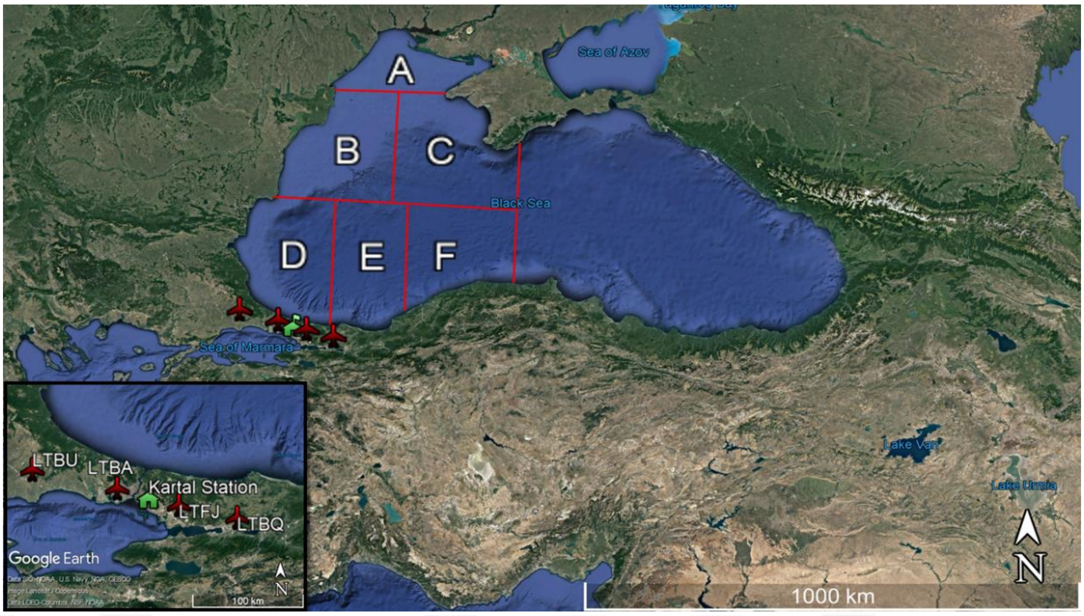

Figure 4.3 : Danube Region (the western part of the Black Sea) (it shows the entire sea area studied); Danube sub-regions (A, B, C, D, E, F); airports (ICAO Codes: LTBA, LTFJ, LTBU, LTBQ) (airports reports were used the determine the snowy days); Kartal Station (the sounding data obtained from this station).

4.2.4 Upper level atmospheric data

Upper level synoptic products published by Plymouth State Weather Center were examined for analysis of upper atmospheric conditions (Plymouth State Weather Service, 2020). Analysis of the upper-level air movements is of great importance especially in determining the direction of the flows on the Black Sea and the source and trajectories of the systems. In the study, synoptic systems of 850 hPa and 700 hPa levels were analysed.

4.2.5 SST data

National Oceanic and Atmospheric Administration High-resolution Blended Analysis (NOAA OI SST V2 High Resolution Dataset) dataset was used to obtain SST data in order to reveal the role of sensible and latent heat fluxes in the formation of SES. Data with a latitude-longitude resolution of 0.25 × 0.25 are available daily from 1981 to the present (APDRC, 2020).

4.3 Results

4.3.1 Snowy times with sea-effect

Within the 10-year period between 2009 and 2018, 186 days were determined as snowy as a result of the examination of METAR and SPECI reports of four airports, and 75 of these days were categorized as sea-effect snowfall as a result of the examination of satellite images. After examining 15-minute satellite images for all snowy times and determining the beginning and end of SES times, the total time that SES was effective was found to be 1163 hours. The times when the SES bands occurred over the Danube Region but did not cause precipitation on the land in the Marmara Region coastline were found to be eight days in total. Although SES bands were formed for 336 hours on an hourly basis throughout the period, SES did not occur over the Danube Region. When the presence of SES bands and the presence of SES were statistically analysed on a monthly basis, the greatest number of daily observations were noted in January, February, December and March, respectively (Figure 4.4). This monthly ranking did not change if the analysis is performed hourly (Figure 4.5). In the examinations made on a daily-scale on an annual basis, the most observations for both cases (presence of SES Bands and SES) occurred in 2012 with 18 days, and the least in 2009 with no observation (Figure 4.6). Similar results were observed in the analysis on an hourly-scale on an annual basis (Figure 4.7). Laird et al. (2009), in the study of lake-effect snow (LES) occurring on Lake Champlain, the majority of 67 LES events occurred in January, followed by December and February, respectively. In this study, the highest number of days with LES was January, followed by February and December.

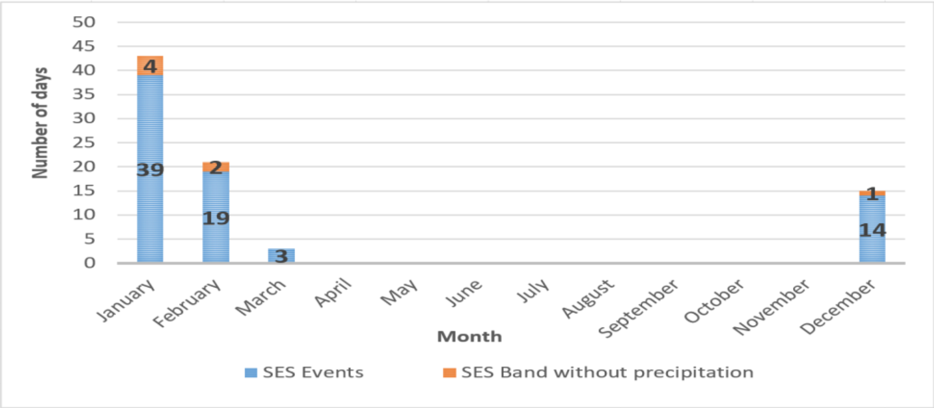

Figure 4.4 : Daily occurrence of SES bands and SES per month of the year.

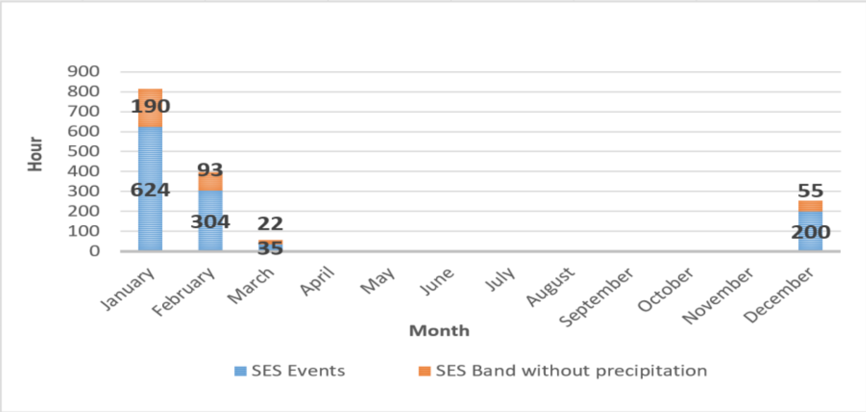

Figure 4.5 : As in Figure 4.4, except for hourly occurrences.

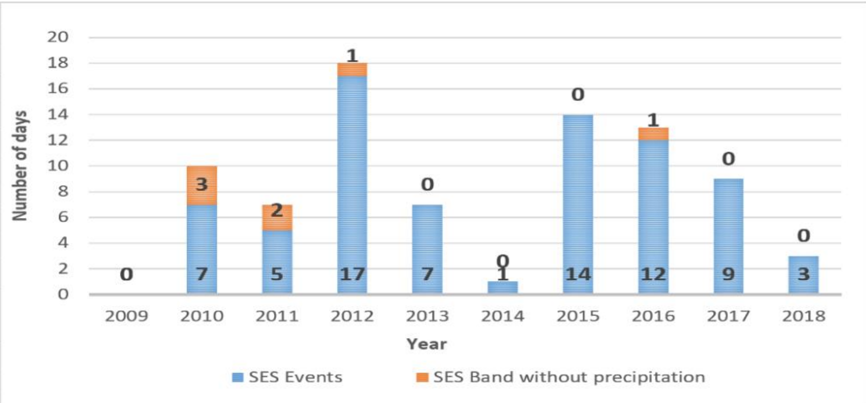

Figure 4.6 : Daily occurrence of SES bands and SES per year.

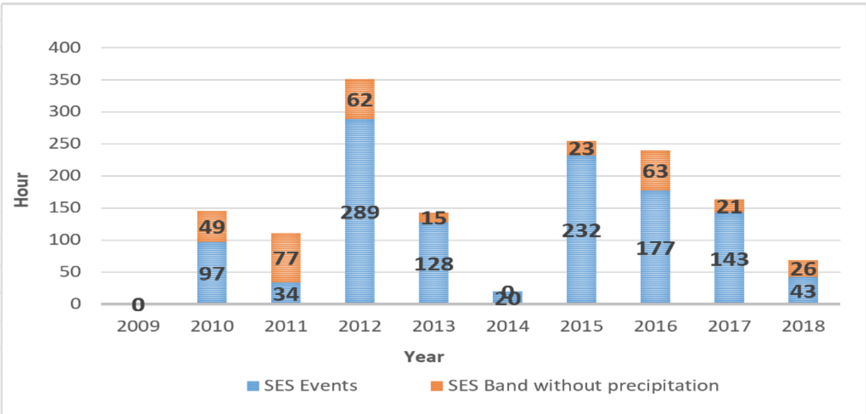

Figure 4.7 : As in Figure 4.6, except for hourly occurrences.

4.3.2 SES band types

4.3.2.1 Frequency of each band type on days with SES

Within the selected 10-year period, the results of the examination performed in accordance with the method in which five different types of band structures are determined by Niziol et al. (1995) are given in Table 4.1. Accordingly, T-2 band type is the most common in Danube Region, followed by T-3, T-4, T-5 and T-1, respectively. Niziol et al. (1995) did not perform any climatological analysis regarding the distribution of band types in his study. The formation of the band types, for which the topographic effects of the region are also extremely important, will differ for each region. In Figure 4.8, examples for five different types of SES bands observed over the Danube Region are presented.

Table 4.1 : Frequency of SES band types over the Danube Region.

TYPES	Total (hr)	Percentage (%)
Type-1 (T-1)	72	1
Type-2 (T-2)	6440	85
Type-3 (T-3)	790	10
Type-4 (T-4)	162	2
Type-5 (T-5)	111	1

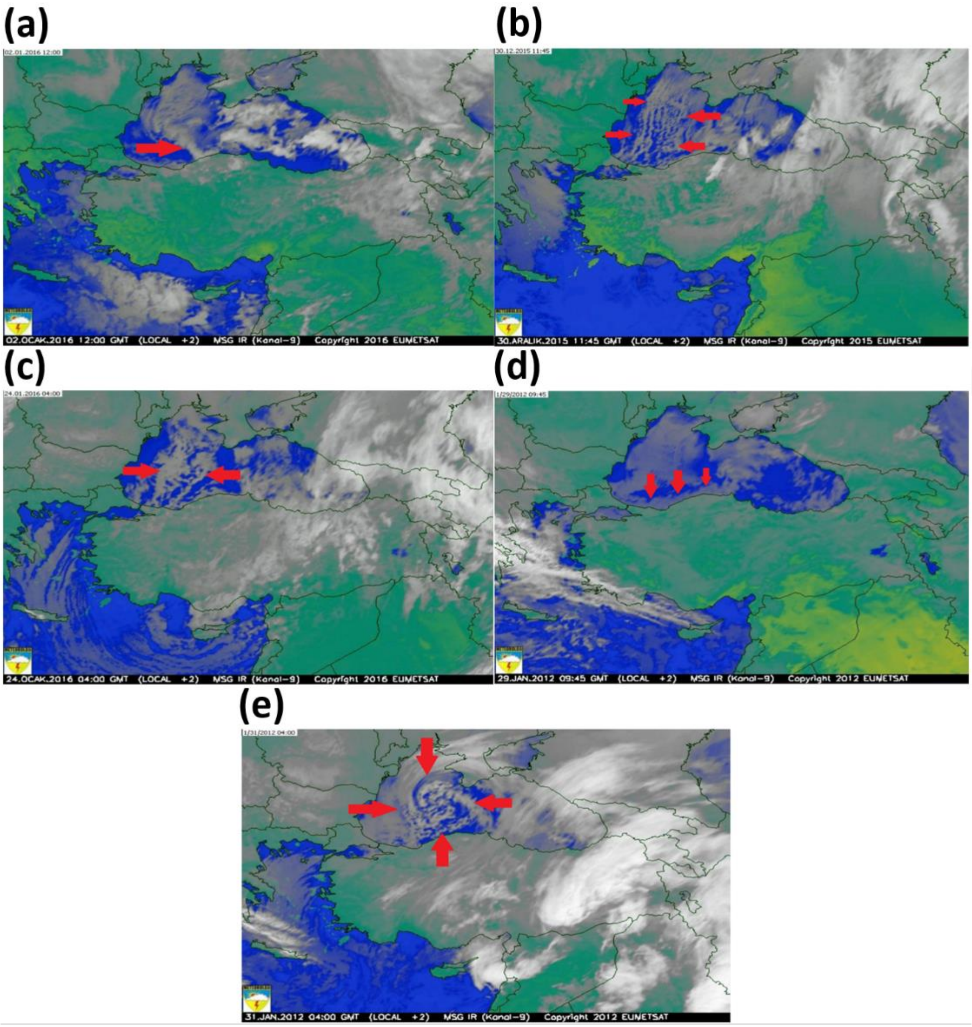

Figure 4.8 : Channel-9-IR satellite images; (a) T-1 band, (b) T-2 band, (c) T-3 band, (d) T-4 band, (e) T-5 band. Red arrows show the location of each band type (TSMS, 2020).

4.3.2.2 Frequency of SES bands in Danube sub-regions

The prevalence of SES bands in each sub-region is given in Table 4.2. The part with the least band in the region was the sub-region "A" in the far north. In our country and the Black Sea, SES bands occur when the Polar and Arctic air masses coming from the north pass over the relatively warmer water surface of the cold air. Since sub-region “A” is the first place to pass from land to sea and cold weather could not reach the sufficient fetch distance in this section, fewer SES bands have occurred. Later, due to the frequent occurrence of the T-2 band type (multiple bands of long-thin structure running parallel to each other from north to south), the occurrence of similar number of SES bands in other sub-regions was observed.

Table 4.2 : Total hours and percentages of SES bands in Danube sub-regions.

DANUBE Sub-regions	Total (h)	Percentage (%)
A	1140	15%
B	1280	17%
C	1262	17%
D	1323	17%
E	1310	17%
F	1260	17%

4.3.2.3 Frequency of each SES band type in Danube sub-regions

Table 4.3 shows the total hours and percentages of five different types of SES bands on the basis of each sub-region throughout the Danube Region. In all six sub-regions, the T-2 band was observed at the highest rate. T-4 band was not observed in “A”, “B” and “C” sub-regions, and T-1 and T-5 bands were observed in very small amounts in all regions.

Table 4.3 : Total hours and percentages of each SES band in Danube sub-regions.

Reg	Type	Tot. (h)	Per.	Reg	Type	Tot. (h)	Per.	Reg	Type	Tot. (h)	Per.
A	T-1	15	1%	B	T-1	15	1%	C	T-1	15	1%
A	T-2	1011	89%	B	T-2	1110	87%	C	T-2	1092	87%
A	T-3	91	8%	B	T-3	132	10%	C	T-3	132	10%
A	T-4	0	0%	B	T-4	0	0%	C	T-4	0	0%
A	T-5	23	2%	B	T-5	23	2%	C	T-5	23	2%
Reg	**Type**	**Tot. (h)**	**Per.**	**Reg**	**Type**	**Tot. (h)**	**Per.**	**Reg**	**Type**	**Tot. (h)**	**Per.**
D	T-1	9	1%	E	T-1	9	1%	F	T-1	9	1%
D	T-2	1098	83%	E	T-2	1085	83%	F	T-2	1044	83%
D	T-3	148	11%	E	T-3	148	11%	F	T-3	139	11%
D	T-4	54	4%	E	T-4	54	4%	F	T-4	54	4%
D	T-5	14	1%	E	T-5	14	1%	F	T-5	14	1%

4.3.3 Inversion layers during SES times

One of the most important factors that play a role in the formation, development and dispersion of SES bands is the presence of the inversion layer, its level and vertical thickness. At the same time, inversion layers have a great role in the variability of band types, in determining their size, duration and trajectory. In this direction, the existence of an inversion layer was determined for 3 different vertical layers by using the data of Kartal Meteorology Station for each day during SES times. These layers are; ground level-850 hPa, 850-700 hPa and 700-500 hPa layers. The total number of inversions in each layer for the 75 SES days are indicated separately. In addition, the average, maximum and minimum thickness values of the determined inversion layers were found statistically throughout the period (Table 4.4). Kindap (2010), in his case study investigating SES for Istanbul, found that there was an inversion with a high thickness value of 850 hPa during the period with SES. At the beginning of the SES, precipitation was less due to a shallow inversion layer (at the level of 925 hPa), while the inversion layer located up to the level of 850 hPa increased the amount and intensity of precipitation. Laird et al. (2009), in their study for a period of 67 SES days, revealed that the inversion occurring between the ground level - 925 hPa layer limits the SES band development. Also, Niziol et al. (1995), in his study examining SES band development in terms of thermodynamic development, determined the importance of inversion and at what level in the model he established by using these parameters as key inputs to the model. Steenburgh et al. (2000), on the other hand, states that the absence of an inversion layer up to 150 hPa from ground level (ground level - 850 hPa, nearly 1.5 km) is an important parameter for SES band development for Great Salt Lake. In this study, when looking at the snow height data taken from Kartal Meteorology Station, where the radiosonde balloon was thrown and vertical sounding data were obtained, the inversion layers were examined in 12 different days where the SES leaves a minimum of 10 cm snow. Considering 12 different days separately, an inversion was observed between 850-700 hPa layer in 10 days, 700-500 hPa layer in 6 days, and ground level - 850 hPa in just two days. In these two days also inversion was observed between 850-700 hPa layer. This result, supports the statement is reported by Steenburgh et al. (2000), "Inversion occurring in the vertical section of the first 150 hPa level from the ground level will reduce the SES band development and therefore the intensity and amount of precipitation". At the station, two different inversion layers were observed in the 850-700 hPa layer on four different days when the amount of snowfall was the highest. The favorable conditions for the development of SES are mostly achieved in terms of inversion are as follows; presence of inversion layer between 850-700 hPa layer in 52 days of 75 SES days, on the other hand, the least amount of inversion layer seen at the first 150 hPa level from the ground (12 days).

Table 4.4 : Number of inversion layers and thickness information on days with SES.

	Inversion Layers	**Total (day)**	
	Surface-850 hPa	12	
	850-700 hPa	52	
	700-500 hPa	34	
Thickness (m)	**Average (m)**	**Maximum (m)**	**Minimum (m)**
Surface-850 hPa	103.1	254	27
850-700 hPa	242.8	829	56
700-500 hPa	344.3	1140	55

When the inversion layer thicknesses are examined in detail, box plot schemes for each layer are given in Figure 4.9. In the first level close to the ground (ground level-850 hPa), the thickness values on average oscillated in the range of 60-160 m. At the second level (850-700 hPa), this value oscillated in the range of 120-280 m. Finally, at the furthest level from the ground (700-500 hPa), this value was found in the range of 180-500 m. The low thickness values at the first 150 hPa level from the ground indicate that the effect of this level is lower than the inversion layers at other levels, mostly in terms of preventing upward movements in terms of thermodynamics. The observation of inversion layers with higher vertical thickness at the other two levels is very important in limiting upward movements and providing a suitable environment for the development of the SES bands.

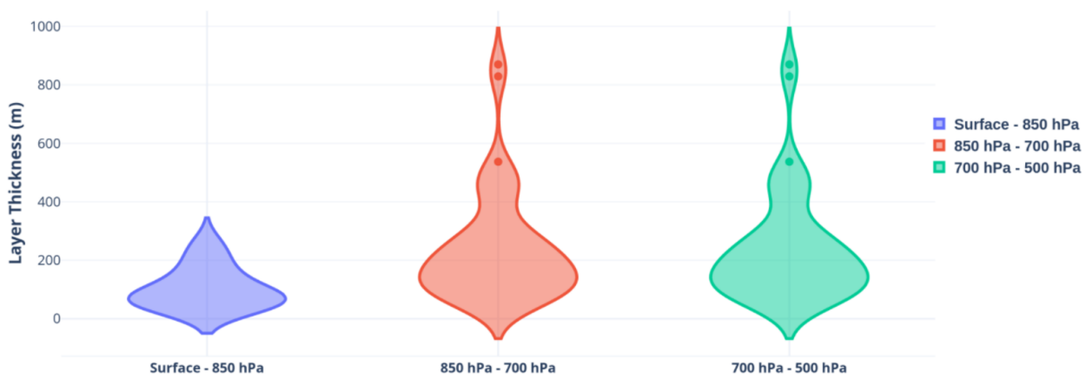

Figure 4.9 : Distribution of inversion layer thicknesses at each vertical level. The dots inside the orange and green plots indicate extreme or outlier values.

4.3.4 Upper level wind flow during SES times

One of the important factors, especially in the formations of the SES bands and the direction they will follow, is the direction information values of the winds below the inversion layer. The results of the analysis performed within the days of the SES bands over the Danube Region are given separately for the 850 hPa and 700 hPa levels (Figures 4.10-4.11). The cases where there is no SES but only SES bands are also included.

The wind direction was 85% northerly (31% North, 36% Northeast, 17% Northwest) for 850 hPa during SES times over the sea throughout the Danube Region. On the other hand, no observation was found from the south direction (180°). In each sub-region of the Danube Region, the wind directions were from the northern directions (80% in sub-region "A", 87% in sub-region "B", 87% in sub-region "C", 84% in sub-region "D", 84% in sub-region "E" and 87% in sub-region "F"). Similar analyses were also made for the 700 hPa level. The wind direction was 81% northerly (28% North, 29% Northeast, 24% Northwest) for 700 hPa level. In each sub-region of the Danube Region, the wind directions were from northern directions similar to the 850 hPa level (89% in sub-region “A”, 86% in sub-region "B", 86% in sub-region "C", 75% in sub-region "D", 75% in sub-region "E" and 73% in sub-region "F").

It is expected that the upper-level wind directions are mostly northerly for both selected levels. Polar and Arctic air masses that are cold and dry at the same time, travel a long fetch distance (in north-south direction) over Danube Region before reaching the Marmara Region and northern parts of Turkey. Therefore, the occurrence of more than one SES bands mostly observed over the region parallel to the wind in each episode and the formation of T-2 bands over the region is also related to the formation of bands in the direction of the wind.

The Polar and Arctic air masses are cold and contain almost no water vapor (quite dry) (Figure 4.12). In snowfall with sea effect, these cold and dry air masses gain moisture as they pass over the Black Sea and become a system that produces snowfall. Unless there is any synoptic or large-scale system, this precipitation is known as SES. Sea/Lake enhanced snow, on the other hand, occurs when a larger-scale (synoptic) storm system supports the existing system in addition to the existing SES mechanism. Following the passage of a frontal system (cold or stationary front) that currently produces precipitation, Sea/Lake enhanced snow is formed by the inclusion of the flows that bring cold air masses from the north. Most of the SES bands occurring on the Black Sea is T-2 bands. In lake enhanced snow, the frontal systems, which move mostly parallel to the air masses coming from the north, also strengthen the existing band structure and do not cause a big change in direction and formation. T-2 multiband type is mostly observed in both cases over Black Sea.

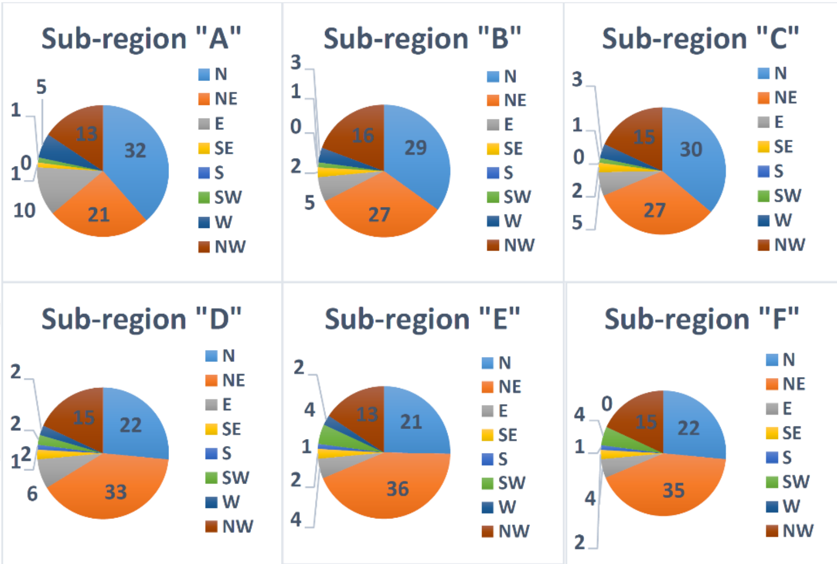

Figure 4.10 : Upper-level wind directions over Danube Region at 850 hPa level. (N=North, NE=Northeast, E=East, SE=Southeast, S=South, SW=Southwest, W=West, NW=Northwest).

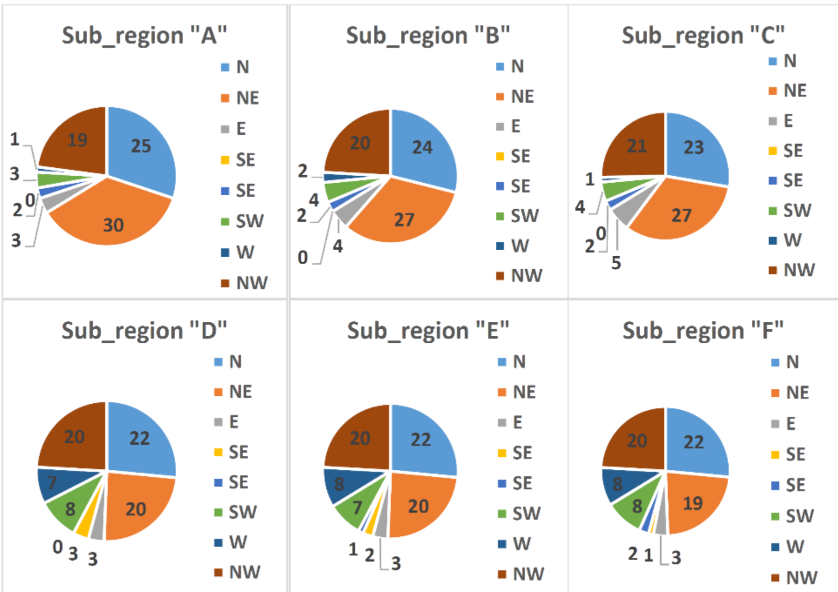

Figure 4.11 : Upper-level wind directions over Danube Region at 700 hPa level. (N=North, NE=Northeast, E=East, SE=Southeast, S=South, SW=Southwest, W=West, NW=Northwest).

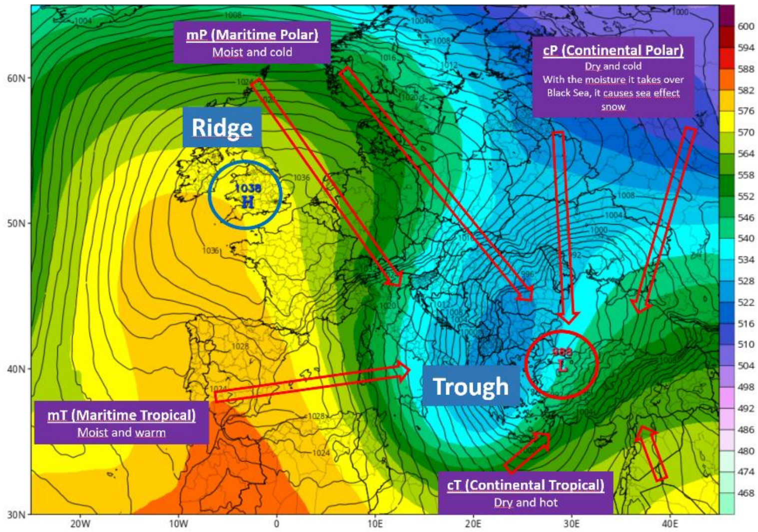

Figure 4.12 : Air masses affecting Turkey, and trough-ridge areas effective in Winter.

4.3.5 The role of air-sea interaction in the formation of SES bands

The air-sea interaction has a great importance in the formation of SES bands and SES. Especially the large difference between the upper level (850 and 700 hPa levels) temperature and SST values will directly affect the formation, intensity and precipitation amount of the SES (Niziol et al., 1995). Sensible and latent heat fluxes from water surfaces towards the atmosphere, cause destabilization of lower atmospheric layer, cloudiness and precipitation in these parts (Ellis and Leathers, 1996). Perturbation will increase as a result of warming of the air mass over the lake or sea by sensible and latent heat fluxes. Hence, a low level of atmospheric instability will occur (Scott and Sousounis, 2001). Accordingly, the increase in the temperature difference of the water surface and the upper air mass will have a triggering/accelerating effect in the formation of SES. In many studies in the literature, results supporting this argument have been obtained for different regions. (Bard and Kristovich, 2012; Clark et al., 2016). In this study, SST values at the time of occurrence of SES bands are analysed. For each band type, the lowest temperatures were observed in the sub-region "A" in the analysis performed within six sub-regions determined within the Danube Region. Similar average temperature values were encountered in other sub-regions, unlike the sub-region "A". In the analyses performed for T-1 band, as a result of the fact that this band type was rarely encountered over the region, an average value was obtained for each region. These values are; 7.42 °C for sub-region "A", 9.51 °C for sub-region "B", 9° C for sub-region "C", 10.47 °C for sub-region "D", 10.44 °C for sub-region "E", 10.14 °C for sub-region "F" (Figure 4.13).

Throughout the period, the lowest SST value in SES times was observed with the value of 3.08 °C when T-2 band occurred in the sub-region "A". The highest temperature value was measured with the value of 12.47 °C in the presence of T-2 band type in the sub-region "C". For the T-2 band, which is the most observed SES band type, the average SST values in all sub-regions of the Danube Region were found to be 7.81 °C. For the T-3 band, which is the most common band after T-2 band type, the average SST value was observed as 7.65 °C.

In another analysis, the difference between SST value and upper air temperature was examined for two different vertical levels. In order to be representative for all regions, SST values were obtained at a point located in the middle part of the Danube Region. With these values, the vertical sounding data obtained from the radiosonde balloon were examined and Table 4.5 was obtained by subtracting the 850 hPa and 700 hPa levels from the SST values obtained from the actual temperature values. It has been stated in previous studies that the temperature difference between the sea surface and the 850 hPa level is greater than 13 °C is sufficient for the formation of the SES band (Rothrock, 1969; Kunkel et al., 2002; Niziol, 1987). Moreover, if the temperature difference is greater than 17 °C, it indicates a strong SES band formation. Therefore, the increase in the temperature difference makes the environment necessary for SES band formation even more suitable. The temperature difference between the sea surface and 700 hPa level is in the range of 17-24 °C, which indicates medium strength band formation, between 24-30 °C indicates strong band formation and greater than 30 °C indicates extreme band formation. As seen in Table 4.5, the average SST and the minimum values of both vertical level difference were observed at the time of the T-2 band. The maximum and minimum temperature difference values were also observed at the time of the T-2 band. As a result, the band type showing the least sensitivity to the temperature difference between sea surface and upper air mass was T-2 band.

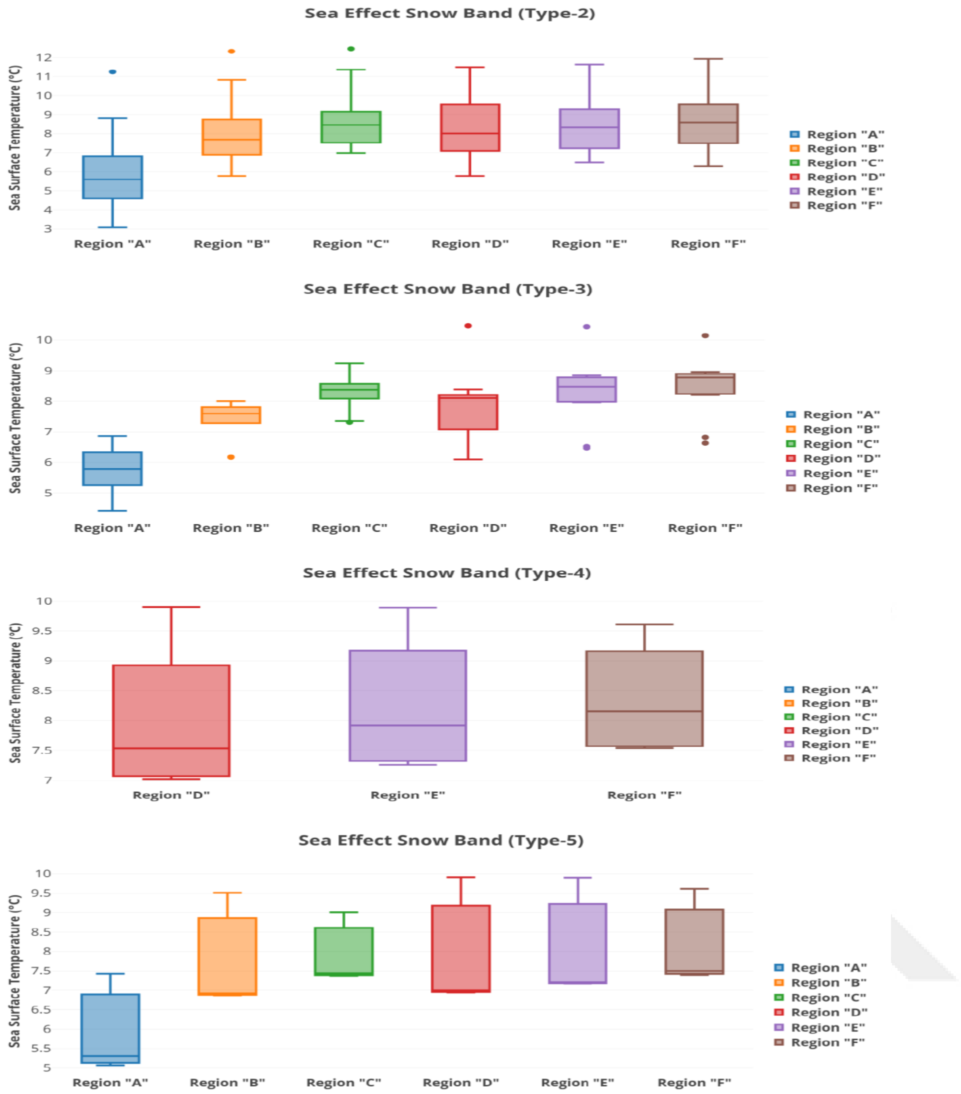

Figure 4.13 : SST values seen in each sub-region of the Danube Region during SES times. The lines in the middle of the colored boxes show the median value, the dots at the bottom or the top show outliers, the lines at the bottom and the top of the box show the minimum and maximum values, and the area between the lower and upper edges of the boxes show the interquartile range.

Table 4.5 : Average, maximum and minimum sea surface-upper level air mass temperature differences observed in each band type.

Band type	Average difference		Maximum difference		Minimum difference	
	SST-850 hPa (°C)	SST-700 hPa (°C)	SST-850 hPa (°C)	SST-700 hPa (°C)	SST-850 hPa (°C)	SST-700 hPa (°C)
T-1	20.37	27.97	20.69	28.65	20.05	27.29
T-2	17.29	24.31	23.21	33.04	10.58	14.96
T-3	18.27	26.23	20.69	32.29	11.18	17.29
T-4	17.95	23.35	20.69	30.49	15.64	17.24
T-5	19.9	25.57	20.69	27.29	18.82	22.42

4.4 Discussion and Conclusions

With this study, the sea-effect snow bands, their formation, types and their statistical relationship with certain meteorological variables for the Danube Region for a period of 10-years have been revealed. Although there are already limited studies on SES events for the Region, thanks to this study, both long-term determination of SES times and the classification of the SES band types has been presented for the first time. In this context, the results obtained and the related evaluations can be summarized as follows:

- T-2 band (85%) was the most observed SES band type within the borders of Danube Region. This was followed by the T-1 band (10%). T-5 band, which is rarely observed in the region, is encountered.
- Although SES bands were observed in the region over the sea for 83 days, SES occurred in 75 days on the shores of the Marmara Region. This is because SES bands have not reached the shore.
- The distribution of SES bands within the six sub-regions identified within the Danube Region was almost the same (17% for each). Only slightly less bands were observed in the sub-region "A" (15%). The reason for this is that in the sub-region "A", there is not enough contact time with the water body over which the cold dry air from the far north passes, and as a result, the required heat and humidity interaction is relatively low.
- One of the basic atmospheric conditions in the formation of SES bands is the presence of an upper inversion layer. In the circulation that starts thermodynamically upwards, the formation of a layer that will limit the movement above and close it is the most important requirement for the formation of the bands. In the region, during 52 days of the 75 days with SES, an inversion was observed between 850-700 hPa levels. Studies in the literature indicate that the inversion formation in the vertical atmosphere column of 150 hPa from ground level will be negative for the onset of vertical movements (Steenburgh *et al.*, 2000). In the study period, this level of inversion was observed in only 12 days, and these layers remained at very low values in terms of thickness. While the inversion layers with the highest vertical thickness values at average and maximum values were at the level of 700-500 hPa, this was followed by the inversion layers at the level of 850-700 hPa.

- The upstream flows are especially important in determining the formation, trajectory and types of SES bands. The most common condition for the T-2 band in the region is the passage of dry cold air over relatively warm water surfaces a long fetch distance in a direction parallel to the wind flow. In this context, the wind direction for the both 850 hPa (85%) and 700 hPa levels (%81) was northerly during the period with SES. On the other hand, in snowy times without sea effect, the wind directions at both levels were again mostly northern, but there were also winds from southern directions (especially southwest). This situation has generally occurred in the presence of a trough extending to the Mediterranean or a deep cyclone emerging over the Aegean Sea.
- T-2 band type has been the most compatible band type with SST value and actual temperature difference conditions of sea surface-upper level air. The average temperature difference between the sea surface-850 hPa level was 17.29 °C and the minimum difference was 10.58 °C. It has been determined for the region that there is a direct proportion between the amount of precipitation and the temperature difference of the sea surface-upper level air. During the selected period, the highest snowfall was observed at Istanbul Sabiha Gokcen Airport with 55 cm. Meanwhile, the temperature between the sea surface-850 hPa level was 20.6 °C, while the temperature difference between the sea surface-700 hPa level was 28.6 °C.

5. ANALYSIS OF A VORTEX CAUSING SEA-EFFECT SNOWFALL IN THE WESTERN PART OF THE BLACK SEA: A CASE STUDY OF EVENTS THAT OCCURRED ON 30-31 JANUARY 2012 [4]

5.1 Introduction

Heavy snowfall was observed in the coastal parts of the Marmara and Black Sea regions under the influence of the vortex-type sea-effect snow (SES) band on 30–31 January 2012. A total of 102 flights planned by a private airline, including 37 international and 65 domestic flights, were cancelled due to adverse weather conditions. Due to the action of strong north- and northeast-trending winds and storms (27–38 kt), there have been problems associated with transportation and daily activities across the Marmara and western Black Sea regions. Traffic disruptions due to icing and snow accumulation led to kilometres of traffic issues on roads across the Marmara region during this event. In cities located along the coastal portions of the western and central Black Sea Region, nearly 700 village roads wereclosed. The Samsun Carsamba Airport, which is close to the Inebolu Meteorological Station, was closed for a certain period of time due to the presence of snow on the runway (TRT, 2020; Dunya, 2020).

SES is a meteorological phenomenon that occurs in the presence of sea-effect snow bands and causes heavy snowfall in areas over which these bands pass. It is generally locally effective and does not cover as large of an area as synoptic-scale snowfall. SES is mostly seen in the Great Lakes Region (in the USA), on the lakes and sea shores of Russia and Japan, and in the northern part of the Marmara and Black Sea regions of Turkey. In studies carried out for the Great Lakes Region, the amount of snowfall, its impact area, and the atmospheric conditions in which SES occurs have been examined ranging from historical to present evaluations (Wiggin, 1950; Pease and Sykes, 1966; Jiusto and Kaplan, 1972; Niziol, 1987; Bolsenga and Norton, 1992; Laird et al., 2001;

---

[4] This chapter is based on the research paper: Yavuz, V., Deniz, A. and Özdemir, E.T. (2021). Analysis of a vortex causing sea-effect snowfall in the western part of the Black Sea: a case study of events that occurred on 30-31 January 2012. *Natural Hazards*, 108, 819-846, doi: https://doi.org/10.1007/s11069-021-04707-8

Hong and Ye, 2014; Veals and Steenburgh, 2015; Suriano and Leathers, 2017). It has also been revealed that the excessive snowfall that occurs as a result of this phenomenon has serious effects, especially on agriculture and transportation (Schmidlin, 1993; Burnett et al., 2003; Burow and Atkinson, 2019).

Many meteorological parameters play an important role in the formation of SES bands. In this regard, the effects of many meteorological parameters on SES formation have been investigated for different regions in the literature. In these studies, it was found that the basic requirement for the formation of SES is the passage of a cold Arctic or polar air mass above a relatively warm water surface (sea or lake surface) (Kindap, 2010; Özdemir and Yetemen, 2019; Yavuz et al., 2021). In this case, sensible and latent heat fluxes emerge from the surface of the water body towards the air mass above, and thermal energy and water vapour fluxes destabilize the cold air mass. Therefore, shallow convection will occur over water bodies (Markowski and Richardson, 2010; Niziol et al., 1995). This convection will generally be characterized by a low-level wind direction, a certain water body shape, and other atmospheric conditions that may occur on a synoptic scale (Niziol et al., 1995). However, for the formation of SES bands, this convection is constrained by a lower-level inversion layer(s) (Niziol, 1987; Hjelmfelt, 1990; Mahoney and Niziol, 1997). Thus, snow bands will be formed as a result of mesoscale-limited circulation that will occur between the water surface and an upper level. In addition, the direction of wind under the inversion layer, the distance travelled by streams over the water body (fetch) (Laird and Kristovich, 2004), and the temperature difference between the sea/lake surface and the 850–700 hPa vertical atmospheric level (Niziol, 1987) play an important role in SES formation (Ballentine, 1992; Niziol et al., 1995; Kunkel et al., 2002).

In earlier studies, based on satellite observations, SES bands were sorted in four categories according to their morphological structures (Kelly, 1986). Later, Niziol et al. (1995) expanded these categories and examined five types of SES bands for operational purposes, i.e. Type-1 (single band), Type-2 (multiband), Type-3 (hybrid band), Type-4 (shoreline parallel band), and Type-5 (mesoscale vortex band). The type-5 band occurs under very stable atmospheric conditions. Shallow cloud structures and vortex cloud types are distinctive features of this band. It occurs very rarely under light wind atmospheric conditions. Additionally, it forms in the centre of seas/lakes, where there is convergence due to the action of sea/lake breezes, and after its formation, this structure is directed towards land. Typically, narrow snow bands are formed under these conditions (Laird, 1999).

In the literature, studies have been performed based on the classification of SES bands, but a special case analysis for the rarely observed vortex-type SES band has not been reported for the Black Sea. In the context of a lack of relevant studies, it is of great importance to study the processes of the Black Sea with respect to SES; in addition, the first study will be conducted for the region over which the vortex-type SES band can be observed. When looking at the studies focused on lakes in the United States of America, Passarelli and Braham (1981) found that under relatively weak synoptic-scale gradient wind conditions, singular and shore-parallel bands are formed over Lake Michigan. At this time, the warming of the air over the warm lake surface creates a large temperature gradient on the lake's shore. Such conditions also cause the development of land breeze circulation on opposite coasts, leading to the formation of convergence over the lake. Accordingly, cloud bands occur in regions where convergence occurs. When the gradient wind intensity increases, the land breeze convergence is dispersed, and the cloud band structure deteriorates. Pease et al. (1988) studied mesoscale spiral vortices embedded in snow bands over Lake Michigan. They concluded that in the absence of any synoptic-scale forcing, strong surface heat fluxes play an important role in mesoscale vortex development.

In addition, surface convergence towards the lake has also been detected by Pease et al. (1988), which resembles that of land breeze circulation. Zhang and Fritsch (1985) found that there could be a common process responsible for the rapid cyclonic rotation of several mesoscale vortices, such as polar lows, tropical cyclones, and lake vortexes. The most important factor driving the development of these circulations is the formation of a dense air mass as a result of the movements of sensible and latent heat fluxes from the lake's surface to the colder air mass at the top. Forbes and Merritt (1984) detected and analysed a total of 14 vortexes over the Michigan, Huron and Superior lakes with the aid of visible and infrared band satellite imagery. Considering the snowfall and meteorological conditions caused by synoptic-scale cyclones, it was determined that the precipitation caused by these vortices was short term (snow showers and squalls) and associated with small amounts of snowfall (less than 2 cm of snow). All 14 vortices were formed by a weak surface pressure gradient and cold polar air. The fact that the air temperature on the lake surface was colder than the lake surface in all analyses also revealed the importance of diabatic warming in the development of vortices. It has also been stated that synoptic-scale forcing is quite weak and insignificant during vortex development. This is due to the negative vorticity measured at 500 hPa in 57% of cases, while a strong positive vorticity has only been observed in one case. Looking at the studies that investigated the vortices occurring over the Sea of Japan, Miyazawa (1967) used various radar products to observe mesocyclonic bands occurring in large snow bands. Asai and Miura (1981) found that the vortices occurring in the same area lasted at least a few hours, and the area they covered was 50–100 km wide and experienced clear cyclonic rotation.

In this study, during the 10-year period between 2009 and 2018, the days with snowfall in the Marmara region were determined from the aviation observations of an airport in the region; the days with SES were distinguished by satellite analyses, and the vortex-type SES band was clearly determined. The main purpose of this study is to examine the meteorological conditions leading to the formation of the vortex-type SES band that took place on 30–31 January 2012 over the western part of the Black Sea. In addition, the precipitation and atmospheric changes caused by SES in the surrounding countries during the time in which the event occurred were also discussed in detail.

5.2 Data and Methodology

The Meteorological Aerodrome Reports (METARs) and the Meteorological Aerodrome Special Reports (SPECIs) of 12 airports belonging to four countries surrounding the western Black Sea were analysed to investigate the vortex-type SES band formation occurring over the western Black Sea on 30–31 January 2012. The reports were obtained from the IOWA Environmental Mesonet website maintained by Iowa State University (IOWA, 2020). Information on the airports were examined, and the start/end times of the observations taken into the assessment are given in Table 5.1.

Various products belonging to two different satellites were used for the analysis of satellite imagery. First, the images were obtained from the Moderate Resolution Imaging Spectroradiometer (MODIS) module of the Terra satellite with a high resolution (0.25° × 0.25° latitude–longitude resolution) and examined once a day for the two-day period. The MODIS module has 36 spectral bands in the 0.4–14.4 μm band range and a resolution of 250–1000 m. Owing to its 2330 km wide monitoring area, it provides an ideal solution for monitoring large-scale changes globally (Zhao and Duan, 2020). MODIS module images taken by the Terra satellite were obtained from the National Aeronautics and Space Administration (NASA) (NASA, 2020). The second-generation MSG-2 and MSG-3 satellite products of the Meteosat satellite series were used as additional satellites. MSG-2 and MSG-3 produce detailed images at 15-min intervals over the continents of Europe and Africa, as well as parts of the Atlantic and Indian Oceans. The spinning enhanced visible and infrared imager (SEVIRI) radiometer on the MSG acquires observations in the four visible (VIS) and near infrared (NIR) channels ranging from 0.4 to 1.6 μm. Additionally, it acquires observations from eight infrared (IR) channels in the range of 3.9–13.4 μm. The data are obtained in the form of 12 spectral bands with a 3-km resolution (Zhao and Duan, 2020; Trigo et al., 2011). In this study, infrared (Channel-9), visible band (Channel-321) and airmass satellite products were analysed. These data were obtained from the Turkish State Meteorological Service (TSMS) (TSMS, 2020).

For the analysis of sounding data, vertical atmospheric information obtained from five radiosonde stations belonging to four different countries was taken into consideration (Figure 5.1). The data were obtained from the University of Wyoming Atmospheric Sciences web page (University of Wyoming, 2020). Skew-T Log-P diagrams and the sounding data of meteorological stations numbered 17062 (Turkey), 17030 (Turkey), 15420 (Romania), 33791 (Poland), and 34731 (Ukraine) were analysed. While data were provided for only 1200 UTC (Universal Time Coordinated) for the dates of 30 and 31 January 2012 at station 33791 in Poland, the data were provided twice a day (for 1200 and 0000 UTC) for all other stations on both days.

NOAA High-Resolution Blended Analysis data were used to obtain sea surface temperature information. Data with a latitude–longitude resolution of 0.25° × 0.25° were obtained from the Asia–Pacific Data-Research Center (APDRC, 2020). The data show the daily average values obtained for the entire western Black Sea.

Table 5.1 : Information on METAR and SPECI reports published by 12 airports, 30–31 January 2012.

Countries and ICAO codes of airports	Airports	Latitude	Longitude	First report time	Last report time
Turkey					
LTBU	Tekirdag Corlu	41°07′46" N	27°54′23" E	30 Jan 2012 0020 UTC	31 Jan 2012 2350 UTC
LTBA	Ataturk	40°58′34" N	28°48′50" E	30 Jan 2012 0020 UTC	31 Jan 2012 2350 UTC
LTFJ	Sabiha Gokcen	40°53′39" N	29°18′30" E	30 Jan 2012 0020 UTC	31 Jan 2012 2350 UTC
LTAS	Zonguldak	41°30′23" N	32°05′19" E	30 Jan 2012 0550 UTC	31 Jan 2012 1450 UTC
LTCM	Sinop	42°00′57" N	35°03′59" E	30 Jan 2012 0550 UTC	31 Jan 2012 1450 UTC
Bulgaria					
LBWN	Varna	43°13′55" N	27°49′30" E	30 Jan 2012 0000 UTC	31 Jan 2012 2330 UTC
LBBG	Burgas	42°34′10" N	27°30′54" E	30 Jan 2012 0000 UTC	31 Jan 2012 2330 UTC
Romania					
LRTC	Tulcea	45°03′28" N	28°42′31" E	30 Jan 2012 0000 UTC	31 Jan 2012 2300 UTC
LRCK	Constanta	44°21′44" N	28°29′18" E	30 Jan 2012 0000 UTC	31 Jan 2012 2330 UTC
Ukraine					
UKFF	Simferopol	42°03′8" N	33°58′31" E	30 Jan 2012 0000 UTC	31 Jan 2012 2358 UTC
UKON	Mykolaiv	47°03′00" N	31°55′00" E	30 Jan 2012 0400 UTC	31 Jan 2012 1800 UTC
UKOO	Odessa	46°25′37" N	30°40′41" E	30 Jan 2012 0000 UTC	31 Jan 2012 2330 UTC

Note: ICAO International Civil Aviation Organization; UTC Universal time coordinated; N North; E East

In the synoptic analysis, the Plymouth State Weather Center and Wetter3 sites were used to obtain surface and upper-level charts (PSWC, 2020; Wetter, 2020). The Meteomanz website was used to obtain the SYNOP observations published by the meteorological stations (Meteomanz, 2020). Many meteorological parameters, such as the amount of snow, relative humidity, pressure, wind speed and direction obtained from a total of 16 meteorological stations belonging to four different countries, were evaluated. The World Meteorological Organization IDs and names of the stations are as follows: 17052-Tekirdag; 17060-Atatürk; 17070-Bolu; 17022-Zonguldak; 17024-Inebolu, 15661-Achtopol; 15655-Burgas; 15552-Varna; 15562-Kallakpa; 15561-

Shabla; 15480-Constanta; 15360-Sulina; 33837-Odessa; 33902-Kherson; and 33924-Cernomorskoe; 33946-Simferopol (Figure 5.1).

Figure 5.1 : Study area. Yellow pins indicate meteorological stations; red balloons indicate meteorolocigal stations where the radiosonde measurements were made. Google Earth, (2020).

5.3 Analyses

5.3.1 METAR and SPECI report analyses

Analyses of the METAR and SPECI reports were carried out considering time periods in which observations were found at the airports listed previously in Table 5.1. For the period of 30–31 January 2012, based on the reports of 12 airports in four different countries during the two-day period, the amount of snow accumulation and some meteorological parameter values were examined. The airports are generally located at an altitude close to sea level, and the airport with the highest average altitude above sea level (AMSL) was the UKFF airport with an altitude of 182 m. During the two-day period, snowfall was observed occasionally or frequently at all airports; it was observed at all times at LTBA, and the lowest observed amount of snowfall occurred at LBBG for a total of five hours. The average actual temperature remained under 0 °C at all stations. The stations located in the northern parts of Turkey had an average relative humidity of 88.8%, and more snowfall was observed there than at other stations (Table 5.2).

Table 5.2 : The snowfall periods observed at the airports between 30-31 January 2012 and the average values of some meteorological parameters.

ICAO codes of airports	Elevation AMSL (m)	Average temperatures (T and Td) (°C)	Average wind speed (kn)	Average r. humidity (%)	Duration of snowy times	Ratio of snowy times
LTBU	175	−7.5/−10	21.1	82.6	14 h	26%
LTBA	50	−2.5/−3.6	16.5	91.9	48 h	100%
LTFJ	95	−2.4/−3.8	11.8	90.5	46 h 30 min	97%
LTAS	4	−1.8/−3.3	6.6	90.0	16 h	84%
LTCM	32	−0.7/−6	7.7	71.1	7 h	39%
LBWN	70	−10.5/−14.2	12.8	74.4	13 h 30 min	28%
LBBG	41	−9.4/−14.3	16.7	67.5	5 h	10%
LRTC	61	−12/−14.5	20.8	81.5	24 h 30 min	51%
LRCK	108	−11.8/−15	13.8	77.4	24 h 30 min	51%
UKFF	182	−12.2/−14.1	16.7	67.5	32 h	67%
UKON	56	−13/−15.3	16.4	82.8	13 h	54%
UKOO	52	−12/−14.7	18.2	80.5	12 h 30 min	26%

5.3.2 Satellite image analyses

Although the MODIS module of the Terra satellite has a high resolution, its biggest disadvantage is that it scans and produces images that cover the western Black Sea only once a day. From this module, which produces images at approximately 1100 UTC over the western Black Sea, images were obtained for 30–31 January 2012. In the image examined on 30 January 2012, no vortex-type SES bands were found, but on the following day, it was observed that a very clear vortex-type SES band was formed over the central and western parts of the Black Sea (Figure 5.2).

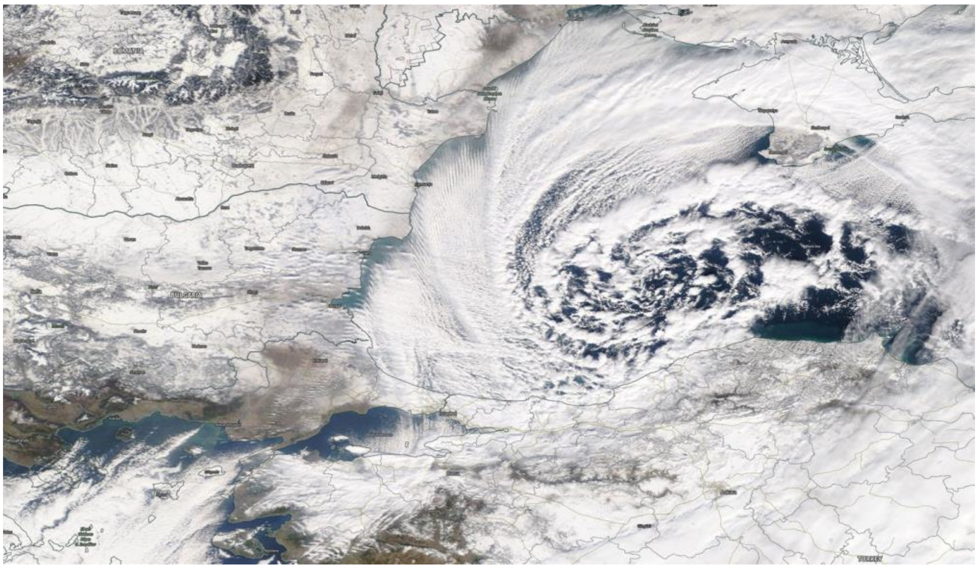

Figure 5.2 : The vortex-type SES band observed over the central and western Black Sea in the satellite image obtained from the MODIS module of the Terra satellite; 31 January 2012. NASA, 2020.

Airmass, infrared (channel-9), and visible band (channel-321) images from the MSG-2 satellite were analysed in detail at intervals of 15 min for a two-day period. In the airmass satellite image taken at 0200 UTC on 30 January 2012, the vortex-type SES band started to appear over the central Black Sea and near the Crimean Peninsula (Figure 5.3a). On the same day, it maintained its position between 0200 and 0800 UTC (Figure 5.3a, b). It became more prominent at approximately 1130 UTC (Figure 5.3c), slowly turned towards the western Black Sea until 2345 UTC, and then deepened and continued its movement by volume expansion (Figure 5.3d–g). The vortex-type SES band, which maintained its position and continued to circulate over nearly the entire western Black Sea from 0000 to 1500 UTC on 31 January 2012 (Figure 5.3h–m), moved towards the east of the Crimean Peninsula and reached the stage of dispersion by filling on 1500 UTC (Figure 5.3n).

Considering the inland extensions of the band on land, between 0200 and 1130 UTC on 30 January 2012, the vortex-type SES band was effective along the Crimean Peninsula and the southern coast of Ukraine (Figure 5.3a–c). In particular, its area of influence expanded between 1000 and 1200 UTC until reaching the city of Odessa (Figure 5.3c). On the same day, between 1200 and 2400 UTC, the centre of the vortex-type SES band maintained its position near the Crimean Peninsula; however, since the morphological structure of the band has shifted to containing a larger volume, the areas affected by the band also included the coastal parts of Romania and Bulgaria (Figure 5.3c–g). In cities close to the shore and those located in the northern part of Turkey, on the same day between 0000 and 1900 UTC, the outer part of the band descended from north to south (similar to the Type-2 band), lowered the cold air along the north–south direction, and caused heavy snowfall due to the cyclonic rotation of the vortex-type SES band (Figure 5.3a–e). In the following hours, the vortex-type SES band continued to dominate here until 2400 UTC (Figure 5.3e–g). The band maintained its presence in all coastal regions surrounding the western Black Sea, thereby increasing its density, especially over the Crimean Peninsula and the southern coastal parts of Ukraine, between 0000 and 1500 UTC on 31 January 2012 (Figure 5.3h–m). From 1500 UTC, the vortex-type SES band filled and started to lose its effect as it slid towards the east (Figure 5.3m, n).

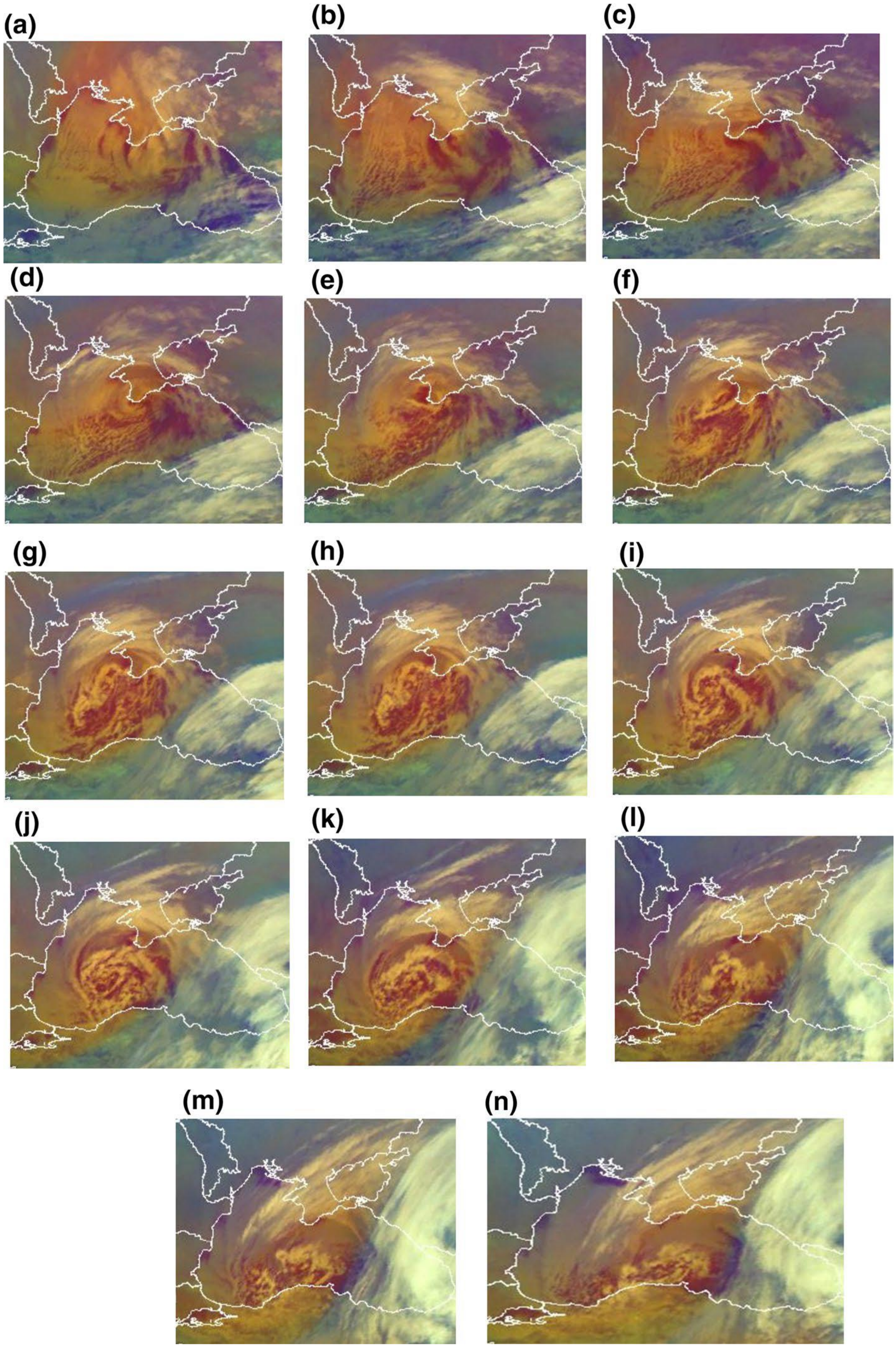

Figure 5.3 : Airmass satellite images obtained from the MSG-2 satellite at a) 0200 UTC, b) 0800 UTC, c) 1130 UTC, d) 1500 UTC, e) 1900 UTC, f) 2100 UTC, and g) 2345 UTC on 30 January 2012 and at h) 0000 UTC, I) 0300 UTC, j) 0600 UTC, k) 0900 UTC, l) 1200 UTC, m) 1500 UTC and n) 1800 UTC on 31 January 2012. TSMS, 2020.

5.3.3 Sounding data analyses

Sounding data were provided for all radiosonde stations at 1200 and 0000 UTC on 30–31 January 2012, excluding station 33,791 in Poland (data could be obtained only at 1200 UTC for two days). First, analyses of the presence, number, and thickness values of the inversion layers for the two-day period were carried out at all stations. At least one inversion layer between the surface and the 500 hPa level was observed at all five stations during the two-day period. While the highest number of inversion layers was observed between the 850 and 700 hPa levels, the lowest number occurred between the 700 and 500 hPa levels. Among the vertical atmospheric levels studied, the average thickness of the inversion layers was 335 m at all stations. This was an indication that a strong and stable structure limiting vertical movement occurred within the upper atmospheric levels. In the formation of SES and the SES bands, the inversion layer is necessary to limit the circulation that occurs as a result of convectional movement in the upper levels and to contribute to cloud development. During the period when the vortex-type SES band was observed over the Black Sea, inversion layers were observed at the upper atmospheric levels at all stations, which showed that atmospheric conditions were favourable for the formation of the SES band (Table 5.3).

Table 5.3 : Inversion layer information obtained from sounding data of five radiosonde stations, 30-31 January 2012.

Station numbers	Date-Hour	No of layers surface-850 hPa	Layer thickness (m)	No of layers 850-700 hPa	Layer thickness (m)	No of layers 700-500 hPa	Layer thickness (m)
17062	30.01.2012 0000 UTC	-	-	1	452	-	-
	30.01.2012 1200 UTC	-	-	2	234/92	1	132
	31.01.2012 0000 UTC	-	-	1	125	1	511
	31.01.2012 1200 UTC	-	-	1	194	1	534
17030	30.01.2012 0000 UTC	1	87	1	344	-	-
	30.01.2012 1200 UTC	-	-	1	418	-	-
	31.01.2012 0000 UTC	-	-	1	324	-	-
	31.01.2012 1200 UTC	-	-	1	110	-	-
15420	30.01.2012 0000 UTC	2	88/274	1	352	-	-
	30.01.2012 1200 UTC	2	8//42	1	263	-	-
	31.01.2012 0000 UTC	3	46/101/464	-	-	-	-
	31.01.2012 1200 UTC	1	190	2	81/130	-	-
34731	30.01.2012 0000 UTC	1	1120	-	-	-	-
	30.01.2012 1200 UTC	1	313	1	516	-	-
	31.01.2012 0000 UTC	1	959	-	-	-	-
	31.01.2012 1200 UTC	1	1176	-	-	-	-
33791	30.01.2012 1200 UTC	1	818	-	-	-	-
	31.01.2012 1200 UTC	2	383/200	-	-	-	-

In another analysis, at similar vertical atmospheric levels viewed for identifying the inversion layers, wind speed and direction changes and backing-veering conditions were analysed. Changes in wind speed and direction, especially within the upper atmospheric levels, are important for the formation of SES bands. Light wind conditions are expected to prevail throughout the region during the formation of the vortex-type SES band. In addition, a wind direction difference between the surface level and the levels of 850–700 hPa of 30° and below indicates strong band organization; if it is between 30° and 60°, band organization is possible. When considering directional changes of 60° and above, SES bands generally pass into the distribution process. The wind speed showed a maximum 8 kt change between the surface and 850 hPa levels when the vortex-type SES band was observed (except station No: 15420). Moreover, wind direction changes were also observed at the surface–850 hPa and 850–700 hPa levels, mostly indicating strong band organization. To evaluate the stability of the atmosphere, it was examined whether the direction change in the wind ran clockwise (veering) or counterclockwise (backing) from the surface to the upper atmospheric levels. There was veering at all stations between the surface and 850 hPa levels (Table 5.4). This again showed that the vertical mobility was lower under the inversion layer and that there was no synoptic scale distortion.

Table 5.4 : Change in wind speed and direction data in each layer in sounding data.

Station numbers	Date-Hour	Ws diff. (kn)			Wd. diff. (°)			B/V		
		S-850	850-700	S-700	S-850	850-700	S-700	S-850	850-700	S-700
17062	30 Jan 0000	-2	5	3	100	130	30	V	B	B
	30 Jan 1200	1	1	2	40	85	45	V	B	B
	31 Jan 0000	3	15	18	30	5	25	V	B	V
	31 Jan 1200	-2	23	21	25	0	25	V	-	V
17030	30 Jan 0000	5	11	16	20	15	35	V	B	B
	30 Jan 1200	-1	17	16	145	35	110	V	B	B
	31 Jan 0000	4	18	22	125	150	275	V	B	V
	31 Jan 1200	1	23	24	5	105	100	V	-	V
15420	30 Jan 0000	29	-10	19	20	30	50	V	V	V
	30 Jan 1200	25	6	31	35	5	40	V	V	V
	31 Jan 0000	27	0	27	40	5	35	V	B	V
	31 Jan 1200	27	-8	19	140	5	135	V	B	V
34731	30 Jan 0000	-10	6	-4	70	25	95	V	V	V
	30 Jan 1200	7	-13	-6	10	25	35	V	V	V
	31 Jan 0000	1	-9	-8	25	15	10	V	B	V
	31 Jan 1200	4	-15	-11	30	20	50	V	V	V
33791	30 Jan 1200	3	2	5	30	0	30	V	-	V
	31 Jan 1200	8	-2	6	0	15	15	0	B	B

5.3.4 SST analyses

Sea surface temperature (SST) values taken on a point-by-point basis according to latitude and longitude are presented for the western Black Sea (Figures 5.4, 5.5). Across the western Black Sea, the daily average SST values for 30–31 January 2012 were 6.8 °C and 6.7 °C, respectively (Figures 5.4, 5.5). In both figures, the SST values decrease from white to red; on the other hand, the SST values increased from white to blue. The daily average SST values between 27 and 29 January 2012 were 7.2, 7.0, and 6.9 °C. A value of 6.5 °C was observed on 1–2 February 2012. The minimum SST value observed over the western Black Sea was 1.9 °C, and the maximum SST value was 8.1 °C on 30 January 2012. The minimum temperature value was 1.6 °C, and the maximum temperature value was 8.0 °C on 31 January 2012. High temperature values on both days over the sea were observed in the area where the core of the vortex-type SES band was located and directly west. In addition, it was determined that the movement direction of the vortex-type SES band was oriented towards the area (west) where high temperature values were observed, excluding those where the core was formed (Figures 5.4, 5.5).

Lat/Lon (°)	27.88E	28.12E	28.38E	28.62E	28.88E	29.12E	29.38E	29.62E	29.88E	30.12E	30.38E	30.62E	30.88E	31.12E	31.38E	31.62E	31.88E	32.12E	32.38E	32.62E
46.88N	....	....	....	....	....	....	....	....	....	....	....	....	....	....	....	....	....	....	....	....
46.62N	....	....	....	....	....	....	....	....	....	....	....	....	....	1.56	1.71	....	....	....	....	....
46.38N	....	....	....	....	....	....	....	....	....	....	....	....	1.9	1.95	2.28	2.96	....	....	....	....
46.12N	....	....	....	....	....	....	....	....	....	....	....	2.46	2.48	2.76	3.19	3.86	4.42	4.69	5.08	....
45.88N	....	....	....	....	....	....	....	....	....	....	3	3.08	3.44	3.91	4.4	5.03	5.24	5.35	5.6	5.55
45.62N	....	....	....	....	....	....	....	....	2.93	3.17	3.49	3.97	4.55	5.12	5.62	6.22	6.28	6.25	6.3	6.07
45.38N	....	....	....	....	....	....	....	....	3.43	3.76	4.27	4.87	5.5	6.06	6.51	7.05	7.06	6.97	6.91	6.66
45.12N	....	....	....	....	....	....	....	....	4.2	4.53	5.04	5.6	6.13	6.58	6.96	7.49	7.5	7.43	7.31	7.15
44.88N	....	....	....	....	....	....	....	5.1	4.97	5.23	5.66	6.1	6.46	6.74	7	7.41	7.47	7.48	7.47	7.44
44.62N	....	....	....	....	....	5.41	5.57	5.63	5.72	5.97	6.34	6.69	6.88	6.97	7.05	7.28	7.31	7.33	7.35	7.4
44.38N	....	....	....	5.16	5.47	5.82	6.22	6.55	6.75	6.95	7.26	7.56	7.58	7.47	7.31	7.23	7.19	7.18	7.18	7.27
44.12N	....	....	....	....	5.88	6.23	6.68	7.03	7.22	7.34	7.6	7.86	7.85	7.72	7.47	7.3	7.21	7.14	7.16	7.22
43.88N	....	....	....	6.34	6.36	6.72	7.12	7.39	7.46	7.47	7.64	7.87	7.88	7.77	7.47	7.28	7.22	7.08	7.09	7.09
43.62N	....	....	....	6.62	6.83	7.21	7.53	7.67	7.57	7.43	7.5	7.66	7.67	7.58	7.36	7.21	7.19	7.09	7.13	7.12
43.38N	....	6.22	6.44	6.76	7.14	7.53	7.79	7.8	7.53	7.27	7.23	7.29	7.3	7.23	7.1	7.04	7.08	7.03	7.07	7.1
43.12N	....	6.16	6.42	6.82	7.26	7.65	7.9	7.82	7.46	7.13	7.01	6.98	6.99	6.93	6.88	6.9	6.98	7	7.03	7.09
42.88N	....	6.07	6.36	6.79	7.24	7.65	7.95	7.86	7.49	7.17	7.02	6.94	6.94	6.89	6.89	6.94	7.02	7.09	7.13	7.21
42.62N	5.71	5.93	6.27	6.68	7.09	7.47	7.82	7.75	7.42	7.17	7.04	6.97	7.01	7	7.06	7.12	7.21	7.3	7.33	7.41
42.38N	5.72	5.94	6.25	6.6	6.96	7.29	7.65	7.6	7.33	7.14	7.04	7.01	7.09	7.13	7.25	7.3	7.4	7.48	7.5	7.56
42.12N	5.83	6.08	6.35	6.64	6.94	7.2	7.5	7.45	7.23	7.08	7	7	7.11	7.19	7.34	7.37	7.49	7.54	7.58	7.6
41.88N	....	6.1	6.31	6.61	6.9	7.12	7.35	7.31	7.17	7.03	6.96	6.98	7.09	7.2	7.32	7.32	7.46	7.42	7.47	7.48
41.62N	....	6.24	6.48	6.85	6.97	7.14	7.27	7.23	7.14	7.01	6.94	7	7.14	7.26	7.35	7.35	7.42	7.38	....	....
41.38N	....	....	....	7.08	7.1	7.21	7.26	7.21	7.17	7.06	6.99	7.1	7.24	7.37	7.46	7.43	....	....	....	....
41.12N	....	....	....	....	....	....	....	....	7.22	7.15	....	7.26	7.37	7.49	7.57	....	....	....	....	....
40.88N	6.67	6.69	6.8	6.96	7.05	7.12	....	....	....	....	....	....	....	....	....	....	....	....	....	....
40.62N	6.68	6.74	6.87	7.04	7.18	7.21	....	....	....	....	....	....	....	....	....	....	....	....	....	....
40.38N	....	6.87	7.03	7.21	7.38	....	....	....	....	....	....	....	....	....	....	....	....	....	....	....
40.12N	....	....	....	....	....	....	....	....	....	....	....	....	....	....	....	....	....	....	....	....

Figure 5.4 : Daily average SST values observed over the western Black Sea, 30 January 2012.

Lat/Lon (°)	27.88E	28.12E	28.38E	28.62E	28.88E	29.12E	29.38E	29.62E	29.88E	30.12E	30.38E	30.62E	30.88E	31.12E	31.38E	31.62E	31.88E	32.12E	32.38E	32.62E
46.88N	....	....	....	....	....	....	....	....	....	....	....	....	....	....	....	....	....	....	....	....
46.62N	....	....	....	....	....	....	....	....	....	....	....	....	....	1.85	2.01	....	....	....	....	....
46.38N	....	....	....	....	....	....	....	....	....	....	....	....	2.25	2.33	2.62	3.24	....	....	....	....
46.12N	....	....	....	....	....	....	....	....	....	....	....	2.84	2.88	3.18	3.56	4.18	4.64	4.86	5.02	....
45.88N	....	....	....	....	....	....	....	....	....	....	3.35	3.48	3.88	4.36	4.8	5.4	5.49	5.55	5.61	5.52
45.62N	....	....	....	....	....	....	....	....	3.15	3.48	3.86	4.39	5	5.59	6.05	6.62	6.55	6.49	6.37	6.08
45.38N	....	....	....	....	....	....	....	....	3.63	4.04	4.62	5.26	5.93	6.49	6.9	7.41	7.31	7.19	6.99	6.68
45.12N	....	....	....	....	....	....	....	....	4.39	4.78	5.31	5.88	6.42	6.85	7.18	7.65	7.59	7.52	7.39	7.18
44.88N	....	....	....	....	....	....	....	5.22	5.12	5.42	5.86	6.31	6.65	6.92	7.13	7.5	7.52	7.55	7.55	7.5
44.62N	....	....	....	....	....	5.43	5.61	5.73	5.81	6.06	6.47	6.82	6.99	7.07	7.12	7.33	7.34	7.37	7.42	7.48
44.38N	....	....	....	5.09	5.39	5.82	6.28	6.65	6.85	7.04	7.36	7.73	7.7	7.53	7.33	7.22	7.19	7.17	7.23	7.35
44.12N	....	....	....	....	5.82	6.22	6.71	7.1	7.28	7.42	7.66	7.99	7.93	7.82	7.53	7.35	7.27	7.2	7.23	7.28
43.88N	....	....	....	6.29	6.32	6.73	7.17	7.47	7.52	7.53	7.69	7.98	7.97	7.89	7.59	7.39	7.31	7.29	7.27	7.22
43.62N	....	....	....	6.62	6.86	7.27	7.6	7.76	7.62	7.48	7.53	7.74	7.75	7.68	7.48	7.29	7.26	7.27	7.3	7.26
43.38N	....	6.19	6.44	6.79	7.19	7.61	7.88	7.89	7.56	7.29	7.24	7.32	7.33	7.27	7.16	7.06	7.09	7.12	7.14	7.16
43.12N	....	6.12	6.41	6.85	7.3	7.71	7.98	7.89	7.45	7.11	6.98	6.94	6.97	6.91	6.85	6.84	6.9	6.93	6.98	7.02
42.88N	....	6.02	6.35	6.82	7.29	7.71	8.07	7.96	7.52	7.18	7.02	6.91	6.94	6.87	6.83	6.85	6.9	6.93	6.97	7.04
42.62N	5.64	5.88	6.25	6.68	7.11	7.51	7.96	7.86	7.47	7.21	7.07	6.98	7.04	7.01	7.01	7.04	7.09	7.1	7.11	7.19
42.38N	5.65	5.89	6.22	6.59	6.96	7.32	7.78	7.71	7.39	7.2	7.09	7.04	7.13	7.17	7.21	7.25	7.31	7.29	7.28	7.3
42.12N	5.76	6.08	6.37	6.66	6.95	7.25	7.63	7.56	7.3	7.15	7.06	7.05	7.17	7.25	7.33	7.35	7.44	7.4	7.37	7.35
41.88N	....	6.14	6.37	6.66	6.96	7.21	7.5	7.43	7.24	7.1	7.03	7.04	7.16	7.26	7.34	7.32	7.46	7.4	7.38	7.33
41.62N	....	6.23	6.48	6.86	7.1	7.3	7.44	7.36	7.2	7.07	7.02	7.07	7.22	7.34	7.42	7.4	7.45	7.38	....	....
41.38N	....	....	....	7.11	7.28	7.4	7.42	7.34	7.22	7.12	7.07	7.18	7.34	7.46	7.56	7.52	....	....	....	....
41.12N	....	....	....	....	....	....	....	....	7.27	7.19	....	7.34	7.47	7.58	7.67	....	....	....	....	....
40.88N	6.91	6.87	6.9	7.01	7.15	7.24	....	....	....	....	....	....	....	....	....	....	....	....	....	....
40.62N	7	6.96	7	7.11	7.25	7.29	....	....	....	....	....	....	....	....	....	....	....	....	....	....
40.38N	....	7.15	7.23	7.33	7.45	....	....	....	....	....	....	....	....	....	....	....	....	....	....	....
40.12N	....	....	....	....	....	....	....	....	....	....	....	....	....	....	....	....	....	....	....	....

Figure 5.5 : Daily average SST values observed over the western Black Sea, 31 January 2012.

In this section, the temperature difference between the sea surface and the upper air layer was analysed. This difference is the most important parameter in the formation of SES and vortex-type SES bands. In this context, the temperature differences between the average and maximum sea surface values observed over the western Black Sea and the 850–700 hPa levels were investigated. Niziol (1987) stated that the minimum difference between the sea/lake surface temperature and the 850 hPa level temperature should be 13 °C for potential SES band development, and if this difference is larger, a more favourable environment will be created for band organization. Similarly, he stated that the difference between the sea/lake surface temperature and the 700 hPa level temperature should be at least 17 °C. If the temperature difference is between 17 °C and 24 °C, moderate instability will occur. If the difference is above 30 °C, extreme instability will occur. In the analysis, temperature values for the 850 and 700 hPa levels were obtained as a result of the measurements made with the radiosonde balloon at five different stations. The temperature differences between the sea surface and the 850–700 hPa level were examined in detail. The average temperature difference between the sea surface and the 850 hPa level was 15.6 °C at minimum and 24.5 °C at maximum on 30 January 2012 at all stations. Similarly, the average temperature difference between the sea surface and 700 hPa level was 20.0 °C at minimum and 28.9 °C at maximum at all stations on the same day. The differences between the maximum SST values and the temperature values at the 850 and 700 hPa levels were found to be 17.8 °C and 21.3 °C on 30 January 2012, respectively. These values were found to be 21.3 °C and 30.2 °C on 31 January 2012, respectively (Table 5.5). The results confirmed that the conditions for vortex-type SES band formation were quite favourable during the two-day period over the region.

Table 5.5 : Temperature differences between sea surface and upper-level air layer (SST-850 hPa, SST-700 hPa), 30-31 January 2012.

Station numbers	Date-Hour	Temperature differences (°C)			
		Sea surface (avg)-850 hPa	Sea surface (avg)-700 hPa	Sea surface (max)-850 hPa	Sea surface (max)-700 hPa
17062	30 Jan 0000 UTC	16.5	20.5	17.8	21.8
	30 Jan 1200 UTC	18.3	21.9	19.6	23.2
	31 Jan 0000 UTC	20.6	26.6	21.9	27.9
	31 Jan 1200 UTC	19.6	26.4	20.9	27.7
17030	30 Jan 0000 UTC	15.7	21.7	18.0	23.0
	30 Jan 1200 UTC	17.7	20.3	19.0	21.6
	31 Jan 0000 UTC	17.6	20.0	18.9	21.3
	31 Jan 1200 UTC	18.0	21.6	19.3	22.9
15420	30 Jan 0000 UTC	20.9	22.1	22.2	23.4
	30 Jan 1200 UTC	24.5	25.9	25.8	27.2
	31 Jan 0000 UTC	18.6	27.6	19.9	28.9
	31 Jan 1200 UTC	20.6	27.0	21.9	28.3
34731	30 Jan 0000 UTC	18.5	28.9	19.8	30.2
	30 Jan 1200 UTC	16.8	27.3	18.2	28.6
	31 Jan 0000 UTC	18.0	26.6	19.3	27.9
	31 Jan 1200 UTC	21.0	27.0	22.3	28.3
33791	30 Jan 1200 UTC	16.7	26.7	18.0	28.0
	31 Jan 1200 UTC	21.0	26.6	22.3	27.9

5.3.5 Synoptic analyses

In this section, synoptic charts belonging to 850, 700, 500, 300 hPa and the corresponding surface levels and meteorological parameter values of 16 meteorological stations were analysed. On the surface level charts, at 0000 UTC on 28 January 2012, a low-pressure centre was located east of the Black Sea, and the Siberian High Pressure Centre reduced the polar air to 40°N, including that west of the Black Sea. The low-pressure centre in the eastern part of the Black Sea region filled and decayed after 1800 UTC on 28 January 2012. The north and northeast flows carrying polar air over the western Black Sea continued to dominate the region at 0000 UTC on 29 January 2012. The flows started to emerge from the southwest across the Black Sea, and at the same time, the low-pressure centre that was formed in the eastern Black Sea the day before was observed again at the same location after 1800 UTC on 29 January 2012. The low-pressure centre in the eastern Black Sea deepened, and the flows in the western and central parts of the Black Sea flowed northeast again at 0000 UTC on 30 January 2012. In addition, an occluded front emerged. The lowpressure centre located east of the Black Sea was partially filled, and it expanded in volume; the area of influence was expanded with the occluded front up to the middle parts of the Black Sea at 1800 UTC on 30 January 2012. A vortex structure similar to a minitropical cyclone occurred over the Black Sea. This structure, which remained until 1200 UTC on 31 January 2012, started to slide towards the southeast-east due to the deepening of the low-pressure centre. The pressure centre completely separated from the Black Sea and shifted towards the southeast after 1200 UTC on 1 February 2012 (Figure 5.6).

Figure 5.6 : Surface level synoptic charts on a 30/01/2012, at a) 0000 UTC, b) 30/01/2012, at 0600 UTC, c) 30/01/2012, at 1200 UTC, d) 30/01/2012, at 1800 UTC, e) 31/01/2012, at 0000 UTC, f) 31/01/2012, at 0600 UTC, g) 31/01/2012, at 1200 UTC and h) 30/01/2012, at 1800 UTC. The red rectangle denotes the Black Sea region. Met Office (2020).

There was a low-pressure centre observed northeast of the Black Sea at the 500 hPa level at 0000 UTC on 30 January 2012. This pressure centre detached from a deeper lowpressure centre above it containing the polar air, preserved its effect, and moved in a southwest-west direction until 0000 UTC on 30 January 2012 until it was finally located over the Crimean Peninsula on that date. On 1 February 2012, the pressure centre, which remained in the same position until 1200 UTC, started to fill and lost its dominance over the region as it shifted towards the east. Strong negative vorticity values were observed at the 500 hPa level where the vortex core was located. On the other hand, low positive or negative vorticity values were observed throughout the western Black Sea (Figure 5.7).

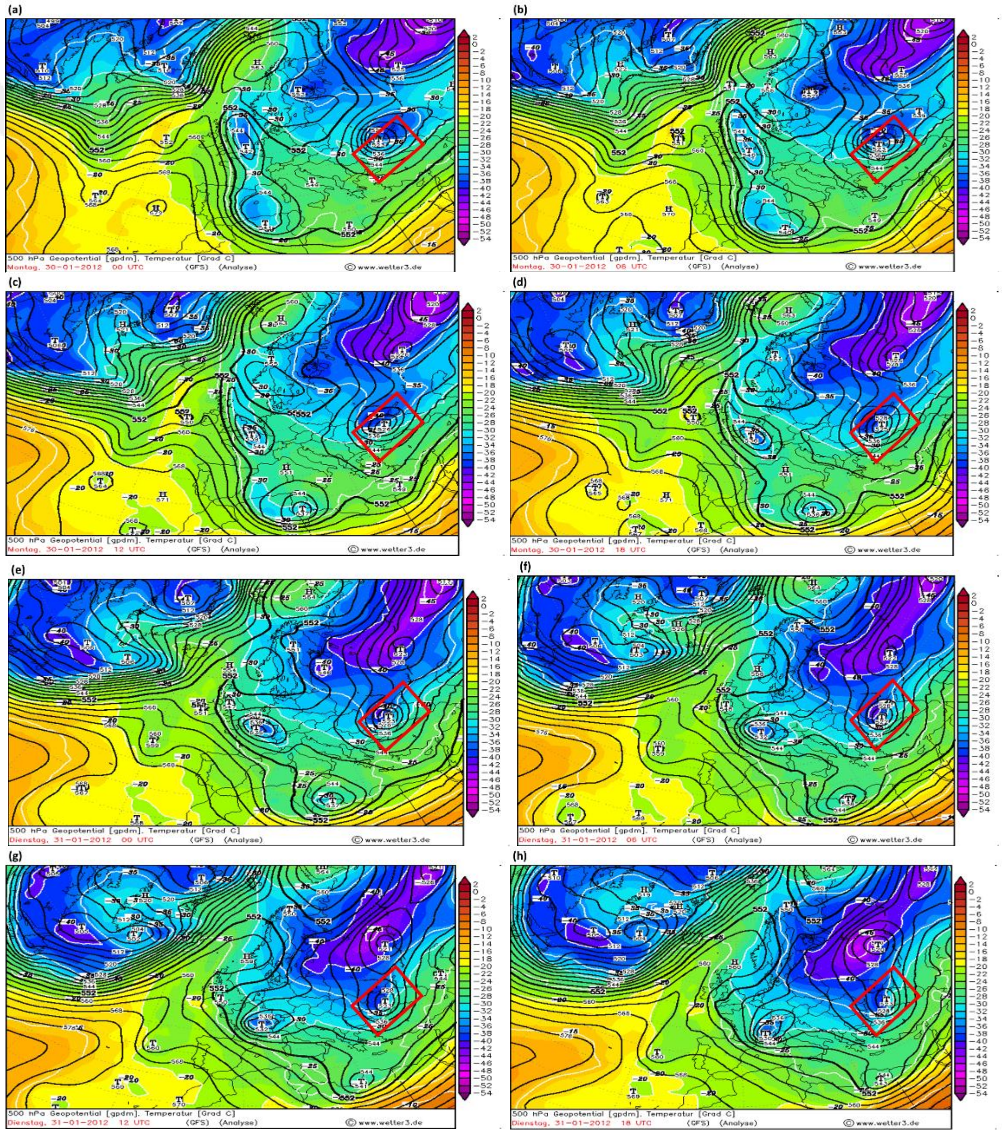

Figure 5.7 : The 500 hPa level synoptic charts collected on a) 30/01/2012, at 0000 UTC, b) 30/01/2012, at 0600 UTC, c) 30/01/2012, at 1200 UTC, d) 30/01/2012, at 1800 UTC, e) 31/01/2012, at 0000 UTC, f) 31/01/2012, at 0600 UTC, g) 31/01/2012, at 1200 UTC, and h) 30/01/2012, at 1800 UTC.

During the event of 30–31 January 2012, a blocking phenomenon was observed in the areas that cover the Black Sea Region according to the blocking data set used in Efe et al. (2020a, b). The blocking event started on 18 January 2012 and decayed until 20 February 2012. The duration of the event was 33 days, which is more than 3 times the average life of blocking events in winter (9.2 days) in the area that affects Turkey. The mean blocking intensity was 2.9, which can be classified as moderate according to Wiedenmann et al. (2002), and was greater than the average blocking intensity of blocking events observed in winter (2.65). The blocking intensity describes the ratio between the geopotential height of the centre and the surroundings of the blocking height. The mean size of this blocking event was approximately 24° in longitude, which is smaller than the average winter blocking event in the area that affects Turkey. The type of blocking (aka high over the low type or dipole type) observed over the period of 26–31 January (Figure 5.8) was of a Rex type, which can be defined as having a high pressure at high latitudes and a low pressure at low altitudes. This event kept the vortex over the Black Sea and allowed it to flow northward and northwest towards Istanbul. The blocking phenomenon plays an important role in the precipitation of Turkey, as mentioned in Efe et al. (2019). The change in the mean precipitation frequency on blocked days during all seasons is positive. In winter, the eastern part of the Marmara Region is a region in which greater changes occur. In addition, Florya is one of the stations that observed the greatest change, with a value of 39%.

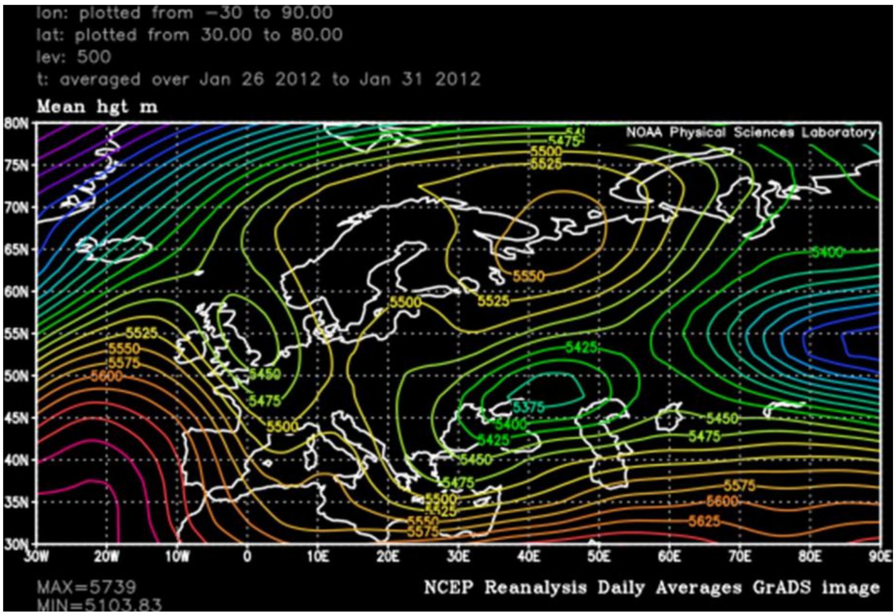

Figure 5.8 : The 500 hPa geopotential height (m) showing Rex-type blocking.

The relative humidity was approximately 90% across the Black Sea for the two-day period at the 700 hPa level (not shown). Low-pressure centres were observed over the Black Sea at the 850 hPa level and the 500 hPa level. Flows at this level showed a full circular cycle between 1200 UTC on 30 January 2012 and 1800 UTC on 31 January 2012 along the central and western parts of the Black Sea. Wind speed values generally oscillated between 20 and 30 kt. The average relative vorticity value was found to be approximately $14 \times 10^{-5}\ s^{-1}$ (not shown).

Some meteorological parameter values and snowfall amounts obtained from the 16 meteorological stations were provided for 30–31 January 2012. Snowfall occurred within the two-day period at all stations except the Tekirdag and Sulina stations. Forbes and Merritt (1984) examined 14 vortices over Michigan, Huron and Superior Lakes and the snowfall they caused and found that the vortex diameters generally ranged from 50 to 120 km. In all cases, the air temperatures were lower than the lake temperatures. All vortexes were observed between midday and midafternoon. In this study, it was determined that the diameter of the vortex SES band, which was effective over the Black Sea for a long period of time (approximately 24 h), was approximately 500 km. Although the western part of the Black Sea has topographic features similar to those of many Great Lakes, the reason why the diameter is larger than the vortex diameters observed over the Great Lakes is the presence of a polar-low structure. Detailed information about this phenomenon is given in the "Discussion, Summary and Conclusions" section. In this study, similar to the study of Forbes and Merritt (1984), the air temperature was higher than the SST at all times. Depending on the bowl-shaped topographic structure of the western Black Sea, the snowfall caused by the presence of the vortex covering almost the entire water body occurred intensely in some places. As a result, a high amount of snowfall was observed regionally in the cities located here. In this context, the highest amount of snow accumulation was observed at the Inebolu Meteorological Station at 24 cm, followed by Zonguldak at 16 cm and the Ataturk Meteorological Station at 10 cm. Other important points here were that the wind directions were mostly trending from northern directions (between 340° and 30°), and the wind intensities were low or medium. Additionally, the relative humidity values were high at most stations (Table 5.6).

Table 5.6 : Snow accumulation amounts and other meteorological parameter values of 12 meteorological stations, 30-31 January 2012.

Station's WMO ID	Station's name	Total snow (cm)		Rel. humidity (%)		Pressure (hPa)		Wind direction (°)		Wind speed (kn)	
		30 Jan	31Jan	30 Jan	31Jan	30 Jan	31Jan	30 Jan	31Jan	30 Jan	31Jan
17056	Tekirdag	0	0	71	68	1029	1027	340	330	8.1	7.0
17060	Ataturk	6	10	95	86	1027	1025	360	350	16.2	17.3
17070	Bolu	4	8	-	-	-	-	-	-	-	-
17022	Zonguldak	12	16	98	88	1026	1021	30	300	5.9	5.9
17024	Inebolu	24	23	97	67	1025	1017	300	220	9.7	10.3
15661	Achtopol	7	7	86	90	1030	1027	340	360	15.1	18.4
15655	Burgas	3	2	68	73	1036	1043	340	320	18.4	13.5
15552	Varna	3	3	77	79	1032	1029	340	320	19.4	19.4
15562	Kallakpa	6	6	-	-	1032	1029	340	360	22.1	29.2
15561	Shabla	0	6	-	-	1031	1028	320	340	19.4	24.3
15480	Constanta	5	4	82	81	1033	1029	340	350	10.3	11.9
15360	Sulina	0	0	84	83	1030	1027	360	360	25.9	28.6
33837	Odessa	0	0.5	85	80	1032	1031	10	20	15.7	16.7
33902	Kherson	1	3	81	73	1029	1030	30	30	15.7	17.3
33924	Cernomorskoe	4	2	82	77	1026	1026	50	50	16.2	21.1
33946	Simferopol	5	5	90	92	1026	1023	20	50	9.2	20.5

5.4 Discussion, Summary and Conclusions

In the literature, vortex-type SES bands have been presented as a phenomenon that induces a small amount of snowfall and is independent of synoptic-scale movements. As the basic formation mechanism, the requirement for the movement of sensible and latent heat fluxes from warm water surfaces to the overlying relatively cold air mass has come to the forefront. It has also been stated that generally light winds have observed in the coastal areas that these bands impact. In these investigations, the diameter of the studied vortex generally varied between 50 and 120 km. The vortex-type SES band that occurred over the western Black Sea between 30 and 31 January 2012, differing from other studies in the literature, exhibited some differences in terms of its formation and the affected area. The diameter of this band, which was effective for 24 h, reached approximately 500 km. There are differences between lake vortices and polar lows in terms of their size and the amount of precipitation they cause. Lake vortices are mesoscale structures with a relatively small diameter. In these structures, troughs are generally observed in low surface pressure areas, and shallow convection occurs. On the other hand, polar lows are structures with larger diameters, in which closed isobars and intense vorticity signals have been observed (Forbes and Lottes, 1982). While lake vortices do not cause notable amounts of precipitation, except for short-term snow showers, polar lows may cause intense precipitation under the effect of intense cyclogenesis. In this study, considering results such as the diameter and duration of the vortex, the amount of precipitation it caused, and the long-term dominance of the upper polar air mass through closed isobars (Rex-type blocking is also present), it was determined that the vortex was similar to a polar low. Within the 10-year study period, vortexes were observed over the region for a short time (approximately 1–2 h), and their cores were smaller, so they did not cause serious snowfall in coastal areas.

In the western Black Sea, during the effective period of the vortex-type SES band, snowfall occurred at all 12 airports. Based on the observations made through satellite images, it was determined that the vortex-type SES band, which was observed over the Black Sea (near the Crimean Peninsula), did not cause much snowfall in the northern parts (Ukraine and Poland coastal areas). The reason why there was little snowfall in these regions was that the northern- and northeastern-trending flows progressed in the terrestrial areas, and as a result of the band circulation, the moist mass from the southeast completed its rotation on land and could not meet the moisture requirement. In countries located west of the vortex-type SES band (Bulgaria and Romania), a small amount of snowfall was observed due to the flows trending north and northeast, and the cold air could not travel far enough over the warm water body. Most snowfall occurred in the coastal areas of the Marmara and Black Sea regions in Turkey. In these areas, daily activities were adversely affected by the snowfall. There were delays in air and sea transportation and accidents on the highways. Snowfalls and storms have impacted many rural areas in the western Black Sea Region and the metropolitan city of Istanbul in the Marmara Region. Compared to other regions surrounded by the western Black Sea, there were several reasons for the occurrence of more snowfall in the northern part of Turkey. The core of the vortex-type SES band was located south of the Crimean Peninsula. As a result of the cyclonic rotation of the band, the north-northeast flow brought cold air from the north (around Odessa) to the south over a long fetch distance. The cold air became saturated with moisture along the long fetch distance and moved the snowfall to the northern coastal parts of the Marmara and Black Seas in the south. Therefore, flows moving parallel to the bands for approximately 600 km in the north–south direction behaved similar to the Type-2 band, resulting in heavy snowfall.

The presence of the inversion layer stands out as the most important condition for the formation of SES bands (Niziol, 1987; Hjelmfelt, 1990; Mahoney and Niziol, 1997). Inversion layer(s) were observed in the vertical atmospheric measurements made by all radiosonde stations on 30–31 January 2012, when the vortex-type SES band was observed. In Turkey's coastal areas (snowfall was observed much more than in other regions), inversion layers were observed in almost all measurements between the 850 and 700 hPa levels. In measurements of other radiosonde stations, inversion layers were mostly seen between the surface and the 850 hPa level. Steenburgh et al. (2000) found that the presence of the inversion layer between the surface and the 850 hPa level has a negative impact on the formation of SES bands throughout the Great Salt Lake Region. Considering the amount of snowfall, the results for the Black Sea confirmed the hypothesis of this study. According to all radiosonde observations made at the stations located in northern Turkey, inversion layers were observed not between the surface and the 850 hPa level but rather between the 850 and 700 hPa levels.

Veering is an indicator of the stability of the atmosphere, and backing is an indicator of instability. During the two-day period, veering was observed at all stations between the surface and 850 hPa levels. The occurrence of a vortex-type SES band under stable atmospheric conditions and a shallow convectional structure compared to other SES band types confirmed the results found. In addition, the slight variation in the wind direction from the surface level up to the 850 and 700 hPa levels (mostly in the range of 0°–50°; this range of values is presented as indicators of strong/moderate band formations and heavy snowfalls) indicated that the atmospheric conditions needed for the formation of the SES band were provided.

Large temperature differences between the sea surface and the upper air will provide atmospheric conditions that are more suitable for the formation of SES bands (Ballentine, 1992; Niziol et al., 1995; Kunkel et al., 2002). In this study, during the observation of the vortex-type SES band, the core of the band was observed, where the temperature differences between the sea surface and the 850–700 hPa levels were highest. Due to the high temperature difference in the region where the core of the band was located, the impact area covered by the band was also large. While the temperature difference between the sea surface and the 850 hPa level should be 13 °C and above, this difference was 21.3 °C on 31 January 2012. Similarly, while a temperature difference between the sea surface and the 700 hPa level of 17 °C and above is required, this difference reached a maximum value of 30.2 °C on 31 January

2012. Unlike the studies in the literature, the main reason why the core of the vortex-type SES band was approximately 3–4 times larger over the Black Sea was due to the high differences between the sea surface and the upper air temperatures.

In the synoptic investigation, it was determined that a low-pressure centre and associated occluded front occurred within the eastern part of the Black Sea on 30 January 2012. The pressure centre and occlusion persisted until the end of 31 January 2012. These structures mostly preserved their position and moved to the west as a result of the partial filling of the pressure centre. This mechanism played an important role in the formation of the vortex-type SES band. Additionally, flows similar to the formation of the vortex-type SES band showed a one-to-one overlap over the low-pressure centre. This pressure centre dominated the region as a result of the falling polar-cold air in the north. Therefore, due to the formation of this cold air pool, the dry and cold air requirements for SES band formation were met. In addition, high relative humidity values (approximately 90%) were observed over the Black Sea during the 700 hPa period. When the vortex-type SES band began to lose its effect, the low-pressure centre also filled and shifted to the east and went over the Black Sea on 1 February 2012.

The prominent results in our study were as follows. First, the vortex diameters occurring over the Great Lakes Region generally vary between 50 and 120 km, while the radius of the vortex examined in this study was found to be approximately 500 km. The most important explanation for this difference was the observation of the polar low structure and the presence of Rex-type blocking. Second, the combination of suitable atmospheric conditions on the western and central Black Sea and the bowl-shaped structure of the topography were important factors driving the formation of the vortex-type band. Third, as a result of the cyclonic rotation of the vortex, cold air was carried over a long fetch distance from the north through the north–south bands from the relatively warm sea surface and became saturated. Along the SES bands, cold and saturated air masses descending south with northern streams entered the northern part of Turkey. Heavy snowfalls occurred in Istanbul, Kastamonu and Zonguldak provinces. Fourth, the inversion layers observed between the 850 and 700 hPa levels were important for the organization of the upstream flows and the vortex-type band. Fifth, the observation of the temperature difference between the sea surface and 700 hPa level at a maximum of 30.2 °C where the vortex core was located played an important role in the large vortex diameter and duration.

6. STATISTICAL CHARACTERISTICS OF SEA-EFFECT SNOW EVENTS OVER THE WESTERN BLACK SEA [5]

6.1 Introduction

Lake-effect snow (LES) occurs as a result of a cold air parcel passing over a relatively warmer water body (lake), transferring heat (sensible and latent) and moisture fluxes from its body, and reaching saturation (Niziol et al., 1995; Kristovich et al., 2003). A similar mechanism applies to sea-effect snow (SES). For the analyses performed in this study, the expression "SES" was preferred instead of "LES". The parameters mentioned in this definition have important meteorological and physical effects in the occurrence of LES/SES events. These parameters are detailed as follows: the origin, moisture content and trajectory of the cold air mass; topographic structure and size of the water body over which the cold air passes; surface temperature of this water body; presence of an upper level mechanism that limits the vertical development of convection; wind speed/direction conditions on the water surface and upper atmospheric levels; wind shears between surface and upper atmospheric levels (850-, 700-hPa levels). In studies examining the effect of meteorological variables on LES/SES events, many case studies have been carried out for the Baltic Sea (Pike and Webb, 2020) and Black Sea (Yavuz et al., 2021a). In addition, climatological analyses were performed for the Black Sea (Yavuz et al., 2021b), Lake Michigan (Kelly, 1982), Lake Erie (Wiley and Mercer, 2020), Lake Ontario (Hartnett et al., 2014; Wiley and Mercer, 2020), Lake Tahoe (Laird et al., 2016), and Pyramid Lake (Laird et al., 2016). In the studies conducted 20th century, LES events have been subjected to various classifications by considering the morphological features of the LES bands and the structural characteristics of the LES events, as well as the determination of the atmospheric conditions in which they occur (Passarelli Jr and Braham Jr., 1981; Kelly, 1982; Braham Jr., 1983; Forbes and Merritt, 1984; Niziol et al., 1995). In the 21st

[5] This chapter is based on the research paper: Yavuz, V., Lupo, A.R., Fox, N.I. and Deniz, A. (2022). Statistical characteristics of sea-effect snow events over the western Black Sea. *Theoretical and Applied Climatology*. doi: 10.1007/s00704-022-04213-2

century, a different classification has been put forward by examining the structural characteristics of the LES events. Laird et al. (2009a) identified 67 LES events that occurred between 1997 and 2006 for Lake Champlain. Afterwards, the structural characteristics of these events were examined in three categories. These categories are as follows: a) LC-Events (well-defined precipitation occurring independently of synoptic/large-scale systems), b) SYNOP-Events (semi-stationary precipitation bands embedded within the synoptic-scale system), c) TRANS-Events (transition between two types). Later, Laird et al (2009b) identified 125 LES events for the New York State Finger Lakes, extending the three categories in the previous study to four categories. Unlike the previous study, Laird et al. (2009b) named the precipitation bands formed as a result of convergence on the lake as " Over Lake Convergence – OLC-Events". A very little or none of these precipitation bands, called the OLC, reach the shore. Finally, Laird et al (2016) identified 62 LES events over 14 winters for Lake Tahoe and Pyramid Lake. They classified these events in four different categories determined before, according to their structural characteristics. Alcott et al. (2012) used a similar classification to classify LES events according to their structural characteristics.

In the classifications made according to the morphological structures of the LES bands and the structural characteristics of the LES events in the following years, some similar situations are handled with different names. For instance, LC-Events and SYNOP-Events in the classification derived by Laird et al. (2016) are similar in structure to the Type-1,2,3 events classified by Niziol et al. (1995). Also, OLC-Events reflect the Type-5 event. In the literature review, a similar classification proposed by Niziol et al. (1995) was made for the western Black Sea by Yavuz et al. (2021b). However, no study could be found in which the classification of the SES events in the Black Sea according to their structural characteristics [similar classification to Laird et al. (2016)]. In general, the case studies were made in the SES studies for the Black Sea (Kindap, 2010; Yavuz et al., 2021a), and climatological analysis of synoptic conditions was performed using the Lamb Weather Type method (Baltaci et al., 2021).

SES occurring in the Marmara Region has negative effects especially on land, air and sea transportations. These effects are shaped by the meso- and synoptic-scale structure of the system. For instance, on 30-31 January 2012, when SYNOP-Events were effective over the Region, a total of 102 flights were cancelled at an international airport in the region. Sea transportation has been temporarily suspended. Dozens of roads were closed to transportation as a result of heavy snow accumulation (Yavuz et al., 2021a). In many events where Black Sea events (BS-Events) were observed, it was stated that the negativities affecting daily life were much more limited compared to Synoptic-scale events (SYNOP-Events) (Yavuz et al., 2022a). The main purpose of this study is to determine the meso- and synoptic-scale structures of SES events for the region and to form the basis for nowcasting and forecasting applications. Accordingly, first, the SES bands that occurred over the western Black Sea between 2009-2018 were analysed by using various satellite and radar products. Over a 10-year period, 95 SES events were identified and these events were classified according to their structural characteristics. After classifying events similar to those found in Laird et al. (2016), the atmospheric conditions in which the SES events occurred were analysed for each type. The data used in the study, the detection of the SES bands, and the classification method are defined in Section 6.2. Statistical results on classification types and atmospheric conditions (meso and synoptic scales) in which these types occur are given in Section 6.3. Finally, some prominent results were compared with similar studies made for different lakes and seas, and their similarities/differences are revealed in Section 6.4.

6.2 Data and Methodology

The study period was chosen as 10 years between 2009-2018. Snow events were determined by using aviation reports at four airports located in the Marmara Region during this period. Then, the availability of the SES events was investigated by using satellite and radar data for all snow events. Accordingly, no SES band could be detected in 2009. In 2014, only two SES events were detected. Although the determination of snow events from airport reports can be made much more than a 10-year period, satellite and radar images are needed to determine whether these snow events are SES events and to classify them. Difficulties in accessing satellite and radar data (especially radar products) and some airport reports were influential in the classification of the study period as 10 years. In addition, the fact that there are too many types of data sets in the study (for example, four images of two different satellites at 15-minute intervals and two images of radar at 7-minute intervals were examined for all snow events) required a heavy workload.

6.2.1 Study region

The Black Sea is bordered by Bulgaria and Romania to the west, Ukraine to the north, Russia and Georgia to the east, and Turkey to the south. Besides being a closed sea, it is also connected to the Marmara and Azov Seas. There is the western Black Sea in the north of the Marmara Region and the Marmara Sea in the south. The region, which has a strait connecting the Black Sea to the Marmara Sea, is home to Turkey's metropolitan city, Istanbul, and its strait connects the continents of Asia and Europe. The surface area of the Marmara Region is approximately 67000 km^2, and the area of the Black Sea is approximately 461000 km^2 (Demirarslan and Akinci, 2018). Especially in the winter season, most precipitation systems enter the region from the north. Therefore, the moisture transfer provided by the western Black Sea to the incoming systems plays an important role in the distribution of precipitation amounts and frequencies. Information about the Black Sea, Marmara Region, radiosonde station and the four airports in the Marmara Region is given in Figure 6.1 and Table 6.1.

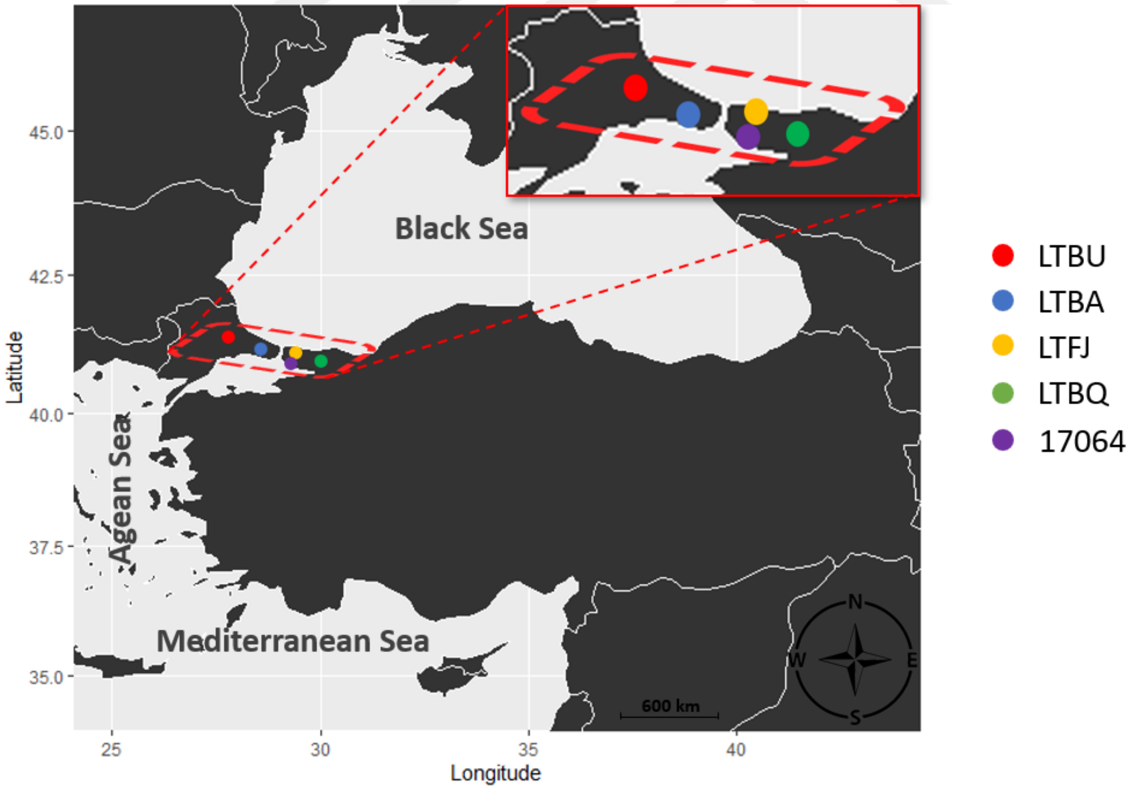

Figure 6.1 : Locations of the airports and the radiosonde station in the Marmara Region. LTBU: Tekirdag Corlu Airport; LTBA: Istanbul Ataturk International Airport; LTFJ: Istanbul Sabiha Gokcen International Airport; LTBQ: Kocaeli Cengiz Topel Airport; 17064: Istanbul Kartal Radiosonde Station.

Table 6.1 : Information about the airports and the radiosonde station.

	Station identifier	Latitude	Longitude	Elevation
Ataturk Int. Airport	LTBA	40°58′34" N	28°48′50" E	50 m
Sabiha Gokcen Int. Airport	LTFJ	40°53′39" N	29°18′30" E	95 m
Kocaeli Cengiz Topel Airport	LTBQ	40°44′10″N	30°5′0″E	55 m
Tekirdag Corlu Airport	LTBU	41°07′46" N	27°54′23" E	16 m
Istanbul Kartal Radiosonde Station	17064	40°54'41"N	29°09'21"E	20 m

6.2.2 Satellite and radar data

All of the satellite products were obtained for the snow events determined within the period. On the other hand, radar products were only available for the years 2014-2018. In the literature, satellite and radar images have been used in most of the studies on detecting SES bands, classifying them according to their formations and determining their trajectories. (Forbes and Merritt, 1984; Kelly, 1982; Kelly, 1986; Niziol, 1987; Niziol et al., 1995; Yavuz et al., 2021a; Yavuz et al., 2022a). In this study, the presence, type and trajectory of SES bands at frequent intervals were tried to be understood by analysing various images of both satellite and radar data. The first satellite product used in the study is high-resolution (0.25° × 0.25° latitude–longitude resolution) images of the Moderate Resolution Imaging Spectroradiometer (MODIS) module of Terra satellite. The MODIS module, which has 36 spectral bands in 0.4-14.4 μm band range (Zhao and Duan, 2020), generates images for the western Black Sea once a day. The images of the MODIS module were accessed from the National Aeronautics and Space Administration (NASA, 2021). The second satellite product used in the study is the satellite images in different channels obtained from the Spinning Enhanced Visible and Infrared Imager (SEVIRI) radiometer of the second-generation MSG-2 (Meteosat-9) and MSG-3 (Meteosat-10) satellites of the Meteosat satellite series. The SEVIRI radiometer produces images in four visible (VIS) and near-infrared (NIR) channels in the 0.4-1.6 μm band range, as well as eight infrared (IR) channels in the 3.9-13.4 μm band range (Trigo et al., 2011; Lazri et al., 2020). In this study, infrared band (Channel-9), visible band (Channel-321), and airmass satellite images were analysed. All satellite images were obtained from the Turkish State Meteorological Service (TSMS, 2021). Radar images used in the study are images of single polarized C-Band radar located in Istanbul-Catalca district. The Plan Position Indicator (PPI) and Max Display (MAX) images of the radar were analysed. The PPI product is a product related to the location and severity of the system. It scans 360° horizontally with a fixed elevation angle. During this scan, electromagnetic waves are sent to the atmosphere, and the signals (echo) received back from scattered objects in the atmosphere are measured. This product does not detect masses below and above the scanning area. For this reason, the MAX product, which uses a volumetric data set, has been examined for more detailed information about the state of the atmosphere. The MAX product is the product in which the maximum values measured by the radar between two horizontal levels are seen using the volumetric scan data (TSMS, 2021). Radar images were obtained from the Turkish State Meteorological Service (TSMS, 2021).

6.2.3 Satellite and radar data

In the study, the Meteorological Aerodrome Reports (METARs) and the Meteorological Aerodrome Special Reports (SPECIs) were obtained for four airports within the borders of the Marmara Region. The reason for choosing these airports is that they represent the majority of the Marmara Region from west to east, and they are the closest airports that meet the systems coming from the Black Sea. The reports were obtained from the IOWA Environmental Mesonet website of IOWA State University (IOWA, 2021). Almost all of the aviation reports (97% to 99%) were published within the period. Information on the airports for which METAR and SPECI reports were obtained for the years 2009-2018 is given in Table 6.1. Three of the four airports (LTBA, LTFJ, and LTBU) are in international and one airport (LTBQ) in the national airport categories. While the METAR reports are prepared at half-hourly intervals at international airports in accordance with regional agreements, these reports are mostly prepared hourly at national airports. The SPECI reports are prepared in the event of a meteorological phenomenon that adversely affects aviation activities between two METAR reports. METAR reports, on the other hand, are prepared in the event of a meteorological event that adversely affects aviation activities (events that reduce the visibility, presence of turbulence and strong wind/wind movements, icing) between two meta reports. These meteorological phenomena are usually heavy rainfalls/snowfalls, turbulence, strong/cross winds, icing, and fog. The most important reason for using aviation reports in the study is data quality and regular preparation of data at frequent intervals. In the study, actual temperature (T), dew point temperature (Td), relative humidity (RH), and wind speed (Ws) information were provided from these reports and used in the analyses.

In order to provide information about the general vertical structure of the atmosphere, inversion information, and wind conditions, the sounding data of Istanbul Kartal Radiosonde Station were provided for 0000 UTC and 1200 UTC for whole period. The data were obtained from the University of Wyoming Atmospheric Sciences website (University of Wyoming, 2021).

6.2.4 Atmospheric vertical level data

Apart from the sounding data, synoptic charts of the 850 hPa and the upper atmospheric levels (700, 500, and 300 hPa) were analysed in order to determine the air movements and to understand the synoptic-scale structure. Air advections, fronts, low/high pressure regions, divergence/convergence areas, and temperature/humidity gradients were analysed on 850 hPa charts. The positions, types and trajectories of long- and short-waves over the study area were determined by these constant pressure level maps provided at 6-hour intervals. The 500 hPa level has been taken as a reference in many studies in examining the effects of long-waves and associated short-wave troughs on SES events at the synoptic-scale (Turtle and Davis, 2013; Metz et al., 2019; Yavuz et al., 2022b). In this study, in addition to these levels, maps of 700 and 300 hPa levels were also examined in order to understand the vertical development of the existing structure along the vertical atmospheric column. Moreover, surface synoptic charts were analysed to examine the structure and position of the frontal systems, low/high pressure centres, and trough/ridge regions. All synoptic charts were obtained from the Plymouth State Weather Center website (PSWC, 2021).

6.2.5 SST data

In the study, the National Oceanic and Atmospheric Administration High-Resolution Blended Analysis (NOAA OI SST V2 High Resolution) dataset was used for the western Black Sea surface temperature information. The dataset was obtained from the Asia-Pacific Data-Research Center website (APDRC, 2021). The data represent daily mean values with a latitude-longitude resolution of 0.25° × 0.25° (APDRC, 2021). Within the scope of the study, the coordinate "29.50°E, 42.50°N" was preferred for the western Black Sea temperature data. The reason for this is that this point has been seen to show nearly an average value for the western Black Sea region (Yavuz et al., 2021a).

6.2.6 Detection of the SES bands

First of all, the aviation reports provided for the four selected airports were examined and snow events were determined throughout the entire period. Then, since radar images could not be obtained between 2009 and 2013, images in various bands obtained from devices belonging to the Terra and the MSG satellites were subjected to visual evaluation. For the years 2014-2018, both the mentioned satellite and radar products were subjected to visual evaluation together. In this visual evaluation, each SES class introduced by Laird et al. (2009a, 2009b, 2016) and Alcott et al. (2012) was taken into account. Thus, all SES bands that occurred over the western Black Sea region within the 10-year period have been examined regardless of whether it caused snowfall or not within the boundaries of the Marmara Region.

6.2.7 SES event classification

The classification introduced by Laird et al. (2009a, 2009b, 2016) and Alcott et al. (2012) (discussed in the Section 6.1) was taken as reference in the determination of the SES events. Visual analyses were made by considering the following conditions while classifying through satellite and radar images. First, the areas where the SES bands appear were determined, then the temporal and spatial analyses of the inland extensions along their trajectories were made. Then, the current precipitation conditions were determined by analysing the aviation reports both before and after the SES bands reached the study area. Thus, it was understood whether SES events are pure or not. Finally, the existence and effects of synoptic-scale structures were revealed by analysing the surface and upper level synoptic charts for each event from the moment the SES bands first appeared to the moment they passed into the disintegration stage. After this preliminary evaluation process, the SES events for the western Black Sea were divided into four types:

- BS-Events (Black Sea Events): These are well-defined events independent of any synoptic-large-scale system over the western Black Sea, with a generally widening structure from north to south, often occurring in more than one parallel band, parallel to flows from the north.
- OSC-Events (Over Sea Convergence): These are the events that usually occur in the middle parts of the western Black Sea, have little or no extension to the northern flows, and usually do not cause any snowfall in the borders of the Marmara Region.

- SYNOP-Events: They are events that occur with a synoptic and large-scale system (embedded within the system) or immediately after the transition of these systems, having the same morphological structure as the BS-Events, but containing stronger and denser bands. They occur under the influence of frontal systems (especially a cold front), low-high pressure centres (especially the low pressure centre and a cold front associated with it), and trough/ridge structure (mostly the part of the trough that represents the flows descending from the north) observed in the surface synoptic charts. In addition, the OSC-Events embedded in a synoptic/large-scale system and occurring immediately after their passages were transferred to the SYNOP-Events category.
- TRANS-Events (Transition Events): They are events that show the transition between different types (e.g., BS-Events – SYNOP Events, BS-Events – OSC Events).

In Figure 6.2, three different satellite images of the visual evaluation made in determining the Events are given. In the image of BS-Event, parallel band structures reaching the Marmara Region over the western Black Sea are seen in the approximately north/northeast-south/southwest direction. In the image of OSC-Event, band structures observed in different directions and in fragments on the western Black Sea, with a very slight extension to the Marmara Region are seen. In the image of SYNOP-Event, the structure consisting of many bands extending in the northeast-southwest direction, parallel to each other and reaching the Marmara Region is seen. The surface chart (the top left of the bottom figure) shows a low pressure centre located approximately in the south of the eastern Black Sea Region and an occluded front associated with it. It is seen that the front passes over the western Black Sea and the flows are in the same parallel with the bands in the satellite image.

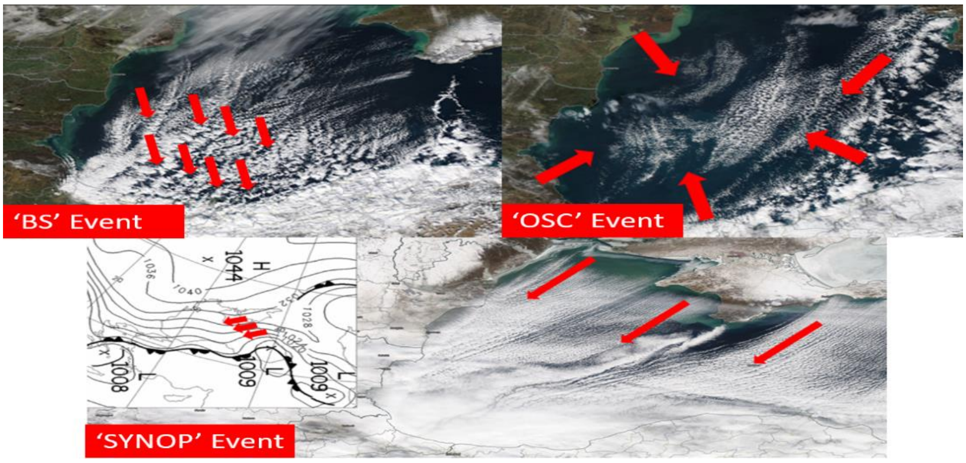

Figure 6.2 : Examples of a) BS-Event, b) OSC-Event, c) SYNOP-Event occurring on the western Black Sea.

In the study, statistical significance levels of the surface and upper-air meteorological variables were examined for each SES class. First, meteorological parameters were subjected to the normality test (Kolmogorov-Smirnov Test). Then, independent two-sample t-test was applied for the parameters that fit the normal distribution. The analysis results of the t-tests performed separately for each airport and SES class are given in Table 6.2.

Table 6.2 : The degrees of statistical significance of the data sets analysed in the study for each SES class.

	Parameter	Statistical significance difference (meaning)			N-size
		BS&SYNOP	***BS&TRANS***	***SYNOP&TRANS***	
LTBA	T (°C)	Not sig.	Statistically sig.	Statistically sig.	BS = 534
	Td (°C)	Statistically sig.	Statistically sig.	Statistically sig.	SYNOP = 782
	RH (%)	Statistically sig.	Statistically sig.	Statistically sig.	OSC = 392
	Ws (kt)	Statistically sig.	Not sig.	Not sig.	TRANS =32
LFTJ	T (°C)	Not sig.	Statistically sig.	Statistically sig.	BS = 662
	Td (°C)	Statistically sig.	Statistically sig.	Statistically sig.	SYNOP = 902
	RH (%)	Statistically sig.	Statistically sig.	Statistically sig.	OSC = 392
	Ws (kt)	Statistically sig.	Not sig.	Not sig.	TRANS = 36
LTBQ	T (°C)	Not sig.	Statistically sig.	Statistically sig.	BS = 394
	Td (°C)	Statistically sig.	Statistically sig.	Statistically sig.	SYNOP = 515
	RH (%)	Statistically sig.	Statistically sig.	Statistically sig.	OSC = 392
	Ws (kt)	Not sig.	Not sig.	Not sig.	TRANS = 30
LTBU	T (°C)	Not sig.	Statistically sig.	Statistically sig.	BS = 292
	Td (°C)	Statistically sig.	Statistically sig.	Statistically sig.	SYNOP = 334
	RH (%)	Statistically sig.	Statistically sig.	Statistically sig.	OSC = 392
	Ws (kt)	Statistically sig.	Not sig.	Not sig.	TRANS = 38
Over sea	$\Delta T_{850\text{-}SS}$(°C)	Statistically sig.	Statistically sig.	Statistically sig.	186
	$\Delta T_{700\text{-}SS}$(°C)	Statistically sig.	Statistically sig.	Statistically sig.	186

6.3 Results

6.3.1 Frequency, duration and classification of the SES events

As a result of the analysis of the METAR and SPECI reports of four airports between 2009 and 2018, it was found that it was snowy for 186 days. These days were examined using satellite and radar products, and the times of the SES band formation over the western Black Sea were identified. As a result, a total of 95 SES events were determined. The information on how long each event lasted is given in Figure 6.3. The mean duration of the SES events was found to be 15.9 hours. The longest SES event lasted 59 h. 38% of the events lasted 10 h or less, 68% of them lasted 20 h or less, and 86% of them lasted 30 h or less. Three events lasted more than 50 h. In studies for the Great Lakes, the average LES event duration was 12.1 h for the Lake Champlain (Laird et al., 2009a), 9.4 h for the New York State Finger Lakes (Laird et al., 2009b), 7.3 h for the Lake Tahoe (Laird et al., 2016), and 5.6 h for the Pyramid Lake (Laird et al., 2016). Alcott et al. (2012) studied 149 LES events for the Great Salt Lake and found the average event duration to be 11.3 h, also found that the events that occurred in the autumn and winter seasons lasted an average of 3.1 h more than those in the spring seasons. Steenburgh et al. (2000) stated that the LES event duration for the Great Salt Lake is often greater than 13 h, while for the Great Lake this time can be from 12 h to several days. It has been stated that this difference in event durations in different lakes and in the western Black Sea is related to the size of the water body and the fetch distance (Laird et al., 2016). It has been determined that the western Black Sea has a fetch distance of approximately 600 km (Kindap, 2010). The long fetch distance contributes positively to the occurrence of LES/SES events in terms of duration and severity (Laird and Kristovich, 2004; Smith and Boris, 2017). The main reason for this is that the amount of sensible and latent heat fluxes that the cold air mass will add to its body during its travel over the warmer water masses will be high (Ellis and Leathers, 1996; Scott and Sousounis, 2001).

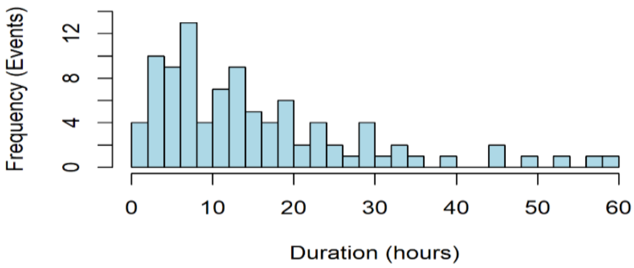

Figure 6.3 : Duration of the SES events.

The durations of the events for the four types identified based on the structural classification of the SES events were also analysed. Accordingly, the most lasting type on average was SYNOP-Events (27.8 h), followed by BS-Events (16.4 h), OSC-Events (8.5 h), and TRANS-Events (4.5 h). The longest lasting event type was SYNOP-Event (59 h) (Figure 6.4). In similar studies in the literature, the average longest event was mostly found as TRANS-Events. For TRANS-Events, Laird et al. (2009a) found this time as 16.6 h and Laird et al. (2009b) as 16.9 h. The most important reason why TRANS-Events had the longest duration was that after the events started as SYNOP-Events, they turned into LC/FL events that were not embedded in the synoptic scale (Laird et al., 2009a; Laird et al., 2009b). In this study, the main reason for the short duration of TRANS-Events was the requirement that the transitions between two different types in TRANS-Events continue uninterruptedly in the transitioned type. In this case, the transition period was determined as a maximum of 6 h without interruption (classification has been carried out in whichever type the switch is made after 6 h), and in interrupted cases (switching to the old type or another type within 6 h), the TRANS-Events category was continued until the uninterrupted condition was met again.

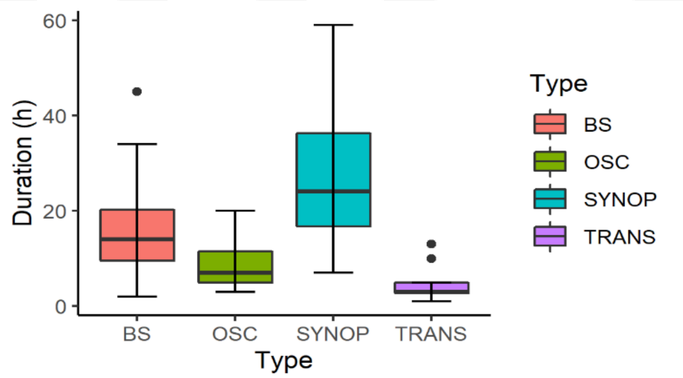

Figure 6.4 : Box plots showing distribution of duration (h) for a) BS-Events, b) OSC-Events, c) SYNOP-Events, d) TRANS-Events.

Annual and monthly frequency analyses of each type of the SES events are given in Figure 6.5 and Figure 6.6, respectively. Each year consists of its own months (Jan, Feb, Mar, and Dec). The greatest number of SES events occurred in 2016 (20 events) and at least in 2014 (2 events). No SES event occurred in 2009. No significant trend was detected within the period. Except for the years 2009 and 2014, at least three different types have been observed each year. On a monthly basis, the greatest number of events (51 events) occurred in January, followed by February (24 events), December

(18 events), and March (2 events). In other months, a SES event was not observed within the period. Except for the years 2009 and 2014, at least three events (average 7 events) occurred each year in January. Laird et al. (2009a) determined that the highest number of the LES events on a monthly basis were December, February and January, respectively. Laird et al. (2016) found that the most LES events occurred in October for the Lake Tahoe and the Pyramid Lake, respectively. It was also determined that at least 50% of the total LES events occurred in October and November. The main reason for this is that October events mostly occur in the last week of October (Laird et al., 2016), and the temperature differences between the air and the lake surface reach their maximum values during the end of October and November (Alcott et al., 2012). In this study, the number of events observed on a monthly basis and the temperature difference between sea surface (SS) and upper level air temperature (SS-850 hPa; SS-700 hPa) do not show one-to-one proportion. However, the highest average differences were observed in December and January, while February and March had relatively lower averages. It is a normal situation that there is no one-to-one overlap since the analysis was based on the dates of occurrence of SES events only. Considering the difference between SS and upper level air temperature on an average monthly basis for all years, it is thought that results close to those found in the literature, or one-to-one results, will be obtained.

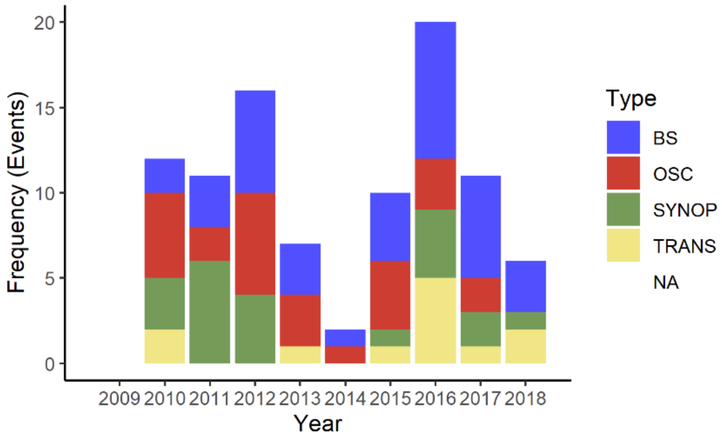

Figure 6.5 : Annual number of each type of the SES events.

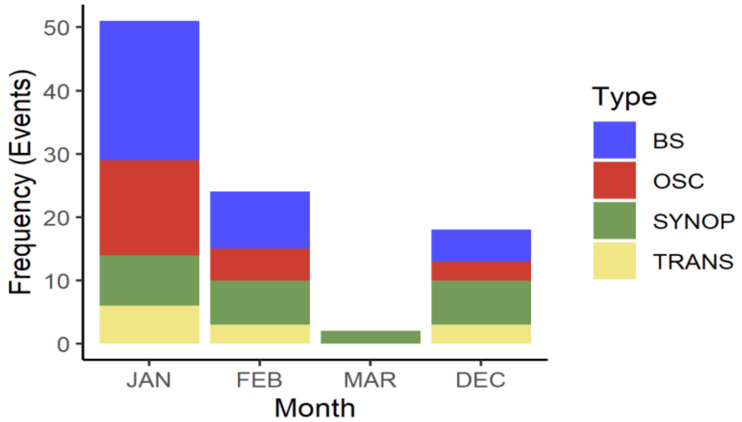

Figure 6.6 : Monthly number of each type of the SES events.

6.3.2 Factors affecting the occurrence of SES events

6.3.2.1 Surface conditions

An analysis was made using surface meteorological information from four airports for the times when the SES Events occurred. For each type of the SES events, analyses were performed for meteorological parameters obtained from the METAR and SPECI reports published by each airport. These meteorological parameters were T, Td, RH, and Ws. In the first analysis made, for each SES event, the analysis was made for the meteorological parameters measured during the event periods, regardless of whether there is precipitation at the airports or not.

In the analyses for actual temperature (T), the average values at four airports in BS-Events varied between -1.6 °C (LTBU) and 1.7 °C (LTBA). Temperature averages in OSC-Events were higher at all airports than in BS-Events. The highest and lowest averages occurred at LTBA (1.8 °C) and LTBU (-0.6 °C), respectively, similar to those in BS-Events. The lowest actual temperature values in SES types were observed at LTBU. In addition, the fact that it is farther from the Marmara Sea in its south compared to other airports causes terrestrial conditions to be more effective than others. This is due to the fact that the airport is located in the north compared to the other. While lower averages were observed mostly (except LTBQ) in SYNOP-Events, higher values were observed in TRANS-Events (Figure 6.7).

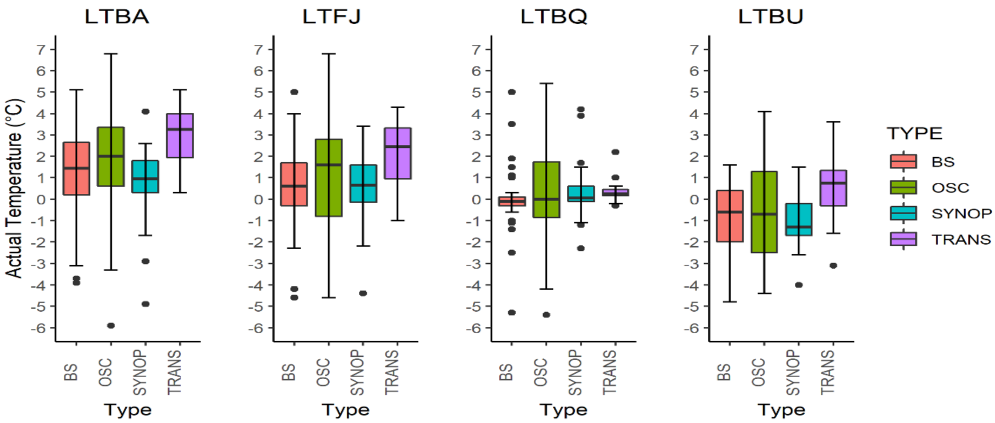

Figure 6.7 : Box plot of actual temperature (°C) at four airports for each type of the SES events.

In the analyses for dew point temperature (Td), the average values at four airports in BS-Events varied between -4.2 °C (LTBU) and -0.7 °C (LTBQ). Lowest and highest dew point temperature averages in OSC-Events occurred at airports similar to those at BS-Events. While higher average values were observed in SYNOP-Events compared to BS-Events (the opposite of the actual temperature), similarly, TRANS-Events had higher values after SYNOP-Events (Figure 6.8).

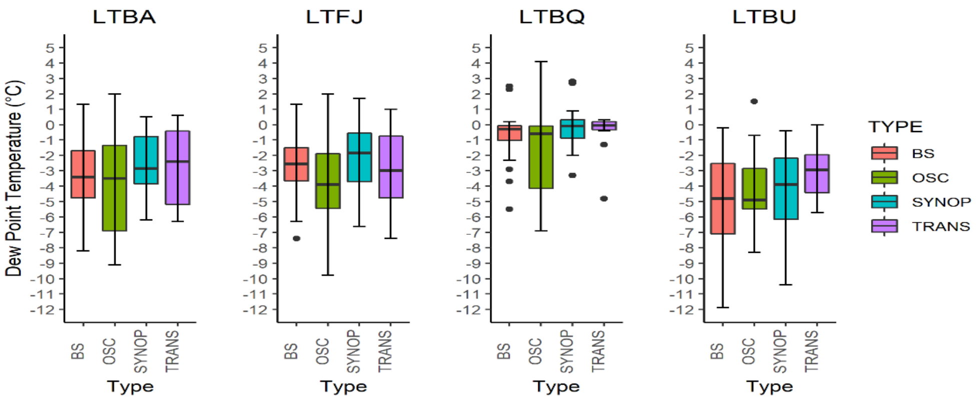

Figure 6.8 : Box plot of dew point temperature (°C) at four airports for each type of the SES events.

In the analyses for relative humidity (RH), the highest average values were observed in SYNOP-Events (between 74.6% and 93.9%) and BS-Events (between 73.4% and 92.1%) at almost all airports. The highest values among all events were observed at LTBQ (between 88.3% and 93.9%). It has been determined that relative humidity values in SYNOP-Events occurred in a narrower range compared to other events. (Figure 6.9).

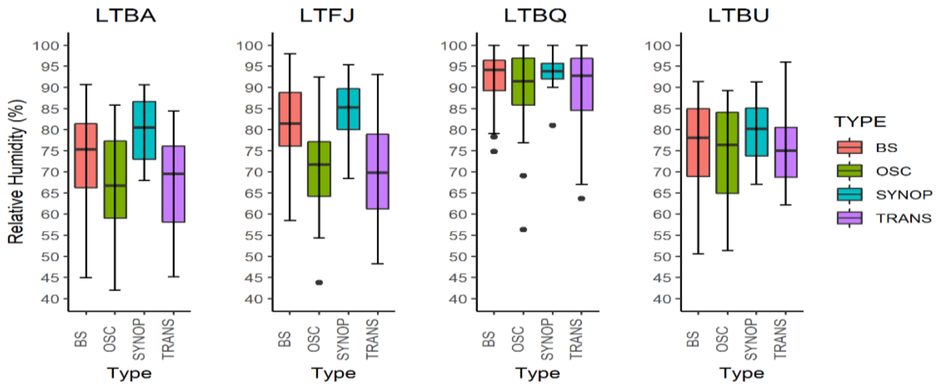

Figure 6.9 : Box plot of relative humidity (%) at four airports for each type of the SES events.

In the analyses for wind speed (kt), the highest average values were observed in SYNOP-Events at all airports. The lowest average values were found in OSC-Events. While the average wind speeds at all airports were 10 kt and above, this value was found to be 3.5 kt at LTBQ (Figure 6.10).

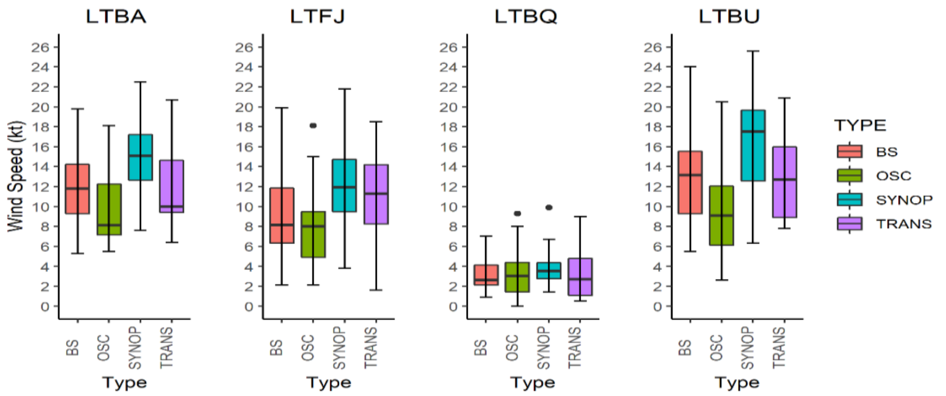

Figure 6.10 : Box plot of wind speed (kt) at four airports for each type of the SES events.

In the above analyses, meteorological parameter analyses for all SES events were carried out regardless of whether there was precipitation at the airports. Therefore, for each SES event, analyses of meteorological parameters at the airports during precipitation were also carried out. In this direction, first, the following results were obtained regarding the snowfall conditions at the airports:

- LTBA: Snowfall occurred in 24 (67%) of 36 BS-Events and 20 (83%) of the 24 SYNOP-Events. While there was no snowfall in OSC-Events, snowfall occurred in 1 (8%) of 12 TRANS-Events.
- LTFJ: Snowfall occurred in 31 (86%) of 36 BS-Events and 22 (92%) of the 24 SYNOP-Events. While there was no snowfall in OSC-Events, snowfall occurred in 1 (8%) of 12 TRANS-Events.

- LTBQ: Snowfall occurred in 31 (86%) of 36 BS-Events and 22 (92%) of the 24 SYNOP-Events. While there was no snowfall in OSC-Events, snowfall occurred in 6 (50%) of 12 TRANS-Events.
- LTBU: Snowfall occurred in 17 (47%) of 36 BS-Events and 14 (58%) of the 24 SYNOP-Events. While there was no snowfall in OSC-Events, snowfall occurred in 1 (8%) of 12 TRANS-Events.

In the light of this information, the average meteorological parameters' analyses at each airport both in snowy times and in the whole period independent of snow are given in Table 6.3. Analyses were only made for BS-Events and SYNOP-Events, since there was no snowfall at the airports in OSC-Events and TRANS-Events were not evaluated because of the low number. The actual temperature value was found to be lower than the average of the whole period during snowy times at all airports. A similar situation was not observed at the dew point temperature values. Relative humidity values were also observed to be higher mostly in snowy times than the whole period, and a trend was not observed in wind speed values.

Table 6.3 : Average values of T, Td, RH and Ws for BS-Events and SYNOP-Event during snowy times at airports and all times.

		Whole Period		Snowy Period	
	Airport	**BS**	**SYNOP**	**BS**	**SYNOP**
T (°C)	LTBA	1.2	0.7	0.2	0.2
	LTFJ	0.5	0.4	0.1	0.0
	LTBQ	0	0.4	-0.6	-0.3
	LTBU	-1.6	-1.9	-1.3	-2.7
Td (°C)	LTBA	-3.3	-2.6	-2.7	-2.3
	LTFJ	-2.5	-2.1	-1.7	-1.1
	LTBQ	-0.7	-0.2	-1.3	-0.9
	LTBU	-4.2	-4.3	-3.8	-5.0
R (%)	LTBA	73.4	80	82.3	86.0
	LTFJ	81.2	84.6	85.1	88.0
	LTBQ	92.1	93.9	94.2	95.5
	LTBU	76.5	79.3	83.5	84.5
Ws (kt)	LTBA	11.9	15.2	12.9	16.7
	LTFJ	9.2	12.3	9.2	12.5
	LTBQ	3.2	3.8	2.4	3.3
	LTBU	12.7	16.2	15.3	18.3

In the LES studies conducted for the Lake Champlain and the Finger Lakes, surface average actual air temperatures were -9 °C and -8 °C, respectively (Laird et al., 2009a;

Laird et al., 2009b). This value was found to be 5.7 °C on average for the Lake Tahoe and the Pyramid Lakes (Laird et al., 2016). Surface average dew point temperatures were -20 °C for the Lake Champlain (Laird et al., 2009a), -11 °C for the Finger Lakes (Laird et al., 2009b), -8.5 °C for the Lake Tahoe (Laird et al., 2016), and -11 °C for the Pyramid Lakes (Laird et al., 2016). In a study conducted for the Great Lakes Region, it was determined that the Lake Effect Rain event occurs when the surface temperature is greater than 0 °C (Miner and Fritsch, 1997). Laird et al. (2009a) determined that SYNOP-Events occur at higher temperatures on average than other events. At the same time, the temperature change range was wider in LC-Events than in SYNOP-Events. In this study, in the analyses made regardless of the snowfall situation for the whole period, the surface actual temperature values were above 0 °C on average at some airports, while it was almost 0 °C or below when snowfall was observed at the airports. Similar to the finding by Laird et al. (2009a), SYNOP-Events occurred at lower temperatures on average and narrower temperature ranges. The main reason for this is that SYNOP-Events occur before the polar or arctic air mass reaches the western Black Sea. The reason for the higher average temperatures at LTBA and LTBU in Istanbul compared to other airports is due to their proximity to the Marmara Sea, which is located in the south, and their location further south. In this study, the average relative humidity values for the snowy period and for the whole period were higher in SYNOP-Events than in BS-Events at all airports. A similar situation was also observed for the average wind speed values. Similar results were also found by Laird et al. (2009a) and Alcott et al. (2012).

6.3.2.2 Sea-atmosphere temperature difference

The temperature difference between SS and 850-hPa level occurred above 17 °C on average for all event types. In the literature, the 13 °C threshold value was used for this difference for the formation of LES events (Rothrock, 1969, Holroyd, 1971; Niziol, 1987, Ballentine, 1992; Villani et al., 2017). In this study, it was determined that this difference was around 13 °C in only five of the 95 events, and mostly higher differences occurred. The average temperature difference in BS-Events was higher than the others. Average temperature differences between SS and 700 hPa level were found above 23 °C. This value is well above the 17 °C threshold set forth in the literature (Niziol, 1987; Ballentine, 1992; Steenburgh et al., 2000; Alcott et al., 2012). Similar to the previous situation, BS-Events had higher differences than the others in almost all averages (Table 6.4). Sensible and latent heat fluxes moving from the SS to the atmosphere will cause degradation in the lower atmospheric layer, cloudiness and associated precipitation (Ellis and Leathers, 1996). The amount of perturbation occurring here will also increase depending on the temperature difference between the SS and the upper atmosphere, and low level atmospheric instability will occur (Scott and Sousounis, 2001).

Table 6.4 : The temperature difference between SS and upper-level air.

	Avg. Temp. Diff. (°C)		**Max. Temp. Diff. (°C)**		**Min. Temp. Diff. (°C)**	
	SS - 850 hPa	**SS - 700 hPa**	**SS - 850 hPa**	**SS - 700 hPa**	**SS - 850 hPa**	**SS - 700 hPa**
BS	18	24.6	22.8	32.4	13.2	15.6
OSC	17.1	23.2	20.5	31	11.8	16.9
SYNOP	17.6	25	21.1	30.1	12.7	15.1
TRANS	17.2	23.6	20.1	30.5	11.2	18

6.3.2.3 Inversion layer

One of the most important parameters in the occurrence of the LES/SES events is the necessity of a mechanism that will restrict the convectional movement occurring over water bodies at upper atmospheric levels. In this context, it has been suggested that an inversion or capping stable layer should exist (Reinking et al., 1993; Kristovich and Laird, 1998). This layer will contribute to the formation of cloudiness and precipitation by limiting perturbation and destabilization due to the transfer of heat and moisture fluxes in the lower atmosphere. While the formation of these layers between 850-700 hPa and 700-500 hPa levels has been put forward as the ideal situation, their occurrence between the surface and the first 150 hPa from the surface has been presented as a negative situation since it will limit the convective movement at very low heights (Steenburgh et al., 2000). In this study, for the specified events, the sounding data published within the period were analysed, and it was revealed whether there was an inversion for each event. The presence of inversion in this observation was given proportionally by examining how many sounding observations there were within the period covered for each event. Among all events, the highest rate of inversion was observed between 850-700 hPa, and the lowest rate was between surface-850 hPa levels (Table 6.5).

Table 6.5 : The frequency of inversions between 1000 hPa and upper atmospheric levels.

	Surface - 850 hPa	850-700 hPa	700-500 hPa
BS	14%	63%	44%
OSC	24%	67%	55%
SYNOP	20%	48%	40%
TRANS	25%	75%	46%

6.3.2.4 Wind shear

The directional change (Backing/Veering-Cyclonic/Anticyclonic) and the amount of this change (wind shear) of the wind that will occur between the surface/near-surface and the upper atmospheric levels (850 and 700 hPa) are some of the most important parameters affecting the structure, occurrence, and stability of the LES/SES bands. For this reason, the fact that the directional change of the wind is less than 30° between the surface and the 850 hPa level (Suriano and Leathers, 2017), and less than 60° between the surface and the 700 hPa level (Niziol, 1987), provides ideal and strong LES/SES band organizations. In this study, these criteria for BS-Events, SYNOP-Events and TRANS-Events were mostly met, but these criteria could not be met in OSC-Events that could not reach the shore due to the wind direction change over the sea (Table 6.6). Since there is no supporting synoptic-scale system in BS-Events, it is more important that the amount of wind shear is less in terms of band formation. In SYNOP-Events, on the other hand, the bands were able to maintain their formation in a few cases where the amount of wind shear was slightly above 60°, thanks to the synoptic-scale system. The main reason for this is that the synoptic-scale system affects the characteristics of these bands both in terms of the direction of the flow and due to the high heat and moisture fluxes it incorporates.

Table 6.6 : Wind direction variation between 1000 hPa and upper atmospheric levels.

	Wind Shear (1000-850 hPa)	Wind Shear (1000-700 hPa)
BS	35°	40°
OSC	60°	80°
SYNOP	40°	35°
TRANS	30°	45°

6.4 Discussion and Conclusions

In previous studies, Baltaci et al. (2021) analysed SES events for the Black Sea using a synoptic climatological approach and emphasized the dominance of northern flows. Yavuz et al. (2021b) classified the SES bands according to their morphological structures and examined the effects over the Marmara Region. Depending on the northern flows, the dominance of Type-2 (multi parallel) band (86%) came to the fore. Yavuz et al. (2021a) examined the Type-5 (meso-scale vortex) structure occurring in the western Black Sea and revealed the importance of SS fluxes and wind direction changes for convectional movements and especially for low-level convergence. This study is the first to reveal the structural characteristics of SES events for the western Black Sea region. In this context, classification methods similar to the studies made by Laird et al. (2009a, 2009b, 2016) and Alcott et al. (2012) were used, but significant variations were found in the results. In this study, the mean event duration occurred as 15.9 h. The closest long duration to this is 12.1 h for Lake Champlain calculated by Laird et al. (2009a). It has been shown that the size and fetch distance of the lakes are directly proportional to the average event durations (Laird et al., 2016; Smith and Boris, 2017). For the Black Sea, which has a fetch distance of approximately 600 km in the north-south direction and is much larger than these lakes, it is normal for the duration times to be high. Unlike similar studies, the most observed SES event for the western Black Sea was SYNOP-Events. This was followed by BS-Events and OSC-Events. In studies by Laird et al. (2009a, 2009b, 2016), SYNOP-Events were mostly in second place. The result of this study is that the western Black Sea (region) is more exposed to synoptic-scale systems, especially in the transition route of northwest-southwest systems. During the SES times, the frontal systems mostly coming from the northern directions, the fronts connected to the low pressure centres over the eastern Black Sea, and the surface level troughs are the mechanisms that make up the SYNOP-Events.

The two most important parameters for SES events are the temperature difference between SS and the upper level air, and a mechanism that will limit the convectional movement that will occur due to this difference above. With regard to the temperature difference, mostly (95%) the 13 °C threshold (between SS-850 hPa), and the 17 °C threshold (between SS-700 hPa) were exceeded. On average, these values were 17 °C and 23 °C, respectively. Therefore, it has been determined that most of the time, fluxes (heat and moisture fluxes) from the SS to the upper atmosphere cause lower atmospheric destabilization. It is also known that perturbation and lower atmospheric instability will increase depending on the increase in temperature differences (Scott and Sousounis 2001). It is very important to restrict this lower level convectional movement and instability occurring at higher levels. The presence of an inversion layer is important for cloudiness and precipitation, especially the presence after the first 150 hPa from the surface (below it would be an early limitation) (Steenburgh et al., 2000). In this study, low rates of inversion were generally observed in BS-Events and SYNOP-Events (14-20%) at the lower level, while this rate was considerably higher in the middle and upper levels (48%-63%).

One of the most important results of the study is that more than half of all events occurred in January. The reason for this is that cold air masses descending from the north pass over the Black Sea more frequently, and meanwhile, sea surface temperatures have positive anomaly values. Another important result of the study is the changes observed in the temperature, dew point temperature and relative humidity values at the airports with and without precipitation. In snowy times, lower temperature and higher relative humidity values were determined compared to the whole period. Also, the whole period temperature average at LTBA was about 0.9 °C during whole period (BS-Events and SYNOP-Events on average), while it was 0.2 °C during snowy times. Therefore, one of the biggest reasons why snow was not observed at LTBA in the presence of BS-Events and SYNOP-Events was the course of surface temperatures around 0.9 °C.

7. THE ROLE OF SHORT-WAVE TROUGHS ON THE FORMATION AND DEVELOPMENT OF SEA-EFFECT SNOWBANDS IN THE WESTERN BLACK SEA [6]

7.1 Introduction

Sea/Lake-effect snow (SES-LES) is a meteorological phenomenon that occurs simply as a result of air-sea interaction, causing extreme instability and snowfall (e.g., Niziol et al., 1995; Bard and Kristovich, 2012; Laird et al., 2017). As the cold air mass passes over the warmer water surfaces (e.g. lake and sea), a temperature gradient occurs between the water surface and the air mass. The temperature gradient allows the transfer of heat and moisture fluxes from the water surfaces to the upper atmosphere. Thus, an unstable boundary layer is formed at the lower tropospheric levels due to the cold air mass destabilized by fluxes and thermal energy (Niziol, 1987). This boundary layer is shaped by the lower atmospheric level wind direction/intensity, the shape of the water body, the water surface temperature, the upper-atmospheric-level air temperature, the convection intensity, and the presence of a layer limiting the convection (Hjelmfelt, 1990; Niziol et al., 1995; Markowski and Richardson, 2010). All these aforementioned parameters directly affect the shape and trajectory of the SES/LES bands and the amount of precipitation they cause (Niziol et al., 1995; Yavuz et al., 2021a). The size of the water body increases the distance (fetch) travelled by the cold air mass. Accordingly, more time is created for the transfer of heat and moisture fluxes from the water surfaces, which increases the intensity of the SES bands (Wiggin, 1950; Dockus, 1985; Smith and Boris, 2017). Local winds due to topographic structure (e.g., mountain-valley breezes) and winds due to intraday atmospheric variations (land-sea breezes) help increase coastal convergence. In this context, convection increases in the mixed layer and intensifies the existing SES/LES bands (Pike and Webb 2020). Synoptic-scale structures (low-high pressure centres, short-

[6] This chapter is based on the research paper: Yavuz, V., Lupo, A.R., Fox, N.I. and Deniz, A. (2022). The role of short-wave troughs on the formation and development of sea-effect snowbands in the western Black Sea. *Theoretical and Applied Climatology*. 149, 501-510, doi: https://doi.org/10.1007/s00704-022-04071-y

long-wave troughs, fronts, etc.) play an important role in increasing the severity of the existing SES/LES. In the SES/LES bands that occur under the influence of these systems, a significant increase is observed in the intensity of the bands, their duration, and the amount of precipitation they cause (Özdemir and Yetemen, 2019, Yavuz et al., 2021a). Finally, the limitation of the unstable convective layer formed with meso- and/or synoptic-scale systems at the upper atmospheric levels is important for cloud/band formations. For this reason, the presence of inversion layer(s) between 850-700 and/or 700-500 hPa is vital for band formation (Niziol, 1987; Mahoney and Niziol, 1987; Kunkel et al., 2002). The fact that this layer does not form at the first 150 hPa from the surface (Surface-850 hPa) is also important in terms of not restricting convection at an early stage and increasing the intensities of SES/LES bands (Steenburgh et al., 2000).

In the studies conducted for the Great Lakes Region of America, the Japan Sea and water bodies influencing Europe, most changes in the lower atmospheric levels were analysed in the SES/LES analyses. Although the lower atmospheric level conditions are important in the formation phase of the SES/LES bands, the changes in the upper atmospheric level also play a role in the formation of the bands, the trajectory it follows, and the amount of precipitation it causes (Ellis and Leathers, 1996; Notaro et al., 2013). The presence, type and position of a long wave of 500 hPa over a region affects the SES bands (Yavuz et al., 2021b). Similarly, short-wave troughs that occur due to long waves play a more active role (Metz et al., 2019). Atmospheric waves are of two types, long (Planetary or Rossby) and short waves (AMS, 2021). Rossby waves are slow-moving waves with a length of about 6,000-8,000 km, which develop due to atmospheric circulation and westerly winds. Short waves are shorter than 6,000 km in length and move faster (37-55 km.h-1) than long waves (e.g., AMS, 2021). It is seen that long and short waves have different effects on the synoptic characteristics of heavy snowfalls. Long-wave troughs and cut-off-low (COL) can affect the severity and duration of existing SES/LES systems. Most importantly, the short-wave troughs located within these long waves directly affect the SES/LES systems with their movement depending on the long wave orientation. In addition, short waves contribute to cyclogenesis (e.g., Kocin et al., 1995). On the other hand, long waves, including those associated with different configurations of blocking (e.g., Rex Blocking, Omega Blocking, Blocking High) has an effect on the formation of extreme precipitation (e.g., Sousa et al., 2017; Rabinowitz et al., 2018; Efe et al., 2019). In studies on heavy snowfalls, a systematic relationship was found between the amount of precipitation and the vorticity maxima of 500-hPa level (Goree and Younkin, 1966; Hanks et al., 1967). The presence and trajectory of the 500-hPa level vorticity maxima have been one of the most important indicators in determining the presence and position of the short-wave troughs that form due to the long wave (Younkin, 1968). The cyclonic vorticity advection occurring just in front of the short-wave trough increases the upward forcing at the lower tropospheric level and causes the atmosphere to destabilize at these levels (Niziol et al., 1995; Holton and Hakim, 2013). Depending on the deepening of the convective boundary layer and the rise of the inversion layer, the amount of precipitation increases where the vorticity maxima is observed (Niziol et al., 1995). Therefore, short-wave troughs are among the most important synoptic-scale structures that provide upstream support to existing SES/LES systems. Although studies on this subject are limited in the literature, Metz et al. (2019) revealed the climatology of seven cold season short-wave troughs and their relationship with LESs. As a result, he stated that short waves survived on the Great Lakes for an average of 24 h, and 65% of these waves were found on at least four lakes during the times of LES. In addition, it has been determined that the number of short-wave troughs being much higher in some years is due to the presence of long waves that are effective on the region for a long time.

There are studies on the climatology of the atmospheric blocking events in association with temperature, including extreme temperature, and precipitation conditions for Turkey. The result of these studies is that many times long-term blockings are effective throughout the country, especially in the winter season (Efe et al., 2019; Efe et al., 2020a, 2020b). It is thought that blocking may influence the development and formation of SES bands that develop due to longitudinal flows to the northern parts of Turkey over the western Black Sea.

Yavuz et al. (2021a) classified the SES bands on the western Black Sea according to their formation. Five types of band structures were detected, and the most common band type found was Type-2 (85%). Type-2 is a band type with a width of 5-20 km and a length of 20-50 km, in which more than one band occurs over a long fetch distance parallel to the wind. The difference from the Type-1 band is that it has a longer fetch distance and more than one parallel band. Type-3 is a hybrid band type that is a mixture of Type-1 and Type-2 (Niziol et al., 1995). Yavuz et al. (2021a) determined that the bands formed almost 95% parallel to the wind (Type-1 and Type-2). Therefore, it is obvious that short-wave troughs and long waves will have an important role on SES bands. In the studies examining the relationship between atmospheric circulation types and precipitation for the Marmara Region, it was revealed that the northern circulation types (NW, N, NE) are dominant for the region in terms of both precipitation frequency and amount in winter season (Baltaci et al., 2015; Baltaci et al., 2017). Also, Baltaci et al. (2021) revealed the effect of synoptic-scale systems in heavy SES in Istanbul province, located in the northwest of Turkey. Besides, many case studies (Kindap, 2010; Özdemir and Yetemen, 2019; Yavuz et al., 2021b) and climatological analyses (Yavuz et al., 2021a; Baltaci et al., 2021) were carried out for western Black Sea effect snowfalls, but no study was found regarding the support of the upper atmospheric level in SES band formation.

The aim of this study is to determine the upper-level mechanisms in the formation of SES bands in the western Black Sea region. In this context, various statistics were made of short-wave troughs and long waves on the western Black Sea in the presence of SES bands between 2010-2018 using the SES band climatology determined by Yavuz et al. (2021a). Short-wave troughs were divided into five classes depending on the direction of movement and long wave relations, and analyses were carried out on a monthly and annual basis for each class. Then, their durations were examined and their relationship with long waves was examined. Statistical analyses were also carried out for long waves. The importance of each short-wave trough in the air-sea interaction was investigated, and the effects of short-wave trough and long waves on SES band types were revealed.

7.2 Data and Methodology

7.2.1 Data

The western Black Sea (also known as the Danube Sea Area) is the western part of a closed inland sea (the Black Sea) located in the north of the Marmara Region, where Turkey's most industrially and economically developed provinces are located, on the longitudinal transit route of polar and arctic air masses in winter. Heavy snowfalls occurring in many provinces (not only in the Marmara Region, but also in the Black Sea Region), especially in Istanbul, occur due to the SES bands of western Black Sea origin with a long fetch distance. Its length in the north-south direction is approximately 600 km and its width is approximately 450 km (Figure 7.1).

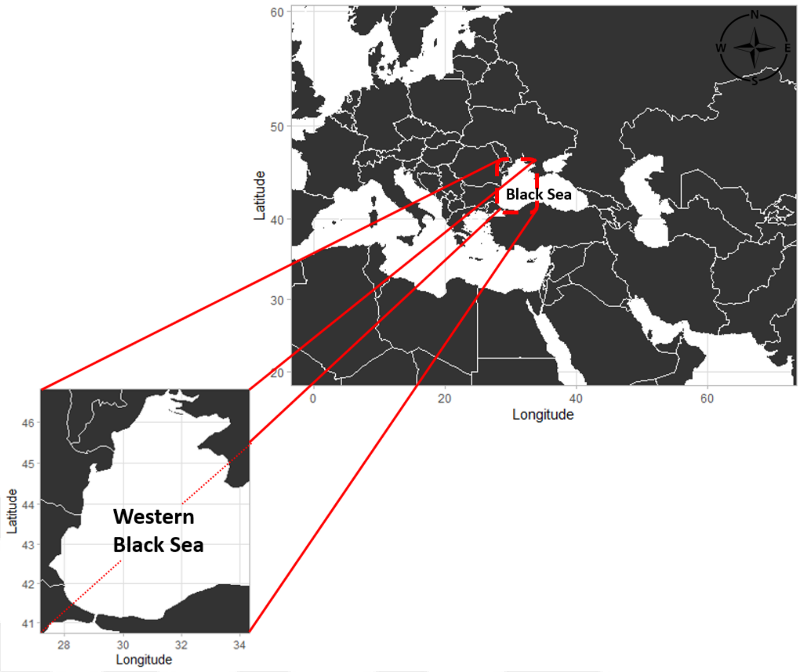

Figure 7.1 : The study area.

In the study, first, sounding data was used to obtain upper-level atmospheric information. In this direction, the data of the Istanbul Kartal Radiosonde Station was provided within the period (University of Wyoming, 2021). These data were used in the determination of inversion layers and in the analysis of meteorological parameters at certain levels (e.g. 850-, 700-, and 500-hPa). The 500-hPa charts were analysed to determine upper atmospheric level long and short waves (University of Wyoming, 2021; Wetter3, 2021).

Finally, sea surface temperature (SST) information was examined to determine the air-sea interaction. The daily average temperature values for the western Black Sea surface were analysed using National Oceanic and Atmospheric Administration (NOAA) High-Resolution Blended Analysis data. The data has a latitude-longitude resolution of 0.25° × 0.25° (APDRC, 2021).

7.2.2 Methodology

The SES band type climatology introduced by Yavuz et al. (2021a) was used in the western Black Sea SES band analyses. Upper atmospheric level analyses were carried out based on the data set of the SES bands, which were put forward for the snowy periods in the Marmara Region between 2010-2018 and classified according to their formations. In the first stage of the study, geopotential heights, wind-height fields, and absolute vorticity parameters of 500-hPa level were analysed in order to determine the short-wave troughs. Since all products were produced at intervals of 6-h, analyses were made at this interval. Several criteria set forth in the literature were used to determine short-wave troughs. These are: a) the cyclonic curvature is visible in 500-hPa wind and height fields, b) the curvature width is limited to a maximum of 1,500 km, and c) the maximum absolute vorticity amount in the curvature is minimum 18×10^{-5} s^{-1} (Tuttle and Davis, 2013; Metz et al., 2019). In the examination of the atmospheric charts of 500-hPa level at 6-h intervals, no short-wave trough definition was made if any of the above-mentioned criteria were not met. These criteria and the determination of short-wave troughs were made on the western Black Sea. After the short-wave troughs were determined in this way, their durations and orientations were determined. In determining the direction of short-wave trough movement, the temporal variation of the point where the vorticity maximum and the axis of the trough intersect was examined. Based on the direction the short-wave trough comes from, it was classified into five different categories. "W" type for troughs coming from the west, "NW" type for troughs coming from north-west, "SW" type for troughs coming from the south-west, "LWT" type for troughs with variable movement due to the long wave, and the "COL" type troughs that meets the three aforementioned criteria (also known as cut-off-low). Monthly- annual analyses, and the durations of troughs were determined for each trough type.

In the second stage of the study, the effects of the upper atmospheric level support on the SES band formations were investigated. Analyses of the temperature difference between the upper atmospheric levels and sea surface (SS) were carried out to examine the change in air-sea interaction in the presence of short-wave troughs. The presence and level of a high-level limiting mechanism due to increasing baroclinity (increase in instability and temperature gradient) and convection in the transitions of short-wave troughs, which are characterized by their maximum absolute vorticity, were also analysed.

In the last stage of the study, analyses of long waves were carried out. For each event, the average geopotential charts were prepared to cover the period, and analyses were made. The National Centers for Environmental Prediction (NCEP) Reanalysis II was used as the data set. This data is provided free of charge by the NOAA Physical Sciences Laboratory four times a day at 17 pressure levels (NOAA, 2021). Unlike the analyses made in short-wave troughs, the types of long waves were determined by looking at their formations on the western Black Sea for each event. Apart from the long-wave troughs, atmospheric blockings were also observed, and these were also classified according to their types. In this context, long waves are evaluated in five different classes. These are: Positive tilted trough (PPT), Negative tilted trough (NTT), and blocking anticyclone or cut-off-low (COL). The axis of the PTT is in the northeast-southwest direction, and the NTT is in the northwest-southeast direction. Atmospheric Blocking is typically characterized as Rex-type or Omega-type events. The Omega-blocking was named because it resembles the Greek Letter omega (Ω). It consists of a combination of two COLs and a blocking-high. The Rex-blocking is characterized by a high-pressure system located over a low-pressure system. The COL refers to stable low-pressure areas disconnected from the main flow (NWS, 2021).

7.3 Results

7.3.1 Classification, frequency, and duration of the short-wave troughs

In the analyses made for the western Black Sea between 2010-2018, a total of 48 short-wave troughs were determined. "NW" type short-wave troughs were observed at the highest rate, while cut-off-lows were the least observed type. "LWT" type troughs, whose direction of movement changed due to long waves, dominated the region in the presence of a significant amount of SES band (Figure 7.2). In similar analyses for the Great Lakes Region, Metz et al. (2019) determined the "W" type short-wave troughs mostly occurred, and attributed the main reason for this to the direction of the upper-level jet streams throughout the region. Similarly, in this study, it was expected that westerly and north-westerly short-wave trough movements were observed due to the fact that the upper level jets and the general prevailing wind direction of the region are north-west.

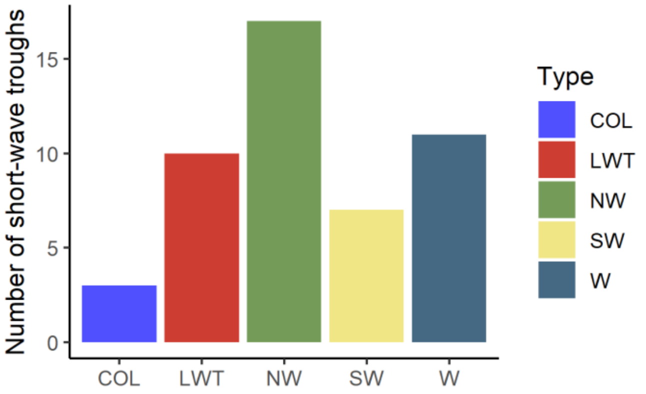

Figure 7.2 : The total number of each type of short-wave trough in the western Black Sea.

In the annual analyses, it was determined that an annual average of 5.3 short-wave troughs crossed over the western Black Sea during the period (Each year is evaluated as January start and December end). No short-wave trough was observed in 2014 when SES bands were observed (this is because the SES band only occurred once this year), and the highest number of troughs (11 short-wave troughs) observed in 2012. While "NW" type short-wave trough was observed in all years except 2014, it was determined that "LWT" type troughs, whose direction of movement was determined by long wave, were observed at least once in all years except 2018 (Figure 7.3). When the "COL" type short-wave trough was detected in 2012, a meso-scale vortex SES band, also known as Type-5, was observed over the western Black Sea.

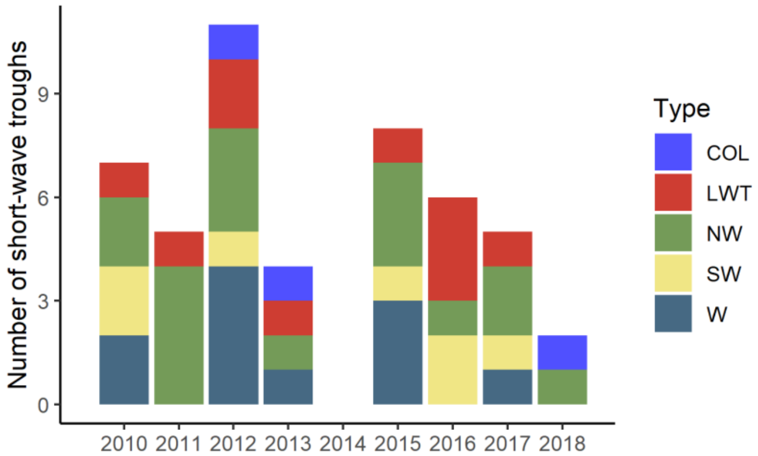

Figure 7.3 : Annual number of each type of the short-wave troughs in the western Black Sea.

In monthly analyses, it was determined that short-wave trough occurred mostly in January (56%), followed by February (23%), December (17%) and March (4%), respectively. According to Yavuz et al. (2021a), since there was no snowfall in the other months and there was no SES band analysis, the analyses related to the short-wave trough were made only for the specified months in this study. While all five types of troughs were observed in January, all types were observed in February and December, except for the "COL" type. In March, only two short-wave troughs were detected, and they were of the “NW” type (Figure 7.4). Metz et al. (2019) observed short-wave trough and LES bands for six months of the year in the Great Lakes Region, and found that “W” and “LWT” type troughs were dominant in all of these months. Generally, an increase trend was observed from October to December and then a decreasing trend towards March. In this study, similarity could not be found due to the fact that far fewer SES events occurred compared to the Great Lakes Region.

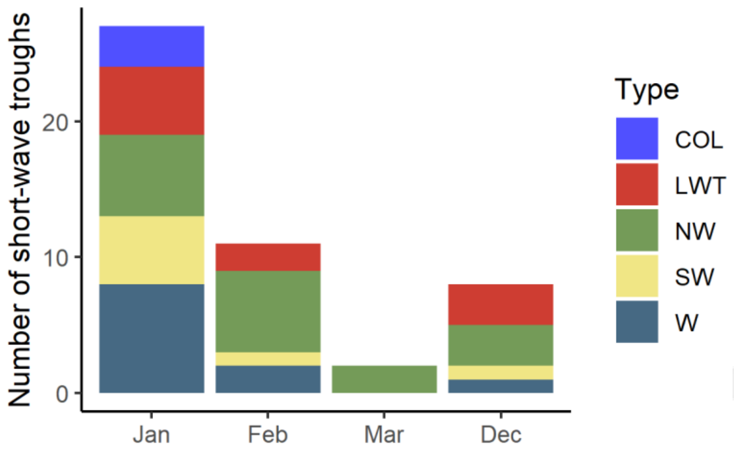

Figure 7.4 : Monthly number of each type of the short-wave troughs in the western Black Sea.

In the western Black Sea, the average duration of short-wave troughs was 27.8 h during the periods when SES bands were observed. While the shortest duration of trough was 6 h, the longest duration of trough was 60 h. On average, the longest durations were observed in the "COL" type (44 h), on the other hand, the lowest durations were observed in the "NW" type (21.2 h) and "SW" type (23.1 h). The “LWT” type with a maximum duration of 60 h was also the short-wave trough with the widest distribution in terms of durations (Figure 7.5). Metz al. (2019) found the average duration for the Great Lakes Region to be 24 h, and observed short-wave troughs lasting a minimum of 6 h and a maximum of 123 h. The short-wave trough type that lasted 123 h was the "COL" type. In this study, the average durations were determined close to Metz al. (2019) found, moreover, the longest duration similarly was seen in the "COL" type.

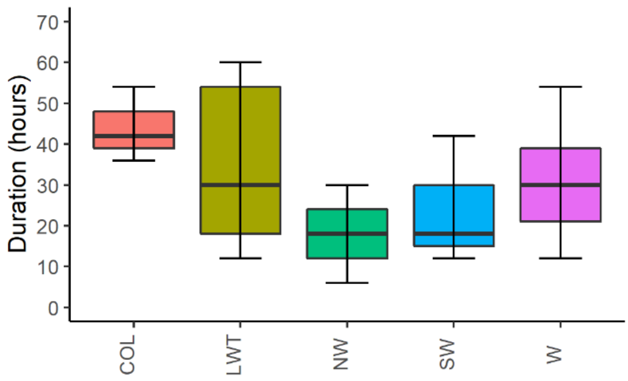

Figure 7.5 : The duration of each type of the short-wave troughs in the western Black Sea.

In the duration of the short-wave troughs on a monthly basis, the longest average duration was found in January (average 29.1 h), February (average 25.6 h), December (average 24 h), and March (average 21 h), respectively. The longest duration occurred in January (60 h), while the shortest duration occurred in December (6 h) (Figure 7.6). Metz al. (2019) stated that shorter durations occur in November and December, while the longest durations occur in October and March. While no large differences were observed in terms of average duration in this study, a wider range was observed in January and February.

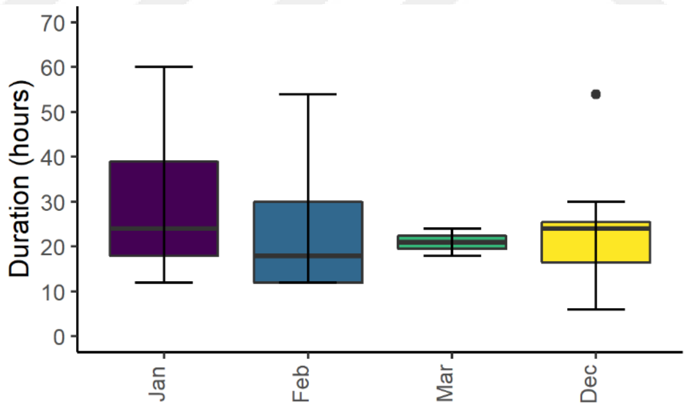

Figure 7.6 : The duration of each type of the short-wave troughs during each month in the western Black Sea.

7.3.2 Short-wave troughs and vertical atmospheric changes

The effects of each type of short-wave trough on air-sea interactions (the temperature difference between upper atmospheric levels and sea surface), and on inversion levels due to baroclinity (increase in instability and convection) were analysed. Different average values and oscillations stand out for each trough type between the air temperatures in the upper atmosphere (T_{850} and T_{700}) and sea surface temperatures (SST). The $\Delta T_{850\text{-}SS}$ has the highest value (18 °C) in "COL" type, also the narrowest oscillation occurred in this type. In the "LWT" type, both the highest $\Delta T_{850\text{-}SS}$ value (21.2 °C) and the widest oscillation were observed. The average $\Delta T_{850\text{-}SS}$ value was 17.7 °C. The lowest average $\Delta T_{850\text{-}SS}$ value was observed in the "NW" type (16.3 °C), while the average values similar to "LWT" were observed in the "SW" and "W" types. In the $\Delta T_{700\text{-}SS}$ analysis, the highest average value was found in the "LWT" type (25.7 °C), and the lowest average value was found in the "NW" type (23.1 °C). The largest change in terms of oscillation was again in the "LWT" type. The highest value was observed in the "W" type (30.7 °C). The increase in the temperature difference between the upper atmospheric levels and sea surfaces has been stated in many studies as a factor that both intensifies the SES bands and increases the amount of precipitation. (Jiusto and Kaplan, 1972; Niziol, 1987, Hjelmfelt, 1990; Hjelmfelt, 1992; Niziol et al., 1995; Yavuz et al., 2021a, 2021b). This value should be a minimum of 13 °C for $\Delta T_{850\text{-}SS}$ and a minimum of 17 °C for $\Delta T_{700\text{-}SS}$ (Hjelmfelt, 1992; Niziol, 1987; Niziol et al., 1995). In this study, the minimum values in the literature were fully met. The average $\Delta T_{850\text{-}SS}$ value was 17.3 °C and the average $\Delta T_{700\text{-}SS}$ value was 24.8 °C. These average values made heavy SES band formations and heavy precipitation possible (Figure 7.7).

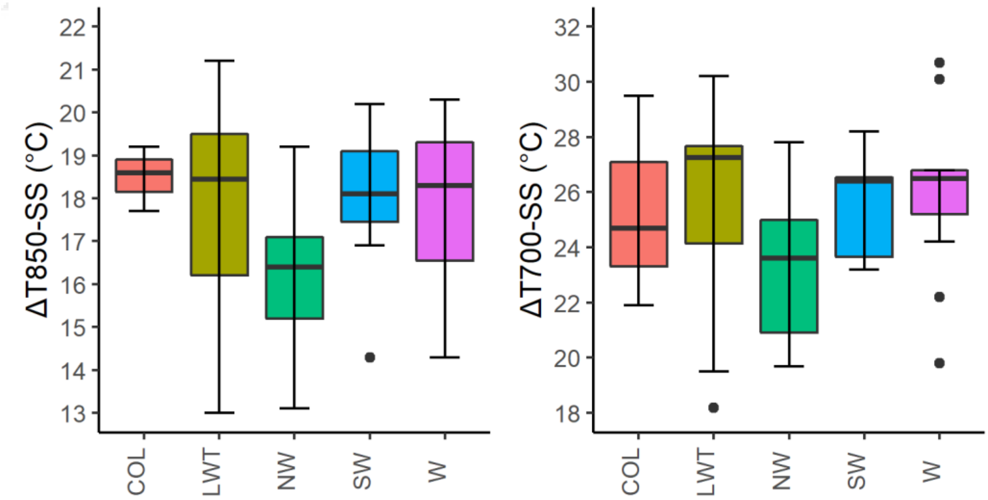

Figure 7.7 : Temperature difference between upper atmospheric levels and sea surface (850 and 700 hPa) during the observation of each type of the short-wave troughs.

The inversion layer is of great importance in limiting the increased convection above and providing this criterion necessary for the formation of SES bands. While the presence of inversion layer in the first 150 hPa (from the surface) is stated as a negative factor as it restricts convection early (Hjelmfelt, 1990; Steenburgh et al., 2000), it is known that inversion layers at higher levels from 850 hPa level increase the strength of the SES bands and have a positive effect on the precipitation amount. (Rothrock, 1969; Niziol, 1987; Hjelmfelt, 1992; Reinking et al., 1993). In the analysis of the short-wave troughs and the levels where the first inversion layer was seen, it was found that the first inversion occurred at an average of 781.8 hPa level in all trough types. Except for the "COL" type, the average values in other types showed oscillation in the range of 770 – 790 hPa levels. In the "COL" type, the average of 824 hPa was found. As a result, when the average values and oscillations of the heights where the first inversion layer was found in all types were examined, it was observed that the inversion layers cut the mixing layer (convective boundary layer) at the upper atmospheric levels (Figure 7.8).

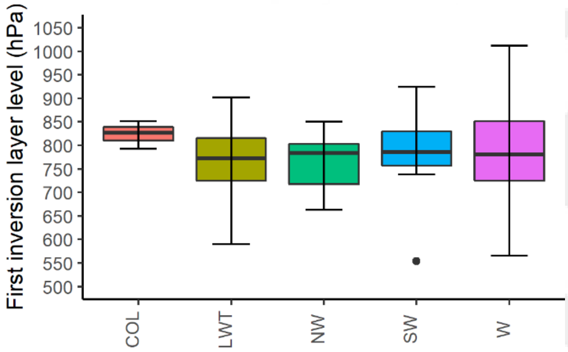

Figure 7.8 : First inversion layer levels (hPa) during the observation of each type of the short-wave troughs.

7.3.3 Long-wave types and their effects on short-wave troughs

Long waves affect the type and direction of travel of short waves. The centres and durations of short-wave troughs also vary depending on long waves. In this study, the long waves observed when there were SES bands were divided into five types (Section 7.2.2). "Omega" and "Rex" blockings in this classification are known as atmospheric blocking types. Atmospheric blocking is expressed as the presence of air parcels in a region for a long time (Aalijahan et al., 2019; Brunner et al., 2018). In the analysis made with long-wave numbers, it was observed that the least number of long waves were observed in blocking types and "NTT" type (Figure 7.9). This may be one of the reasons why durations or lifespans of short-wave troughs were short on average. Because in the analysis made for each short-wave trough types, the average duration was calculated as 27.8 h, and in the presence of blocking type long waves, this duration was 31.5 h on average. In "PTT" and "COL" long-wave types, short-wave troughs mostly appeared in the northwest of the western Black Sea and continued their transition with western (north/southwest) movements.

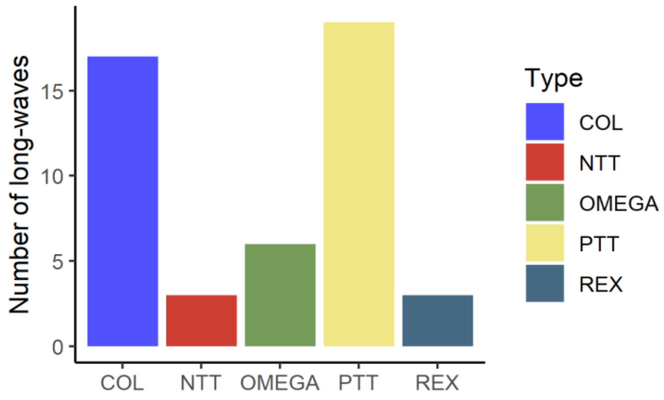

Figure 7.9 : The total number of each type of long wave in the western Black Sea.

7.3.4 The effect of short-wave troughs and long waves on the SES band type

According to Yavuz et al. (2021a), Type-2 band was the most observed (85%) SES band type over the western Black Sea. It was determined that Type-2 bands mostly occur in the north-south, northwest-southeast and northeast-southwest directions. In this type, in which more than one parallel band was observed, the positions of the short-wave troughs and the long waves that manage them on the western Black Sea were highly similar to the detected band trajectories. In the presence of SES bands concurred with short-wave troughs, 79% of bands were found to be Type-2. In the presence of SES bands concurred with long waves, 77% of bands were found to be Type-2. These were followed by Type-3 with 10% in both short-wave troughs and long waves (Table 7.1).

Table 7.1 : The SES band types detected over the western Black Sea for each event where short-wave troughs and long waves were observed.

	Band type	Type-1	Type-2	Type-3	Type-4	Type-5
Long-waves	COL	-	16	3	2	-
	NTT	-	3	-	-	-
	OMEGA	-	6	-	-	1
	PTT	-	19	3	-	-
	REX	1	2	-	1	1
Short-wave troughs	COL	-	3	1	-	1
	LWT	1	10	2	1	-
	NW	-	15	-	1	-
	SW	1	7	1	1	1
	W	-	10	2	-	-

7.4 Discussion and Conclusions

This is the first study to examine the short-wave trough and long wave climatology of the western Black Sea region for sea-effect snow events. Although the direct effect of long waves on the formation and characteristics of SES bands is limited, short-wave troughs that arise due to these waves have important effects. These effects are generally; the increase in instability in the atmospheric boundary layer (increasing baroclinity), change of position and structure of wind fields and restrictive upper level mechanisms in the layer, changes in the types and orientation of SES bands depending on the aforementioned effects.

It was determined that short-wave troughs and long waves play an active role in the region in almost all times when the SES bands were observed in the western Black Sea. The most important effect of long waves was that they play a role in the formation of short-wave troughs on the region, and also carried arctic and polar air masses over long distances thanks to their length/oscillations. Therefore, most of the short-wave troughs that arose due to long waves on the region occurred within the cold air mass coming from the north. The movements of most short-wave trough types with western component were observed on the region (SW, W, NW). A part of it consisted of "LWT" type, which was exposed to direction changes due to long waves. The prevailing north-westerly wind direction of the region and upstream jets also play a major role in this distribution. Long waves have an effect on the determination of the average duration of short-wave troughs. Atmospheric blocking was observed in a small part of the long waves, mostly "COL" and "PTT" types were dominant. In the presence of atmospheric blocking, the average duration of short-wave troughs increased over the region, this was due to the long-term presence of an air parcel on a region due to the nature of blocking.

The movements of the long-waves, mostly with a western component, caused the short-wave troughs that develop due to them to emerge especially in the northwest of the western Black Sea and moved towards the southeast. Accordingly, more than one SES band parallel to each other (parallel to the sub-inversion level wind direction) followed the north-south and northwest-southeast trajectories over the region. According to Yavuz et al. (2021a), it was found that 85% of the SES bands over the western Black Sea between 2009-2018 occurred as Type-2 and 10% as Type-3. In this study, 79% of the SES bands in the presence of short-wave troughs and 77% of the SES bands in the presence of long waves were Type-2. In a case where a “COL” type short wave was observed, a meso-scale vortex structure (Type-5), which did not reach the shore, was observed on the western Black Sea. This is a result of the positive contribution of short-wave troughs to baroclinity by increasing convergence. Changes in the atmospheric boundary layer over the sea, depending on the increasing baroclinity, also determine the band structure and trajectories. Similarly, Type-4 band, also known as shoreline parallel band, was formed by the effect of the “COL” type long waves having a western component along the coast to cover the entire western Black Sea. A support was provided to the formation of a parallel band to the coast by contributing to coastal convergence. Similar structure was also observed in “Omega” blocking. In short-wave troughs, the parallel structure of the northwest and southwest components (NW, SW) and the movement of the “LWT” type along the “COL” type long wave also contributed to the coastal convergence and the formation of Type-4 bands.

In the presence of short-wave troughs, it was found that the convective boundary layer deepened and there were high temperature differences between the upper atmospheric levels and the sea surface. The occurrence of convection-restricting inversion layers at high levels increased the baroclinity and caused the bands to intensify. Also, the high temperature differences made it possible to transfer heat and moisture fluxes from the sea surfaces to the air mass above in greater quantities. Therefore, in the presence of these two conditions, a positive contribution was made to the SES bands. The most important mechanism triggering these situations was the high amount of vorticity and the associated cyclonic vorticity advection in regions with short-wave troughs.

8. MESO-SCALE COMPARISON OF NON-SEA-EFFECT AND SEA-EFFECT SNOWFALLS, AND DEVELOPMENT OF PREDICTION ALGORITHM FOR MEGACITY ISTANBUL AIRPORTS IN TURKEY [7]

8.1 Introduction

It is seen in many regions around the world that arctic, polar, and similar cold air masses incorporate heat and moisture fluxes depending on the temperature difference during their passage over any water body (e.g., lake, sea, and ocean) and leave this moisture loading in the form of snowfall on their route (Kristovich et al., 2000; Kunkel et al., 2002; Cordeira et al., 2008). These snowfalls are expressed in the literature as lake-effect snow (LES) and sea-effect snow (SES) depending on the type of water source. Many studies of LES for the Great Lakes and Great Salt Lake (in the USA) are available in the literature. In the first studies, atmospheric conditions for LES formation were analysed (Wiggin, 1950; Petterssen, 1956), and the effects of meso- and synoptic-scale mechanisms were investigated (Peace and Sykes, 1966; Niziol, 1987). Afterwards, operational forecasting methods were developed (Niziol, 1987; Dockus, 1985), climatological analyses were performed (Alcott et al., 2012; Laird et al., 2016), and model projections were created (Theeuwes et al., 2010; Notaro et al., 2015; Saslo and Greybush, 2017). Regarding the SES, analyses were performed for the Japan Sea (Estoque and Ninomiya, 1976; Veals et al., 2019), Caspian Sea (Nicholls and Toumi, 2014; Ghafarian et al., 2017; Ghafarian, 2021), Adriatic Sea (Stocci and Davolio, 2017), Baltic Sea (Olsson et al., 2018), and Black Sea (Kindap 2010; Yavuz et al., 2021a; Yavuz et al., 2021b; Baltaci et al., 2021). In these studies, similarly to those in the Great Lakes, the atmospheric conditions, climatology, and predictions of SES were investigated. The SES event that occurred in eastern Massachusetts (in the

[7] This chapter is based on the research paper: Yavuz, V., Lupo, A.R., Fox, N.I. and Deniz, A. (2022). Meso-Scale Comparison of Non-Sea-Effect and Sea-Effect Snowfalls, and Development of Prediction Algorithm for Megacity Istanbul Airports in Turkey. *Atmosphere*. 13(5), 657, doi: https://doi.org/10.3390/atmos13050657

USA) in 1999 was one of the rare events with the effect of ocean forcing (Waldstreicher, 2002).

In studies on the determination and prediction of precipitation types (rain, snow), the most important meteorological parameter was the critical air temperature value (Collins et al., 2004; Özgür and Koçak, 2019; Özgür and Koçak, 2021). In addition, discrimination can be made based on particle characteristics using remote sensing products (satellite and radar images) (Grenfell and Putkonen, 2008). In order to make a similar distinction between snowfall and LES/SES, threshold values of various meteorological parameters were set, and operational classifications were made according to the morphological characteristics of snow bands using remote sensing products. The threshold values for some key parameters in LES and SES in the literature are as follows:

- Fetch distance: The distance that the cold air parcel travels over the relatively warmer water body should be long enough (Wiggin, 1950; Niziol, 1987; Eichenlaub, 1970; Jiustı and Kaplan, 1972; Kristovich and Laird, 1998; Fujisaki-Manome et al., 2017). This distance determines how much heat and moisture flux will be taken from the lake/sea surface (LS/SS) (Andersson and Gustafsson, 1994; Mazon et al., 1994). The amount of snowfall increases depending on the increase in this distance (Petterssen 1956; Kelly, 1982). For enhanced lake/sea effect snow, the fetch distance should be at least 80 km. If there is no synoptic scale support, this distance should be a minimum of 160 km for pure LES (Dockus, 1985).
- Inversion layer: The existence of a mechanism that limits the convection that starts on the water body at higher levels often contributes to the development of LES/SES and increases their intensity (Petterssen 1956; Rothrock, 1969; Niziol et al. 1995). It also affects their morphological structure and trajectory (Niziol, 1987). The formation of this layer in the range of 1000–850 hPa has a negative effect, as it will limit the convection early. Accordingly, band formations cannot be observed, or weak bands occur (Hjelmfelt 1990; Laird et al. 2009; Steenburgh et al., 2000). When the inversion layer is deeper and located at higher atmospheric levels, the unstable layer deepens, allowing the LES/SES to increase in intensity (Niziol, 1987; Reinking et al., 1993).

- Temperature difference: The high temperature difference between the upper level air parcel and the LS/SS is one of the most important parameters for LES/SES band formation (Lavoie, 1972; Passarelli and Braham, 1981; Hjelmfelt and Braham, 1983; Hjelmfelt 1992; Wiley and Mercer, 2020). It was revealed that the difference between 850 hPa and LS/SS should be a minimum of 13 °C (Kunkel et al., 2002; Niziol, 1987; Rothrock, 1969; Niziol et al., 1995; Laird et al., 2009; Holrody, 1971), while the difference between 700 hPa and LS/SS should be a minimum of 16–17 °C (Niziol, 1987; Steenburgh et al., 2000; Carpenter, 1993). It was also stated that vertical fluxes of momentum, heat and moisture decrease depending on the decrease in temperature differences (Jiusto and Kaplan, 1972).
- Wind speed and direction: Variations in wind speed and direction between LS/SS and upper levels play an important role in the formation, development and dissipation of LES/SES bands (Niziol, 1987; Carpenter, 1993; Steenburgh and Onton, 2001; Laird et al., 2003; Laird and Kristovich, 2004). The difference in wind speed has two different consequences. If the wind speed is high, more heat and moisture flux are transferred from the LS/SS to the air parcel. However, there is not enough time for this transfer at short fetch distances. Therefore, high wind speeds at long fetch distances and lower wind speeds at short fetch distances contribute positively to band formation (Lang et al., 2018). Suriano and Leathers found the average wind speed for the Great Lakes to be between 8–17.3 kt (Suriano and Leathers, 2017); Campbell and Steenburgh found this value to be 5.8–11.7 kt for Tug Hill in New York State, USA (Campbell and Steenburgh, 2017). Directional wind shear of 60° and below between 700 hPa and LS/SS supports band formation, while higher changes cause bands to disperse (Niziol, 1987; Kristovich and Laird, 1998; Steenburgh et al., 2000). Stronger band formations are observed at 30° wind shear and below (Niziol, 1987; Suriano and Leathers, 2017; Ghafarian et al., 2021).
- Heat Fluxes: One of the most important factors in the formation of LES/SES is how much heat and moisture flux will be transferred from the warm water surfaces to the air parcel above. Due to the air–sea interaction, heat and moisture fluxes moving from the water surfaces destabilize the lower atmospheric layer (Gerbush et al., 2008), and a shallow convection layer forms

(Niziol et al., 1995; Scott and Sousounis, 2001; Markowski and Richardson, 2010). This layer generally varies according to the downstream wind direction and strength, the shape of the water body, and the presence of synoptic-scale systems (Niziol et al., 1995). Lang and co-workers stated that the sensible and latent heat flux values for Lake Erie and Lake Ontario were 50–150 W m^{-2} at times with LES (Lang et al., 2018), while Sousounis and Mann determined that wind speeds in the range of 10–15 kt on the lake produce sensible and latent heat flux in the range of 200–500 W m^{-2} (Sousounis and Mann, 2000).

- Humidity: In LES/SES studies, specific and relative humidity parameters were analysed. Wiley and Mercer (2000) found that the specific humidity value is in the range of 2.5–3.0 g kg^{-1} in heavy snowfalls in the Great Lakes (Wiley and Mercer, 2020). Relative humidity values were determined as 80–90% at 850/700 hPa levels for the heavy snowfalls due to SES (Yavuz et al., 2021a; Yavuz et al., 2021b).

Throughout the history of Istanbul, snowfalls have sometimes become a meteorological disaster. In the first half of the 20th century, the Bosphorus, the Golden Horn, and the dams were frozen, which prevented electricity and water needs from being met (Yavuz et al., 2007). In 1987, snowfalls that continued for days under the effect of cyclone and atmospheric blocking caused snow depths in the order of meters. Electricity and water cuts were experienced, and disruptions and cancellations occurred in all types of transportation (Tayanç et al., 1998). In the 2000s, heavy snowfall occurred four times, and snow depths between half a meter and one meter were measured in areas affected by cyclone and SES bands. Especially in the 21st century, snowfalls have negatively affected aviation activities at airports in Istanbul. These effects can often lead to flight cancellations and various accidents or incidents. In a study examining the accident-incident reports in the European region between 2005 and 2014, the effect of weather conditions was found to be 15% among the accident-causing factors. Most of the adverse weather conditions were the occurrence of events that reduce horizontal visibility (heavy snowfall and rainfall, fog) and cause icing (Yavuz et al., 2015). In this study, an analysis of snow events that took place in Istanbul was performed. Between 2009–2018, SES and non-SES events were differentiated using satellite images for the snow events determined from the two airport reports. Then, the threshold values were determined due to the changes in meteorological parameters (surface air temperature, surface dew point, relative humidity, pressure, wind speed/direction), the results of air–sea interaction (sea surface temperature—SST, specific humidity, latent and sensible heat fluxes, inversion layer), and the changes in the amount of snowfall (snow depth). The goal of the study was to develop an algorithm that will allow nowcasting and forecasting of SES events at both airports. Accordingly, information in the literature on SES events and the meteorological parameters affecting them is presented in Section 8.1; the study area, airports, and the data used were introduced, and the method is specified in Section 8.2. Statistical analyses of SES and non-SES events were performed at both airports during the period, snow depth analyses were conducted for both event types, and a 12-item algorithm was developed to identify SES events, as presented in Section 8.3. Finally, general evaluations of the results of the study are given in Section 8.4.

8.2 Materials and Methods

The meso-scale analysis of snow events that occurred in Istanbul province between 2009–2018 was carried out. Istanbul is located in the Marmara Region, which is the most economically and industrially developed region of Turkey. While Black Sea climate features are observed in the northern parts of Istanbul with hot summers, mild winters and precipitation in all seasons and Mediterranean climate characteristics are observed in the southern parts with hot, dry summers and warm, rainy winters. A large part of the population in the province is located in the southern part of the region. In the city, which does not have significant elevation, precipitation variability is observed in the north–south direction. Istanbul is the only city that has a coastline on the Black Sea and the Marmara Sea, has the Bosphorus between these two seas, and has land on both the Asian and European continents. Istanbul Atatürk International Airport (ICAO Code: LTBA) and Istanbul Sabiha Gökçen Airport (ICAO Code: LTFJ) are located on two different continents. Their height above sea level is in the range of 50–100 m (IMM, 2021). The Istanbul Kartal Radiosonde station, where meteorological parameters of the upper atmospheric levels were provided, is located on the Asian continent and is at approximately sea level. The information about the study area, the airports and radiosonde station where the data were provided, and the specific points determined on the western Black Sea are shown in Figure 8.1.

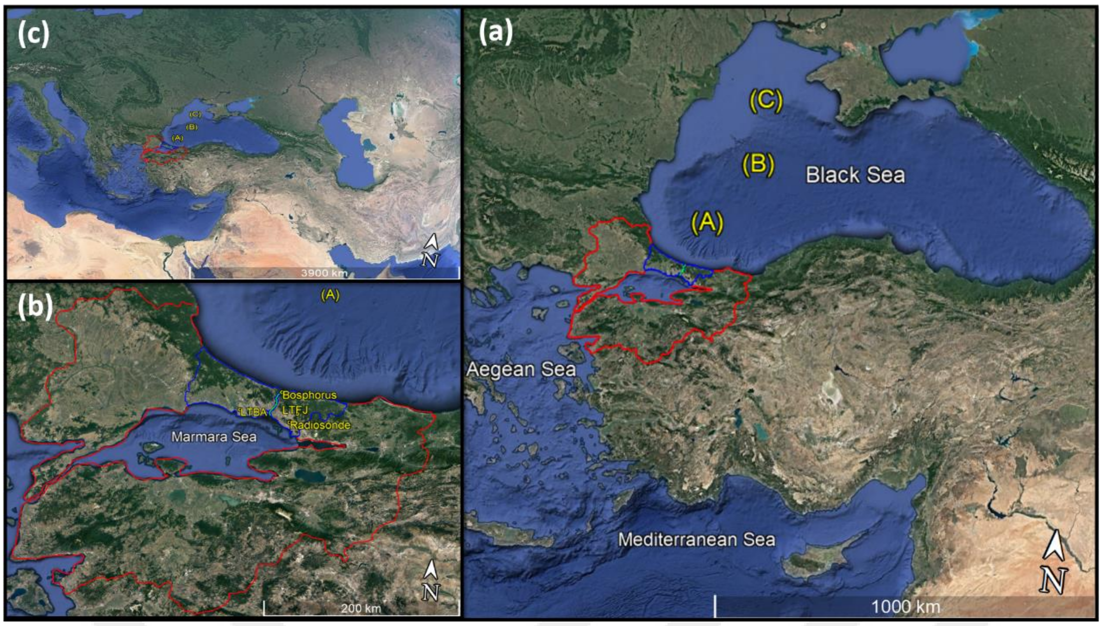

Figure 8.1 : Study area. The large black rectangle shows the study area (a), the black square in the lower left shows the study area in detail (b), and the black square in the top left shows the study area in large scale (c). The area covered with red lines shows the Marmara Region. The area covered with blue lines within the red lines shows Istanbul. The green line, which cuts the blue lined area almost in half, represents the Bosphorus. The west of this line is the European Continent, and the east is the Asian Continent. The locations of LTBA, LTFJ, and Istanbul Kartal Radiosonde Station are indicated in the figure. The coordinate information of points A, B, and C are as follows, respectively: 29.5° E, 42.5° N; 30.5° E, 43.5° N; 30.5° E, 44.5° N.

The Meteorological Aerodrome Reports (METARs) and the Meteorological Aerodrome Special Reports (SPECIs) published by the LTBA and LTFJ were obtained from the IOWA Environmental Mesonet website accessible by Iowa State University (IOWA, 2021). Since both airports are international airports, METAR reports contain real data published at half-hourly intervals. SPECI reports are published when situations affecting aviation activity arise between two METAR reports. The air temperature (T), dew point (Td), relative humidity (RH), pressure (P), snow depth, wind speed (Ws), and wind direction (Wd) data from surface level meteorological parameters were provided from these reports for the years 2009–2018. The information on the upper atmospheric level meteorological parameters (T, Td, Ws and Wd at 850, 700 and 500 hPa levels; inversion layers between surface–850 hPa, 850–700 hPa, and 700–500 hPa) was obtained from the sounding data provided by the Istanbul Kartal Radiosonde station. These data are the actual observation data obtained from the measurement devices connected to a meteorological balloon that is sent into the atmosphere twice a day (at 0000 and 1200 UTC). These data were accessed from the

University of Wyoming Atmospheric Science’s website (University of Wyoming, 2021).

After the determination of snow events in Istanbul, various satellite images were used to distinguish between the SES and non-SES events. At this stage, the study in which SES bands were classified according to the morphological structure within the same period for the same study area was taken as reference (Yavuz et al. 2021a). Satellite images of all times with snowfall were re-examined and confirmed by the method of detecting LES bands by means of satellite images for the eastern United States (Niziol et al. 1995). First, the Moderate Resolution Imaging Spectroradiometer (MODIS) module images of the Terra satellite were examined. Although this module offers high resolution (0.25° × 0.25° latitude–longitude resolution) images, it only provided one image per day for the study area. The images from the module were obtained from the National Aeronautics and Space Administration (NASA) (NASA, 2021). Then, some of the second-generation MSG-2 and MSG-3 satellite products of the Meteosat satellite series were analysed. MSG-2 and MSG-3 provide images at 15 min intervals, covering the continents of Europe and Africa. In this study, satellite images on different channels of the spinning enhanced visible and infrared imager (SEVIRI) radiometer on the MSG-2 and MSG-3 satellites were evaluated. Infrared (channel 9), visible band (channel 321) and airmass satellite images were analysed in detail throughout the entire period at 15 min intervals. These data have a resolution of 3 km (Zhao and Duran, 2020). The SEVIRI radiometer images used in the study were obtained from the Turkish State Meteorological Service (TSMS) (TSMS, 2021).

The SST information was obtained from NOAA High-Resolution Blended Analysis in order to analyse air–sea interactions. The data with a latitude–longitude resolution of 0.25° × 0.25° were analysed for three different points (“A”: 29.5° E, 42.5° N; “B”: 30.5° E, 43.5° N; “C”: 30.5° E, 44.5° N) determined in the western Black Sea within the entire snowy period. The data consist of a global scale grid of multiple observation data obtained from satellites, buoys, and floats. The data, which present average daily SST values, were obtained from the Asia-Pacific Data-Research Center (APDRC) (APDRC, 2021). In addition, in order to detect the heat fluxes from the SS to the upper atmosphere, sensible and latent heat flux data at the level of 1000 hPa were obtained for the three points (A, B, C) determined in the study from the Woods Hole Oceanographic Institution (WHOI)—Objectively Analyzed Air-Sea Fluxes (OAFlux) data set. Specific humidity data for the 1000 hPa level were also taken from the same data set. The data set is a product created by integrating satellite observations, ship reports, and atmospheric model data run with reanalysis data. All of these data are presented as daily average values (WHOI, 2021).

In the study, statistical significance levels of the average values were examined for all discrete data sets analysed for SES and non-SES events (except for wind direction information and inversion conditions). Data belonging to the same meteorological parameter from both even types were first subjected to a normality test (Kolmogorov–Smirnov test). Since no significant deviation from the normal distribution was observed in all of the data sets, the t-test was applied. p-values and interpretations obtained by applying the independent two samples t-test are given in Table 8.1.

Table 8.1 : The degrees of statistical significance of the data sets analysed in the study for SES and non-SES events.

	Parameters	**t-test P-values (95% confidence interval)**	**Statistical significance difference (meaning)**
LTBA	T (°C)	0.1089	Not significant
	Td (°C)	0.0001	Statistically significant
	Ws (kt)	0.1423	Not significant
	R (%)	0.0064	Statistically significant
	P (hPa)	0.0001	Statistically significant
LTFJ	T (°C)	0.0771	Not significant
	Td (°C)	0.0001	Statistically significant
	Ws (kt)	0.1576	Not significant
	R (%)	0.0006	Statistically significant
	P (hPa)	0.0011	Statistically significant
Over Sea	ΔT_{SS-850} (°C)	0.0001	Statistically significant
	ΔT_{SS-700} (°C)	0.0001	Statistically significant
	ΔWS_{SS-850} (kt)	0.0893	Statistically significant
	ΔWS_{SS-700} (kt)	0.0046	Statistically significant
	SH (g/kg)	0.0001	Statistically significant
	SHF (W/m^2)	0.0001	Statistically significant
	LHF (W/m^2)	0.0001	Statistically significant

At the end of the study, a 12-item algorithm was developed for LTBA and LTFJ to be used in the operational estimation of SES events. The algorithm was then validated with reference to a total of three different SES events that occurred separately and simultaneously at both airports. In these events, the algorithm scored 11 out of 12 (92%) and 12 out of 12 (100%).

8.3 Results

8.3.1 SES and Non-SES events

A total of 118 days of snowfall were identified at LTBA and LTFJ between 2009 and 2018. According to the analyses made with satellite images, 73 days were detected as SES events and 45 days as non-SES events. At LTBA, 57 days of SES events and 28 days of non-SES events were determined, while similarly at LTFJ, 72 days of SES events and 38 days of non-SES events were recorded. Total snowfall duration at LTBA was found to be 632 h for SES events and 215 h for non-SES events. At LTFJ, these values were 745 h and 260 h, respectively. No SES events were observed in 2009; the most SES and non-SES events occurred in 2012 (Figure 8.2a). On a monthly basis, it was observed that both SES and non-SES events occurred mostly in January and least often in March (Figure 8.2b).

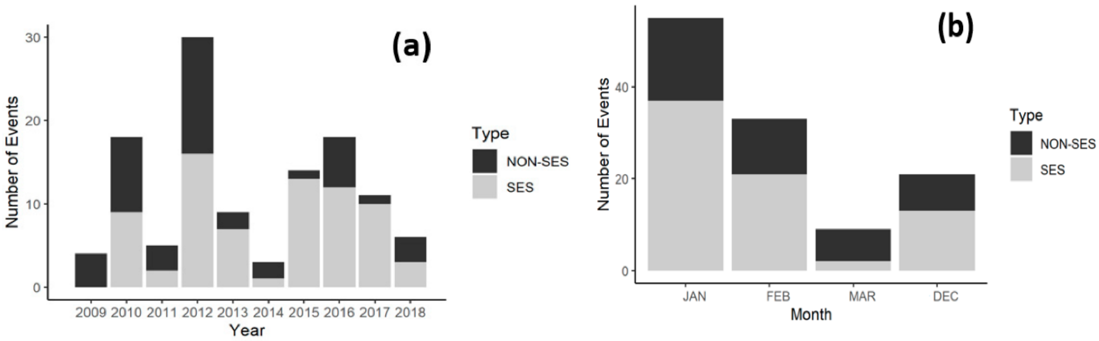

Figure 8.2 : Annual distribution of sea-effect snow (SES) and non-SES events in the left panel (a), monthly distribution in the right panel (b).

8.3.2 Meteorological conditions at LTBA and LTFJ

At both airports, the average air temperature, dew point and relative humidity were higher in non-SES events (Figure 8.3). On the other hand, average wind speed values were close to each other. In the presence of SES events at LTBA, the average air temperature was −0.1 °C, dew point −2.4 °C, wind speed 14.4 kt, and relative humidity 84.3%, while in the presence of non-SES events, the average values were 0.5 °C, −0.5 °C, 16 kt and 89.6%, respectively (Figure 8.3a). In the presence of SES events at LTFJ, the average air temperature was 0 °C, dew point −2.2 °C, wind speed 10.6 kt, and relative humidity 86.1%, while in the presence of non-SES events, the average values were 0.5 °C, −0.8 °C, 9.3 kt and 91.5%, respectively (Figure 8.3b). Temperature and dew point values showed a wider variation in SES events than in non-SES events at both airports. Although almost similar variations were observed in wind intensities, relative humidity values also showed much larger variation in SES events than in non-SES events (Figure 8.3).

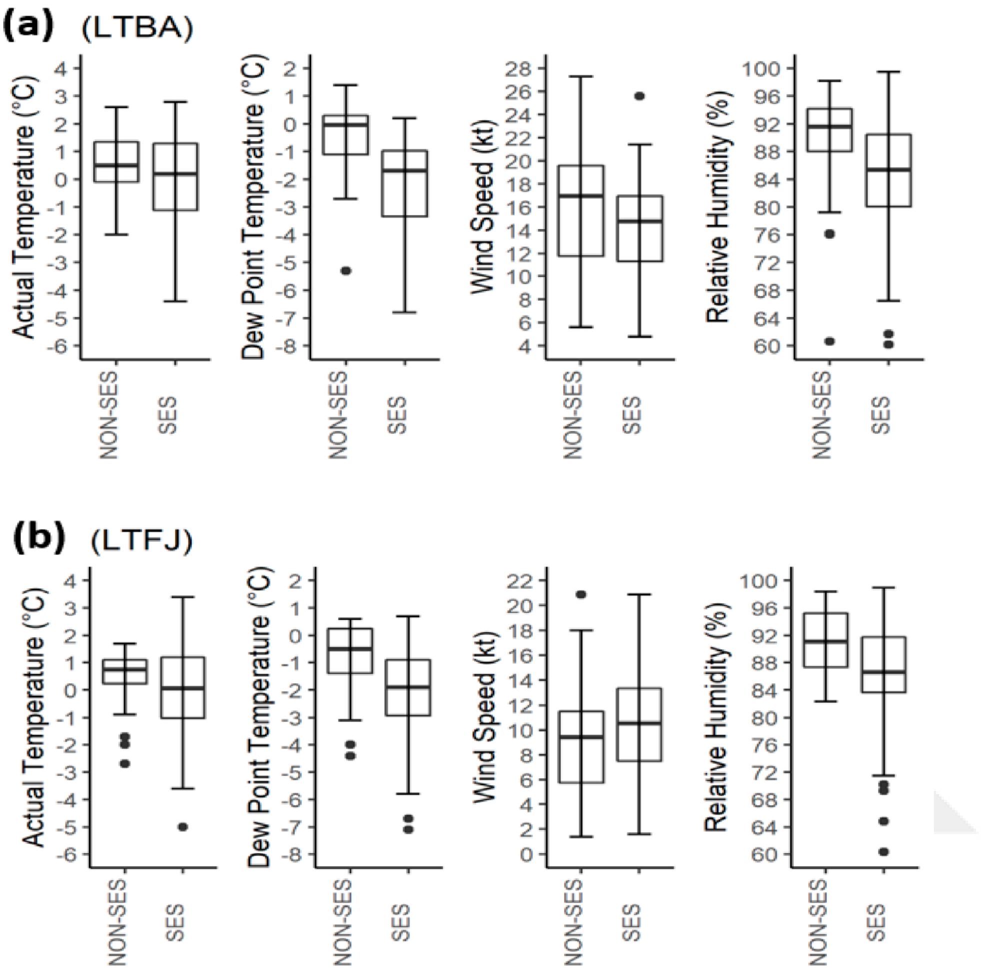

Figure 8.3 : The comparison of meteorological parameters in SES and non-SES events at (a) LTBA and (b) LTFJ.

In the SES and non-SES events, the prevailing wind direction information observed at the airports is given in Table 8.2. While it was observed that the northerly winds predominate (NW, N, NE) at both airports in SES events, almost similar results were observed in non-SES events. The most significant difference between SES and non-SES in terms of prevailing wind direction was that variable wind conditions (VRB) were observed more in non-SES events. In addition, a small amount of westerly and south-westerly wind directions were also observed in non-SES events. In the studies carried out for the Caspian Sea, which is located at almost the same latitudes as the Black Sea, it was determined that the prevailing wind direction in SES events is mostly northerly (Ghafarian et al., 2017; Ghafarian, 2021).

Table 8.2 : The wind direction frequencies in SES and non-SES events at LTBA and LTFJ.

Wind Direction	SES Events		NON-SES Events	
	LTBA	**LTFJ**	**LTBA**	**LTFJ**
Southwest (SW)	0%	0%	3%	3%
West (W)	0%	0%	0%	3%
Northwest (NW)	20%	11%	20%	3%
North (N)	62%	44%	63%	34%
Northeast (NE)	15%	40%	3%	34%
Variable (VRB)	2%	4%	10%	24%

8.3.3 Meteorological conditions on the western Black Sea

In the formation of SES bands that caused SESs at LTBA and LTFJ, the water source where the necessary heat and moisture fluxes were supplied was the western Black Sea. In this direction, within the scope of the study, three different points were selected to observe the changes in the specific humidity, heat fluxes and, SST over the western Black Sea in SES and non-SES events. These points are shown in Figure 8.1. The changes in the aforementioned parameters at each point are given in Figure 8.4a–c. The data obtained at three different points for four different parameters were handled separately to observe the effects on the formation, development and dissipation processes of SES bands. The main reason for choosing these points is that the coordinates for each data set exactly coincide with the grid points.

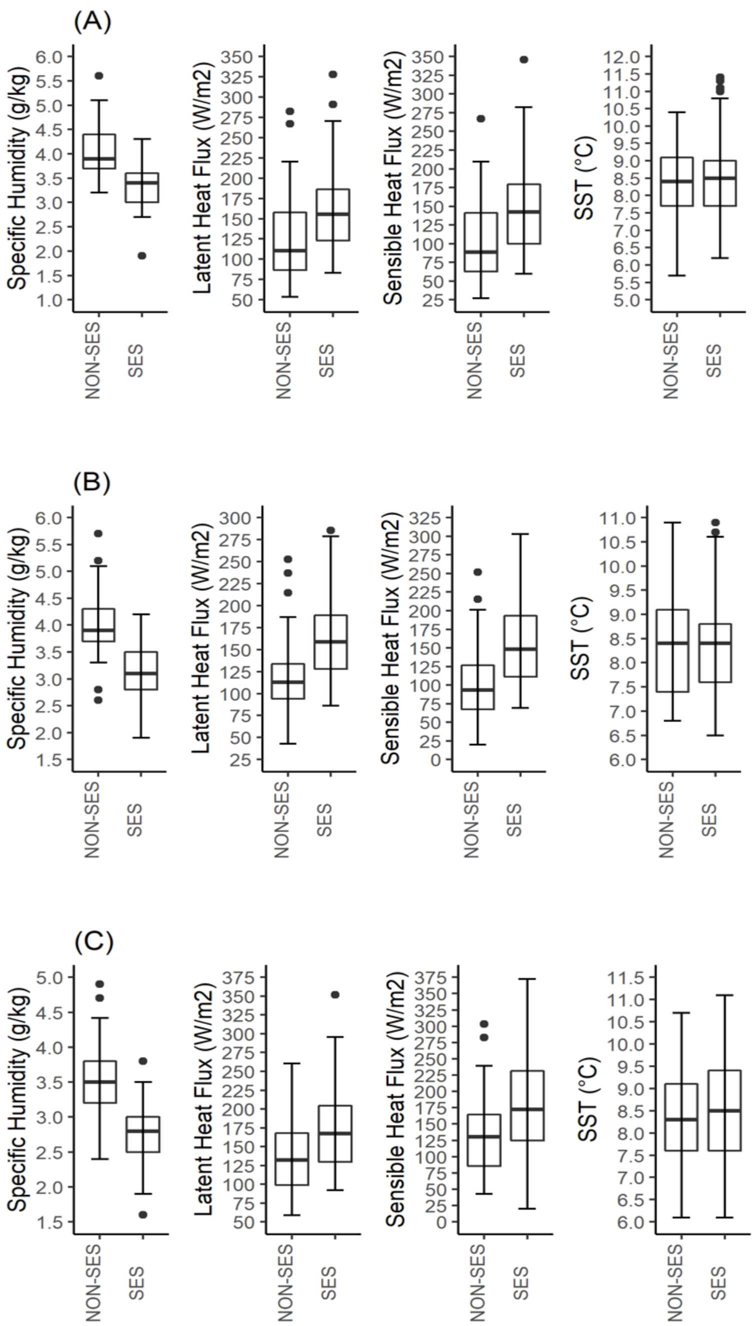

Figure 8.4 : Changes in meteorological parameters in SES and non-SES events at (a) point “A”, (b) point “B”, and (c) point “C” on the western Black Sea surface.

Specific humidity values were observed to be between 17.5% and 22.5% lower in SES events than in non-SES events at all three points. The highest mean values were observed at point “A” and the lowest values at point “C”. The average latent heat flux values were 27% higher at point “A”, 37% higher at point “B”, and 25% higher at point “C” in SES events compared to non-SES events. The average sensible heat flux values were found to be 27% higher at point “A”, 37% at point “B”, and 25% higher at point “C” in SES events compared to non-SES events. In both heat fluxes, the highest values in SES events were observed at point “C” and the lowest values at point “A”. In SST values, the average value in SES events was determined as 8.5 °C at all three points. Relatively lower average values (2–3% less) were found in non-SES events. The results obtained in this section, especially regarding heat fluxes, are similar to those of many studies in the literature (Niziol et al., 1995; Ghafarian et al., 2021; Scott and Sousounis, 2001; Markowski and Richardson, 2010). Lang and co-workers stated that in cases of sufficient fetch distance, the wind speed varies in direct proportion to the heat and moisture fluxes upwards from the SS (Lang et al. 2018). Additionally, Sousounis and Mann stated that 10–15 kt high wind speeds generate heat fluxes in the range of approximately 200–500 W m^{-2} (Sousounis and Mann, 2000). In this study, high wind speed values were observed over the sea when high sensible and latent heat flux values were observed (not shown). Increasing wind speed values make a positive contribution to heat and moisture fluxes, as there is sufficient fetch distance (400–600 km) over the western Black Sea; on the other hand, they make a negative contribution to the specific humidity values on the SS. For this reason, lower specific humidity values were observed in SES events compared to non-SES events.

8.3.4 Air–Sea Interaction over the Western Black Sea

One of the most important parameters that plays a role in the occurrence of LES/SES events is a certain temperature difference between the cold air mass and the relatively warmer water source over which it passes. In this regard, some limit values have been revealed in the studies conducted for different regions where LES/SES events were observed (Section 8.1). In this study, the average $\Delta T_{SS\text{-}850}$ value was found to be 17.6 °C for SES events and 12.2 °C for non-SES events (Figure 8.5a). Similarly, the average $\Delta T_{SS\text{-}700}$ value was found to be 24.9 °C for SES events and 19.3 °C for non-SES events (Figure 8.5a). In SES events, the highest $\Delta T_{SS\text{-}850}$ value was 24.1 °C and the highest $\Delta T_{SS\text{-}700}$ value was 33.1 °C. The lowest temperature differences for $\Delta T_{SS\text{-}850}$ and $\Delta T_{SS\text{-}700}$ were 9.8 °C and 14.6 °C, respectively. In addition, 94% of the $\Delta T_{SS\text{-}850}$ data was 13 °C and above, and 99% of the $\Delta T_{SS\text{-}700}$ data was 17 °C and over. In these analyses, point “B” was taken as a reference for SST information (Figure 8.5a,b). Similar results were obtained in the analyses made on the other two points determined on the western Black Sea.

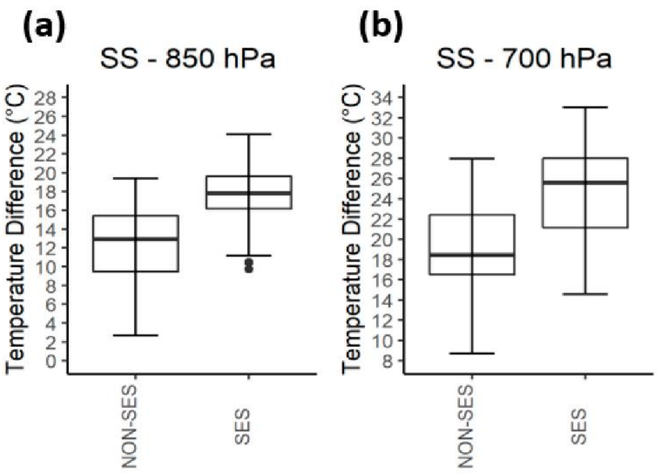

Figure 8.5 : The variation in the temperature difference between the upper atmospheric level air (850 and 700 hPa levels) and point "B" (specified on the western Black Sea surface) in SES and non-SES events. (a) the temperature difference between the 850 hPa level and point "B", (b) the temperature difference between the 700 hPa level and point "B".

Wind speed and direction changes in the convective layer (especially just below the inversion layer) have an important effect on the formation, intensity and trajectory of the LES/SES bands. The low wind direction change from the LS/SS to the upper atmospheric levels is an important parameter that increases the formation and strength of the bands. Regarding this, in the literature, between LS/SS and 700 hPa, 30° and below were specified as the appropriate range for strong band formations, and 60° and below for band formation (Niziol 1987; Kristovich and Laird, 1998). In this study, wind direction changes between 850/700 hPa levels and point "B" specified on the western Black Sea ($\Delta W_{SS\text{-}850}$ and $\Delta W_{SS\text{-}700}$) are discussed separately for SES and non-SES events. In SES events, the $\Delta W_{SS\text{-}700}$ value was 60° and below at a rate of 59%, while this rate decreased to 26% in non-SES events. The $\Delta W_{SS\text{-}850}$ value was 60° and below in both SES and non-SES events, at rates of 71% and 52%, respectively (Table 8.3).

Table 8.3 : The wind direction frequencies in SES and non-SES events at LTBA and LTFJ.

	SES Events		**NON-SES Events**	
	$\Delta WD_{SS\text{-}850}$	$\Delta WD_{SS\text{-}700}$	$\Delta WD_{SS\text{-}850}$	$\Delta WD_{SS\text{-}700}$
≤ 30°	43%	39%	23%	8%
30°- 60°	28%	20%	29%	18%
≥ 60°	29%	41%	49%	74%

The variation in the wind speed over the LS/SS up to the upper atmospheric levels is a critical parameter that determines the band structures and formations as well as the wind direction changes (Suriano and Leathers, 2017). In this study, wind speed differences between 850/700 hPa levels and SS were observed in a relatively narrow range in SES events compared to non-SES events. This difference was 12.1 kt for $\Delta WS_{SS\text{-}850}$ (Figure 8.6a) and 14.1 kt for $\Delta WS_{SS\text{-}700}$ (Figure 8.6b) in SES events, while it was 14.5 kt (Figure 8.6a) and 18.4 kt (Figure 8.6b) in non-SES events, respectively.

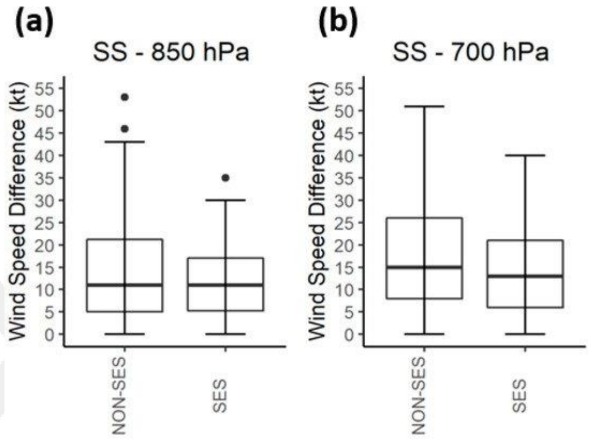

Figure 8.6 : The variation in the wind speed difference between the upper atmospheric levels (850 and 700 hPa levels) and point "B" (specified on the western Black Sea surface) in SES and non-SES events. (a) the wind speed difference between the 850 hPa level and point "B", (b) the wind speed difference between the 700 hPa level and point "B".

The limitation of the convective boundary layer, which develops due to the air–sea interaction, at the upper atmospheric levels is important in the LES/SES band formation. The formation of this layer in the first 150 hPa from LS/SS is stated to be unfavourable in terms of band formation (Steenburgh et al., 2000), while its presence at higher atmospheric levels increases baroclinity and contributes to strong band formations (Niziol et al., 1995; Laird et al., 2009). In this study, an inversion layer between SS and 500 hPa was observed in 79.5% of SES events, while this rate was 67.9% in non-SES events. Additionally, in SES events, the proportion of inversion layers occurring only within the first 150 hPa was 4.8%, whereas in non-SES events, this rate was 25%. The presence of an inversion only between 850–500 hPa, which is important for the formation of strong SES bands, was 61% in total in SES events and 33.3% in non-SES events (Table 8.4).

Table 8.4 : Presence and location of inversion layers in SES and non-SES events.

Inversion Layer	Freq. of SES Events	Freq. of NON-SES Events
1st	4.8%	25.0%
2nd	26.0%	23.8%
3rd	15.1%	8.3%
1st and 2nd	5.5%	8.3%
1st and 3rd	5.5%	0.0%
2nd and 3rd	19.9%	1.2%
1st, 2nd, 3rd	1.4%	1.2%
None	20.5%	32.1%

8.3.5 Snow Depths and Influencing Meteorological Parameters in SES and Non-SES Events

In the SES events, the maximum daily fresh snow depths measured at LTBA and LTFJ were 35 cm and 36 cm, respectively. In non-SES events, these values were measured as 7 cm and 13 cm, respectively. The dates on which the maximum fresh snow depths were measured were different at both airports. At LTBA, most of the daily fresh snow depths in SES events occurred at 1 cm and below, and a significant amount was between 1–5 cm. In addition, values over 15 cm were measured at a rate of 8%. On the other hand, in non-SES events, a larger part of the daily fresh snow depths occurred at 1 cm and below compared to SES events, while the ratio of values measured between 1–5 cm was similar. In addition, values above 10 cm did not occur. At LTFJ, daily fresh snow depths in SES events were similar to those at LTBA. The most important differences were that the ratios of 1–5 cm and over 15 cm were higher at LTFJ. Unlike non-SES events at LTBA, measurements were made in the range of 11–15 cm in non-SES events at LTFJ, and measurements of 1 cm and above were also found at a higher rate (Figure 8.7).

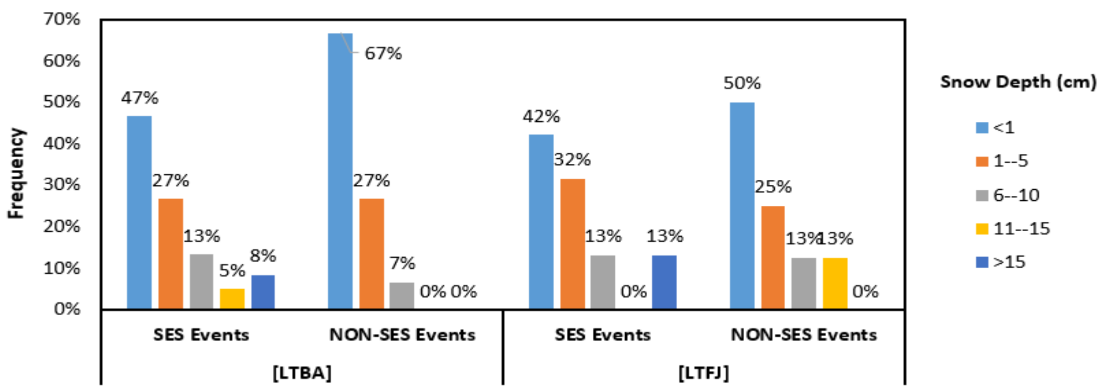

Figure 8.7 : Distribution of snow depths in SES and non-SES events at LTBA and LTFJ.

In SES and non-SES events, changes in snow depths depending on meteorological parameters were analysed for both airports (Table 8.5 and Table 8.6). For each snow depth range in Figure 7, SES and non-SES events were handled separately. In this process, the average meteorological parameter values at the airport, SS and upper atmospheric levels were determined. At both airports, snow depths often increased in both SES and non-SES events as air temperatures decreased. The average dew point depression (T-Td) was mostly higher in SES events than in non-SES events. Moreover, as dew point depression decreased in both SES and non-SES events, snow depth mostly increased for both airports. The average wind speed values were higher in non-SES events compared to SES events, and as the snow depth increased, wind intensity was generally higher in both events. In all SES events, northerly wind directions were dominant; on the other hand, in non-SES events, although similarly northerly directions were dominant, variable wind directions were also semi-dominant. The average relative humidity values were directly proportional to snow depths at both airports during SES events. This trend was mostly observed in non-SES events. At snow depths above 1 cm, the minimum relative humidity value was 84.3% at LTBA and 86.2% at LTFJ for both types of events. The average pressure values were mostly measured higher at LTBA than at LTFJ in both events. The average pressure values in SES events were found in the range of 1022–1024 hPa at LTBA and in the range of 1016.5–1019.4 hPa at LTFJ (excluding snow depths over 15 cm). The average ΔTSS-850 values were found to be a minimum of 16.7 °C (at LTFJ) and a maximum of 19.7 °C (at LTFJ) in SES events. In non-SES events, these values were 4.7 °C (at LTFJ) and 15.8 °C (at LTFJ), respectively. The average ΔTSS-700 values were found to be a minimum of 22.8 °C (at LTFJ) and a maximum of 27.9 °C (at LTFJ) in SES events. In non-SES events, these values were 15.0 °C (at LTFJ) and 21.1 °C (at LTFJ), respectively. The average sensible and latent heat flux values were higher for SES events than for non-SES events at both airports at the same snow depth ranges. In SES events, the highest flux values were observed at snow depths above 15 cm. The average specific humidity values, on the other hand, were higher in non-SES events than in SES events, which were the exact opposite of flux values at the same snow depths. Minimum values in SES events were also observed at the highest snow depth. Almost all SES events had one or more inversion layers. In non-SES events, this rate was half as low as in SES events.

Table 8.5 : Average values of meteorological parameters in SES and non-SES events according to snow depth intervals at LTBA.

LTBA	Snow Depth (cm)	T (°C)	Td (°C)	Ws (kt)	Wd (°)	RH (%)	P (hPa)	ΔT_{SS-850} (°C)	ΔT_{SS-700} (°C)	SHF (Wm^{-2})	LHF (Wm^{-2})	Spe. Hum. (gkg^{-1})	Inver. Layer
SES	<1	0.7	-2.3	14	N-NE	79.1	1023.2	17.3	23.6	162.9	166	3.2	93%
NON-SES		0.8	-0.1	15.5	NW-NE	91.2	1015.3	11.8	18.4	98.7	113.9	4	80%
SES	1-5	-0.2	-2.4	14.8	N	86.3	1024.5	16.9	24	160.6	156.9	3	100%
NON-SES		0.3	-1	16.2	VRB	84.3	1015.5	14.2	21.1	129.1	136.2	3.7	50%
SES	6-10	-0.8	-2.5	12.9	NW-N	88.5	1022	19	27.9	170.9	173.1	3.1	100%
NON-SES		-2	-2.7	20.5	NW-N	94.3	1023	8.9	16.9	117	133.8	4.1	50%
SES	11-15	-1.9	-2.6	15	N-NE	94.9	1023.9	19.5	27.5	189.7	169.2	3	100%
NON-SES		-	-	-	-	-	-	-	-	-	-	-	-
SES	>15	-1.9	-2.8	17.2	N-NE	93.8	1027.1	19	26.7	209	189.4	2.9	100%
NON-SES		-	-	-	-	-	-	-	-	-	-	-	-

Table 8.6 : Average values of meteorological parameters in SES and non-SES events according to snow depth intervals at LTFJ.

LTFJ	Snow Depth (cm)	T (°C)	Td (°C)	Ws (kt)	Wd (°)	RH (%)	P (hPa)	ΔT_{SS-850} (°C)	ΔT_{SS-700} (°C)	SHF (Wm^{-2})	LHF (Wm^{-2})	Spe. Hum. (gkg^{-1})	Inver. Layer
SES	<1	1.1	-1.6	11.3	N-NE	82.8	1016.5	16.7	22.8	129.8	141.1	3.3	100%
NON-SES		0.6	-0.8	9.1	VRB	90.9	1015.5	10.6	17.6	96.9	107.6	4.3	66%
SES	1-5	0.1	-2.1	10.8	N-NE	86.2	1019.4	18.6	26.8	174.2	176.5	3	100%
NON-SES		0.1	-0.7	12.7	N-NE	95	1019.7	15.8	20.2	146.1	143.5	3.9	50%
SES	6-10	-0.7	-2.3	13.1	N-NE	89	1018	17	26.4	177.3	178.9	3.1	100%
NON-SES		0.1	-1.8	8	VRB	88.5	1019	4.7	15	78.5	102.6	4.5	100%
SES	11-15	-	-	-	-	-	-	-	-	-	-	-	-
NON-SES		-	-	-	-	-	-	-	-	-	-	-	-
SES	>15	-2.1	-3.3	9.8	N-NE	91.5	1030.1	19.7	26.9	200	179.4	2.9	100%
NON-SES		-	-	-	-	-	-	-	-	-	-	-	-

Note: *T actual temperature; Td dew point temperature; Ws wind speed; Wd wind dir*ection; *RH relative humidity*; *P pressure*; *SS sea surface*; *SHF sensible heat flux*; *LHF latent heat flux*; *Spe. Hum. Specific humidity*; *VRB variable.*

8.3.6 An Algorithm for the Prediction of SES Events at LTBA and LTFJ

In this study, SES and non-SES events were analysed at the meso-scale. In this context, the changes in many meteorological parameters in both types of events, both at airports and on/over the sea, were analysed separately, and the results were shared. After revealing the difference between SES and non-SES events at meso-scale, the changes in average meteorological parameter values from small to large were identified in the frequency ranges determined for the times when SES events occurred at LTBA and LTFJ (Figure 8.8).

SES Events Frequency

		0% – 10%	10% – 25%	25% – 75%	75% – 90%	90% – 100%
ΔTSS-850 (°C)		9.8 - 14.6	14.6 - 16.2	16.2 - 19.7	19.7 - 20.4	20.4 - 24.1
ΔTSS-700 (°C)		14.6 - 18.4	18.4 - 21.0	21.0 - 28.0	28.0 - 30.4	30.4 - 33.1
ΔWSS-850 (kt)		0 - 3	3 - 6	6 - 19	19 - 25	25 - 35
ΔWSS-700 (kt)		0 - 4	4 - 7	7 - 22	22 - 29	29 - 40
SH (g/kg)		1.9 - 2.6	2.6 – 2.8	2.8 - 3.4	3.4 - 3.6	3.6 - 4.2
SHF (W/m2)		69 - 92	92 - 110	110 - 191	191 - 238	238 - 303
LHF (W/m2)		86 - 104	104 - 126	126 - 188	188 - 223	223 - 286
Inv. Layer (?)		No Layer	Mostly No Layer	YES	YES	YES
T (°C)	LTBA	-4.4 / -2.2	-2.2 / -1.2	-1.2 / 1.3	1.3 / 1.7	1.7 / 2.8
Td (°C)	LTBA	-6.8 / -5.5	-5.5 / -3.3	-3.3 / -0.9	-0.9 / -0.3	-0.3 / -0.2
Ws (kt)	LTBA	4.8 - 8.9	8.9 - 11.3	11.3 - 17.0	17 - 20.6	20.6 - 25.6
Rh (%)	LTBA	60 - 75	75 - 80	80 - 91	91 - 95	95 - 100
P (hPa)	LTBA	1009-1012	1012-1019	1019-1029	1029-1030	1030-1038
T (°C)	LTFJ	-5.0 / -2.1	-2.1 / -1.0	-1.0 / 1.2	1.2 / 2.2	2.2 / 3.4
Td (°C)	LTFJ	-7.1 / -4.6	-4.6 / -2.9	-2.9 / -0.9	-0.9 / 0.0	0.0 / 0.7
Ws (kt)	LTFJ	1.6 - 5.0	5.0 - 7.5	7.5 - 13.4	13.4 / 16.3	16.3 - 20.9
Rh (%)	LTFJ	60 - 75	75 - 84	84 - 92	92 - 95	95 - 100
P (hPa)	LTFJ	1004-1010	1010-1015	1015-1027	1027 - 1030	1030 - 1036

Figure 8.8 : Changes in average meteorological parameter values in SES events at LTBA and LTFJ.

A 12-item algorithm was created for the operational prediction of SES events at LTBA and LTFJ. Each of these conditions is important for the formation, development and trajectory of SES bands over the western Black Sea. All of the conditions specified in the algorithm below were met in 90% of the SES events that occurred at LTBA and LTFJ. As stated in Table 8.1, since the air temperature and wind speed values at the airports in SES and non-SES events were not statistically significantly different from each other, at least 10 conditions out of the 12 should be expected to be met (usually condition 9 and/or condition 12 were/was not met in 10% of the SES events). It was observed that in some rare cases where more than two conditions were not met (at most, four conditions were not met), one or more of the additional conditions listed at the bottom of the algorithm occurred. Additionally, these additional conditions increased the severity of the SES events (i.e., strengthening of the bands, increasing the amount of snowfall, etc.). Besides all of the conditions of this 12-item algorithm and additional conditions, the formation of suitable atmospheric conditions at airports and the monitoring the formations and trajectories of SES bands with remote sensing products (e.g., radar and satellite observations) have critical importance in terms of determining the regions to be affected by SES bands. The Algorithm created for the SES prediction is as follows:

Algorithm for the SES prediction at LTBA & LTBJ (in Istanbul)

I. Is the ΔTSS-850 14.6 °C or more?
   - If yes, SES likely
   - If not, SES not likely**
   - If above 16.2 °C, well-defined SES banding possible
   - The increase in the difference directly affects the amount of snowfall

II. Is the ΔTSS-700 18.4 °C or more?
   - If yes, SES likely
   - If not, SES not likely**
   - If above 21.0 °C, well-defined SES banding possible
   - The increase in the difference directly affects the amount of snowfall

III. Is there any inversion layer(s) or stable layer(s) below 600-hPa?
   - If yes, SES likely
     - If between the sea surface and 850-hPa, SES not likely or weak SES banding
     - If between the 850- and 700-hPa, SES most likely
     - If above 700-hPa, well-defined SES banding possible (If too above 700-hPa, SES not likely
   - If no, SES not likely**

IV. Is the fetch distance over the western Black Sea 80 km or greater?
   - If yes, SES likely, but pure SES not likely** below 160 km
   - If above 160 km, SES most likely [pure SES – well-defined SES banding possible]

V. Is the wind direction northerly (NW, N, NE) just below the inversion/stable layer?
   - If yes, SES likely
   - If not, SES not likely

VI. Is the ΔWD_{SS-700} 60° or below?

- If below 30°, well-defined SES banding possible
- If between 30°-60°, SES likely
- If above 60°, SES not likely**

VII. Is the specific humidity between 2.6 and 3.6 g.kg-1 at 1000-hPa over the western Black Sea?

- If yes, SES likely
- If below 2.6 g kg-1, SES not likely**
- If above 3.6 g kg-1, SES not likely**

VIII. Are the sensible and latent heat fluxes at 1000-hPa over the western Black Sea 92 W m^{-2} or more?

- If yes, SES likely
- If not, SES not likely
- If above 191 W/m^2, well-defined SES banding possible, heavy snowfall possible
- The increase in these fluxes strengthens the SES bands and directly affects the amount of snowfall positively.

IX. Is the actual temperature below 1.3 °C at LTBA and 1.2 °C at LTFJ?

- If yes, SES likely
- If not, SES not/less likely**

X. Is the dew point temperature below -0.3 °C at LTBA and 0.0 °C at LTFJ?

- If yes, SES likely
- If not, SES not likely**

XI. Is the relative humidity above 75% at LTBA and LTFJ?

- If yes, SES likely
- If between 60%-75%, SES less likely**
- If below 60%, SES not likely

XII. Is the wind speed greater than 8.9 kt at LTBA and 5.0 kt at LTFJ?

- If yes, SES likely
- If not, SES less likely
- If above 25.6 kt at LTBA and 20.9 kt at LTFJ, SES less/not likely**

Additional Conditions:

**SES possible if the strong upper-level dynamics (sea-enhanced) exists:

- Presence of a meso-scale low-pressure centre
- Presence of a front (e.g., a cold front, stationary front)
- Presence of a positive/negative tilted trough (e.g., long-wave trough)
- Presence of a blocking pattern (e.g., Omega, Rex, Blocking High, Cut-off-low)
- Presence of a short-wave trough (Note: position of the max vorticity is important)

**SES also possible if the following considerations are maximized:

- Upper-level air temperature to sea surface temperature gradient
- Depth of the convective layer (between inversion/stable layer and sea surface)
- Shoreline frictional convergence and land breeze
- Orographic effects (do not generate bands, affects distribution and intensity)
- Positive vorticity advection
- Ice cover (Not applicable for the western Black Sea)
- Increase in total fluxes (heat and moisture fluxes).

8.4 Discussion and Conclusions

One of the most important parameters that negatively affects operational activities in the aviation sector is adverse weather conditions (Yavuz et al., 2020; Özdemir et al., 2017). Meteorological events that reduce or obstruct visibility can cause accident-incident events, especially during the landing and take-off phases (Yavuz et al., 2015; Özdemir et al., 2016). Snowfall and SES are meteorological parameters that reduce visibility. SES bands can cause long-term heavy snowfalls in narrow or wide areas depending on their formation and inland extension. The type and trajectory of these bands can usually be detected on radar images. However, knowing the answers to the following questions in nowcasting/forecasting applications will contribute to operational forecasts. (1) What are the atmospheric conditions required for SES bands to begin to form over water bodies (at SS and upper atmospheric levels) and, accordingly, when will they begin to form/dissipate? (2) How will they behave with the effect of atmospheric conditions at surface and upper atmospheric levels on their trajectory along their inland extension, and what will be the surface level types of precipitation? In this study, the analyses of meteorological parameters at surface level, SS and upper atmospheric levels affecting SES were performed, value ranges were determined for two international airports, and a 12-item algorithm was created to contribute to operational activities.

Although the atmospheric conditions for the formation of SES and SES bands in similar studies in the literature were often similar in this study, some different results also emerged. For example, 13 °C and 17 °C threshold values for $\Delta T_{SS\text{-}850}$ and $\Delta T_{SS\text{-}850}$ have been determined in the literature, respectively (Niziol, 1987; Rothrock, 1969; Laird et al., 2009; Holroyd, 1971; Carpenter, 1993). In this study, these values were 17.6 °C and 24.9 °C on average, respectively. The most important reason for this is that SES events are mostly supported by synoptic-scale systems. SES events that occur in this way are called sea-enhanced snow. Similarly, for the formation of SES bands, certain threshold values are available for wind speeds and vertical wind variation. In this study, SES band formations were also observed above these threshold values. The main reason for this is that the fetch was at least two times longer than the fetches in the studies in the literature. This situation does not prevent the high wind speeds at sub-inversion level from adding the necessary heat and moisture fluxes to the air parcel since the distance covered over the sea is long. The sensitivity of strong SES bands, which occur in parallel with high heat and moisture fluxes, to wind direction changes also decreased in this way.

Finally, the 12-item algorithm for LTBA and LTFJ was validated by selecting various cases. In this context, three of the events were selected. One of them was chosen from events that took place at LTBA only, one at LTFJ only, and finally one at both airports. Then, the data on these events were extracted from all the data sets analysed in the algorithm. Later, the revised algorithm was analysed separately for these three events. The results were as follows: 11 out of 12 items in the algorithm were met for the event that occurred at LTBA, 11 out of 12 for the event that occurred at LTFJ, and 12 out of 12 for the event that occurred at both airports.

9. A LONG-TERM ANALYSIS OF THUNDERSNOW EVENTS OVER THE MARMARA REGION, TURKEY [8]

9.1 Introduction

A thunderstorm (TS) is a weather phenomenon commonly characterized by lightning and thunder, causing heavy rainfall, strong winds (also wind gusts) and may also generate tornadoes (Yavuz et al., 2020). The relatively high moisture content of the air parcel, the presence of buoyancy forces that will carry the air parcel upwards (i.e., convection, convergence, orographic ascent, or frontal lifting) and the unstable atmospheric conditions are important in terms of the formation of the necessary atmospheric environment for the occurrence of TS (Ackerman and Knox, 2002; Özdemir et al., 2017; Wahiduzzaman et al., 2022). In addition, vertical wind shear is often critical in the formation of TS (Doswell and Evans, 2003; Özdemir, 2021; Yavuz et al., 2022a). TSs can occur mostly with heavy rain (TSRA) (Özdemir et al., 2019), occasionally singularly (TS), and rarely with snow (TSSN) (Crowe et al., 2006; Bech et al., 2013) and sleet (TSSNRA) (Bech et al., 2013).

TSSN, also known as a convective snowfall event, usually occurs with synoptic-scale systems, and sometimes occurs at meso-scale depending on local effects (i.e., coastal convergence-frictional convergence, orographic ascent). Schultz and Varek (2009) described it as a rare/unusual weather phenomenon when compared with other snowfall and thunder events. The fact that lightning and thunder events occur mostly during seasonal transitions and spring months when the atmospheric instability is high, and that TSSN occurs in the winter season when more stable atmospheric conditions prevail, strengthens the definition of "rare weather phenomenon". TSSN has the potential to significantly reduce horizontal and vertical visibility with the combination of lightning and snow. This negatively affects land, sea and especially air transport activities (Wilkinson et al., 2013; Zook, 2014). In this study, the TSSN event, which

---

[8] This chapter is based on the research paper: Yavuz, V., Lupo, A.R., Fox, N.I. and Deniz, A. (2022). A long-term analysis of thundersnow events over the Marmara Region, Turkey. *Natural Hazards*. doi: https://doi.org/10.1007/s11069-022-05393-w

was detected at different times on 12 January 2015 at seven airports in the Marmara Region, led to cancellation of most of the flights due to the severe storm and decrease in visibility because of heavy snowfall (Dunya, 2015). This unexpected event also caused people to be more exposed to the possibility of lightning strikes in open areas (for example, skiing activities) (Cherington, 2001). Climatological analyses and case studies were carried out mostly for North America and Canada regarding TSSN events (Crowe et al., 2006; Market et al., 2006; Market et al., 2007). For Europe, Munzar and Franc (2003) examined winter thunderstorms, but did not directly address the thundersnow event.

Curran and Pearson (1971), in their study in which they analysed hourly surface observations for the United States (USA) between 1968 and 1971, detected TSSN in only 76 reports out of 114,924 reports. Elkins (1987) detected 43 thundersnow events by following the Daily Weather Map series between 1971-1986 in the USA. In this study, the origins of cyclones and the air parcel within the cyclone were investigated. Colman's work (1990a, b) classified elevated TS events according to precipitation types (i.e., rain, snow, sleet, etc.), and revealed their meso- and synoptic-scale environmental conditions. Schultz (1999), based on the surface meteorological station data, analysed the thunders that occurred between October and May for the USA, and found snow in only 1.3% of them.

In studies on convective precipitation in the cold-season, it was stated that atmospheric contents (such as, atmospheric instability, a lifting mechanism and high moisture content) similar to those in the warm-season are required. However, the physical and dynamic processes that produce these contents must be different in the cold-season. Although the TSSN event seems to be a meso-scale event, the effects of synoptic-scale systems were mostly observed in its formation mechanisms (Market et al., 2002). Schultz and Vavrek (2009) revealed a recipe for TSSNs that occur in the USA. Four basic components (moisture, lifting, unstable temperature profile and cold air) required for TSSN have been determined. It was determined that the moisture source can be met by local sources, as well as by long-distance transport (from Gulf of Mexico), and even in the Great Lakes region, TSSNs were formed by the lake-effect mechanism. Regarding the lifting mechanism, the rising of warm air parcel required for convective storm occurred by frontal systems or orographic effects. Unstable temperature gradient profiles can also occur under the influence of synoptic-scale systems and irregular distributions of upper-level jet streams. Finally, the cold air pool (which must be below the freezing point) was expected to form within the clouds near the ground.

Compared to summer convective TSs, lower convective available potential energy (CAPE) values were observed in winter TSSNs (Stuart, 2001; Halcomb and Market, 2003; Mäkelä et al., 2013, Kumjian and Dierling, 2015). Market et al. (2002) found no direct effect on the time of day occurrence of TSSNs. In the sounding analyses of TSSN events, it was determined that the temperatures were formed below 0 °C in almost all of the atmospheric column from the surface (Çurran and Pearson, 1971; Market et al., 2006; Market et al., 2007). In these cases, when the data obtained from the surrounding stations were examined, the effect of cold air advection observed especially in the lower levels of the atmosphere (below relatively warmer and humid air mass) was seen. In the presence of TSSN, although the temperatures in that station decreased to 0°C and below, 10 °C values were observed in the surrounding stations (Kumjian and Dierling, 2015).

The formation types of TSSNs were classified under six sub-classes by Market et al. (2002). These are cyclone, orographic ascent, coastal cyclone, frontal, lake-effect, and upslope. In order for TSSNs to be included in the cyclone class, they must have at least two closed isobars in the contour range of 4 hPa at the start of the event. Such events usually occur near the front (especially the warm front). Two criteria have been set for the orographic class. These should not occur heavily in the surrounding stations and should be substantially different in terms of the characteristics of the surrounding stations. If these events, which occur in isolation from neighboring stations, are observed at more than one station, they may have occurred in this cyclone class. If TSSN is observed at more than one station along the coast in the presence of an open cyclone in the open sea, it is included in the coastal cyclone class. The frontal class includes events occurring at the ends of the region that are typically stable and do not have a well-defined cyclonic circulation. In the events in the lake-effect class, the presence of lake-effect bands is sought, and TSSNs associated or not associated with synoptic-scale systems are found in this class. In upslope events, a weak cyclonic circulation is required in the presence of an anticyclone or a reverse trough (Market et al., 2002).

In this study, the Meteorological Aerodrome Report (METAR) and the Special Aerodrome Reports (SPECI) reports from 11 airports in the Marmara Region were analysed for a 22-year period between 2000-2021. In total, TSSN (thundersnow) was detected in 31 reports and TSSNRA (thundersnow with rain) in 4 reports. International airports publish half-hourly reports, while national and military airports publish hourly reports. For this reason, a daily scale was preferred to statistical analysis of the TSSN events. Accordingly, 19 TSSN events were identified. Statistical analyses were carried out for TSSN events on a daily, monthly and annual basis, and the atmospheric conditions in which each event occurred were examined in detail. TSSN events were classified according to the formation types, but this classification was slightly different from Market et al. (2002), so that the formation mechanisms of TSSNs occurring throughout the region were more inclusive. Together with these, the changes of meteorological parameters on the land surface (LS), sea surface (SS) and upper atmosphere were analysed at the meso-scale, and the thermodynamic structure of the events and the atmospheric instability conditions were determined by using the sounding data.

9.2 Data and Methodology

The TSSN events that occurred in the Marmara Region, one of Turkey's seven geographical regions, were analysed within the period between 2000 and 2021. The region is located around the Marmara Sea, which is an inland sea, and the Black Sea is located to the north. The prevailing wind direction is southwest in summer and northeast in winter. Summers are warm/hot and dry, and winters are mostly rainy. In terms of climate type, it is stated that there is a Mediterranean climate in summer and Black Sea climate types are observed in winter. (Yavuz et al., 2021a). One of Turkey's most important ski resorts is located in the province of Bursa, located in the south of the Marmara Sea. Similarly, Kocaeli province, located in the north of the Marmara Region, is home to the Kartepe ski resort. There are 11 airports in total within the boundaries of the region. Six of these airports are in the international category, while the rest are in the national and military category (GDSAA, 2021). TSSN events and current surface meteorological parameter values were determined and analysed by examining the METAR and SPECI reports published by the airports throughout the period. While these reports are prepared at half-hourly intervals at international airports in accordance with regional agreements, reports are mostly published at hourly intervals at national airports. One airport examined in the study started to serve in

2011. Although other airports published reports within the period, especially national and military airports do not publish reports in a specific order. In some airports, reports are prepared only during a certain period of the day (for example, in an 8-hour period of the day), while at the airports where flights are made regularly at certain hours, reports are published only at those hour intervals. For this reason, the existence of any TSSN events, except airport reports, was investigated by conducting newspaper, magazine and internet searches to determine TSSN events. Each event was defined as one event per day, regardless of the time and duration of the day. Information about the airports is given in Table 9.1. METAR and SPECI reports were obtained from the IOWA Environmental Mesonet website (IOWA, 2021). Istanbul Kartal Radiosonde station data were used to determine the change in upper level atmospheric conditions for the region. The closest sounding observation to the time interval in which the TSSN occurred was used. If it occurred almost halfway between two observations, the average values of the two observations were used. All of the sounding data within the specified events were obtained from the University of Wyoming Atmospheric Science's website (University of Wyoming, 2021). The indexes used in the determination of the stability of the atmosphere were also obtained from these sounding data. The study area, airports and radiosonde station are shown in Figure 9.1.

Table 9.1 : Information about the airports in the Marmara Region (FGA, 2021).

Province	**Airport**	**ICAO Code**	**Altitute (m)**	**Opening data**	**Latitude-Longitude**
Istanbul	Ataturk Airport	LTBA	49	1953	40°58'34"N - 28°48'51"E
Istanbul	Sabiha Gokcen Airport	LTFJ	95	2001	40°53'54"N - 29°18'33"E
Istanbul	Samandira Airport	LTBX	123	1988	40°59'34"N - 29°12'56"E
Yalova	Taskopru Airport	LTBP	13	-	40°41'11"N - 29°22'48"E
Kocaeli	Cengiz Topel Airport	LTBQ	56	2011	40°44'6"N - 30°4'60"E
Tekirdag	Corlu Airport	LTBU	31	1998	41°8'18"N - 27°55'9"E
Bursa	Yenisehir Airport	LTBR	100	2000	40°15'18"N - 29°33'45"E
Balikesir	Bandirma Airport	LTBG	52	1960	40°19'4"N - 27°58'39"E
Balikesir	Kocaseyit Airport	LTFD	5	1997	39°33'16"N - 27°0'49"E
Balikesir	Balikesir Airport	LTBF	104	1998	39°37'9"N - 27°55'33"E
Canakkale	Canakkale Airport	LTBH	7	1995	40°8'15"N - 26°25'36"E

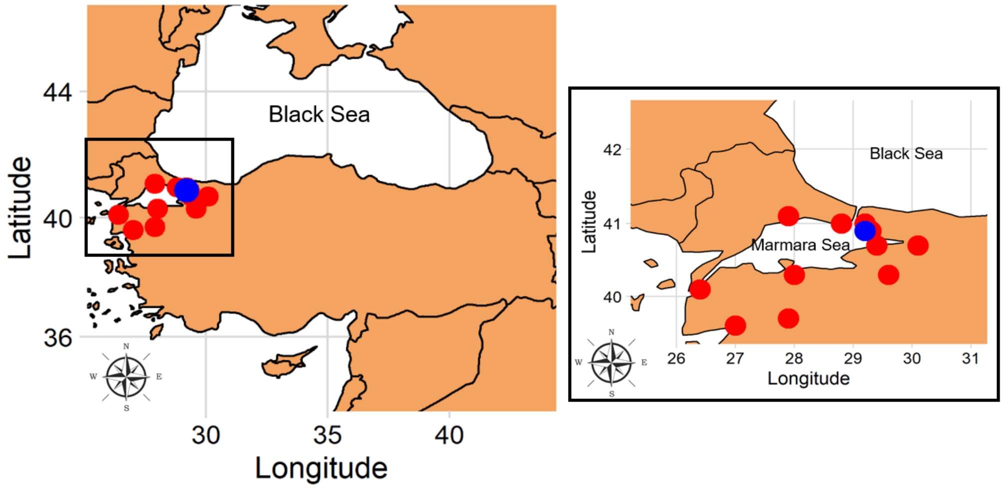

Figure 9.1 : Study area, location of airports (red dots), and location of Istanbul Kartal radiosonde station (blue dot).

In the study, first, the intraday change of TSSN events, their monthly and annual distributions were determined. Then, the events were classified according to the formation types revealed by Market et al. (2002). Apart from surface meteorological data, other data sets were also needed to perform these classifications. Accordingly, synoptic-scale evaluations were made using the images of the Spinning Enhanced Visible and Infrared Imager (SEVIRI) module of MSG-2 and MSG-3 satellites. Infrared (Channel-9), Visible (Channel-321) and airmass satellite images presented at 15-minute intervals and 3-km resolution were analysed (Zhao and Duan, 2020). Satellite images were obtained from the Turkish State Meteorological Service (TSMS 2021). In addition, the western Black Sea surface temperature data were obtained from the NOAA High-Resolution Blended Analysis data set (The data with a latitude-longitude resolution of $0.25° \times 0.25°$) in order to be useful in the detection of events occurring especially with sea-effect (NOAA, 2021). For the same purpose, the Woods Hole Oceanographic Institution (WHOI) - Objectively Analyzed Air-Sea Fluxes (OAFlux) data set was used for sensible and latent heat fluxes (WHOI, 2021).

Within the scope of the study, Convective Available Potential Energy (CAPE), Convective Inhibition (CIN), and Bulk Richardson Number (BRN) were analysed to reveal the stability of the atmosphere in detail. In addition, Lifted Index (LI), Showalter Index (SI), Severe Weather Index (SWEAT), Total Total Index (TTI) and TQ Index (TQI) values were analysed. Finally, the Pressure of Lifting Condensation Level (LCLP) and Precipitable Water (PWAT) values were calculated. The information about these parameters and indices used to determine the stability of the atmosphere is briefly as follows:

- CAPE: It is an indicator of atmospheric convection. It is calculated by integrating along the vertical profile of the atmosphere. Its high values are indicative of the instability of the atmosphere. (Lucas et al., 1994; Ye et al., 1998).
- CIN: It is the negative part of CAPE (Zhang, 2003). Its high values are an indication of the stability of the boundary layer.
- BRN: It is directly related to CAPE. It gives the relationship between CAPE and wind shear vector difference. Its high values indicate the instability of the atmosphere. (Weisman and Klemp, 1982).
- LI: It is the temperature difference between an adiabatically lifted air parcel and the environment at a given pressure. It is used to determine the stability of the lower troposphere. Its low values are an indication of the instability of the atmosphere. (Galway, 1956).
- SWEAT: It is very important for severe weather events. High values of this index are also an indication of high temperature and humidity in the lower atmosphere, the veering of the wind direction with height, the presence of a cooler air pool at the upper levels, and the presence of large vertical wind shear. (Miller, 1972).
- SI: It is a popular severe weather index. It is calculated similarly to LI but less comprehensive. Its low values are an indication of the instability of the atmosphere. (Showalter, 1953).
- TTI: It is calculated using the temperature and dew point temperature values at the 850 and 500 hPa levels. Its high values are indicative of atmospheric instability. (Miller, 1972; Pepler and Lamb, 1989).
- TQI: It uses the temperature information at 850 hPa and 700 hPa levels. For low-topped thunderstorm formation, this value must be 12 and above (Henry, 2000).
- LCLP: Higher values indicate that the lower levels of the atmosphere are drier
- PWAT: It gives the amount of water vapor available for precipitation along the vertical column of the atmosphere in mm.

9.3 Results

9.3.1 Frequency and duration of the TSSN events

A total of 19 TSSN events were identified over a 22-year period using aviation reports from 11 airports (Figure 9.2a). In addition, reports of thunder and snowfall occurring together were analysed by looking at newspapers and other online news sites over the internet. Except for the events determined by looking at the airport reports, no extra events were found. Although there is no obvious trend in annual analyses, the observation of six events (almost one third of all events) in 2015 came to the fore. In the study conducted by Market et al. (2002) covering the entire United States of America (USA), data from 204 stations over a 30-year period were used, and a total of 191 events were determined based on 3-hour reports. Approximately the annual average number of events was around six. Since TSSN event is known as a rare meteorological phenomenon, it is an important result that while the USA is 143 times larger than the Marmara Region in terms of surface area, the events in the USA are only six times more frequent. In monthly analyses, TSSN events were observed in four months of the year, almost similar numbers were observed in winter months, while only two events occurred in November (Figure 9.2b). In the USA, events were observed for seven months from October to April, and peak values were reached especially in February and March (Market et al., 2002). Similar results have also been found in the study by Adhikari and Liu (2019). No significant distribution or trend was found in diurnal cycle. However, only 3% of the events were observed between 0000 UTC and 0600 UTC. Maximum frequencies were observed approximately 5-6 hours after sunrise until 3 hours after sunset (Figure 9.2c). Market et al (2002) did not observe a significant trend in intraday changes of TSSN events, whereas Adhikari and Liu (2019) observed maximum frequencies between 1700 and 2400 UTC. The majority of the events (74%) lasted less than an hour, rarely (10%) over 2.5 hours (Figure 9.2d). Market et al (2002) also determined that one of the longest durations was 5 hours at a single station.

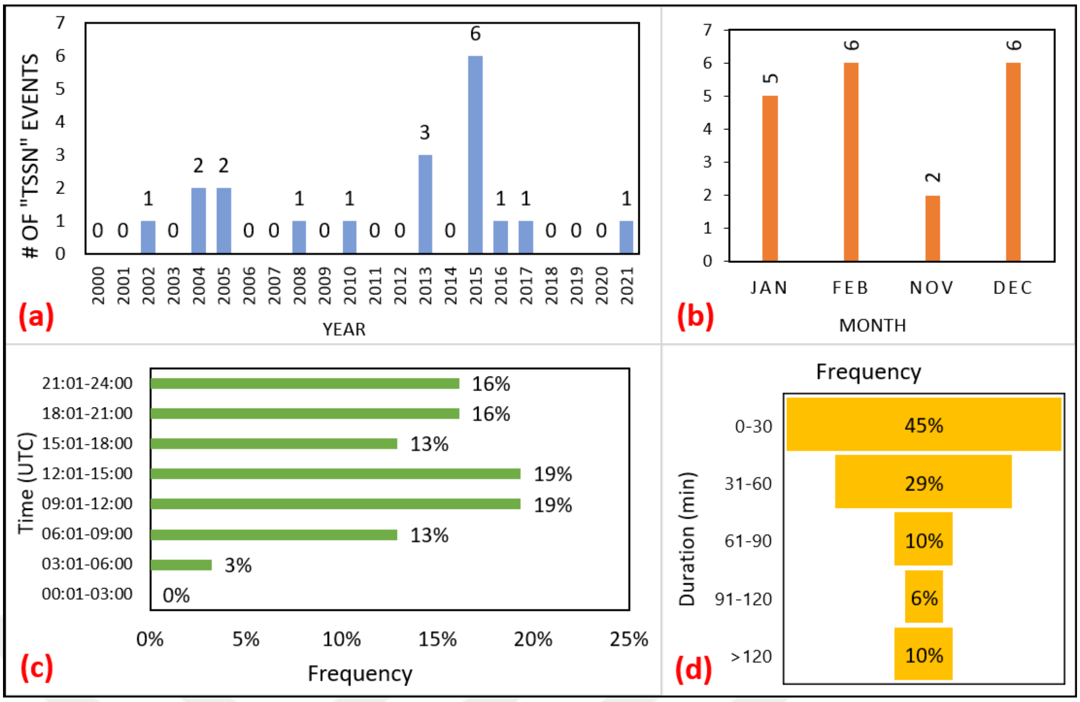

Figure 9.2 : Annual (a), monthly (b), intraday (c) distributions, and durations (d) of TSSN events.

9.3.2 Airport-based surface meteorological analyses

No TSSN events were encountered during the period in 4 of 11 airports (LTBH, LTBQ, LTBR, and LTFD) in the Marmara Region. On 12 January 2015, TSSNs were observed at all seven airports at different times during the day. On this date, at all airports except LTFJ, the TSSN event durations were one hour at the most. At LTFJ, TSSNs lasted 5.5 hours in a single day, 4.5 hours in the afternoon and 1 hour before midnight. Overall, 84% of the events occurred at LTBA and LTFJ, while the rest occurred at other airports excluding these two airports. At three airports (LTBP, LTBU, and LTBX), the TSSN event occurred only on 12 January 2015. In Fig. 3, ranges in the actual/dew point temperature values and relative humidity values at the time of TSSN events at seven airports are given. In Table 9.2, the average values of meteorological parameters at the time of TSSN events at seven airports are given. As can be seen in Figure 9.3, the actual temperature value at airports mostly did not exceed 2 °C, and rarely went below -1 °C. Considering the event frequencies at LTBA and LTFJ, a wider variation at LTBA and values above 0 °C in almost all events at LTFJ were noted. Market et al. (2002) analysed the TSSNs and found the mean surface temperatures to be -1 °C. In similar studies, this value was around 0 °C (Holle et al., 1998; Schultz, 1999; Stuart, 2001). The dew point temperature values were mostly below 0 °C on average, and oscillation was observed around 0 °C at the LTFJ. In the relative humidity values, the minimum value was seen at LTBA (73%), but mostly it occurred at 87% and above.

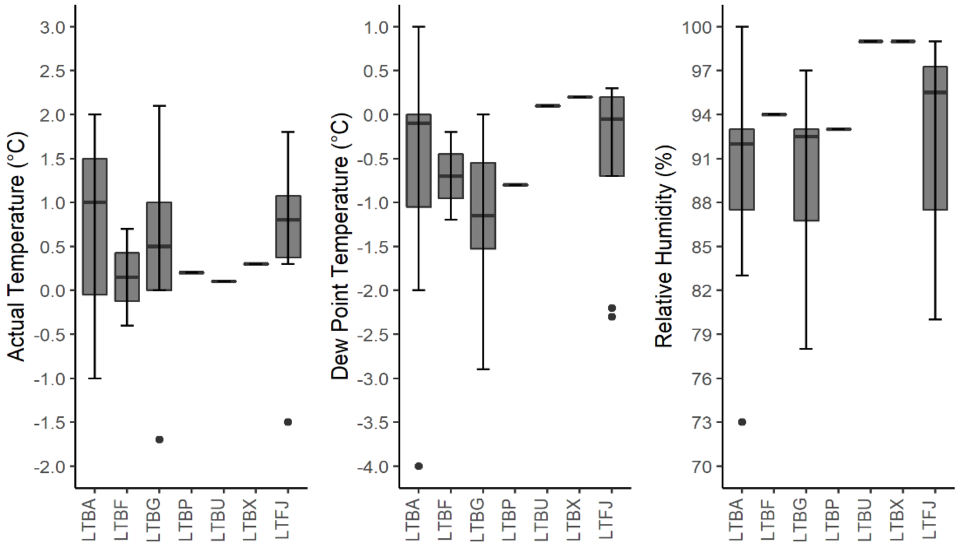

Figure 9.3 : The variation of actual/dew point temperature and relative humidity values in TSSN events at seven airports.

In Table 9.2, it is seen that the average of the actual temperature values for all airports was minimum 0.1 °C and maximum 0.7 °C. The dew point temperature values were slightly above 0 °C at only two airports. While the mean values of wind speeds were close to each other (11.5 kt and 10.6 kt) at LTBA and LTFJ, a high mean value (17.7 kt) was observed at LTBG. Almost all of the prevailing wind directions at the airports were northerly, and most of them are from the north. Average relative humidity values were 90% and above at all airports. While TSSN events were observed at higher station pressure values on average at LTBA compared to LTFJ, no significant difference was found at other airports.

Table 9.2 : Average values of meteorological parameters measured at airports in TSSN events.

Airport	T (°C)	Td (°C)	Ws (kt)	Wd	RH (%)	P (hPa)
LTBA	0.7	-0.6	11.5	N	90.0	1028.0
LTBF	0.2	-0.7	11.0	N	94.0	1023.5
LTBG	0.4	-1.2	17.7	N	90.0	1025.7
LTBP	0.2	-0.8	CALM	VRB	93.0	1020.0
LTBU	0.1	0.1	7.0	NW	99.0	1018.0
LTBX	0.3	0.2	9.0	N	99.0	1019.0
LTFJ	0.6	-0.5	10.6	N	92.4	1018.3

Note: CALM a wind speed less than 1 kt; VRB wind direction varies by 60 degrees or more

9.3.3 Analyses of sea surface and upper atmospheric parameters

Air-sea interaction plays an important role in the occurrence of TSSN events. Many processes occur depending on the air-sea interaction. For instance, the source of moisture required for cloud and precipitation formation, buoyancy forces that will carry this moisture to the upper atmospheric levels and initiate convective movements, the presence of convergence to support convective vertical development, advections to carry cold air within the cloud and lower atmospheric levels, etc. In this study, the average daily sea surface temperatures (SSTs) for the western Black Sea were obtained separately for all TSSN events, and the temperature differences between the upper atmospheric levels (850 and 700 hPa) and SS were analysed (Figure 9.4). In addition, average and maximum values of sensible and latent heat fluxes for all events were also investigated.

The average SST value for all TSSN events was 8.9 °C. The lowest value observed was 6.6 °C, the highest was 13.0 °C. However, the most important thing here is to determine the temperature difference between upper atmospheric levels and SS. Accordingly, ΔT_{SS-850} and ΔT_{SS-700} values were analysed for all events. Higher values increase the temperature gradient in the region, support the necessary lifting mechanisms to carry more heat and moisture fluxes from the SS to the upper atmospheric levels, and as a result, a more unstable atmosphere occurs due to increased convection. In studies on lake/sea effect snowfalls (LES/SES) in the literature, threshold values were generally used for ΔT_{SS-850} and ΔT_{SS-700} so that heat and moisture fluxes over water bodies could initiate cloud band formations at higher atmospheric levels. These values were 13.0 °C (Holroyd, 1971; Niziol et al., 1995; Kunkel et al., 2002; Laird et al., 2009, Yavuz et al., 2021b; Yavuz et al., 2022b) and 17.0 °C (Niziol, 1987; Carpenter, 1993; Steenburgh et al., 2000), respectively. Values above these thresholds both strengthen cloud band structures and increase the amount of precipitation. However, when these conditions occur, it has been stated that an inversion layer that limits the convective movements at higher atmospheric levels must also occur (Pettersen, 1956; Rothrock, 1969; Hjelmfelt, 1990; Reinking et al., 1993; Yavuz et al., 2021c; Yavuz et al., 2022c). At the same time, the longer the distance (fetch distance) that the cold air parcel travels on the relatively warm water surfaces, the more the heat and moisture fluxes pass through the water bodies to the upper atmosphere, which supports the instability (Jiusto and Kaplan, 1972; Kristovich and

Laird, 1998; Fujisaki-Manome et al., 2017). It is also important that the directional wind shear in the convective boundary layer is less than 60° in the formation of cloud band structures and in the determination of their trajectories (Carpenter, 1993; Steenburgh and Onton, 2001; Laird et al., 2003; Laird and Kristovich, 2004). In this study, the ΔT_{SS-850} value was calculated as an average of 17.0 °C for all events, and the ΔT_{SS-700} value was calculated as an average of 27.0 °C. The ΔT_{SS-850} value was found to be minimum 4.3 °C (but the smallest value after this value was 10.2 °C), and the highest value was 21.8 °C. The minimum value for ΔT_{SS-700} was found to be 15.4 °C and the maximum value as 33.0 °C (Figure 9.4). Inversion layers were detected at various atmospheric levels in all sounding data analysed within 19 events. The majority of these layers were located between 800-650 hPa (not shown). Heat and moisture fluxes are very important as they destabilize lower atmospheric levels over water bodies (Gerbush et al., 2008). These fluxes, which are necessary for the formation of the convective layer, have different effects depending on the shape of the water body, the presence of synoptic- and large-scale systems, and the wind conditions at the surface of the water bodies (Scott and Sousounis, 2001; Markowski and Richardson, 2010). Sensible and latent heat fluxes in LES events varied in the range of 50-150 W m^{-2} (Lang et al., 2018), these values were observed in the range of 200-500 W m^{-2} when strong bands and heavy snowfalls occur due to increased instability and convection (Sousounis and Mann, 2000). In this study, the average values of sensible and latent heat fluxes were 140.4 W m^{-2} and 161.2 W m^{-2}, respectively. A minimum of 20 W m-2 and a maximum of 306 W m-2 were determined in the sensible heat flux. A minimum of 83 W m^{-2} and a maximum of 352 W m^{-2} were observed in the latent heat flux (Fig. 5). In the final analysis made in this section, it was determined that 84% of the wind directions from surface level to 700 hPa level were veering (anticyclonic turning of wind direction with height). Similarly, Market et al. (2006) determined that veering was dominant in the sounding analyses for TSSNs.

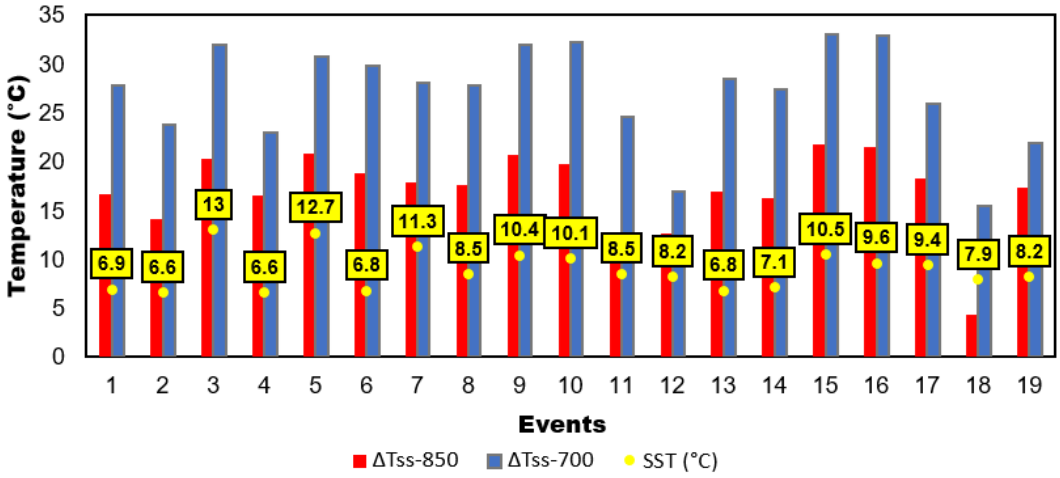

Figure 9.4 : The red and blue bar graphs show ΔTSS-850 and ΔTSS-700 for the western Black Sea, respectively. The values in the boxes determined by the yellow dots give the daily average SST value for each TSSN event.

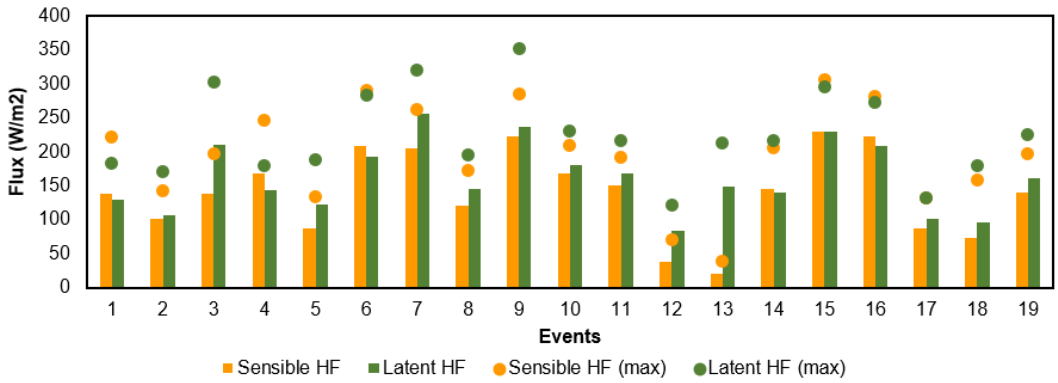

Figure 9.5 : Orange and green bars show sensible and latent heat fluxes, respectively. Dots of the same colour on the bars also give the maximum values of the both heat fluxes.

9.3.4 Formation types of the TSSN events

In this study, initially the aim was to complete an analysis similar to the classification of TSSN events according to the formation types made by Market et al. (2002), but the classification was slightly different. The most important reason for the difference in classification was that 17 of 19 TSSN events had a distinctly SES mechanism. For this reason, it was determined whether SES events occur singularly or together with synoptic-scale systems (such as: cyclone; front; trough).

SESs were observed in 17 of 19 events, and the other two SES-independent events also occurred within the frontal and cyclone effects. In general, cyclones were observed on and in the immediate vicinity of the study area in 10 of 19 events. Similarly, in 12 of the 19 events, a front was observed on and in the immediate vicinity of the study area. Therefore, the SES that occurred after the frontal and cyclone transitions was effective as sea-enhanced snowfall. This increased both the intensity of the SES bands and the total amount of snowfall. Considering the analyses made in Section (9.3.3), it was determined that the requirements for the SES mechanism were more than met in most of the cases, in terms of air-sea interaction. In the classification made by Market et al. (2002), almost half of the TSSN events took place in the cyclone class. In this study, most of the events took place with the SES mechanism, and more than half of them occurred after the transition of cyclone and frontal systems.

9.3.5 Atmospheric stability analyses

In this section, atmospheric stability indexes and analyses of some sounding parameters were carried out. The information about the values of these indexes and parameters, in which intervals, and what they mean is given in Table 9.3. Each parameter has its own distinct value range. In addition, many parameters not only give information about the stability of the atmosphere, but also provide information about the severity and distribution of TSs, whether the necessary conditions for the formation of supercell and multicell are met, and the probability and severity of tornado formation. No criteria were found for LCLP, but it was still included in the table. Because this parameter provides important information about the moisture content in the lower troposphere. Similarly, the PWAT value gives information about the moisture content, not about the stability of the atmosphere. In the analyses, in addition to the PWAT values, the relative humidity (RH) values at 850- and 700-hPa levels were also analysed.

Table 9.3 : The ranges and meanings of atmospheric stability indexes’ values and values of some sounding parameters (NWS, 2021).

	Severe Weather Activitiy
CAPE	"CAPE < 300, stable" "300 < CAPE < 1000, marginally unstable" "1000 < CAPE < 2500, moderately unstable" "CAPE > 2500, very to extremely unstable"
CIN	"CIN < 100, potential instability" "100 < CIN < 200, marginally stable" "200 < CIN < 300, moderately stable" "CIN > 400, very stable"
BRN	"BRN < 10, much more shear than buoyancy, TSs unlikely" "10 < BRN < 45, balance between shear and buoyancy, supercells possible" "BRN > 45, buoyancy dominates over shear, multicells more likely"
LI	LI > 2, stable "0 < LI < 2, weak convection, TSs possible with other source of lift" "-2 < LI < 0, TSs possible, trigger needed, marginally unstable" "-4 < LI < -2, TSs probable, moderately unstable" " LI < -4, severe TSs possible, tornado possible, very unstable"
SWEAT	"SWEAT < 150, TSs unlikely" "150 < SWEAT < 300, slight severe, no severe TSs" "300 < SWEAT < 400, severe TSs possible" "SWEAT > 400, severe TSs probable, tornadoes possible"
SI	SI > 3, stable "1 < SI < 3, rain showers, thundershowers possible with other source of lift" "-2 < SI < 1, TSs possible, marginally unstable" "-3 < LI < -2, TSs probable, moderately unstable" "-6 < SI < -4, severe TSs, very unstable" " SI < -6, strong/severe TSs more probable, tornado possible, extreme unstable"
TTI	"44-45, isolated TSs "46-47, scattered moderate TSs, "48-49, scattered severe TSs "50-51, scattered severe TSs, isolated tornadoes" "52-55, scattered to numerous TSs, few tornadoes"
TQI	TTI > 55, numerous TSs, scattered tornadoes Low-topped thunderstorms possible with the threshold value of 12.
LCLP	"No scale was found. High values indicate how dry the atmosphere is up to that level" "A low LCLP (closer to surface) increases tornadogenesis"
PWAT	"PWAT < 12.7 mm, very low moisture content" "12.8 < PWAT < 31.8 mm, low moisture content" "31.8 < PWAT < 44.5 mm, moderate moisture content" "44.5 < PWAT < 50.8 mm, high moisture content"

In terms of representing the vertical profile of the atmosphere, the Skew-T Log-P diagram at 1200 UTC on 12 January 2015, when the TSSN events occurred at all seven airports, is given in Figure 9.6. The TSSN event occurred longest at LTFJ (285 min) and shortest at LTBA (38 min). In the presence of TSSN events, the average relative humidity at airports was 96%. As can be seen in the diagram, the surface level air temperature is around 0 °C. The actual and dew point temperature lines are nearly overlapped from surface level to about 375 hPa level. The parcel lapse rate usually starts from the surface in the warm season. This may not be the case in the cold season. Elevated convection can be observed in TSSN events. Most atmospheric stability indexes cannot make accurate predictions due to elevated convection. In this diagram, the atmosphere is stable below 600 hPa, and above that is looks unstable, so any convection leading to the lightning and thunder is elevated above the stable layer (an inversion layer). It is also seen that there is a serious cooling above from the 300 hPa level. This is an indication that a large-scale system may exist. The fact that the wind veering with height at this level indicates that there may be a warm advection layer here.

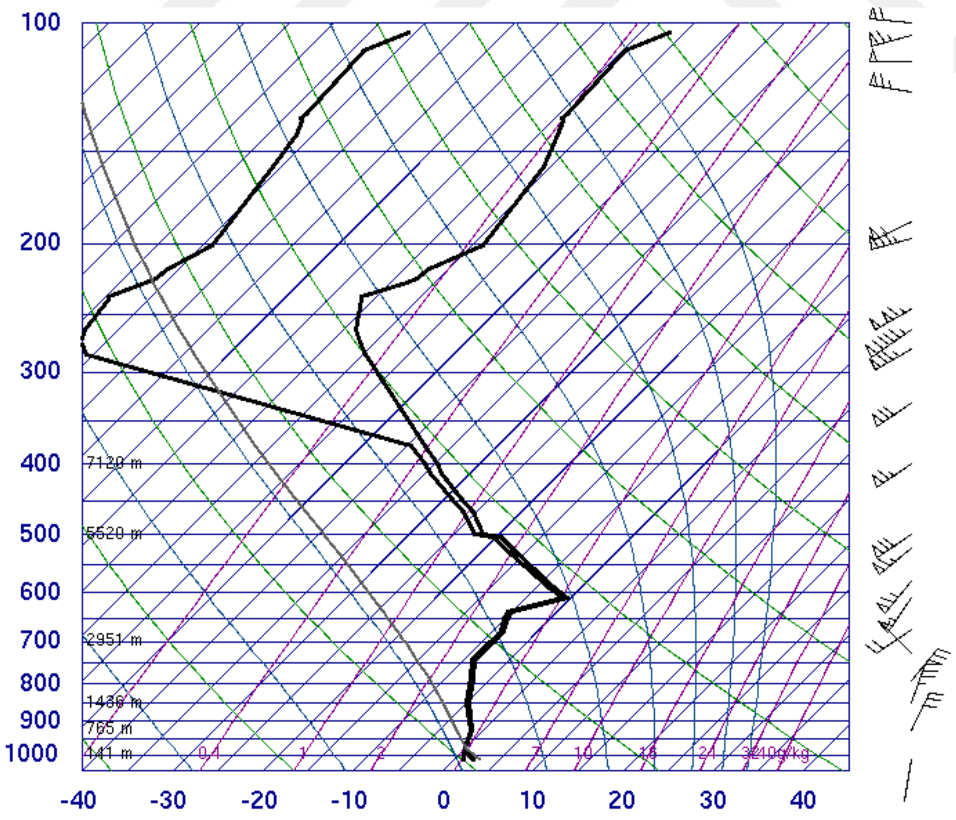

Figure 9.6 : Skew-T Log-P diagram at 1200 UTC on 12 January 2015 (University of Wyoming 2021).

In parallel with the information in the literature for CAPE values (Section 9.1), much lower CAPE values were observed in winter TSs compared to summer TSs. In the TS analyses conducted by Özdemir et al. (2017) at LTBA within the 2008-2013 period, the annual average CAPE values in the winter period varied between 0 W m^{-2} and 30.6 W m^{-2}. Similarly, in the same study, CIN values were found to be between -75.5 W m^{-2} and 0 W m^{-2} on annual averages. In this study, results similar to those in the literature were obtained in all TSSN events, except for Event-14. In Event 14, it was determined that the atmosphere was marginally unstable in terms of the CAPE value. A similar structure was observed in BRN values as well as CAPE values. Event 14 was the only event where buoyant forces dominated vertical shear, and a multicell structure was most likely to be observed (Table 9.4). Therefore, although these three sounding parameters gave good results for summer TSs, they were not successful for winter TSs. In the atmospheric stability indexes, some indexes were almost unsuccessful, while clear information about the instability of the atmosphere could be obtained from some of them. While LI only showed that the atmosphere was very unstable in Event 14, TS and tornadoes were possible, it could not make a similar determination for other events. The SWEAT index showed that slight severe conditions were present in three events and not a severe TS, that severe TS could occur in one event, and finally, severe TS and tornadoes were possible for Event 14. SI showed that thundershowers were possible in an event if there was another source of lift, and for Event 14, extreme unstable atmospheric conditions were present and severe TSs and tornadoes could be seen. The TTI was the second most successful index in revealing the instability of the atmosphere among the indexes. It showed that in 12 of the 19 TSSN events, unstable atmospheric conditions were present. In one of these, it was found that TSs from scattered to enormous would occur and it was possible to see a few tornadoes. It also showed that it was quite possible to observe enormous TSs and scattered tornadoes for Events 13 and 14. Finally, the TQI was the most successful index to reveal the instability of the atmosphere. This index, which is calculated depending on the air temperature and dew point temperature at 850 hPa and the air temperature at 700 hPa, is free from surface level characteristics and daily changes in the characteristics of the layer close to the surface.

LCLP indicates the pressure level at which the LCL value was found. This sounding parameter gives important information about the moisture content in the lower atmosphere. In almost all TSSN events, these levels were determined to vary between 840 hPa and 986 hPa (with the exception of Event 14, 768.9 hPa was detected in that event). Therefore, the lower parts of the atmosphere were not very dry in TSSN events. In PWAT values, mostly very low and low moisture content values were determined. However, this value does not directly look at the humidity for the lower levels of the troposphere, but gives information about the precipitable water content in the entire sounding. A deep column of water vapor is not expected for cold season events, so the same PWAT values confined to low levels are better than it being distributed through a depth. For this reason, humidity information at 850 hPa and 700 hPa levels was also examined. For TSSN events, the average relative humidity value at the 850 hPa level was 81.7%, and this value was 64.1% at the 700 hPa level (Table 9.4). These values indicated that the lower tropospheric levels near the ground (especially around 850 hPa) were rich in moisture content, as observed LCL pressure levels.

Table 9.4 : Atmospheric stability indexes and some parameters that give information about the vertical atmosphere structure. In some values, bold font was used to express important values for each SES event.

	CAPE	**CIN**	**BRN**	**LI**	**SWEAT**	**SI**	**TTI**	**TQI**	**LCLP**	**PWAT**	**RH_{850}**	**RH_{700}**
E-1	0	**0**	0	16.2	106	15	34.4	**14.1**	938	8.2	85	76
E-2	0	**0**	0	9.2	**155**	7	**49.6**	**12.5**	892	8	88	80
E-3	5	**-8**	0.3	11.1	63	11.6	**51.2**	**11.6**	938	6.3	85	10
E-4	0	**0**	0	5	91	5.5	**51.2**	5.9	893	6.3	62	13
E-5	7	**0**	0.3	7.1	109	8.6	**48**	8.6	942	5.8	75	65
E-6	0	**0**	0	7.3	97	7.6	**48.9**	10.9	894	6.1	78	75
E-7	20	**-24**	0.4	11.7	134	12	40.2	**13.9**	946	7	81	22
E-8	0	**0**	0	17.7	142	14.1	34.1	**11.6**	979	17.2	98	98
E-9	0	**0**	0	10	124	9.2	**45.8**	**12.9**	950	8.2	87	78
E-10	12	**-1**	0.9	7.7	79	9.9	**49.5**	**15.6**	986	6.9	96	77
E-11	0	**0**	0	3	**168**	3.6	**54.8**	**19.0**	849	5.6	62	28
E-12	0	**0**	0	10	114	10	43.3	5.5	936	9.6	89	81
E-13	3	**-12**	0.3	4.9	**302**	**1**	**61.7**	**14.1**	953	8.6	89	81
E-14	**501**	**-207**	**67.2**	**-9.1**	**495**	**-4.7**	**69.8**	**14.5**	769	14.6	69	83
E-15	0	**0**	0	16.3	65	16	31.8	**14.1**	879	5.9	79	17
E-16	0	**0**	0	12.7	74	12.7	39.6	**15.3**	973	6.9	88	84
E-17	20	**-7**	2	14.9	83	15.8	32.6	8.0	921	7	81	79
E-18	11	**-1**	5.9	10.9	50	9.6	**44.3**	**16.0**	956	8.5	85	79
E-19	0	**0**	0	4.9	**223**	3.2	**51**	2.1	931	18.5	75	91

9.4 Discussion and Conclusions

In this study, the temporal analyses of TSSN events over a 22-year period were made based on airport reports and the atmospheric conditions in which they occurred were investigated. Such a short-term and rare event has several serious negative effects, especially in terms of aviation activities. In most of the events, it was found that the horizontal visibility decreased drastically when TSSN was observed. In addition, high wind speeds, which often have gust, have been the common adverse condition observed at all airports where TSSN was observed. TSSN events were mostly observed in restricted areas and for a short time (0-1 h). These events were observed only in winter and in November (only two events) during the period. Considering the intraday distributions, no trend was found as in Market et al. (2002). However, very few TSSN events were observed from midnight to sunrise. There are two important points for TS coding at airports. One of them is the hearing of the thunder by the observer and the other is the observation of the lightning. For this reason, it was not thought that less TSSN occurrence in the hours from midnight to sunrise is an observation deficiency or error, but on the contrary, it is known that better observation is made during night hours.

It was determined that in the airport reports that TSSN events were observed in the range of -1 °C and 2 °C. Market et al. (2002) found this value to be around -1 °C, and Schultz (1999) and Stuart (2001) found it around 0 °C. In this study, actual temperature values close to 2 °C were rarely observed, but mostly there were variations around 0 °C. The high relative humidity values (90% and above) observed in these reports indicate that the humidity required for unstable atmospheric conditions and convective movements was available. In addition, when TSSN events were observed, at almost all airports, the wind direction was northerly. This is directly proportional to the fact that the systems that bring precipitation in the Marmara Region, especially in winter, enter from the north. Most of the heavy snowfall caused by the synoptic-scale systems (long-wave troughs, short-wave troughs, fronts, low pressure centres, sea-effect mechanisms) in the region is dominated by northern flows. It was not a coincidence that 6 of the 19 events during the period were observed in 2015, and that one event was detected at different times during the day at all airports where TSSN was observed on 12 January in the same year. It was related to the existence of four different SES systems in total throughout the region that year, and the formation of intense and sea-enhanced snow band structures as a result of almost all of these systems being supported by synoptic-scale systems (mostly after cyclone and frontal passages) (Yavuz et al., 2021b).

The classification of TSSN events according to their formation was similar to the classification made by Market et al. (2002), but the dominance of a single class (SES mechanism) was decisive throughout the period. Sea-effect or sea-enhanced snow mechanisms were observed in 17 of 19 events. On the other hand, Market et al. (2002) approximately found 10% of the TSSN times when the LES mechanism was effective. Air-sea interaction is an important parameter in SES mechanisms, which occur at the meso-scale and exacerbate from time to time with synoptic-scale systems. From this point of view, TSSN and SES event mechanisms are similar to each other due to the atmospheric conditions they require. The arctic and polar origin cold air parcel transported over the western Black Sea during the long fetch (150-600 km) distance could easily meet the humidity requirement (heat and moisture fluxes) for both TS and SES in most of the events analysed during the period. The average values of ΔTSS-850 and ΔT_{SS-700} for all TSSN events were observed as 17 °C and 27 °C, respectively. Due to these high temperature differences between the upper atmosphere and the SS, heat and moisture fluxes from the SS to the upper atmosphere were easily transferred, when the long fetch distance is also taken into account. It is known that sensible and latent heat flux values are directly proportional to the aforementioned temperature differences, and it was determined in this study as well. These high heat and moisture fluxes were caused by or contributed to the formation of high humidity, unstable atmospheric conditions, lifting mechanism, and additionally directional wind shear along the convective boundary layer required for the TS mechanisms. Similar to the result found by Market et al. (2006) in the sounding analyses, veering movements were observed in most cases (84%). In addition, cold air advections were observed in most of the sounding analyses.

Although CAPE values are a suitable analysis parameter to evaluate summer TSs, it is the opposite for winter TSs. Almost all of the CAPE values (except for one event) seem to have stable atmospheric conditions during TSSN events. The fact that TSSN events usually occur as a result from slantwise convection causes the CAPE values to be low. The potential for this is not captured by CAPE as the buoyancy gradient does not exist in the vertical. TTI was the index that made the second most successful prediction in the analyses made by considering the atmospheric stability indexes. There are several reasons for this. TTI, which is used as a measure of TS potential, consists of two basic components: vertical totals (VT) and Cross Totals (CT). VT takes into account lapse rate and static stability between 850- and 500-hPa, while CT takes into account the lower-level moisture throughout 850-hPa. The higher the value of these components, the higher the index value. Increasing values of the index also show that the TS potential is increasing. There are also some disadvantages of the index. Since only parameters in the range of 850 and 500 hPa are used, it does not take into account inversion layers, and moist or dry layers that exist below the 850 hPa level. In addition to these disadvantages of the TTI, directional wind shear, which is critical in the formation of TS, is an important parameter that the index does not take into account. It is also important that the study area should be below the 850-hPa level for the index to be usable. All of the airports analysed in this study are located at altitudes close to sea level. In addition, analyses were carried out considering the airport reports and sounding data on directional wind shear, and it was observed in these analyses that sufficient conditions for TS were created. On the other hand, it was known that the moisture content 850 hPa and below was quite sufficient according to the analysis results obtained from both the sounding data and the airport reports. Finally, in the sounding analyses made, inversion layers were detected in only a few observations at 850 hPa and below, but these also had very low thickness values (45-130 m). When analysing TTI values, it was seen that high consistency estimates can be made for TSSN with the additional analyses to be made for the above-mentioned 850-hPa and lower levels. Besides the TTI, the TQI has the most successful performance among indexes. One of the most important factors that makes this index successful is that it takes into account the instability in the range of 700-500 hPa levels. Although the TQI is more successful in deeply unstable warm season convective environments, it was successful in detecting the TSSN events considered in this study.

For the two airports (LTBA and LTFJ) where the majority of TSSN events occurred, analyses of TS events occurring in January, February, November and December were carried out within the study period (Figure 9.7). As the TSSN events within the period occurred only in these four months, analyses of the TS events were performed for similar months. An increasing linear trend at LTFJ and a decreasing linear trend at LTBA were noted. However, a similar trend was not observed both between cold-season TS and TSSN events, and between airports located in two different regions in the same province. Therefore, it is necessary to conduct a comprehensive study on the forecast of cold-season TS and TSSN events for the region.

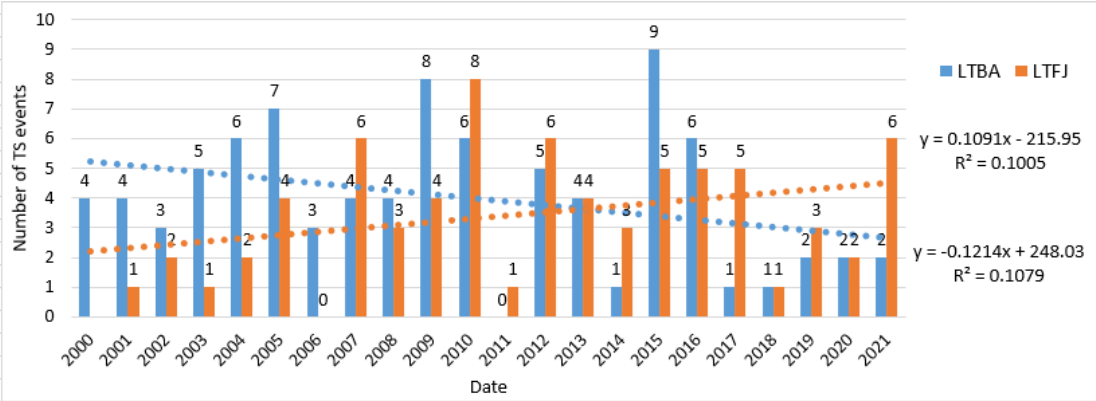

Figure 9.7 : Total number of TS events that occurred in January, February, November, and December at LTBA and LTFJ from 2000-2021.

10. HISTORICAL EXTREME WINTERS OF ISTANBUL: THE FACTORS THAT CONTRIBUTED TO SEVERE WINTERS DURING THE 20TH AND 21ST CENTURIES [9]

10.1 Overview of Istanbul's historical extreme winters

Istanbul is located in a unique geopolitical position in the world. The province, which has a piece of land on the continents of Asia and Europe, connects the Black Sea and the Marmara Sea with a narrow S-shaped channel (throat-also known as the Bosphorus) (Figure 10.1). In order to examine the extreme winters of Istanbul and to compile the records of these winters, it is necessary to divide the period the last 1700 years into three sub-periods. These periods are the Byzantine Empire period (330-1453), the Ottoman Empire period (1453-1922), and the Turkish Republic (1923-continue). The first important event related to the extreme winter conditions in the history of Istanbul occurred in 401. It was stated that the Bosphorus and the Golden Horn were completely frozen during the time of the Byzantine Emperor Arkadius, and ice floes were observed even in March (Yavuz et al., 2007). Since this date, there was a period of harsh winter in almost every century (except the 9th century). In the 9th century, although there were very harsh winters in Europe in six different years and even the Adriatic Sea and the Danube Rivers froze, no written records of extreme winters for Istanbul or the freezing of the Bosphorus could be found.

---

[9] This chapter is based on the research paper: Yavuz, V., Özdaş, M., Lupo, A.R., Fox, N.I. and Deniz, A. (2022). Historical extreme winters of Istanbul: The factors that contributed to severe winters during the 20th and 21st centuries. *International Journal of Global Warming*.

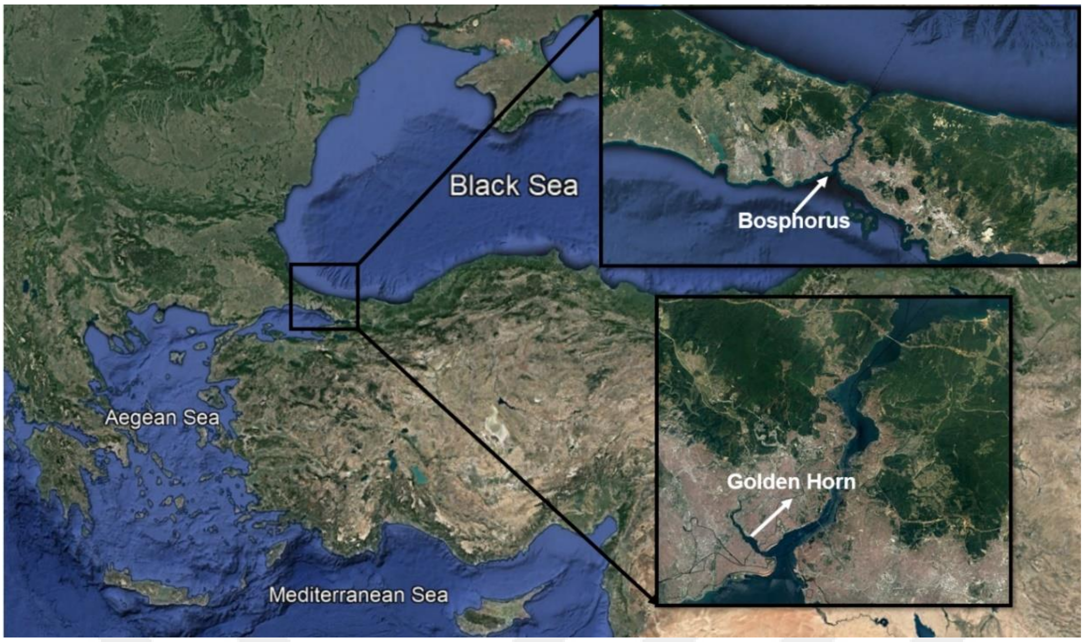

Figure 10.1 : The black small square represents Istanbul. In the upper right corner, the S-type formation separating the two continents is the Bosphorus. In the lower right corner, the Golden Horn with connection to the Bosphorus can be seen.

According to Yavuz et al. (2007), the Bosphorus and the Golden Horn were frozen and the periods when severe cold were experienced were discussed during three historical periods. These extreme conditions were encountered between the 400s, 700-1250 and 1600-2000. It was stated that since the first century AD, the Bosphorus froze 12 times completely and six times in parts, and the Golden Horn was frozen 15 times completely and six times in parts (Yavuz et al., 2007). In the same study, it was stated that the climatic conditions of the region changed depending on the North Atlantic Oscillation (NAO) and the Siberian High-Pressure Centre and these effects were observed between 1621-1954. As a result of the analyses carried out through various newspaper news, literary sources, books, and publications, it was determined that a total of 48 extreme winters occurred in Istanbul between the years 401-2022. In this context, the information obtained about the events and the problems experienced are given in Table 10.1.

Table 10.1: The years of Istanbul's extreme winters and the consequences.

Years	Effects and Consequences
401, 472	The Black Sea was partially frozen, and the ice masses coming from here blocked the Bosphorus and caused it to freeze for 20 days.
545	There was a one-day winter in summer (in August), the waters of the Bosphorus swelled due to the tidal wave, and all the Bosphorus villages were flooded.
660	Extreme colds were observed and Istanbul was covered with snow for months.
739, 753, 755, 756, 763	The Bosphorus and Golden Horn partially frozen, extreme cold and strong winds were observed in 753.
9th century	-
905, 928, 934, 993	In 905, the Bosphorus was frozen, in 928 the Golden Horn was partially frozen and ice masses were observed in the Bosphorus, in 934 ice blocks were observed floating in the Marmara Sea, and in 993 freezing temperatures occurred.
1011	The Bosporus was frozen.
1124	Very low temperature values were encountered in Europe and Istanbul.
1232, 1297	The Bosphorus and the Golden Horn were partially frozen.
1341, 1342, 1343	Freezing temperatures in Europe and Istanbul showed themselves 3 winters in a row.
1402	Icebergs were observed in the Bosphorus.
1573	Snowfalls and freezing temperatures were observed for at least a month.
1620, 1621, 1669	In 1620, thick ice masses connected the two continents, in 1621 the Bosphorus and the Golden Horn were covered with ice, and in 1669 partial freezing occurred in the Bosphorus.
1754, 1755, 1778, 1779, 1782	In 1754, it snowed for 2 months without interruption and the Bosphorus was frozen, in 1755 there were frosts in places in the Bosphorus, and in 1778, 1779 and 1782, very severe winter conditions occurred.
1808, 1823, 1849, 1857, 1862, 1878, 1893	In 1808, snow depths of 1.5 men heights were observed between the neighborhoods, in 1823, the long and harsh winter conditions froze part of the Sea of Marmara and the water flowing from the taps. The Golden Horn was frozen during the years 1849, 1857, 1862, 1878 and 1893, and the Bosphorus was partially frozen in 1862, 1878 and 1893.
1928	The Bosphorus and the Golden Horn partially frozen.
1929	Heavy snowfalls and colds occurred all over Europe and Istanbul, and it snowed nonstop for 2 months. Every day, a few people froze to death, the ceilings of many houses collapsed due to the snow load, the Bosphorus was partially frozen, many of the dam lakes that supplied the city with water were completely frozen, the water pipes burst, hungry wolves and wild boars came to the city.
1942	Long-term freezing cold prevailed.
1954	The Bosphorus was covered with ice floes from the Black Sea. Freezing cold and snow stopped transportation in the Bosphorus. There was a shortage of bread and wood.
1963	Terkos Dam froze and water could not be supplied to the city for days. Freezing temperatures observed.
1969	3 dams in Istanbul were frozen and water could not be supplied to the city.
1987	In March, snowfall continued during the days under the influence of blocking and cyclones, and freezing temperatures were present. Meter-thick snow heights were measured.
2004	Electricity and water were cut off, natural gas could not be supplied.
2012	One of the coldest days in the last 33 years was experienced.
2017	The heaviest snowfall was observed after 1987. Snow heights exceeding 1 meter were measured in some places.
2022	Snow heights were measured in meters from places under the effect of sea-effect snow bands and cyclones.

10.2 Overview of Istanbul's historical extreme winters

The occurrence of one or more of the following criteria has been taken into account in the determination of extreme winter conditions:

- Partial or complete freezing of the Bosphorus or Golden Horn (especially for the first half of the 20th century)
- Freezing of dams in the province
- More than half a meter of snow depth and this situation adversely affects aviation activities, sea transportation, land transportation and energy/water supply for several days
- The occurrence of the coldest days of at least the last 30 years, which do not freeze the Bosphorus, Golden Horn or Dams.

A total of seven winters in the 20th century and four severe or extreme winters in the 21st century up to 2022 were determined in Istanbul. In the 20th century, the Bosphorus and the Golden Horn were partially frozen only in 1928, and in some years, partial or complete freezing occurred in the dams and lake/stream type formations that only supplied water to Istanbul. Images of the Bosphorus, snowfall and freezing throughout Istanbul in the 20th century are given in Figure 10.2 (TRT, 2022).

Figure 10.2 : Istanbul winter landscapes of the 20th century (Vatan, 2022; Milliyet, 2022; Kanalistanbul, 2022).

Following 1928, the year 1929 was the year when the severe winter conditions were observed both in Istanbul and in Europe. In 1942, temperatures were measured below 0 °C for 10 days, 1 °C for 14 days, 3 °C for 27 days and below 5 °C for 44 days at the meteorological station in Goztepe district, located on the Anatolian side of the province. In 1954, the highest daily temperatures remained below 0 °C for days, and after 1929 and 1942, it was the year in which the most severe winter conditions were experienced. At this date, the ice masses coming from the Black Sea covered the Bosphorus, and people were able to walk on these masses in the Bosphorus. The cold temperatures that froze the dams in Istanbul in 1963 and 1969 were also effective in Europe. Mostly the NAO was in the positive phase, causing relatively warm waters to come over Europe from the Atlantic. Longitudinal movements of the Arctic and Polar air masses to the south, the Siberian High-Pressure Centre being located further south, and the blocking effect that lasted for days over Europe caused severe winter conditions to be effective for days.

The first specially prepared study in the literature on the hard winter conditions observed in Istanbul was conducted for the 1987 Istanbul winter (Tayanç et al., 1998). Blocking observed at 250- and 850-hPa geopotential levels over northern Europe contributed to cyclogenesis and led to heavy snowfall. Atmospheric mechanisms showed similarity in the severe winter conditions that took place in the 21st century. The polar cold air, which descends from the north, over central Europe, and sometimes to the Mediterranean, allows the pressure centres to descend continuously with the blocking effect, allowing cyclones to be produced and to pass over Istanbul. In addition, the high temperature differences between sea surfaces and air masses at upper atmospheric levels activate the sea-effect snow (SES) mechanism. These bands, which are currently formed with cyclone and frontal transitions, support the formation of enhanced-sea effect snowfall. Especially in the northern parts of Istanbul, snow depths in the order of meters have been observed from time to time in places where SES bands were impactful.

Yavuz et al. (2021a) determined that SES mechanisms occurred during 75 of the 186 snow events that occurred within the borders of the Marmara Region between 2009 and 2018. In addition, it was determined that these SES bands were formed due to the high temperature differences between the western Black Sea surface and the polar and arctic air masses as a result of the longitudinal movements of these to the south. These bands were stated to be effective in the northern parts of Istanbul in the north-south direction of more than one parallel band with a rate of 85%. According to Yavuz et al. (2021b), it was stated that the heavy snowfalls that took place in 2012 occurred due to the high temperature difference between the sea surface and the air parcels at the level of 850/700 hPa. In addition, it was determined that vortex-type SES bands observed in the western Black Sea region left heavy snowfalls to Istanbul with north-northeast flows during the long fetch distance. For this reason, cyclogenesis, the passage of frontal systems connected to pressure centres over the region, the location and survival times of long waves (predominance of blocking types), short-wave troughs, and SES mechanisms played an important role in the heavy snowfalls and severe cold periods of the 21st century.

10.3 Atmospheric Circulation types and effects on snowfall

In studies conducted for the Marmara Region, it has been stated that northern atmospheric circulation types (NW, N, NE) dominate the frequency and amount of precipitation in the region (Baltaci et al., 2015; Baltacı et al., 2017). Efe et al. (2019) analysed the atmospheric blocking and precipitation changes in Turkey for the period 1977-2016, and determined that Omega-type blocking dominates Turkey in the winter season. They also found that blocking increases the average precipitation frequency. Efe et al. (2020) found an anomaly of -2 °C in the presence of blocking in the northern parts of the Marmara Region (in provinces close to Istanbul) in their study for a similar period. Therefore, it is seen that the winter season blocking systems may cause lower temperature values for the region. Yavuz et al. (2022) studied long waves and short-wave troughs in the formation of SES bands in the western Black Sea. It has been stated that short-wave troughs mostly enter the western Black Sea from western directions (due to long waves), and have high absolute vorticity values depending on the sea surface and upper atmosphere air temperature difference. It has been determined that long waves are effective on the region mostly in cut-off low (COL) and positively-tilted trough forms, and Omega- and Rex-type blocking structures were also observed in the presence of SES systems in addition to these forms. Therefore, the positions of the positively-tilted long-wave troughs, the structures and trajectories of the short-wave troughs acting on them, and ultimately the presence of the components that will form these systems play an important role in the activation, development and trajectory of SES mechanisms. The structure and positions of long waves at 500 hPa in heavy snowfalls that took place in Istanbul in the 2000s in four different years are shown in Figure 10.3, as the average values of the snowy period in those years. It was determined that the positive-tilted trough structure in the region in all figures and the north and north-east flows related to it, carried the cold air pool in the north over the region (Figure 10.3).

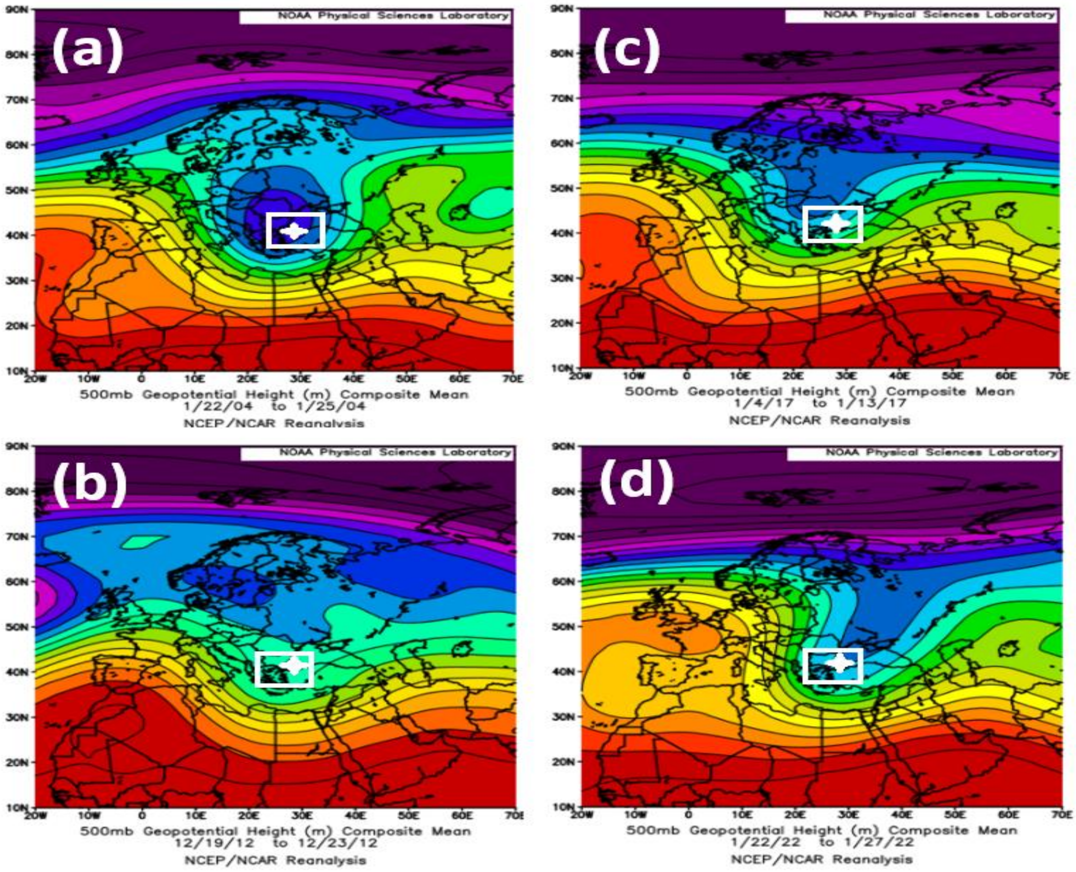

Figure 10.3 : The structure and positions of the long waves at 500 hPa level on a) 22-25 January 2004, b) 19-23 December 2012, c) 4-13 January 2017, d) 22-27 January 2022. The star in the white square indicates Istanbul.

10.4 Black Sea surface temperature anomalies

It has been reported in many studies that changes in Black Sea surface temperatures have direct effects on the formation and effects of SES bands in provinces located in the north of Istanbul and the Marmara Region (Kindap, 2010; Yavuz et al., 2021a, 2021b, Baltaci et al., 2021). The high temperature differences between sea surface and upper atmosphere air contributes positively to the formation and intensification of SES bands (Niziol, 1987; Niziol et al., 1995). For this reason, increasing values of sea surface temperatures will make a positive contribution in terms of SES band formation. In order to analyse the changes in SSTs, the anomaly graph of SST values between 1860 and 2020 for the 30°E and 42°N point (corresponding to the western Black Sea) was obtained from the NOAA Extended Reconstructed Sea Surface Temperature V5 data set (Figure 10.4). The anomaly values showed variations around 0 °C until the 2000s, sometimes values above 4 °C and sometimes below -3 °C were detected. However, it is obvious that anomaly values that have increased on average since the 2000s. If the increasing trend in SST anomaly values continues, it can be said that SES bands with greater frequency and intensity will be effective throughout the region.

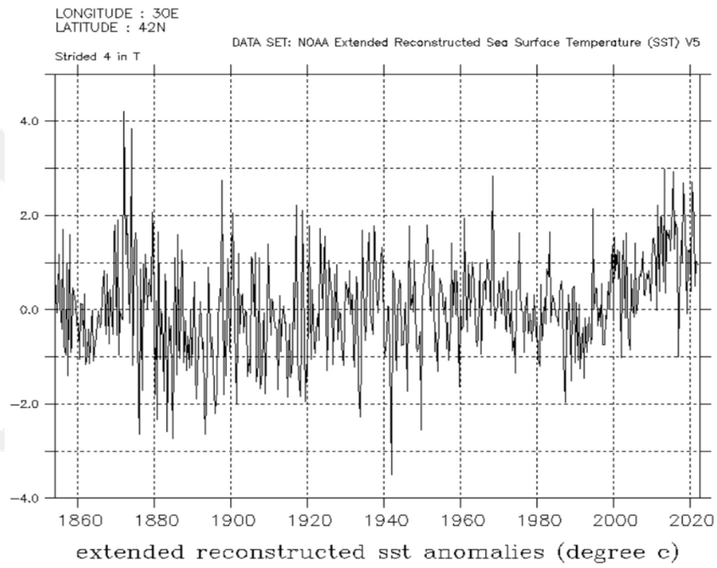

Figure 10.4 : SST anomalies (°C) on the Black Sea.

10.5 The possibility of extreme winter conditions in the period until 2050 and 2100

In this section, the probability of occurrence of these events from 2022 to 2050 and 2100 for Istanbul was analysed based on 23 extreme winter conditions that occurred in the 18th, 19th, 20th, and 21st centuries. First, all data between the 18th and 21st centuries were analysed as the first period, and then only the 20th and 21st centuries data were analysed as the second period. Although the average times between events were known, the Poisson distribution, one of the statistical methods used in event series where the exact timing of events is random, was preferred for analysis. In order to use the Poisson distribution, events must be independent from each other, and one event should not affect the other. At the same time, events should not be simultaneous.

The Poisson distribution gives us how many (k) times an event is likely to be observed in a certain time period (the period from 2022 to 2050 and 2100 in this study), and the average duration (λ) of this event according to time. The equation of the Poisson distribution is as follows.

$$P\ (k;\lambda) = \frac{\lambda^{k} e^{-\lambda}}{k!} \tag{10.1}$$

Projections made until 2050 and 2100 with reference to the extreme winters that took place between the 1^{8th} and 21st centuries are given in Table 10.2, and projections made until 2050 and 2100 with reference to the events that took place in the 20th and 21st centuries are given in Table 10.3. In both projections, there were a possibility of a maximum of 7 severe winters until 2050 and a maximum of 15 severe winters until 2100. In addition, in the projection made by taking the events that occurred in the 20th and 21st centuries as a reference, the probability of the occurrence of events was higher than the other. The probability of more than 7 severe winters by 2050 and 15 or more severe winters by 2100 was found to be slightly higher. This shows the trend of increasing, albeit low, event rates in the 20th and 21st centuries within the entire period.

Table 10.2: Projections made using data between the 18th and 21st centuries.

2022-2050 Projection			**2022-2100 Projection**		
Number of occurrences	**Exact Probability**	**Cumulative Probability**	**Number of occurrences**	**Exact Probability**	**Cumulative Probability**
0	0.091	0.091	0	0.001	0.001
1	0.218	0.308	1	0.008	0.010
2	0.261	0.570	2	0.028	0.037
3	0.209	0.779	3	0.062	0.099
4	0.125	0.904	4	0.104	0.203
5	0.060	0.964	5	0.139	0.341
6	0.024	0.988	6	0.155	0.496
7	0.008	0.997	7	0.148	0.644
>7	0.003	1.000	8	0.124	0.768
			9	0.092	0.860
			10	0.062	0.922
			11	0.038	0.959
			12	0.021	0.980
			13	0.011	0.991
			14	0.005	0.996
			15	0.002	0.998
			>15	0. 002	1.000

Table 10.3: Projections using only data from the 20th and 21st centuries.

2022-2050 Projection			2022-2100 Projection		
Number of occurrences	**Exact Probability**	**Cumulative Probability**	**Number of occurrences**	**Exact Probability**	**Cumulative Probability**
0	0.038	0.038	0	0	0
1	0.124	0.162	1	0.001	0.001
2	0.203	0.364	2	0.005	0.006
3	0.221	0.586	3	0.014	0.019
4	0.181	0.767	4	0.031	0.051
5	0.119	0.886	5	0.057	0.108
6	0.065	0.951	6	0.087	0.195
7	0.030	0.981	7	0.114	0.309
> 7	0.019	1.000	8	0.130	0.439
			9	0.132	0.571
			10	0.120	0.691
			11	0.100	0.79
			12	0.076	0.866
			13	0.053	0.92
			14	0.035	0.954
			15	0.021	0.975
			> 15	0.024	1.000

10.6 Conclusions and Discussion

Turkey's metropolitan city, Istanbul, has been exposed to many natural disasters over the centuries. Extreme precipitation and cold weather, which is one of the meteorological natural disasters, caused the Golden Horn to freeze from time to time, and sometimes even the Bosphorus. In the 20th century, it has been determined that Istanbul has experienced severe winter conditions seven times, on the other hand, in the 21st century, severe winter conditions have occurred only four times in 22 years. In 2012, the coldest day of the last 33 years was experienced, and snow depths exceeding one meter were measured in 2017. Projections for the future, based on Istanbul's extreme winter past, have shown that the megacity will be more exposed to these events in an increasing trend as a result of climate change. When the events that took place in the second half of the 20th century and the 21st century are analysed, the most important reason for the winter systems affecting Istanbul, and especially for the precipitation they leave, is the moisture transport originating from the Black Sea. Sea-effect snow mechanisms, which occur together with meso- and synoptic-scale systems, have become the main mechanism in recent events. The most important parameter that triggers the formation of sea-effect snow bands over the Black Sea is the high sea surface temperatures (SSTs). The increase in SST anomalies, which was responsible for the occurrence of four events in a short time in the 21st century, draws attention. As can be seen from the statistical projections made for the coming years in the analysis section, it is expected that Istanbul will be exposed to extreme winter conditions more frequently in the future.

11. CONCLUSIONS

In this thesis study, it is aimed to carry out detailed analyses on case studies, climatological evaluations, and prediction methods related to thunderstorm and sea-effect snow (SES), which are meteorological events that occur due to air-sea interaction. In the first study, it was revealed that the nowcasting of the thunderstorm that occurred at an international airport in the Marmara Region could be made approximately 42 to 57 minutes before the event time. This result is an important finding for decision makers in the field of meteorology, especially for the aviation sector. In the second study, long-term climatological analyses of thunderstorms were carried out for 11 national and international airports in the Marmara Region. During the 15-year period, intraday, monthly, and annual distributions of thunderstorms were revealed and the atmospheric conditions in which they occurred were determined. The precipitation and non-precipitation conditions of the thunderstorms in the region were determined, and the effects of the changes in sea surface temperatures (SSTs) were analysed. It has been observed that the majority of thunderstorms occur at the airports located in the north of the Marmara Region. The most important reason for this is that the airports in the north are more exposed to the effect of the Black Sea, and the Marmara Sea is smaller than the Black Sea. The second reason is the SSTs are lower in spring and summer.

In the third study, the SES bands occurring over the western Black Sea were classified according to their morphological structures. It was determined that Type-2 band occurred at the highest rate with 85%. Since the sea effect mechanism is in its initial stage in the northern end of the western Black Sea, fewer intense bands were observed in these regions. The number and intensity of the bands increased as one went south on the western Black Sea, depending on the increase in the fetch distance. The main mechanisms in the formation of the band types are the air-sea surface temperature difference, the presence of the inversion layer, the prevailing wind direction under the inversion, and wind shear. The Type-2 band was also the band type in which the highest air-sea surface temperature difference was observed. In the fourth study, vortex, a rare meteorological phenomenon over the Black Sea, and the snowfalls it causes were analysed. It has been determined that the diameter of the vortex varies between 400-500 km, and it maintains its dominance for about 24 hours. The most important mechanism that helped the vortex to form, intensify, and maintain its position was the location of a low pressure centre exactly on the vortex core. While the effect of the vortex in terms of snowfall in the north of the western Black Sea is quite limited, it caused a snow height of 24 cm at the İnebolu Station located in the Marmara Region in the south.

In the fifth study, statistical characteristics of SES events were determined and meso- and synoptic-scale characteristics of events were analysed. It has been determined that most of the SES events occur in January, and the main reason for this is that the dry and cold air masses coming from the north mostly pass over the western Black Sea in January. In all classification types, the temperatures at the airports oscillated around 0 °C. Heavy snowfalls mostly observed in SYNOP events than in other types. In the sixth study, the roles of short-wave troughs and long waves in SES events were investigated. The main role of long waves was to determine the directional determination of short-wave troughs. Shor-wave troughs, on the other hand, moved parallel to the direction of movement of the SES bands in the majority of events, and played a role in reinforcing them. All five different short-wave trough and long wave types caused the convective boundary layer to deepen and the bands to intensify.

In seventh study, statistical analyses of thundersnow events for many years have been carried out. It has been determined that these events are mostly short-term (0-1 hours), and they are mostly effective in the winter season. Temperature differences between sea surface and upper atmospheric levels had high differences in all events. In the analyses made with atmospheric stability indices, it was determined that the most successful indexes in the detection of these events were Total Total Index and TQ Index. In eighth study, an algorithm has been developed to be used in SES prediction for Istanbul Ataturk International Airport and Sabiha Gökçen International Airport. In addition, the snow depth value ranges of sea-effect and non-sea-effect snowfalls were determined and atmospheric conditions were revealed. In the ninth study, the extreme winters and snowfalls that occurred in Istanbul during the 17th century were analysed. Afterwards, predictions for 2050 and 2100 were created based on heavy snowfalls and harsh winters in the last few centuries. Depending on the increasing anomaly values in SSTs, it is predicted that such events will occur more in the future.

REFERENCES

Aalijahan, M., Salahi, B., Rahimi, Y. G. & Asl, M. F. (2019). A new approach in temporal-spatial reconstruction and synoptic analysis of cold waves in the northwest of Iran, *Theor. Appl. Climatol., 137,* 341-352.

ACI (2015). Airports Council International. Available at: http://www.aci.aero/News/Releases/Most-Recent/2015/03/26/ACI-World-releases-preliminary-world-airport-traffic-and-rankings-for-2014--DXB-becomes-busiest-airport-for-international-passenger-traffic- (accessed 16 August 2017).

Ackerman, S. & Knox, J. A. (2013). Meteorology: Understanding the atmosphere, Third edition, chapter 9, 260-272.

Adhikari, A. & Liu, C. (2019). Geographical Distribution of Thundersnow Events and Their Properties from GPM Ku-Band Radar, *J. of Geophy. Res: Atmospheres, 124(4), 2031-*2048.

Alcott, T. I., Steenburgh, W. J. & Laird, N.F. (2012). Great salt lakeeffect precipitation: observed frequency, characteristics, and associated environmental factors, *Weather and Forecasting, 27,* 954–971.

Agnihotri, G., Venugopal, R. & Hatwar, H. R. (2013). Climatology of thunderstorms and squalls over Bangalore, *Mausam, 64(4),* 735-740.

AMS (2021) American Meteorological Society: Glossary of Meteorology. Available at: https://glossary.ametsoc.org/wiki/Long_wave (accessed 12 October 2021).

Andersson, T. & Gustafsson, N. (1994). Coast of Departure and Coast of Arrival: Two Important Concepts for the Formation and Structure of Convective Snowbands over Seas and Lakes, *Mon. Weather Rev., 122,* 1036–1049.

APDRC (2020). Asia-Pasific Data-Research Center: sea surface temperatures. Available at: http://apdrc.soest.hawaii.edu (accessed 15 August 2020).

APDRC (2021). Asia-Pasific Data-Research Center: sea surface temperatures. Available at: http://apdrc.soest.hawaii.edu (accessed 15 August 2021).

Asai, T. & Miura, Y. (1981). An analytical study of meso-scale vortex-like disturbances observed around Wakasa Bay Area, *J. Meteor. Soc. Jpn. 59(6),* 832–843.

Asia-Pasific Data-Research Center (APDRC) (2020). Sea surface temperatures. Available at: http://apdrc.soest.hawaii.edu (accessed 14 August 2020).

Ballentine, R. J. (1992). Numerical simulation of land-breeze-induced snow bands along the western shore of Lake Michigan, *Mon. Wea. Rev., 110(11),* 1544–1553.

Ballentine, R. J., Stamm, A. J., Chermack, E. E., Byrd, G. P. & Schleede, D. (1998). Mesoscale model simulations of the 4–5 January 1995 lake-effect snowstorm, Weather and Forecasting, 13, 893–920.

Baltaci, H., Gokturk, O. M., Kindap, T., Unal, A. & Karaca, M. (2015). Atmospheric circulation types in Marmara Region (NW Turkey) and their influence on precipitation, *Int. J. Climatol., 35(8),* 1810-1820.

Baltaci, H., Kindap, T., Unal, A. & Karaca, M. (2017). The influence of atmospheric circulation types on regional patterns of precipitation in Marmara (NW Turkey), *Theor. Appl. Climatol., 127,* 563-572.

Baltaci, H., da Silva, M. C. L. & Gomes, H. B. (2021). Climatological conditions of the Black Sea-effect snowfall events in Istanbul, Turkey, *Int. J. Clim., 41,* 2017–2028.

Bard, L. & Kristovich, D. A. R. (2012). Trend reversal in Lake Michigan contribution to snowfall. *J. Appl. Meteor. Climatol., 51(11),* 2038-2046.

Braham, R.R. Jr. (1983). The Midwest snowstorm of 8-11 December 1977, *Mon. Wea. Rev., 111(2),* 253– 272.

Bard, L. & Kristovich, D. A. R. (2012). Trend reversal in Lake Michigan contribution to snowfall, *Journal of Applied Climatology, 51,* 2038–2046.

Bech, J., Pineda, N., Rigo, T. & Aran, M. (2013). Remote sensing analysis of a Mediterranean thundersnow and low-altitude heavy snowfall event, *Atmos. Res., 123,* 305-322.

Beşiktepe, Ş. T., Özsoy, E., Abdullatif, M. A. & Oğuz, T. (2000). Hydrography and circulation of the Marmara Sea. Marmara Sea 2000 Symposium, Symposium Book, 284-291. (in Turkish).

Bolsenga, S. J. & Norton, D. C. (1992). Maximum snowfall at long-term stations in the U.S./Canadian Great Lakes. *Nat. Hazards, 5,* 221–232.

Bowler, N. E., Pierce, C. E. & Seed, A. W. (2006). STEPS: A probabilistic precipitation forecasting scheme which merges an extrapolation nowcast with downscaled NWP, *Quartely Journal of the Royal Meteorological Society, 132(620),* 2127-2155.

Braham, R. R., Jr. (1983). The Midwest snowstorm of 8-11 December 1977, *Monthly Weather Review, 111,* 253–272.

Braham, R. R., Jr. (1990) Snow particle size spectra in lake effect snows. *Journal of Applied Meteorology and Climatology, 29(3),* 200–207.

Brunner, L., Schaller, N., Anstey, J., Sillmann, J. & Steiner, A. K. (2018). Dependence of present and future European temperature extremes on the location of atmospheric blocking, *Geophys. Res. Lett., 45,* 6311–6320.

Burnett, A. W., Kirby, M. E., Mullins, H. T. & Patterson, W. P. (2003). Increasing great lake-effect snowfall during the twentieth century: a regional response to global warming, *J. Clim., 16,* 3535–3542.

Burow, D. & Atkinson, C. (2019). An examination of traffic volume during snow events in northeast Ohio, *Nat. Hazards, 99,* 1179–1189.

Campbell, L. S. & Steenburgh, W. J. (2017). The OWleS IOP2b Lake-effect Snowstorm: Mechanisms contributing to the Tug Hill precipitation maximum, *Mon. Weather Rev., 145,* 2461–2478.

Carpenter, D. M. (1993). The Lake Effect of the Great Salt Lake: Overview and Forecast Problems, *Weather Forecast., 8,* 181–193.

Chen, Z. & Wang, Y. (2019). Impacts of severe weather events on high-speed rail and aviation delays, *Transportation Research Part D: Transport and Environment,* 69, 168-183.

Cherington, M. (2001). Lightning injuries in sports: Situations to avoid. *Sports Medicine, 31(4)*, 301-308.

Christian, H. J., Blakeslee, R. J., Boccippio, D. J., Boeck, W. L., Buechler, D. E., Driscoll, K. T., … Stewart, M.F. (2003). Global frequency and distribution of lightning as observed from space by the Optical Transient Detector, *Journal of Geophysical Research,* 108, 4000.

Clark, C. A., Elless, T. J., Lyza, A. W., Ganesh-Babu, B., Koning, D. M., Carne, A. R., … Barrick, J. M. (2016). Spatiotemporal variability in the Lake Michigan region: how is warming affecting wintertime snowfall, *Journal of Applied Meteorology and Climatology, 55,* 1813–1830.

Collins, W., Rasch, P., Boville, B., McCaa, J., Williamson, D., Kiehl, J., … Zhang, M. (2004). Description of the NCAR Community Atmosphere Model (CAM 3.0), University Corporation for Atmospheric Research: Boulder, (CO), USA, Publisher: City, (State Abbreviation), Country.

Colman, B. R. (1990a). Thunderstorms above frontal surfaces in environments without positive CAPE. Part I: Climatology, *Mon. Wea. Rev., 118(5),* 1103-1122.

Colman, B. R. (1990b). Thunderstorms above frontal surfaces in environments without positive CAPE. Part II: Organization and instability mechanisms, *Mon. Wea. Rev., 118(5),* 1123-1144.

Cordeira, J. M. & Laird, N. F. (2008). The influence of ice cover on two lake-effect snow events over Lake Erie, *Monthly Weather Review, 136,* 2747–2763.

Crowe, C., Market, P., Pettegrew, B., Melick, C. & Podzimek, J. (2006). An investigation of thundersnow and deep snow accumulations, *Geophys. Res. Lett., 33(24),* L24812.

Curran, J. T & Pearson A. D. (1971). Proximity soundings for thunderstorms with snow. *Preprints, Seventh Conference on Severe Local Storms,* American Meteorological Society: Kansas City, MO. 118–119.

Das, S., Tomar, C. S., Giri, R. K., Bhattacharjee, K. & Barman, B. (2014). The severe thunderstorm of 5th April, 2010 at Guwahati Airport: An observational study, *Mausam, 65(1),* 99-102.

Demirarslan, K.O. & Akinci, H. (2018). Assessment of Winter Season Air Quality in the Marmara Region Using GIS and Air Quality Data, *Journal of Natural Hazards and Environment, 4(1), 11*-27.

Dockus, D. A. (1985). Lake effect snow forecasting in the computer age. *Natl. Weather Dig., 10,* 5–19.

Doswell, C. A. III. & Evans, J. S. (2003). Proximity sounding analysis for derechos and supercells: an assessment of similarities and differences, *Atmos. Res., 67-68*, 117-133.

Drozdov, A., Grigoriev, A. & Malyshkin, Y. (2013). Assessment of thunderstorm neutron radiation environment at altitudes of aviation flights, *Journal of Geophysical Research: Space Physics*, 118(2), 947-955.

Dunya (2015) Severe storm affected flights at Sabiha Gokçen Airport. Available at: https://www.dunya.com/gundem/siddetli-ruzgar-ucak-seferlerini-de-etkiledi-haberi-268222 (accessed 5 November 2021).

Dunya (2020) Kar çilesi devam edecek. Available at: https://www.dunya.com/gundem/kar-cilesi-devam-edecek-haberi-164923 (accessed 6 September 2020).

Ellis, A. W. & Leathers, D. J. (1996). A synoptic climatological approach to the analysis of lake-effect snowfall: potential forecasting applications, *Weather and Forecasting, 11,* 216–229.

Dixon, M. & Wiener, G. (1993). TITAN: Thunderstorm identification, tracking, analysis and nowcasting - A radar-based methodology, *Journal of Atmospheric and Oceanic Technology, 10(6),* 785-797.

Efe, B., Lupo, A. R. & Deniz, A. (2019). The relationship between atmospheric blocking and precipitation changes in Turkey between 1977 and 2016, *Theor. Appl. Climatol., 138(3–4),* 1573–1590.

Efe, B., Sezen, İ., Lupo, A. R. & Deniz, A. (2020a). The relationship between atmospheric blocking and temperature anomalies in Turkey between 1977 and 2016, *Int. J. Climatol., 40(2),* 1022–1037.

Efe, B., Lupo, A. R. & Deniz, A. (2020b). Extreme temperatures linked to the atmospheric blocking events in Turkey between 1977 and 2016, *Nat. Hazards, 104(2),* 1879–1898.

Eichenlaub, V. L. (1970). Lake Effect Snowfall to the Lee of the Great Lakes: Its Role in Michigan, *Bull. Am. Meteorol. Soc., 51,* 403–412.

Elkins, H. A. (1987). Thunderstorms with snow: A comprehensive, empirical study of their occurrence, development and structure (Master's thesis), Saint Louis University, 79 pp.

Ellis, A. W. & Leathers, D. J. (1996). A synoptic climatological approach to the analysis of lake-effect snowfall: potential forecasting applications, *Weather and Forecasting, 11,* 216–229.

Enno, S. E., Sugier, J., Alber, R. & Seltzer, M. (2020). Lightning flash density in Europe based on 10 years of ATDnet data, *Atmospheric Research, 235,* 104769.

Estoque, M. A. & Ninomiya, K. (1976). Numerical simulation of Japan Sea effect snowfall. *Tellus, 28,* 243–253.

FGA (2021). Future Generation Aviation: airports in Turkey, Available at: http://www.tr.auto-gyro.com/sayfa/ucus-hazirligi/turkiye-havaalanlari.html (accessed 18 April 2021).

Forbes, G. S. & Lottes, W. D. (1982). Characteristics and evolution of mesoscale cloud vortices occurring in polar airstreams. Preprints Conf Cloud Phys, Chicago, *Amer. Meteor. Soc.*, 310–313.

Forbes, G. S. & Merritt, J. H. (1984). Mesoscale vortices over the Great Lakes in wintertime. *Monthly Weather Review, 112*, 377–382.

Fujisaki-Manome, A., Fitzpatrick, L. E., Gronewold, A. D., Anderson, E. J., Lofgren, B. M., Spence, C., … Xiao, C. (2017). Turbulent Heat Fluxes during an Extreme Lake-Effect Snow Event, *J. Hydrometeorol., 18,* 3145–3163.

Galway, J. G. (1956). The lifted index as a predictor of latent instability, *Bull. Amer. Meteor. Soc., 43,* 528–529.

GDSAA (2015). General Directorate of State Airports Authority. Available at: http://www.dhmi.gov.tr/home.aspx (accessed 16 August 2017).

GDSAA (2021) General Directorate of State Airports Authority, Republic of Turkey Ministry of Transport and Infrastructure: Airport information. Available at: https://www.dhmi.gov.tr/Sayfalar/HavaLimanlari.aspx (accessed 5 March 2021).

Gerbush, M. R., Kristovich, D. A. R. & Laird, N. F. (2008). Mesoscale Boundary Layer and Heat Flux Variations over Pack Ice Covered Lake Erie, *J. Appl. Meteorol. Clim., 47,* 668–682.

Germann, U. & Zawadzki, I. (2002). Scale-dependence of the predictability of precipitation from continental radar images. Part I: Description of the methodology, *Monthly Weather Review, 130(12),* 2859-2873.

Ghafarian, P., Pegahfar, N. & Owlad, E. (2018). Multiscale analysis of lake-effect snow over the southwest coast of the Caspian Sea (31 January-February 5, 2014). *Weather, 73*, 9–14.

Ghafarian, P. (2021). Impact of physical parameterizations on simulation of the Caspian Sea lake-effect snow, *Dyn. Atmos. Oceans, 94,* 101219.

Ghafarian, P., Delju, A. H., Tajbakhsh, S. & Penchah, M. M. (2021). Simulation of the role of Caspian Sea surface temperature and air temperature on precipitation intensity in lake-effect snow, *J. Atmos. Sol.-Terr. Phys., 225,* 105777.

Google Earth (2020). Maps. Available at: https:// www. google. com/ earth (accessed 3 September 2020).

Goree, P. A. & Younkin, R. J. (1966). Synoptic climatology of heavy snowfall over the central and eastern United States, *Mon. Wea. Rev., 94(11),* 663-668.

Grenfell, T. C. & Putkonen, J. (2008). A method for the detection of the severe rain-on-snow event on Banks Island, October 2003, using passive microwave remote sensing, *Water Resour. Res., 44,* 03425.

Halcomb, C. E. & Market, P. S. (2003). Forcing, instability, and equivalent potential vorticity in a midwestern U. S. convective snowstorm, *Meteorol. Appl. 10,* 273– 280.

Hall, J. V., Zhang, R., Schroeder, W., Huang, C. & Giglio, L. (2019). Validation of GOES-16 ABI and MSG SEVIRI active fire products, *International Journal of Applied Earth Observation and Geoinformation*, *83,* 1–14.

Hanks, H. H., de Harpporte, D. R. Jr. & Grueber, E. C. (1967). Snow forecasting procedures in the central United States. Final Report, Contract, Cwb-11353, Atmospheric Research and Development Corp., Kansas City, MO, 33.

Hartnett, J. J., Collins, J. M., Baxter, M. A. & Chambers, D. P. (2014). Spatiotemporal snowfall trends in Central New York. *Journal of Applied Meteorology and Climatology, 53(12),* 2685-2697.

Henry, N. L. (2000). A Static Stability Index for Low-Topped Convection, *Wea. Forecasting, 15(2),* 246-254.

Hjelmfelt, M. R. & Braham, R. R. (1983). Numerical Simulation of the Airflow over Lake Michigan for a Major Lake-Effect Snow Event, *Mon. Weather Rev., 111,* 205–219.

Hjelmfelt, M. R. (1990). Numerical study of the influence of environmental conditions on lake-effect snow-storms on Lake Michigan, *Mon. Wea. Rev., 118*, 138–150.

Hjelmfelt, M. R. (1992). Orographic Effects in Simulated Lake-Effect Snowstorms over Lake Michigan, *Mon. Weather Rev., 120*, 373–377.

Holle, R. L., Cortinas, J. V. & Robbins, C. C. (1998). Winter thunderstorms in the United States. Preprints, *16th Conf. on Weather Analysis and Forecasting,* Phoenix, AZ, *Amer. Meteor. Soc*., 298–300.

Holroyd, E. W., III. (1971). Lake-effect cloud bands as seen from weather satellites, *Journal of the Atmospheric Sciences*, *28(7),* 1165–1170.

Holton, J. R. & Hakim, G. J. (2013). An Introduction to Dynamic Meteorology. Waltham, MA: Academic Press.

Hong, H. P., Ye, W. (2014). Analysis of extreme ground snow loads for Canada using snow depth records, *Nat. Hazards, 73,* 355–371.

Hoyle, B. D. (2008). Climate change, in context: Sea temperatures and storm intensity. Available at: Encloypedia.com (accessed 18 September 2017).

IMM (2021). Istanbul Metropolitan Municipality: Climate of Istanbul. Available at: https://www.ibb.istanbul/ (accessed 23 November 2021).

IOWA (2020). Environmental Mesonet: ASOS-AWOS-METAR data. Available at: https://mesonet.agron.iastate.edu/request/download.phtml (accessed 19 August 2020).

IOWA (2021). Environmental Mesonet: ASOS-AWOS-METAR data. Available at: https://mesonet.agron.iastate.edu/request/download.phtml (accessed 19 June 2021).

Ismail, P. & Siadari, E. L. (2015). Atmospheric conditions analysis of the heavy rain phenomenon in Biak (case study 4-5 December 2014), *IOP Conference Series: Journal of Physics, 795*, IOS Publishing.

Jebson, S. (2011). The Derby Day thunderstorm of 31 May 1911, *Weather, 66(6),* 156-157.

Jiusto, J. E. & Kaplan, M. L. (1972). Snowfall from lake-effect storms, *Mon. Wea. Rev., 100,* 62–66.

Kaltenböck, R., Diendorfer, G. & Dotzek, N. (2009). Evaluation of Thunderstorm Indices from ECMWF Analyses, Lightning Data and Severe Storm Reports, *Atmospheric Research, 93*, 381-396.

Kanalistanbul (2022). The year the Bosphorus froze. Available at: http://www.kanalistanbul.com.tr/istanbul-bogazinin-dondugu-yil/ (accessed 21 February 2022).

Karan, H. (2007). Thermodynamic and Kinematic Characteristics of Low-level Convergence Zones Observed by the Mobile Integrated Profiling System (Ph.D. thesis). University of Alabama.

Kawai, Y. & Wada, A. (2007). Diurnal sea surface temperature variation and its impact on the atmosphere and ocean: A review, *Journal of Oceanography, 63,* 721-744.

Kelly, R. D. (1982). A single doppler radar study of horizontal-roll convection in a lake-effect snow storm, *Journal of the Atmospheric Sciences, 39,* 1521–1531.

Kelly, R. D. (1986). Mesoscale frequencies and seasonal snowfalls for different types of Lake Michigan snow storms, *J. Atmos. Appl. Meteorol., 25,* 308–312.

Kindap, T. (2010). A severe sea-effect snow episode over the city of Istanbul, *Natural Hazards, 54, 707*–723.

Kocin, P. J., Schumacher, P. N., Morales, Jr. R. F. & Uccellini, L. W. (1995). Overview of the 12-14 March 1993 superstorm, *Bull. Americ. Met. Soc., 76(2),* 165-182.

Kohn M., Galanti, E., Price, C., Lagouvardos, K. & Kotroni, V. (2011). Nowcasting thunderstorms in the Mediterranean region using lightning data, *Atmospheric Research, 100(4),* 489-502.

Kristovich, D. A. R. & Laird, N. F. (1998). Observations of Widespread Lake-Effect Cloudiness: Influences of Lake Surface Temperature and Upwind Conditions, *Weather Forecast., 13,* 811–821.

Kristovich, D. A. R., Laird, N. F. & Hjelmfelt, M. R. (2003). Convective evolution across Lake Michigan during a widespread lake-effect snow event, *Mon. Wea. Rev., 131(4),* 643-655.

Kristovich, D. A. R., Young, G. S., Verlinde, J., Sousounis, P. J., Mourad, P., Lenschow, D., … Young, J. (2000). The lake-induced convection experiment and the snowband Dynamics Project, *Bulletin of the American Meteorological Society, 81(3),* 519–542.

Kumijan, M.R. & Dierling, W. (2015). Analysis of Thundersnow Storms over Northern Colorado, *Wea. Forecasting 30(6),* 1469-1490.

Kunkel, K. E., Westcott, N. E. & Kristovich, D. A. R. (2002). Assessment of potential effects of climate change on heavy lake-effect snowstorms near Lake Erie, *Journal of Great Lakes Research, 28,* 521–536.

Laird, N. F. (1999). Observation of coexisting mesoscale lake-effect vortices over the western Great Lakes, *Mon. Wea. Rev., 127,* 1137–1141.

Laird, N. F., Miller, L. J. & Kristovich D. A. R. (2001). Synthetic dual-Doppler analysis of a winter mesoscale vortex, *Mon. Wea. Rev., 129,* 312–331.

Laird, N. F., Kristovich, D. A. R. & Walsh, J. E. (2003). Idealized Model Simulations Examining the Mesoscale Structure of Winter Lake-Effect Circulations, *Mon. Weather Rev., 131*, 206–221.

Laird, N. F. & Kristovich, D.A.R. (2004). Comparison of observations with idealized model results for a method to resolve winter lake-effect mesoscale morphology, *Mon. Wea. Rev., 132,* 1093–1103.

Laird, N. F., Desrochers, J. & Payer, M. (2009a). Climatology of lake-effect precipitation events over Lake Champlain, *Journal of Applied Meteorology, 48,* 232–250.

Laird, N. F., Sobash, R. & Hodas, N. (2009b). The Frequency and Characteristics of Lake-Effect Precipitation Events Associated with the New York State Finger Lakes, *Journal of Applied Meteorology and Climatology 48(4),* 873-886.

Laird, N. F., Bentley, A. M., Ganetis, S. A., Stieneke, A. & Tushaus, S. A. (2016). Climatology of lake-effect precipitation events over Lake Tahoe and Pyramid Lake, *Journal of Applied Meteorology and Climatology, 55(2),* 297-312.

Laird, N. F., Metz, N. D., Gaudet, L., Grasmick, C., Higgins, L., Loeser, C., … Zelinsky, D. A. (2017). Climatology of cold season lake-effect cloud bands for the North American Great Lakes, *Int. J. Climatol., 37(4),* 2111-2121.

Lang, C. E., McDonald, J. M., Gaudet, L., Doeblin, D., Jones, E. A. & Laird, N. F. (2018). The Influence of a Lake-to-Lake Connection from Lake Huron on the Lake-Effect Snowfall in the Vicinity of Lake Ontario, *J. Appl. Meteorol. Clim., 57,* 1423–1439.

Lavoie, R. L. (1972). A mesoscale numerical model of lake-effect storms, *J. Atmos. Sci., 29,* 1025–1040.

Lazri, M., Labadi, K., Brucker, J. M. & Ameur, S. (2020). Imrpoving satellite rainfall estimation from MSG data in Northern Algeria by using a multi-classifier model based on machine learning, *Journal of Hydrology, 584,* 1–16.

Li, P. & Lai, E. S. (2004). Short-range quantitative precipitation forecasting in Hong Kong, *Journal of Hydrology, 288(1),* 189-209.

Lucas, C., Zipser, E. J. & LeMone, M. A. (1994). Convective Available Potential Energy in the Environment of Oceanic and Continental Clouds: Correction and Comments, *J. Atmos. Sci. 51(24),* 3829-3830.

Ma, R., Sun, J. & Yang, X. (2021). An eight-year climatology of the warm-season severe thunderstorm environments over North China, *Atmospheric Research, 254,* 105519.

Magono, C., Kikuchi, K., Kimura, T., Tazawa, S. & Kasai, T. (1966). A study on the snowfall in the winter monsoon season in Hokkaido with special reference to low land snowfall, *Journal of Faculty of Science, Hokkaido University Series, 11,* 287–308.

Mahoney, E. A. & Niziol, T.A. (1997). BUFKIT: a software application tool kit for predicting lake-effect snow. Preprints, 13th Int. Con. on Interactive information and processing systems for meteorology, oceanography, and hydrology, Long Beach, CA, Amer. Meteor. Soc. Mesoscale meteorology in mid-latitudes. Wiley-Blackwel, 388-391.

Mäkelä, A., Saltikoff, E., Julkunen, J., Juga, I., Gregow, E. & Niemelä, S. (2013). Cold-season thunderstorms in Finland and their effect on aviation safety, *Bull. of Amer. Meteor. Soc., 94(6),* 847-858.

Manzato, A. (2007). The 6 h climatology of thunderstorms and rainfalls in the Friuli Venezia Giulia Plain, *Atmospheric Research, 83*, 336-348.

Market, P. S., Halcomb, C. E. & Ebert, R. L. (2002). A Climatology of Thundersnow Events over the Contiguous United States, *Wea. Forecasting, 17(6),* 1290-1295.

Market, P. S., Oravetz, A. M., Gaede, D., et al. (2006). Proximity soundings of thundersnow in the central United States, *J. of Geophy. Res: Atmospheres,* 111(D19).

Market, P. S., Ebert-Cripe, R. L. & Bodner, M. (2007). Case study of a longlived thundersnow event, *National Weather Digest, 31,* 103-120.

Markowski, P. & Richardson, Y. (2010). Mesoscale Meteorology in Midlatitudes; Wiley: Hoboken, NJ, USA, 2010, 407.

Mass, C. F. (2011). Nowcasting: The next revolution in weather prediction, Bulletin of the American Society. Available at: https://www.atmos.washington.edu/~cliff/BAMSNowcast7.11.pdf (accessed 18 September 2017).

Mazon, J., Niemelä, S., Pino, D., Savijärvi, H. & Vihma, T. (2015). Snow bands over the Gulf of Finland in wintertime, *Tellus A Dyn. Meteorol. Oceanogr., 67,* 25102.

Meteomanz (2020). SYNOP/BUFR recorded data. Available at: http://meteomanz.com/index?l=1 (accessed 19 August 2020).

Meteorology (2005). JAA ATPL theoretical training manual: Meteorology, Oxford Academy. Chapter 20, 1.

Met Office (2020). Surface pressure charts. Available at: https://www.metoffice.gov.uk/weather/maps-and-charts/surface pressure (accessed 1 September 2020).

Metz, N. D., Bruick, Z. S., Capute, P. K., Neureuter, M. M., Ott, E. W. & Sessa, M. F. (2019). An investigation of cold-season short-wave troughs in the great lakes region and their concurrence with lake-effect clouds, *J. Appl. Meteorol. Climatol., 58(3),* 605–614.

Miller R. C. (1972). Notes on the analysis of severe storm forecasting procedures of the air force global weather center AFGWC Tech Rep 200, *Air Weather Service,* Scott AFB, IL.

Milliyet (2022). Istanbul has seen very dark winters in 5 thousand years. Available at: https://www.milliyet.com.tr/gundem/istanbul-5-bin-yilda-cok-kara-kislar-gordu-1496801 (accessed 22 February 2022).

Miner, T. J. & Fritsch, J. M. (1997). Lake-effect rain events, Mon. Wea. Rev., 125(12), 3231–3248.

Miyazawa, S. (1967). On vertical mesoscale disturbances observed during the period of heavy snow or rain in the hokuriku district, *J. Meteor. Soc. Jpn., 45,* 166–176.

Munzar, J. & Franc, M. (2003), Winter thunderstorms in central Europe in the past and the present, *Atmos. Res. 67-68,* 501-515.

Nakai, S., Iwanami, K., Misumi, R., Park, S. G. & Kobayashi, T. (2005). A classification of snow clouds by Doppler radar observations at Nagaoka, Japan, *Scientific Online Letters on the Atmosphere, 1,* 161–164.

NASA (2020). National Aeronautics and Atmospheric Administration. Available at: http://lance-modis.eosdis.nasa.gov/cgibin/imagery/realtime.cgi?date=2009058 (accessed 11 September 2020).

NASA (2021). National Aeronautics and Atmospheric Administration. Available at: http://lance-modis.eosdis.nasa.gov/cgibin/imagery/realtime.cgi?date=2009058 (accessed 15 July 2021).

Nicholls, J. F. & Toumi, R. (2014). On the lake effects of the Caspian Sea, *Q. J. R. Meteorol. Soc., 140,* 1399–1408.

Niziol, T. A. (1987). Operational forecasting of lake-effect snowfall in western and central New York, *Weather and Forecasting, 2,* 310–321.

Niziol, T. A., Snyder, W. R. & Waldstreicher, J. S. (1995). Winter weather forecasting throughout the eastern United States. Part IV: lake effect snow, *Weather and Forecasting, 10,* 61–77.

NOAA (2015). National Oceanic and Atmospheric Administration. Available at: http://www.srh.noaa.gov/ffc/?n=gloss2 (accessed 12 August 2017).

NWS (2021) National Weather Service: Basic wave patterns. Available at: https://www.weather.gov/jetstream/basic (accessed 7 October 2021).

Notaro, M., Zarrin, A., Vavrus, S. & Bennington, V. (2013). Simulation of heavy-lake effect snowstorms across the Great Lakes basin by RegCM4: synoptic climatology and variability, *Monthly Weather Review, 141(6),* 1990–2014.

Notaro, M., Bennington, V. & Vavrus, S. (2015). Dynamically Downscaled Projections of Lake-Effect Snow in the Great Lakes Basin, *J. Clim., 28,* 1661–1684.

Olsson, T., Post, P., Rannat, K., Keernik, H., Perttula, T., Luomaranta, A., … Voormansik, T. (2018). Sea-effect snow-fall case in the Baltic Sea region analysed by reanalysis, remote sensing data and convection-permitting mesoscale modelling, *Geophysica, 53,* 65–91.

Olsson, T., Perttula, T., Jokinen, P., Luomarata, A., Kamarainen, M., Laurila, T., … Jylha, K. (2018). Severe seaeffect snowfall on the Finnish Coast, *Finnish Meteorological Institute*, SAFIR2018.

Özdemir, E. T. & Deniz, A. (2016). Severe thunderstorm over Esenboğa International Airport in Turkey on 15 July 2013, *Weather, 71(7),* 157-161.

Özdemir, E. T., Deniz, A., Sezen, İ., Aslan, Z. & Yavuz, V. (2017). Investigation of thunderstorms over Atatürk International Airport (LTBA), *Mausam, 68(1),* 175-180.

Özdemir, E. T. & Yetemen, Ö. (2019). Deniz etkisi arttırılmıs¸ kar yağışının meteorolojik analizi, 17-19 Şubat 2015, Istanbul olayı, *Journal of Anatolian Environmental and Animal Sciences, 2,* 115–121 (in Turkish).

Özdemir, E. T., Yavuz, V., Deniz, A., Karan, H., Kartal, M. & Kent, S. (2019). Squall line over Antalya: a case study of the events of 25 October 2014, *Weather, 74(S1),* S1-S6.

Özdemir, E. T. (2021). A Case Study of a Multicell Severe Convective Storm in Ankara, Turkey, *Pure Appl. Geophys., 178,* 4107-4126.

Özgür, E. & Koçak, K. (2019). Climatology of snowfall/total precipitation days over Turkey, *Arch. Meteorol. Geophys. Bioclimatol. Ser. B, 137,* 2487–2495.

Özgür, E. & Koçak, K. (2021). Spatial variation of critical temperatures between snow and rain over Turkey, *Arab. J. Geosci., 14,* 1–10.

Öztopal, A. (2017). Investigation of Turkey's lightning observation, *Dokuz Eylül University Journal of Science and Engineering, 19(56),* 304-313.

Paolo, S. & Davolio, S. (2017). Intense air-sea exchanges and heavy orographic precipitation over Italy: the role of Adriatic Sea surface temperature uncertainty, *Atmospheric Research, 196,* 62–82.

Passarelli, R. E. & Braham, R. R., Jr. (1981). The role of the winter land breeze in the formation of Great Lakes snowstorms, *Bulletion of American Meteorological Society, 82,* 482–491.

Peace, R. L. & Sykes, R. B. (1966). Mesoscale study of a lake effect sow storm, *Monthly Weather Review, 94,* 495–507.

Pease, S. R., Lyons, W. A., Keen, C. S. & Hjelmfelt, M. (1988). Mesoscale spiral vortex embedded within a Lake Michigan snow squall band: high resolution satellite observations and numerical model simulations, *Mon. Wea. Rev., 116,* 1374–1380.

Pepler, R. A. & Lamb, P. J. (1989). Tropospheric Static Stability and Central North American Growing Season Rainfall, *Mon. Wea. Rev., 117(6),* 1156-1180.

Pettersen, S. (1956). Weather analysis and forecasting: Volume II. Weather and Weather Systems. McGraw-Hill, 266 p.

Pike, W. S. & Webb, J. D. C. (2020). The very deep cold pool, and lake-effect snowfalls of 27 February–1 March 2018. *Weather, 75(3),* 88-98.

Piper, D. & Kunz, M. (2017). Spatiotemporal variability of lightning activity in Europe and the relation to the North Atlantic Oscillation teleconnection pattern, *Natural Hazards and Earth System Sciences, 17(8),* 1319-1336.

Plymouth State Weather Center (PSWC) (2020). Upper air charts. Available at: https://vortex.plymouth.edu/myo/upa (accessed 2nd August 2020).

Pradhan, D., De, U. K. & Singh, U. V. (2012). Development of nowcasting technique and evaluation of convective indices for thunderstorm prediction in Gangetic West Bengal (India) using Doppler Weather Radar and upper air data, *Mausam, 63(2),* 299-318.

Proseus, E. A. (2000). A Meteorological Analysis of the American Airlines Flight 1420 Accident, *Ninth Conf. on Aviation, Range, and Aerospace Meteorology,* 11-15 September 2000, 209-211.

PSWC (2020). Plymouth State Weather Center: upper air charts. Available at: https:// vortex.plymouth.edu/myo/upa (accessed 18 August 2020).

PSWC (2021). Plymouth State Weather Center: upper air charts. Available at: https:// vortex.plymouth.edu/myo/upa (accessed 18 June 2021).

Punkka, A. J., Teittinen, J. & Johns, R. H. (2006). Synoptic and Mesoscale Analysis of a High-Latitude Derecho–Severe Thunderstorm Outbreak in Finland on 5 July 2002, *Weather and Forecasting, 21(5),* 752-763.

Rabinowitz, J. L, Lupo, A. R. & Guinan, P. E. (2018). Evaluating linkages between atmospheric blocking patterns and heavy rainfall events across the north-central Mississippi River valley for different ENSO phases. *Adv. Meteorol.*, Article ID 1217830.

Raghavendra, A., Zhou, L., Jiang, Y. & Hua, W. (2018). Increasing extent and intensity of thunderstorms observed over the Congo Basin from 1982 to 2016, *Atmospheric Research, 213,* 17-26.

Reinking, R. F., Caiazza, R., Kropfli, R. A., Orr, B. W., Martner, B. E., Niziol, T. A., … Koscielny, A. J. (1993). The Lake Ontario Winter Storms (LOWS) project, *Bulletin of the American Meteorological Society, 74,* 1828–1849.

Rothrock, H. J. (1969). An aid in forecasting significant lake snows. Tech. Memo. WBTM CR-30, National Weather Service Central. *The Region, 16*.

Ryley, T., Baumeister, S. & Coulter, L. (2020). Climate change influences on aviation: A literature review, *Transport Policy, 92,* 55-64.

Saslo, S. & Greybush, S. J. (2017). Prediction of lake-effect snow using convection-allowing ensemble forecasts and regional data as-sim-ilation, *Weather Forecast, 32,* 1727–1744.

Schmidlin, T. W. (1993). Impacts on severe winter weather during December 1989 in the Lake Erie snow belt, *J. Clim., 6*, 759–767.

Schrom, R., Stamm, A., Ruth, D., Jaszka, K., Kress, T., Rathbun, B., … Kosiba, K. (2013). Circulations, bounded weak echo regions, and horizontal vortices observed within long-lake-axis-parallel-lake-effect storms by the Doppler on wheels. *Monthly Weather Review, 141(8),* 2821–2840.

Schultz, D. M. (1999). Lake-Effect Snowstorms in Northern Utah and Western New York with and without Lightning, *Wea. Forecasting, 14(6),* 1023-1031.

Schultz, D. M. & Vavrek, R. J. (2009). An overview of thundersnow. *Weather 64(10),* 274-277.

Scott, C. P. J. & Sousounis, P. J. (2001). The utility of additional soundings for forecasting lake-effect snow in the Great Lakes Region, *Weather and Forecasting, 16,* 448–462.

Showalter, A. K. (1953). A stability index for forecasting thunderstorms, *Bull. Amer. Meteor. Soc., 34(6),* 250–252.

Sibley, A. (2012). Thunderstorms from a Spanish Plume event on 28 June 2011, *Weather, 67(6),* 143-146.

Sikora, T. D. & Halverson, D. M. (2002). Multiyear observations of cloud lines associated with the Cheasepeake and Delaware Bays, *Journal of Applied Meteorology, 41,* 825–831.

Singh, C., Yadav, B. P., Das, S. & Saha, D. (2014). Thunderstorm accompanied with squalls over Agartala for consecutive two days on 30 April and 1 May, 2012, *Mausam, 65(4),* 539-552.

Sills, D. M. (2009). On the MSC forecasters forums and the future role of the human forecaster, *Bulletin of the American Meteorological Society, 90(5),* 619-627.

Smith, B. B. & Boris, J. P. (2017). Lake snow parameter. National Weather Service Forecast Office, Gaylord, MI. Available at: https://www.weather.gov/apx/lake_snow_parameter (accessed 5 September 2021).

Sousa, P. M., Trigo, R. M., Barriopedro, D., Soares, P. M. M., Ramos, A. M., Liberato, M. L. R. (2017). Responses of European precipitation distributions and regimes to different blocking locations, *Clim. Dyn., 48(3),* 1141–1160.

Sousounis, W. J. & Mann, G. E. (2000). Lake-aggregate mesoscale disturbances. Part V: Impacts on lake-effect precipitation, *Mon. Weather Rev., 128,* 728–745.

Sousounis, P. J. (2001). Lake-effect storms. In: Encylopedia of Atmospheric Sciences. Cambridge, *MA: Academic Press,* 1104–1115.

Steenburgh, W. J., Halvorson, S. F. & Onton, D. J. (2000). Climatology of lake-effect snowstorms of the Great Salt Lake, *Monthly Weather Review, 128(3),* 709–727.

Steenburgh, W. J. & Onton, D. J. (2001). Multiscale Analysis of the 7 December 1998 Great Salt Lake–Effect Snowstorm, *Mon. Weather Rev., 129,* 1296–1317.

Stocci, P. & Davolio, S. (2017). Intense air-sea exchanges and heavy orographic precipitation over Italy: The role of the Adriatic Sea surface temperature uncertainty, *Atmos. Res., 196,* 62–82.

Stuart, N. A. (2001). Multi-dimensional analysis of an extreme thundersnow event during the 30 December 2000 snowstorm. In 18th Conference on Weather Analysis and Forecasting, Fort Lauderdale, FL, *Amer. Meteor. Soc., 18*, 223–226.

Stuart, N. A., Market, P. S., Telfeyan, B., Lackmann, G. M., Carey, K., Brooks, H. E., … Reeves, K. (2006). The future of humans in an increasingly automated forecast process, *Bulletin of the American Meteorological Society, 87(11)* 1497-1502.

Stuart, N. A., Schultz, D. M. & Klein, G. (2007). Maintaining the role of humans in the forecast process: Analyzing the psyche of expert forecasters, *Bulletin of the American Meteorological Society, 88(12)* 1893-1898.

Suriano, Z. J. & Leathers, D. J. (2016). Twenty-first century snowfall projections within the eastern Great Lakes region: detecting the presence of a lake-induced snowfall signal in GCMs, *International Journal of Climatology, 36,* 2200–2209.

Suriano, Z. J. & Leathers, D. J. (2017). Synoptic climatology of lake effect snowfall conditions in the eastern Great Lakes region. *International Journal of Climatology, 37,* 4377–4389.

Tafferner, A., Forster, C., Guillou, Y., Hauf, T., Lunnon, B. & Zinner, T. (2010). Improved thunderstorm weather information for pilots through ground and satellite based observing systems, *EUMETSAT Meteorological Satellite Conference,* September, 2010.

Taszarek, M., Allen, J., Pucik, T., Groenemeijer, P., Czernecki, B., Kolendowicz, L., … Schulz, W. (2019). A Climatology of Thunderstorms across Europe from a Synthesis of Multiple Data Sources, *Journal of Climate, 32(6),* 1813-1837.

Taszarek, M., Kendzierski, S. & Pilguj, N. (2020). Hazardous weather affecting European airports: Climatological estimates of situations with limited visibility, thunderstorm, low-level wind shear and snowfall from ERA5, *Weather and Climate Extremes*, 28, 100243.

Tayanç, M., Karaca, M. & Dalfes, H. N. (1998). March 1987 Cyclone (Blizzard) over the Eastern Mediterranean and Balkan Region Associated with Blocking, *Mon. Weather Rev., 126,* 3036–3047.

Theeuwes, N. E., Steeneveld, G. J., Krikken, F. & Holtslag, A. A. M. (2010). Mesoscale modeling of lake effect snow over Lake Erie—Sensitivity to convection, microphysics and the water temperature, *Adv. Sci. Res., 4,* 15–22.

Trenberth, K. (2005). Uncertainty in hurricanes and global warming, *Science, 308,* 1753-1754.

Trigo, I. F., Dacamara, C. C., Viterbo, P., Roujean, J. L., Olesen, F., Barroso, C., … Arboleda, A. (2011). The satellite application facility for land surface analysis, *Int. J. Remote Sens., 32*, 2725–2744.

TRT (2020). Karadeniz’de kar hayatı olumsuz etkiledi. Available at: https://www.trthaber.com/haber/turkiye/karadenizde-karhayati-olumsuz-etkiledi-26534.html (accessed 5 September 2020).

TRT (2022). Unforgettable cold winters of Istanbul. Available at: https://www.trthaber.com/haber/turkiye/istanbulun-unutulmayan-soguk-kislari-458541.html (accessed 23 February 2022).

TSMS (2020). Satellite and radar images. Available at: http://www.mgm.gov.tr (in Turkish) (accessed 15th July 2020).

TSMS (2021). Turkish State Meteorological Service. Available at: http://www.mgm.gov.tr (in Turkish) (accessed 15 April 2021).

Tusboki, K., Fujiyoshi, Y. & Wakahama, G. (1989). Structure of land breeze and snowfall enhancement at the leading edge, *Journal of the Meteorological Society of Japan, 67, 757*–770.

Tuttle, J.D. & Davis, C.A. (2013). Modulation of the diurnal cycle of warm-season precipitation by short-wave troughs, *J. Atmos. Sci., 70,* 1710–1726.

Türkeş, M. (2010). Climatology and Meteorology, Kriter Publishing, 406. University of Wyoming. (2021). Sounding data. Available at: http://weather.uwyo.edu/upperair/sounding.html (accessed 15 April 2021).

University of Wyoming (2020). http://weather.uwyo.edu/upperair/sounding.html. (accessed 29 August 2020).

University of Wyoming (2021). http://weather.uwyo.edu/upperair/sounding.html. (accessed 19 July 2021).

Vatan (2022). Istanbul's coldest winters! 20 times since 1621. Available at: https://www.gazetevatan.com/galeri/istanbulun-en-soguk-kislari-1621-yilindan- itibaren-20-kez-2016769/22 (accessed 22 February 2022).

Veals, P.G. & Steenburgh, W.J. (2015). Climatological characteristics and orographic enhancement of lake-effect precipitation east of Lake Ontario and over the Tug Hill Plateau, *Mon. Wea. Rev., 143*, 3591–3609.

Veals, P. G., Steenburgh, W. J., Nakai, S. & Yamaguchi, S. (2019). Factors Affecting the Inland and Orographic Enhancement of Sea-Effect Snowfall in the Hokuriku Region of Japan, *Mon. Weather Rev., 147,* 3121–3143.

Villani, J.P., Jurewicz, M.L. & Sr. Reinhold, K. (2017). Forecasting the Inland Extent of Lake Effect Snow Bands Downwind of Lake Ontario, *J. Oper. Meteorol. 5(5),* 53–70.

Wahiduzzaman, M., Ali, M. A., Luo, J. J., et al. (2022). Effects of convective available potential energy, temperature and humidity on the variability of thunderstorm frequency over Bangladesh, *Theor. Appl. Climatol., 147,* 325–346.

Waldstreicher, J. S. (2002). A foot of snow from a 3000-foot cloud: The Ocean-Effect Snowstorm of 14 January 1999, *Bull. Am. Meteorol. Soc., 83,* 19–22.

Wang, Y. & Kulkarni, D. (2011). Modeling weather impact on ground delay programs, *SAE Int. J. Aerosp., 4*, 1207-1215.

Weisman, M. L. & Klemp, J. B. (1982). The dependence of numerically simulated convective storms on vertical wind shear and buoyancy, *Mon. Wea. Rev., 110*, 504–520.

Wetter3 (2020). Charts. Available at: http://www.wetter3.de (accessed 9 March 2020).

Wetter3 (2021). Charts. Available at: http://www.wetter3.de (accessed 19 June 2021).

WHOI (2021). Woods Hole Oceanographic Institute. Available at: http://apdrc.soest.hawaii.edu/datadoc/whoioafluxday.php (accessed 10 July 2021).

Wiedenmann, J. M., Lupo, A. R., Mokhov, II. & Tikhonova, E. A. (2002). The climatology of blocking anticyclones for the Northern and Southern Hemispheres: block intensity as a diagnostic, *J. Clim., 15(23),* 3459–3473.

Wiggin, B. L. (1950). Great snows of the Great Lakes, *Weatherwise, 3,* 123–126.

Wiley, J. & Mercer, A. (2020). An updated synoptic climatology of Lake Erie and Lake Ontario heavy lake-effect snow events, *Atmosphere, 11(8),* 872.

Wilkinson, J. M., Wells, H., Field, P. R. & Agnew, P. (2013), Investigation and prediction of helicopter-triggered lightning over the North Sea, *Meteor. Appl. 20(1),* 94-106.

Williams, E. & Stanfill, S. (2002). The physical origin of the land–ocean contrast in lightning activity, *Comptes Rendus Physique, 3(10),* 1277-1292.

Wilson, J. W., Crook, N. A., Mueller, C. K., Sun, J. & Dixon, M. (1998). Nowcasting thunderstorms: A status report, *Bulletin of the American Meteorological Society, 79(10),* 2079-2099.

Yang, J., Liu, N., Sato, M., Lu, G., Wang, Y. & Feng, G. (2018). Characteristics of Thunderstorm Structure and Lightning Activity Causing Negative and Positive Sprites, *Journal of Geophysical Research: Atmospheres, 123(15),* 8190-8207.

Yavuz, V., Akcar, N. & Schlüchter, C. (2007). The frozen Bosphorus and its paleoclimatic implications based on a summary of the his-torical data. In the Black Sea Flood Question: Changes in Coastline, Climate, and Human Settlement; Yanko-Hombach, V., Gilbert, A.S., Panin, N., Dolukhanov, P.M., Eds.; Springer: Dordrecht, The Netherlands.

Yavuz, V., Temiz, C., Özdemir, E. T. & Deniz, A. (2015). Investigation of accident incident in-flight reports for the European Region, *Eur. J. Sci. Technol., 2,* 155–160.

Yavuz, V. (2016). Investigation of the relationship between aviation reports and instrumental observations for lightning incident in Marmara Region (Master's thesis). Available at: https://tez.yok.gov.tr/UlusalTezMerkezi/tezSorguSonucYeni.jsp (Thesis no: 439621).

Yavuz, V., Özdemir, E. T. & Deniz, A. (2020). Nowcasting of a thunderstorm: The case study of 2 February, 2015 at Istanbul Ataturk International Airport, *Mausam, 71(1),* 21-32.

Yavuz, V., Deniz, A., Özdemir, E.T., Kolay, O. & Karan, H. (2021a). Classification and analysis of sea-effect snowbands for Danube Sea area in Black Sea. Int. J, Climatol., 41(5), 3139-3152.

Yavuz, V., Deniz, A. & Özdemir, E. T. (2021b). Analysis of a vortex causing sea-effect snowfall in the western part of the Black Sea: a case study of events that occurred on 30–31 January 2012, *Nat. Hazards, 108,* 819-846.

Yavuz, V., Özen, C., Çapraz, Ö., Özdemir, E. T., Deniz, A., Akbayır, İ., … Temur, H. (2021c). Analysing of atmospheric conditions and their effects on air quality in Istanbul using Sodar and Ceilometer. *Environ. Sci. Pollut. Res.*

Yavuz, V., Lupo, A. R., Fox, N. I. & Deniz, A. (2022a). Meso-scale comparison of non-sea-effect and sea-effect snowfalls, and development of prediction algorithm for megacity Istanbul airports in Turkey, *Atmosphere 13(5),* 657.

Yavuz, V., Lupo, A. R., Fox, N. I. & Deniz, A. (2022b). The role of short-wave troughs on the formation and development of sea-effect snowbands in the western Black Sea, *Theor. Appl. Climatol., 149,* 501-510.

Yavuz, V., Deniz, A., Özdemir, E. T., Karan, H. & Temiz, C. (2022c). Long-term thunderstorm analysis at airports in the Marmara Region: types and favourable atmospheric conditions, *Int. J. Global. Warming*.

Yazmuhammedov, S., Deniz, A. & Özdemir, E. T. (2014). Cb and thunderstorm analysis of Istanbul airports", 5th National Aeronautics and Space Conference, 8-10 September 2014, Kayseri, Turkey.

Ye, B., Genio, A. D. D. & Lo, K. K. W. (1998). CAPE Variations in the Current Climate and in a Climate Change, *J. Climate, 11(8),* 1997-2015.

Young, M. V. (2007). Severe thunderstorms over southern England on 10 May 2006, *Weather, 62(5*), 116-120.

Zhang, D. L. & Fritsch, J. M. (1985). Numerical simulation of a meso-beta scale warm-core vortex over land. Preprints, 14th Conf on Severe Local Storms, Amer. Meteor. Soc., 29–32.

Zhang, G. J. (2003). Diurnal cycle of convection at the ARM SGP site: role of large-scale forcing, surface fluxes, and convective inhibition. *13th ARM Science Team Meeting Proceedings*, Broomfield, Colorado.

Zhao, W. & Duan, S. B. (2020). Reconstruction of daytime land surface temperatures under cloud-covered conditions using integrated MODIS/Terra land products and MSG geostationary satellite data. *Remote Sens. Environ., 247,* 1–15.

Zook, D. (2014) When lightning strikes. *Ski Area Manage, 53(4),* 36.

CIRRICULUM VITAE

Name Surname **:** Veli YAVUZ

- **B.Sc.** **:** 2014, Istanbul Technical University, Faculty of Aeronautics and Astronautics, Meteorological Engineering Department
- **M.Sc.** **:** 2016, Istanbul Technical University, Faculty of Aeronautics and Astronautics, Meteorological Engineering Department

PROFESSIONAL EXPERIENCE AND REWARDS:

- 2021-2022: Visiting Scholar at University of Missouri – United States of America.
- 2021: TÜBİTAK 2214-A Scholarship.
- 2014-Continued: Research Assisstant – Istanbul Technical University.

PUBLICATIONS, PRESENTATIONS AND PATENTS ON THE THESIS:

- **Yavuz, V.,** Özdemir, E. T. & Deniz, A. (2020). Nowcasting of a thunderstorm: The case study of 2 February, 2015 at Istanbul Ataturk International Airport, *Mausam, 71(1)*, 21-32.
- **Yavuz, V.,** Deniz, A., Özdemir, E.T., Kolay, O. & Karan, H. (2021). Classification and analysis of sea-effect snowbands for Danube Sea area in Black Sea. *Int. J, Climatol., 41(5)*, 3139-3152.
- **Yavuz, V.,** Deniz, A. & Özdemir, E. T. (2021). Analysis of a vortex causing sea-effect snowfall in the western part of the Black Sea: a case study of events that occurred on 30–31 January 2012, *Nat. Hazards, 108*, 819-846.
- **Yavuz, V.,** Deniz, A., Özdemir, E. T., Karan, H. & Temiz, C. (2022). Long-term thunderstorm analysis at airports in the Marmara Region: types and favourable atmospheric conditions, *Int. J. Global. Warming.* 10.1504/IJGW.2022.125083.

- **Yavuz, V.,** Lupo, A. R., Fox, N. I. & Deniz, A. (2022). Meso-scale comparison of non-sea-effect and sea-effect snowfalls, and development of prediction algorithm for megacity Istanbul airports in Turkey, *Atmosphere 13(5)*, 657.
- **Yavuz, V.,** Lupo, A. R., Fox, N. I. & Deniz, A. (2022). The role of short-wave troughs on the formation and development of sea-effect snowbands in the western Black Sea, *Theor. Appl. Climatol., 149,* 501-510.
- **Yavuz, V.,** Lupo, A. R., Fox, N. I. & Deniz, A. (2022). Statistical characteristics of sea-effect snow events over the western Black Sea, *Theor. Appl. Climatol.* 10.1007/s00704-022-04213-2.
- **Yavuz, V.,** Lupo, A. R., Fox, N. I. & Deniz, A. (2022). A long-term analysis of thundersnow events over the Marmara Region, Turkey, *Nat. Hazards*, 10.1007/s11069-022-05393-w.
- **Yavuz, V.,** Lupo, A. R., Fox, N. I. & Deniz, A. (2022). Historical extreme winters of Istanbul: The factors that contributed to severe winters during the 20^{th} and 21^{st} centuries, International Journal of Global Warming (Accepted article).

OTHER PUBLICATIONS, PRESENTATIONS AND PATENTS:

- **Yavuz, V.,** Özen, C., Çapraz, Ö., Özdemir, E. T., Deniz, A., Akbayır, İ. & Temur, H. (2021). Analysing of atmospheric conditions and their effects on air quality in Istanbul using SODAR and CEILOMETER, *Environ. Sci. Pollut. Res.*, 29(11), 16213-16232.
- Özdemir, E. T., **Yavuz, V.,** Deniz, A., Karan, H., Kartal, M. & Kent, S. (2019). Squall line over Antalya: a case study of the events of 25 October 2014, *Weather, 74(S1),* 1-6.
- Özdemir, E. T., Korkmaz, F. M. & **Yavuz, V.** (2018). Synoptic analysis of dust storm over Arabian Peninsula: a case study on February 28, 2009, *Nat. Hazards, 92,* 805-827.
- Özdemir, E. T., Deniz, A., **Yavuz, V.,** Doğan, N. & Akbayır, İ. (2018). Investigation of Fog-Air Quality Relationship in Istanbul, *Fres.Environ. Bull., 27(1),* 30-36.
- Özdemir, E. T., Deniz, A., Sezen, İ., Aslan, Z. & **Yavuz, V.** (2017). Investigation of Thunderstorms over Ataturk International Airport (LTBA), Istanbul, *Mausam, 68(1), 175*-180.
- Özdemir, E. T., Deniz, A., Sezen, İ., Menteş, Ş. S. & **Yavuz, V.** (2016). Fog Analysis at Istanbul Ataturk International Airport, *Weather, 71(11),* 279-284.
- **Yavuz, V.,** Akbayır, İ., Özen, C. & Deniz, A. (2017). Analysis of Hail Incident for Two Different Provinces in Turkey: A Case Study Using Synoptic Analysis and Numerical Weather Prediction Model (WRF), *International Journal of Engineering and Computing (IJESC), 7(12),* 15822-15826.
- **Yavuz, V.,** Akbayır, İ., Özen, C., & Deniz, A. (2017). The Method for forecasting Relative Humidity with Height, *International Journal of Engineering and Computing (IJESC), 7(12),* 15827-15828.
- **Yavuz, V.,** Deniz, A., Çavuş, P. C., Doğan, N. & Akbayır, İ. (2016). Investigation of Wind Characteristics for Bergama in Terms of Wind Energy, *International Journal of Innovative Research in Science, Engineering and Technology – (IJIRSET), 5(12),* 129-137.

- Akbayır, İ., **Yavuz, V.** & Deniz, A. (2016). Evaluation of Air Quality in terms of Health on a Regional Basis in Istanbul, *International Journal of Engineering and Computing (IJESC), 6(11),* 3308-3311.
- Çavuş, P. C., Deniz, A., Doğan, N., Akbayır, İ. & **Yavuz, V.** (2016). Comparison of Three Stations' PM10 Data for Istanbul, Turkey, *International Journal of Innovative Research in Science, Engineering and Technology (IJIRSET), 5(12),* 138-150.
- **Yavuz, V.,** Temiz C., Özdemir, E.T. & Deniz, A. (2014). Investigation of Accident-Incident Reports (Aviation) for the European Region, *European Journal of Science and Technology, 1(2*), 28-38.
- Akbayır, İ., **Yavuz, V.,** Deniz, A. & Özdemir, E.T. (2018). Temporal distribution of fog events at the airports in Turkey. *El-Cezeri Journal of Science and Engineering, 5(2), 327*-330.
- Özen, C., **Yavuz, V.,** Dinç, U., Özdemir, E.T. & Deniz, A. (2019). Short Power Curve Verification of Wind Turbines by Using the Nacelle Mounted Anemometer, *Journal of Research in Atmospheric Science, 1(1),* 32-34.
- Özdemir, E. T., Kolay, O., **Yavuz, V.,** Özen, C., Yetemen, Ö. & Deniz, A. (2019). Queensland Townsville Floods in Australia in Feb 2019, *ATMOS'19 (9th Atmospheric Sciences Symposium),* 80-87, İstanbul, Turkey, 23-26 October 2019. (in Turkish).
- Özen, C., **Yavuz, V.,** Özdemir, E. T. & Deniz, A. (2019). Power Curve Verification on Wind Turbines by Using the Nacelle Mounted Anemometer, *ATMOS'19 (9th Atmospheric Sciences Symposium),* İstanbul, Turkey, 23-26 October 2019. (in Turkish).
- Deniz, A., **Yavuz, V.** & Özdemir, E. T. (2018). Synoptic Situation Analysis on Fog Formation of Istanbul Sabiha Gökçen International Airport, *Turkish National Union of Geodesy and Geophysics Scientific Congress,* 225-228, İzmir, Turkey, 30 May – 2 June 2018. (in Turkish).
- **Yavuz, V.,** Deniz, A. & Özdemir, E. T. (2018). Fog Analysis Using FOGSI Index of Istanbul Sabiha Gökçen International Airport to Minimize Safe Flight and Economic Losses, *Turkish National Union of Geodesy and Geophysics Scientific Congress,* 221-224, İzmir, Turkey, 30 May – 2 June 2018. (in Turkish).
- **Yavuz, V.,** Doğan, N., Akbayır, İ., Toros, H. & Özen, C. (2017). Evaluation on Air Pollution in Karabük, *MENSEC'17 (International Mediterranean Natural Sciences and Engineering Congress,* 151-156, Podgorica, Montenegro, 19-22 October 2017.
- Doğan, N., Akbayır, İ., **Yavuz, V.** & Toros, H. (2017). Investigation of Spatial Variation of Air Pollution in Dilovası-Turkey, *MENSEC'17 (International Mediterranean Natural Sciences and Engineering Congress,* 169-174, Podgorica, Montenegro, 19-22 October 2017.
- **Yavuz, V.,** Deniz, A., Karan, H., Öztopal, A. & Özdemir, E. T. (2017). Climatology of Lightning Events for Marmara Region Airports, *IAREC'17 (International Advanced Researches & Engineering Congress-2017),* 1-5, Osmaniye, Turkey, 16-18 November 2017. (in Turkish).
- **Yavuz, V.,** Deniz, A., Karan, H., Öztopal, A. & Özdemir, E. T. (2017). Examination of Two Different Observations in terms of Lightning Incident at Marmara Region Airports, *IAREC'17 (International Advanced Researches & Engineering Congress-2017),* 1-5, Osmaniye, Turkey, 16-18 November 2017. (in Turkish).

- Akbayır, İ., **Yavuz, V.,** Deniz, A. & Özdemir, E. T. (2017). Temporal Analysis of Fog Incident at Airports in Turkey, *IAREC'17 (International Advanced Researches & Engineering Congress-2017),* 1-5, Osmaniye, Turkey, 16-18 November 2017. (in Turkish).
- Akbayır, İ., Doğan, N., **Yavuz, V.** & Toros, H. (2017). Investigation of the Relationship Between Bolu and Kocaeli Dilovası Air Pollution Parameters by WRF-Chem Model, *IAREC'17 (International Advanced Researches & Engineering Congress-2017),* 1-5, Osmaniye, Turkey, 16-18 November 2017. (in Turkish).
- Akbayır, İ., **Yavuz, V.,** Deniz, A. & Özdemir, E. T. (2017). Fog Analysis at Adana City Airports, *IAREC'17 (International Advanced Researches & Engineering Congress-2017),* 1-5, Osmaniye, Turkey, 16-18 November 2017. (in Turkish).
- Özdemir, E. T., **Yavuz, V.** & Müslüm, M. (2017). Investigation of Downburst Incident at Atatürk International Airport, *UZALMET'17 (3rd Meteorological Remote Sensing Symposium),* Belek-Antalya, Turkey, 16-19 October 2017. (in Turkish).
- Doğan, N., Akbayır, İ., **Yavuz, V.,** Deniz, A. & Çavuş, P. C. (2016). Seasonal Pollution Analysis for Yenibosna, Istanbul, *1st International Conference on Engineering Technology and Applied Sciences,* 1505-1508. Afyonkarahisar, Turkey. (in Turkish).
- **Yavuz, V.,** Deniz, A., Çavuş, P. C., Doğan, N. & Akbayır, İ. (2016). Investigation of Wind Characteristics for Bergama in terms of Wind Energy, *1st International Conference on Engineering Technology and Applied Sciences*, 1415-1424. Afyonkarahisar, Turkey. (in Turkish).
- **Yavuz, V.,** Deniz, A., Çavuş, P. C., Doğan, N. & Akbayır, İ. (2016). Investigation of Wind Characteristics for Bergama in terms of Wind Energy, **ICETAS'16 (1st International Conference on Engeneering Technology and Applied Sciences),** 1492-1496, Afyonkarahisar, Turkey, 21-22 April 2016. (in Turkish).
- Çavuş, P. C., Deniz, A., Doğan, N., Akbayır, İ. & **Yavuz, V.** (2016). Temporal Air Pollution Analysis for Afyon, *1st International Conference on Engineering Technology and Applied Sciences*, 1429-1532. Afyonkarahisar, Turkey. 21-22 April 2016. (in Turkish).
- Çavuş, P. C., Deniz, A., Doğan, N., Akbayır, İ. & **Yavuz, V.** (2016). Comparison of PM10 Data of Three Stations for Istanbul, Turkey, *ICETAS'16 (1st International Conference on Engeneering Technology and Applied Sciences),* 1522-1528, Afyonkarahisar, Turkey, 21-22 April 2016. (in Turkish).
- Doğan, N., Akbayır, İ., **Yavuz, V.,** Deniz, A. & Çavuş, P. C. (2016). Fog Probability Calculation Method and Criteria with FOGSI Index, *ICETAS'16 (1st International Conference on Engeneering Technology and Applied Sciences),* 1509-1511, Afyonkarahisar, Turkey, 21-22 April 2016. (in Turkish).
- Akbayır, İ., **Yavuz, V.,** Deniz, A., Çavuş, P. C. & Doğan, N. (2016). Fog Prediction for Istanbul Atatürk Airport Using Decision Tree Model, *ICETAS'16 (1st International Conference on Engeneering Technology and Applied Sciences),* 1517-1521, Afyonkarahisar, Turkey, 21-22 April 2016. (in Turkish).
- Doğan, N., Akbayır, İ., **Yavuz, V.,** Deniz, A. & Çavuş, P. C. (2016). Seasonal Pollution Analysis for Istanbul Yenibosna, *ICETAS'16 (1st International Conference on Engeneering Technology and Applied Sciences),* 1505-1508, Afyonkarahisar, Turkey, 21-22 April 2016. (in Turkish).

- Akbayır, İ., **Yavuz, V.,** Deniz, A., Çavuş, P. C. & Doğan, N. (2016). Fog Analysis and Forecasting Using Data Mining Methods for Trabzon Airport, *ICETAS'16 (1st International Conference on Engeneering Technology and Applied Sciences),* 1512-1515, Afyonkarahisar, Turkey, 21-22 April 2016. (in Turkish).
- **Yavuz, V.,** Temiz, C., Özdemir, E. T. & Deniz, A. (2015). Squall Line over Antalya, *OSTIV Meteorological Panel Meeting, p. 32,* February 6-7, Winterthur, Switzerland.
- Çakın, A., Ceyhan, İ., **Yavuz, V.,** Özdemir, E. T., Temiz, C. & Deniz, A. (2015). Investigation of the Effect of Snowfall on the flights in Turkey, *OSTIV Meteorological Panel Meeting, p. 32,* February 6-7, Winterthur, Switzerland.
- Temiz, C., **Yavuz, V.** & Deniz, A. (2015) Computational Fluid Dynamics Approach to Wind Energy Calculation and Assessment of Wind Resource of Aegean Region in Turkey, *MESAEP-18th International Symposium on Environmental Pollution and Its Impact on Life in the Mediterranean Region, p. 261,* September 26-30, Crete, Greece.
- Temiz, C., **Yavuz, V.,** Özdemir, E. T. & Deniz, A. (2015) Comparison with Linear and Non-linear Models in Long-term Wind Energy Production, *MESAEP-18th International Symposium on Environmental Pollution and Its Impact on Life in the Mediterranean Region,* 262-262, Crete, Greece, 26-30 September 2015.
- Çavuş, P. C., **Yavuz, V.,** Özen, C. & Deniz, A. (2015) Temporal and Spatial Analysis of Hail in Turkey, *MESAEP-18th International Symposium on Environmental Pollution and Its Impact on Life in the Mediterranean Region,* p. 98, September 26-30, Crete, Greece.
- **Yavuz, V.,** Temiz, C., Özdemir, E. T. & Deniz, A. (2015) Investigation of Accident-Incident Reports (Aviation) for the European Region, *7th Atmospheric Sciences Symposium.* 434-441. Istanbul, Turkey. (in Turkish).
- **Yavuz, V.,** Temiz, C., Özdemir, E. T. & Deniz, A. (2015) Investigation of CODA Reports, *7th Atmospheric Sciences Symposium.* 422-433. Istanbul, Turkey. (in Turkish).
- **Yavuz, V.,** Çavuş, P. C., Özen, C. & Deniz, A. (2015) Temporal and Spatial Analysis of Thunderstorm Cases in Turkey, *7th Atmospheric Sciences Symposium.* 79-85. Istanbul, Turkey. (in Turkish).
- Temiz, C., Özdemir, E. T., **Yavuz, V.,** Durukan, M., Uluyazı, M. & Deniz, A. (2015) Investigation of thunderstorm incident in Ankara Esenboğa Airport on July 15, 2013, *7th Atmospheric Sciences Symposium.* 465-474. Istanbul, Turkey. (in Turkish).
- Ceyhan, İ, Çakın, A., Temiz, C., **Yavuz, V.,** Koçak, K. & Kahya, C. (2014) Analysis of the Wind Persistence in Southwest Anatolia terms of Paragliding, *OSTIV Congress*, p. 43, Poznan, Poland.